Characterisation of the Lysosomal Integral Membrane Protein Type 2 (LIMP-2) in Murine Brain

Dissertation

in fulfilment of the requirement for the degree “Dr. rer. nat”

of the Faculty of Mathematics and Natural Sciences

at Kiel University

submitted by

Michelle Danaher

Kiel 2013

Referee: Prof. Dr. Paul Saftig

Co-referee: Prof. Dr. Thomas Roeder

Date of oral examination: 29.05.2013

Approved for publication: 29.05.2013

Prof. Dr. Wolfgang J. Duschl

(The Dean)

Contents

1 Abstract

Neuron specific functions of the Lysosomal Integral Membrane Protein type 2 (LIMP-2) have not yet been identified. Mutations within LIMP-2 are known to cause a human disease called the Action Myoclonus Renal Failure syndrome (AMRF) where patients present with progressive neurological symptoms including myoclonic epilepsy. Additionally, LIMP-2 was identified as a sorting receptor of the lysosomal hydrolase β-glucocerobrosidase (β-GC). Mutations in β-GC result in a reduction in enzyme activity and ultimately cause Gaucher disease, the most common lysosomal storage disorder. This leads to an accumulation of the enzyme´s substrate glucosylceramide (GluCer) which can stabilise α-synuclein oligomers, the neurotoxic species in synucleinopathies such as Parkinson´s disease (PD). To date it has not been elucidated whether missorting of β-GC or neurological anomalies manifest as a consequence of loss of LIMP-2.

LIMP-2 deficiency in mice resulted in mistrafficking and significant reduction in activity of β-GC in the central nervous system (CNS) accompanied by an accumulation of lipids and carbohydrate-conjugates in primary neurons and brain, respectively. In addition to the previously reported ataxic gait, loss of LIMP-2 led to behavioural abnormalities such as hind-limb clasping, paralysis and tremor consistent with CNS impairment. Astrogliosis, microglial activation and neuronal shrinkage, particularly within dopaminergic neurons, accompanied by an accumulation of α-synuclein, increased apoptosis and indications of lysosomal dysfunction were observed in LIMP-2-deficient murine brain. Similarly, α-synuclein aggregation was detected in primary neurons deficient in LIMP-2. Interestingly, by increasing the targeting of β-GC to the lysosome and thus its activity, using heterologous expression of LIMP-2, the steady state level of α-synuclein could be significantly reduced.

In summary, LIMP-2 appears to play a critical role in the trafficking of β-GC in neuronal populations and its loss leads to abnormal behaviour and disturbed metabolism of several substances within the CNS of mice. Furthermore, attenuating levels of LIMP-2 in order to increase lysosomal β-GC activity and lower levels of intracellular, neurotoxic α-synuclein should be considered as a therapeutic approach for treatment of synucleinopathies.

2 Zusammenfassung

In der vorliegenden Arbeit wurde das *Lysosomal Integral Membrane Protein type-2* (LIMP-2) auf seine -bislang unbeschriebene- neuronale Funktion untersucht. Seit einiger Zeit ist LIMP-2 in seiner Rolle als Rezeptor und Transporter der lysosomalen Hydrolase β-Glukocerobrosidase (β-GC) gut charakterisiert. Dabei führen β-GC-Mutationen zu verminderter Enzymaktivität, einhergehend mit einer Anhäufung des Substrates Glukosylceramid (GluCer). Dieses führt schließlich zur Ausprägung der Gaucher-Erkrankung, einer der häufigsten lysosomalen Speichererkrankungen. Darüber hinaus ist bekannt, dass Mutationen innerhalb des kodierenden Gens für LIMP-2 zur Ausbildung des *Action Myoclonus Renal Failure* (AMRF) -Syndroms führen, welches beim Menschen durch progressive neurologische Symptome, einschließlich myoklonischer Epilepsie, charakterisiert ist. Erst kürzlich konnten Mutationen des LIMP-2-Liganden β-GC als Risikofaktor für die Parkinson-Erkrankung identifiziert werden. Dabei wurde gezeigt, dass GluCer in der Lage ist α-Synuklein-Oligomere zu stabilisieren. Diese führen in Synukleinopathien, wie bei der Parkinson-Erkrankung beobachtet, zu neurotoxischen α-Synuklein-Aggregationen.

Im Rahmen dieser Arbeit konnte gezeigt werden, dass LIMP-2-Defizienz in Mäusen zu einer signifikanten Verringerung der β-GC-Aktivität im zentralen Nervensystem (ZNS) führt. Daraus resultierend kommt es in primären Neuronen bzw. im Gehirn zu einer Anhäufung von Lipid- und Kohlenhydrat-Konjugaten. Zusätzlich konnten Verhaltensauffälligkeiten, wie die Ausprägung eines ataktischen Ganges und die Verkrampfung der Hinterbeine, sowie Lähmungen und Zuckungen beobachtet werden, die als Funktionsstörung des ZNS zu werten sind. Des Weiteren wurde in Gehirnen der LIMP-2-defizienten Mäuse eine lysosomale Dysfunktion einhergehend mit Astrogliose, Mikrogliaaktivierung sowie neuronaler Degradierung und vermehrter Apoptose beobachtet. Insbesondere konnten Anhäufungen von α-Synuklein im ZNS sowie der Verlust von dopaminergen Neuronen beobacht werden. Ebenso wurden α-Synuklein-Akkumulationen in LIMP-2-defizienten primären Neuronen festgestellt. Interessanterweise konnte durch heterologe Expression von LIMP-2 ein vermehrter Transport von β-GC zum Lysosom und somit eine Enzym-Aktivitätserhöhung beobachtet werden, wodurch eine Reduzierung des stationären α-Synuklein erreicht werden konnte. Dieser Ansatz stellt eine potenzielle innovative Therapie zur Behandlung von Synukleinopathien dar.

3 Introduction

3.1 The lysosome

The discovery of lysosomes at the end of the fifties by Christian de Duve led to the birth of a new field of biology (de Duve, 1959). Their physiological importance is highlighted by the increasing number of diseases that are associated with lysosomal dysfunction (Cox and Cachon-Gonzalez, 2012; Shachar et al., 2011).

3.1.1 Constituents of the lysosomal proteome

Lysosomal integral membrane proteins and lysosomal hydrolases are the main constituents necessary for correct function of the lysosome. Four of the major players in maintenance of lysosomal biogenesis are the Lysosomal Associated Membrane Proteins type 1 and 2 (LAMP-1, -2), Lysosomal Integral Membrane Protein type 2 (LIMP-2 or SCARB2), and LIMP-1 (also known as CD63) (fig. 3.1). Other components of the lysosomal/endosomal membrane include the putative ion channel mucolipin 1 (TRP-ML-1) (Dong et al., 2008), the cholesterol transporter Nieman-Pick type C1 (NPC1) (Infante et al., 2008), the multi-subunit proton transporter responsible for acidification of the lysosome, the H^+ vacuolar-type ATPase (Forgac, 1998), the chloride/proton exchanger CLC-7 (Graves et al., 2008) and several others.

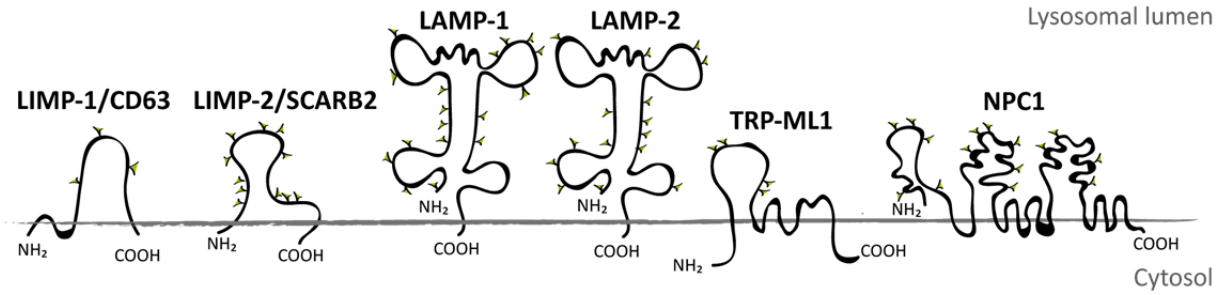

Figure 3.1 ***Lysosomal membrane proteins.*** The topology of selected integral membrane proteins is depicted (adapted from: Eskelinen et al., 2003; Ioannou, 2000; Kiselyov et al., 2005).

One essential role of the limiting membrane of the lysosome is the protection of cytosolic components from the degradative properties of acidic hydrolases. Over 50 hydrolases are found within the lysosomal lumen which includes glucosidases, phosphatases, nucleases, proteases, peptidases, sulphatases and lipases (Bainton, 1981). These enzymes are responsible for catabolism of macromolecules delivered to the lysosome via various routes

both of intracellular and extracellular origin destined for degradation and require an acidic environment for optimal function (De Duve and Beaufay, 1959).

Recently the Coordinated Lysosomal Expression And Regulation (CLEAR) network was shown to be responsible for transcriptional control of many lysosomal proteins including cathepsin D, LAMP-1, LAMP-2, β-Glucocerebrosidase (β-GC) but not LIMP-2 (Sardiello et al., 2009). CLEAR elements, when present in the promoter region of certain genes, can bind the Transcription Factor EB (TFEB) to activate transcription. Overexpression of TFEB results in the formation of more lysosomes and increased exocytosis and its activation is intimately connected to autophagy (Settembre et al., 2011). Dephosphorylation of TFEB via the kinase in mammalian Target Of Rapamycin Complex 1 (mTORC1) during nutrient deprivation leads to transport of the transcription factor through the nuclear membrane followed by the transcription of lysosomal genes (Settembre et al., 2012).

3.1.2 Trafficking of soluble lysosomal proteins

3.1.2.1 Mannose-6-phosphate receptor dependent transport

Proteins destined for the lysosome must have a lysosomal targeting sequence or, in the case of soluble lysosomal proteins, bind to a specific transporter. One such pathway involves the binding of the phosphomonoester residues by one of the Mannose-6-Phosphate Receptors (M-6-PRs) (Huynh-Ba et al., 2008; Martinez-Pineiro et al., 1996)**.** Binding takes place in the trans-Golgi (Lazzarino and Gabel, 1988). Due to acidification of endosomes that bud from the trans-Golgi, the receptor dissociates from the trafficked hydrolase (Gonzalez-Noriega et al., 1980). Then, the receptor may be recycled back to the Golgi or translocate to the plasma membrane (Duncan and Kornfeld, 1988) (fig. 3.2-1).

3.1.2.2 Mannose-6-phosphate receptor independent transport

Some proteins, including hydrolases, are still directed to the lysosome in an M-6-PR independent manner (fig. 3.2-2). In fact fibroblasts from patients suffering from Inclusion-cell (I-cell) disease, in which the N-acetylgluosamine-phosphotransferase is mutated, some hydrolases, such as the acid hydrolase β-GC and sphingolipid activator, are still correctly transported to the lysosome (Rijnboutt et al., 1991) even though these proteins

do not have the M-6-P tag (Owada and Neufeld, 1982; Waheed et al., 1982). Similarly, knockout mice of subunits of the N-acetlygluosamine-phosphotransferase or M-6-PR still have some lysosomally targeted hydrolases (Dittmer et al., 1999; Gelfman et al., 2007). Such findings indicate that an alternative route for hydrolases to be directed to the lysosome must exist.

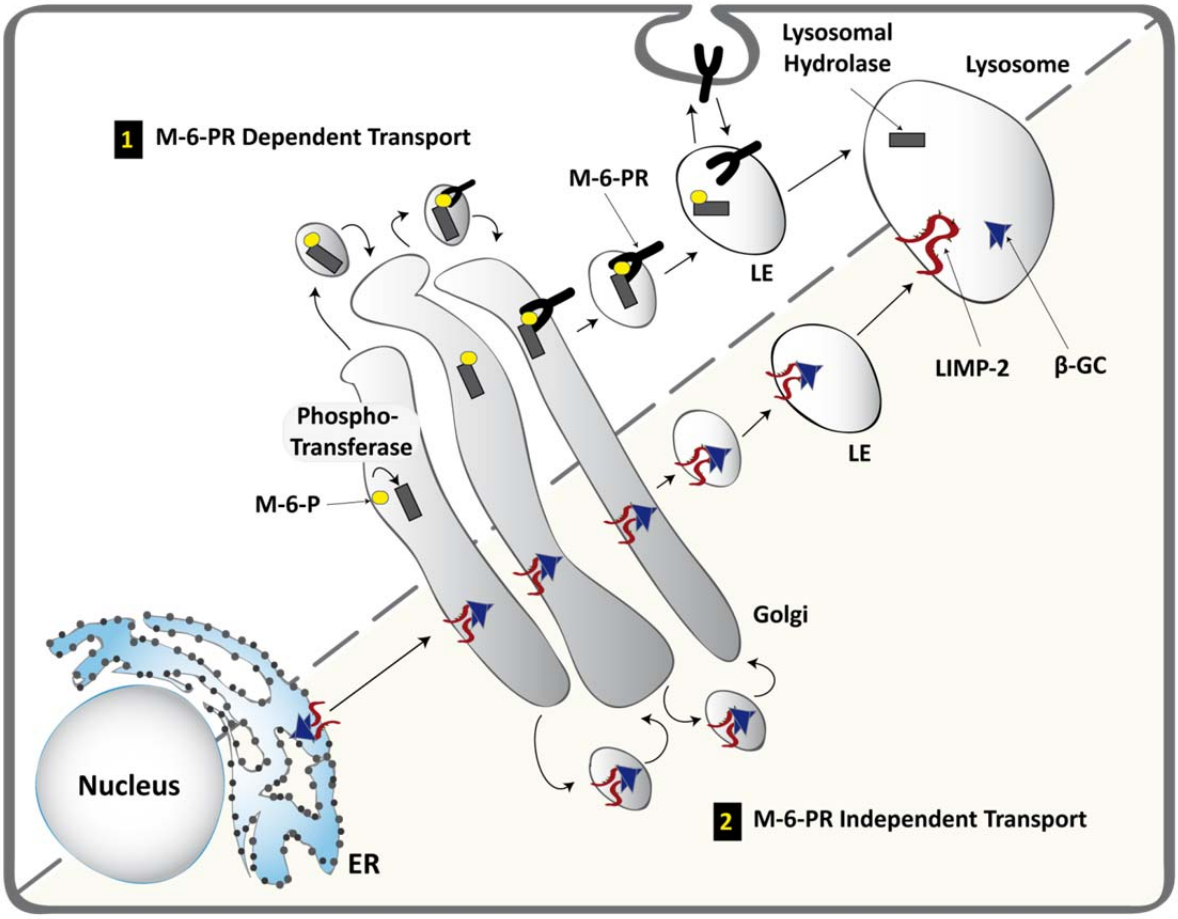

Figure 3.2 ***Trafficking to the lysosome.*** **1-** Mannose-6-Phosphate Receptor (M-6-PR) dependent pathway. Soluble lysosomal proteins obtain a Mannose-6-Phosphate (M-6-P) tag in the cis-Golgi via the phosphotransferase. The receptor-ligand complex is then transported to the late endosome (LE) where the soluble, tagged protein dissociates from the M-6-PR due to the reduction in pH. **2-** M-6-PR independent/LIMP-2 pathway. LIMP-2 binds its ligand β-GC already in the ER and transports the hydrolase to the lysosome where it dissociates into the lumen due to the acidic pH.

Targeting of lysosomal enzymes is thought to be cell type specific. Within the trans-Golgi, sortilin is a type 1 transmembrane protein with a short cytoplasmic tail and large lumenal domain (Petersen et al., 1997). Cathepsin D is found to be trafficked in an M-6-PR dependent manner in fibroblasts but is mediated by sortilin in other cell types (Canuel et al., 2008; Dittmer et al., 1999). Additionally, sortilin has been identified as the primary transporter for sphingolipid activator proteins (Lefrancois et al., 2003) and acid sphingomyelinase (Wahe et

al., 2010). Furthermore, β-GC is transported to the lysosome in an M-6-PR independent manner by LIMP-2 (Reczek et al., 2007) (fig. 3.2-2). Within the ER, LIMP-2 binds β-GC. The receptor-ligand complex travels through the Golgi apparatus to endosomes. Finally, due to a reduction in pH, β-GC dissociates into the lumen of the lysosome (Zachos et al., 2012).

3.2 LIMP-2

3.2.1 Structure and function

LIMP-2, encoded by the SCAvenger Receptor class B member 2 (SCARB2) gene, belonging to the CD36 superfamily, is one of the most abundant proteins of the lysosomal membrane along with the LAMPs 1 and 2 (Marsh et al., 1987). Synonyms for the protein include SR-BII, LGP85, CD36L2, HLGP85 and LIMPII. It is a type 3 transmembrane protein consisting of a large lumenal domain and short cytosolic N- and C- termini (Fujita et al., 1991; Tabuchi et al., 1997; Vega et al., 1991) proposed to be important for lysosomal biogenesis and maintenance (Kuronita et al., 2002; Kuronita et al., 2005). However, its precise role within this process remains unknown. Its large lumenal domain has 11 putative glycosylation sites in humans. In addition to its trafficking functions for lysosomal targeting of β-GC, LIMP-2 has been described as a receptor for the causative agent in hand, foot and mouth disease, enterovirus 71 (Yamayoshi et al., 2009). Adaptor protein 1 (AP-1) is thought to interact with LIMP-2 and thereby mediates its packaging into clathrin coated vesicles (Janvier et al., 2003). Similarly, AP-3 interacts with the dileucine motif in the C-terminus of LIMP-2 and thus guides its trafficking from endosomes to lysosomes (Honing et al., 1998).

3.2.2 Human disease

Mutations within the SCARB2 gene cause Action Myoclonus Renal Failure syndrome (AMRF), a rare form of progressive myoclonic epilepsy (PME) associated with renal failure (Berkovic et al., 2008), deafness (Perandones et al., 2012), demyelinating peripheral neuropathy (Hopfner et al., 2011) and premature death (Badhwar et al., 2004). Patients present with neurological symptoms including PME and ataxia but no cognitive decline with uncharacterised storage material in brain (Berkovic et al., 2008). The majority of patients lack immunodetectable LIMP-2 and knockout mice (Gamp et al., 2003) have been shown to be a valid mouse model (Berkovic et al., 2008) with additional symptoms to those seen in

AMRF patients (Desmond et al., 2011; Gamp et al., 2003; Knipper et al., 2006; Schroen et al., 2007). To date about 13 splice site, missense and nonsense LIMP-2 mutations have been identified in AMRF as well as some PME cases (Balreira et al., 2008; Dardis et al., 2009; Dibbens et al., 2009; Hopfner et al., 2011). Biochemical analysis of selected LIMP-2 mutants revealed low levels of expression, mislocalisation and reduced β-GC binding when compared to LIMP-2 wild-type protein (Blanz et al., 2010; Zachos et al., 2012).

3.2.3 LIMP-2 knockout mice

An array of phenotypes has been attributed to the deficiency of LIMP-2 in mice (table 3.1). The most obvious consequences caused by loss of LIMP-2 function are the initial observations outlined in the first published knockout description including hydronophoresis, deafness and ataxia attributed to peripheral neuropathy (Gamp et al., 2003).

Table 3.1 ***Phenotypes in mice and symptoms in humans due to LIMP-2 deficiency.***

Organ/cell type	Phenotype	Species	Reference
Inner ear	Deafness	Mouse & human	Gamp *et al*., 2003 Perandones *et al*., 2012
Kidney	Hydronophoresis (caused by pelvic junction obstruction), glomerularsclerosis, proteinurea	Mouse	Gamp *et al*., 2003
Kidney	Proteinurea, nephrotic syndrome	Human	Balreira *et al*., 2008, Dardis *et al*., 2009, Desmond *et al*., 2011
Peripheral nerve	Peripheral demyelination (reduced conductance in peripheral nerves)	Mouse & human	Gamp *et al*., 2003, Chaves *et al*., 2011
Brain	Ataxia, slight hyperactivity	Mouse	Berkovic *et al*., 2008
Brain	Myoclonic epilepsy	Human	Berkovic *et al*., 2008, Dardis *et al*., 2009, Chaves *et al*., 2011
Heart	Dilated cardiomyopathy in response to high blood pressure	Mouse & human	Schroen *et al*., 2007
Immune system	Increased susceptibility to Listeria infection	Mouse	Carrasco-Marín *et al*., 2011
Liver, lung, brain	Reduced β-GC activity	Mouse	(Reczek et al., 2007)
Liver and lung	Accumulation glucosylceramide	Mouse	(Reczek et al., 2007)
Brain	Accumulation of unidentified carbohydrate-conjugate product	Mouse & human	Berkovic *et al*., 2008

3.3 The nervous system

The central nervous system (CNS) is comprised of two basic cell types: neurons and metabolic/structural glia and is separated from circulating blood via the blood-brain-barrier.

3.3.1.1 Neurons

Due to the post-mitotic state of neurons they require an efficient way of recycling proteins, dealing with any abnormal aggregates and clearance of aged/damaged organelles. As a result, they possess a well-developed lysosomal system. Endosomes within neurons actively form in dendrites and are transported towards the soma, which contains the highest concentration of lysosomes (Overly and Hollenbeck, 1996). Dysfunction of a multitude of components involved in lysosomal degradation and transport is associated with neurodegenerative diseases (Fukuda et al., 2006; Nixon et al., 2000; Qi et al., 2012) and may be the primary contributor to age-related neurodegeneration. In fact, a general decrease in lysosomal function is associated with ageing and is thought to underlie the increased prevalence of neurodegenerative diseases observed in the elderly (Cuervo and Dice, 2000).

3.3.1.2 Glial cells

Glial cells can be further subdivided into astrocytes, oligodendrocytes and microglia. Astrocytes are star shape cells capable of mitosis with many processes extending from a large soma. Microglial cells are the “macrophages of the CNS” and embody the key innate immunity cells of this organ. Neuroinflammation is encompassed by the activation of both astrocytes and microglia, as seen in many neurodegenerative disorders including Parkinson´s disease (PD) (Block and Hong, 2005; Zhang et al., 2005). In fact, microglia can be activated after lipopolysaccharide stimulation or endocytosis of extracellular proteinaceous aggregates (Reynolds et al., 2008; Zhang et al., 2005). However, whether gliosis in general contributes to neurotoxicity or has protective properties is still under debate.

3.4 Lysosomal metabolism and neurodegenerative disease

3.4.1 Delivery of material to the lysosome (Autophagy)

The sequestration of soluble cytosolic proteins, defective organelles or damaged proteins for degradation and recycling in the lysosome occurs through a process called autophagy which

can be further sub-categorised into microautophagy, chaperone mediated autophagy (CMA) and macroautophagy. These three forms are distinguishable from one another by the processes that are involved in transportation of cargo across the lysosomal membrane and by means of differential induction (review: Cuervo et al., 2005).

In CMA, soluble, cytosolic proteins are transported across the lysosomal membrane via a specific receptor complex thought to consist of a LAMP-2A multimer, Elongation Factor-1 alpha (EF1a) and Glial Fibrillary Acidic Protein (GFAP) (review: Sridhar et al., 2012) and is upregulated in response to stress/nutrient deprivation (Komatsu et al., 2005; Young et al., 2009).

The sequestration of cargo within double-membrane vesicles and their fusion with the lysosome is predominantly used for the degradation of organelles (Mizushima et al., 2008) and aggregated protein (Verhoef et al., 2002; Yamamoto and Simonsen, 2011) within eukaryotic cells and is termed macroautophagy. Targets for degradation are sequestered into double-membrane vesicles. When autophagy is initiated Light Chain 3-I (LC3-I) is conjugated to phosphotidylethanolamine to form LC3-II which localises to autophagosome membranes (Kabeya et al., 2000). Damaged organelles and protein aggregates in the cytosol may be polyubiquitinated (Arrasate et al., 2004; Kopito, 2000). The polyubiquitin tag is then bound by the adaptor protein sequestosome 1 (SQSTM1/p62) which in turn binds LC3-II on autophagic vesicles for fusion with the lysosome for degradation (Komatsu et al., 2007; Pankiv et al., 2007). Thus, an increase in p62 is an indication of inefficient autophagic clearance of aggregated proteins.

3.4.2 Glycosphingolipids and storage disease

The importance of correct function of the lysosome is highlighted by the prevalence of inborn lysosomal diseases of which approximately 40 distinct forms are known with a collective frequency of 1 in 8,000 live births (Meikle et al., 1999). Lysosomal disease usually involves a cryptic cascade of events leading to the manifestation of often crippling symptoms. A clear connection between clinical-pathological manifestations and a unique molecular defect is difficult to establish due to the heterogeneity of symptoms presented by patients. The disease may be categorised based on the nature of the degradative pathway

affected. A well-studied metabolic process that takes place within the lysosome is the degradation of glycosphingolipids (GSLs).

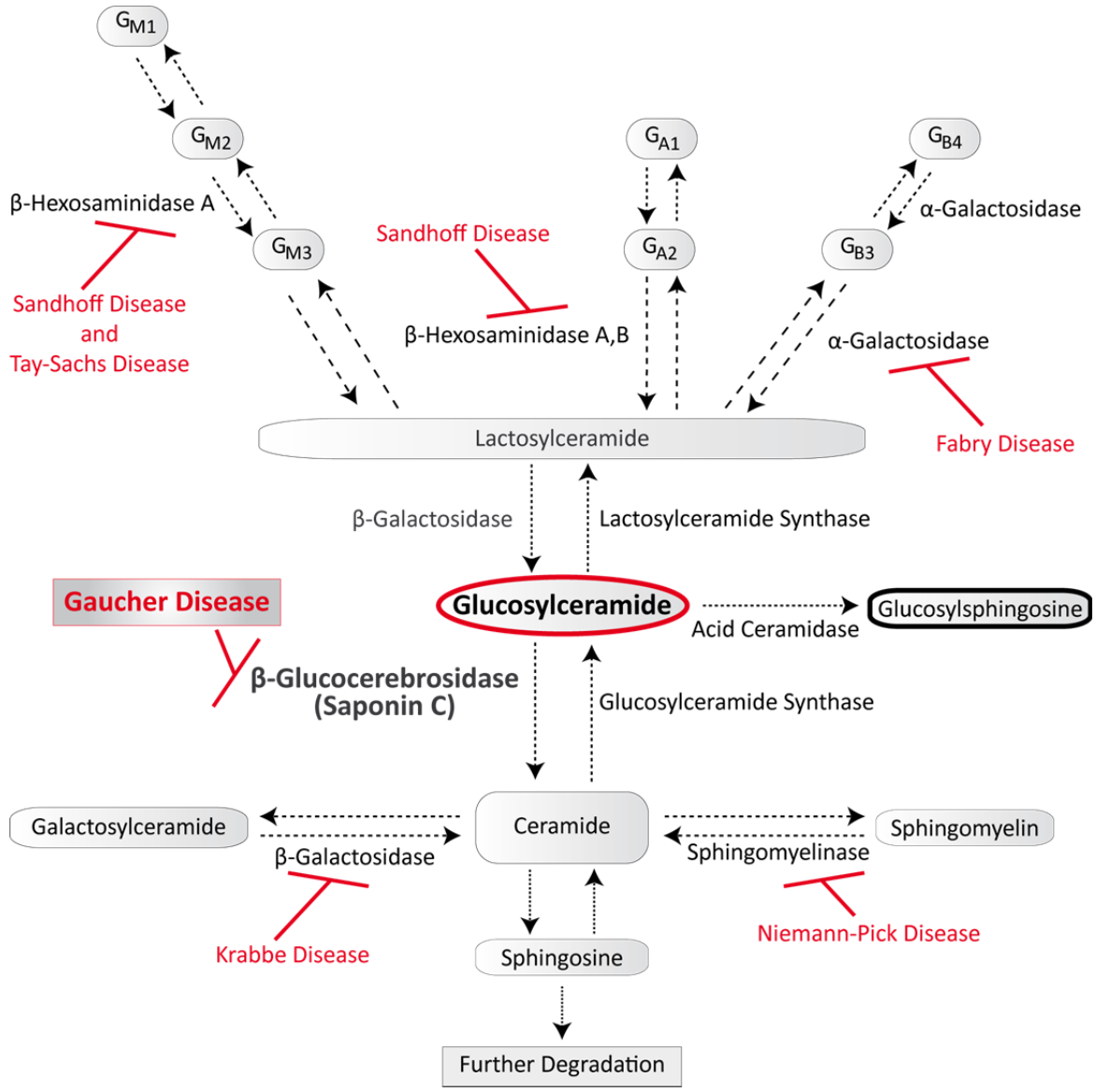

Figure 3.3 ***Metabolism of glycosphingolipids.*** Complex glycosphingolipids (GSLs) are degraded in a sequential manner to give rise to glucosylceramide, which is further metabolised into ceramide via β-glucocerebrosidase and its co-factor saponin C. Glucosylceramide may also be converted into glucosylsphingosine through removal of a fatty acid moiety. Dysfunction of several enzymes in this process cause lysosomal storage diseases shown in red. (GSLs: Gangliosides (G_M) are distinguished by the presence of a sialic acid group; Globosides (G_A) have an N-acetylgalactosamine group but no sialic acid; Lactosides (G_B) have additional galactose groups added to lactoslyceramide but possess neither a sialic acid nor an N-acetylgalactosamine group. Adapted from: Ginzburg et al., 2004; Sawkar et al., 2006; Xu et al., 2010; Yamaguchi et al., 1994).

Sphingolipids are synthesised *de novo* in the ER and are modified via an array of enzymes in the Golgi apparatus (Futerman and Pagano, 1991). The addition of sugar-moieties to the sphingolipid ceramide results in the production of a more complex subgroup called GSLs that play significant roles in membrane biology and provide many bioactive metabolites that

regulate cellular function. They are transported to the plasma membrane by vesicular transport from the Golgi and are endocytosed for degradation mediated by calveolin- and clathrin-mediated endocytosis (Sillence and Platt, 2004). During metabolism, complex lipids are constitutively degraded in the lysosome by soluble hydrolases in a sequential manner. Inefficient activity, trafficking defects or incorrect/absent post-translational modification of one of the enzymes involved in metabolism of GSLs can affect enzymatic activity leading to build-up of its natural substrate causing a glycosphingolipidosis (fig. 3.3). It is not surprising that many glycosphingolipidosis present with neurological symptoms since GSLs are found at the highest level in neurons (Yu et al., 2009). Additionally, the majority, but not all, of lysosomal diseases show storage material within the lysosome. For example electron microscopy of tissue from patients with Krabbe disease, caused by a defect in galactosylceramidase (fig. 3.3), show many non-lysosomal bound cytoplasmic inclusions (Del Bigio et al., 2004). Furthermore, in Pompe disease caused by defective α-glucosidase, storage is seen within lysosomes and in the cytoplasm (Raben et al., 2002). Intralysosomal storage material has not been reported for patients suffering from AMRF caused by mutations in LIMP-2.

Several co-factors and modifying proteins are essential for optimal function of lysosomal enzymes. One such protein is the SUlfatase Modifying Factor SUMF1. Multiple sulfatase deficiency (Austin´s disease) is caused by mutations in the SUMF1 gene resulting in a deficiency in function of all 12 known sulfatases (Cosma et al., 2003). Another family of well-studied co-factors are the sphingolipid activator proteins, saposins A-D, all derived from a common precursor prosaposin (Leonova et al., 1996; Vielhaber et al., 1996). In fact, saposin C plays a role in the optimal activity of β-GC (fig. 3.3) (Qi and Grabowski, 1998; Sun et al., 2003) and other lysosomal GSL metabolic hydrolases (Furst and Sandhoff, 1992).

3.4.3 β-Glucocerebrosidase and Gaucher disease

The lysosomal hydrolase β-GC is responsible for the intralysosomal degradation of the sphingolipid glucosylceramide (GluCer) and is transcribed from the Glucosidase Beta 1 (GBA1) gene. β-GC catalyses the removal of glucose from the central ceramide group within the lysosome (fig. 3.4). A related enzyme, Glucosidase Beta 2 (GBA2), located in the ER and Golgi (Korschen et al., 2013), is responsible for metabolism of GluCer outside of the

lysosome (Yildiz et al., 2006). Gaucher disease (GD) is the most common lysosomal storage disorder with an incidence of 1:50,000 live births with fifty times increased prevalence within the Ashkenazi Jewish population probably due to founder effects (Horowitz and Zimran, 1994). It is caused by defective function of β-GC (Brady et al., 1966) which leads to accumulation of GluCer within affected cells. In some rare cases Gaucher patients with mutations in saposin C have been reported (Vaccaro et al., 2010).

One of the striking features of GD is the pathological enlargement of macrophages in the form of "Gaucher cells". Glucosylsphingosine (GluSph) is another metabolite of GluCer which is found increased 100-fold in GD patient brain and mouse models (Nilsson and Svennerholm, 1982; Orvisky et al., 2000). GluSph is known to be a neurotoxin (Schueler et al., 2003) and is potentially the cause of neuropathology seen in type 2 and 3 GD. Similarly, in Krabbe disease concentrations of the GluCer structurally related β-galactosylceramide is not dramatically increased in brain. Nonetheless, up to 100-fold increased levels of galactosylphingosine have been detected (Svennerholm et al., 1980). Furthermore galactosylsphingosine is proposed to be the toxic metabolite responsible for neuropathology (Suzuki, 1998).

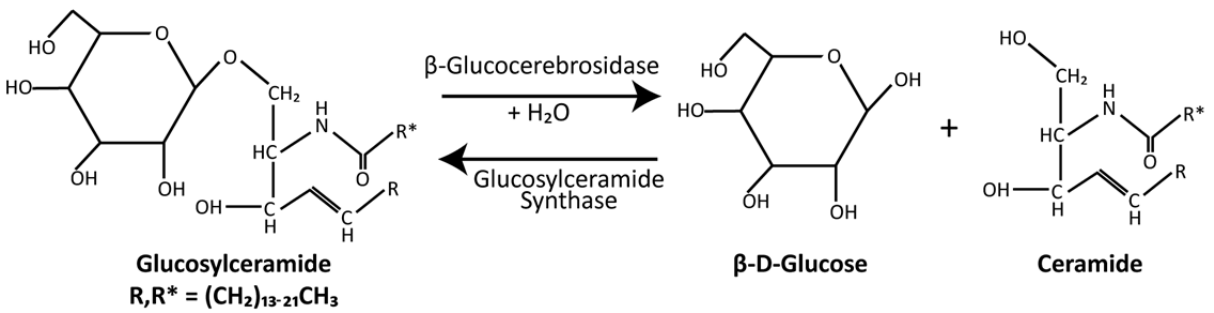

Figure 3.4 ***Hydrolysis of glucosylceramide.*** Glucosylceramide is hydrolysed via the enzymatic activity of β-GC thereby releasing one glucose group from the core ceramide structure. The addition of a glucose ring onto ceramide is mediated by the action of glucosylceramide synthase in a condensation reaction. (Adapted from: Dvir et al., 2003).

Manifestations of GD are highly variable but correlate in severity to remaining enzyme activity and can be categorised into 3 types. GD usually presents as a mild, non-neuronopathic form, type-1 (OMIM #230800) or severe forms with CNS involvement, type-2 (OMIM #230900) and type-3 (OMIM #231000). However, this classification is under revision

since type 1 GD has been associated with a higher risk of developing PD (review: Sidransky, 2005).

3.4.4 Treatment of Gaucher and AMRF

A number of different methods are used in the treatment of lysosomal storage disorders, all with a common purpose of reducing the accumulating metabolic product within the cell. By increasing β-GC activity within the lysosome or directly influencing its synthesis, reduction of GluCer levels can be achieved.

In many cases where a defective hydrolase is responsible for the disease, exogenous administration of recombinant enzyme (Enzyme Replacement Therapy, ERT) has proven effective in the treatment of peripheral GD (Goldblatt et al., 2005; Grabowski et al., 1998; Weinreb et al., 2002). However, with the exception of some storage diseases where high doses of enzyme are administered such as alpha-mannosidosis (Blanz et al., 2008) and mucopolysaccharidosis VII (Vogler et al., 2005) ERT has not proven successful in the amelioration of CNS impairment seen in lysosomal diseases, a classic example being GD (Altarescu et al., 2001). Therefore, compounds capable of penetrating the blood-brain barrier have more attractive therapeutic potential. One such compound is N-butyl-deoxynojirimycin (miglustat), used in substrate reduction therapy (SRT) for some lysosomal diseases (Lachmann, 2006), particularly GD (Cox et al., 2000). Miglustat exerts its effects by inhibiting glucosyltransferase (fig. 3.4) (Platt et al., 1994). Thus, less GluCer is produced leading to an altogether decrease in GSL within the cell. In fact, miglustat treatment resulted in an improvement of symptoms in type 1 GD patients (Cox et al., 2000) and CNS symptoms in one patient with AMRF (Chaves et al., 2011). Interestingly, combined treatment of miglustat and recombinant β-GC improved symptoms in a GD type 3 patient (Capablo et al., 2007). However, reduction of GSLs in general may not be the safest method of targeting the reduction of GluCer within the lysosome as GSLs essential roles in normal cell physiology is not fully understood (Buccoliero et al., 2002).

Chemical chaperones are small molecules that reduce ER associated degradation (ERAD) of misfolded proteins within the ER and thereby increase the probability that they are transported to their destination within the cell, in this case the lysosome. Several

chaperones have been identified capable of enhancing lysosomal localisation and thus activity of GD associated mutated proteins. In addition to its inhibitory effects on the catabolism of GluCer, miglustat appears to act as a chaperone for misfolded β-GC by stabilising the protein in the ER thereby preventing its degradation by the proteasome and enhancing its trafficking to the lysosome (Alfonso et al., 2005; Sawkar et al., 2005). Similarly, ambroxol hydrochloride (Bendikov-Bar et al., 2011) and isofagomine chloride (Khanna et al., 2010) are capable of stabilisation of a β-GC mutant, L444P, causing severe GD and thus enhancing its activity and trafficking to the lysosome.

3.5 Parkinson´s disease

In an ageing population PD is the most common neurodegenerative movement disorder. It is a disease predominantly afflicting the elderly involving a number of both motor and non-motor symptoms and is pathologically characterised by the loss of dopaminergic motor neurons within the substantia nigra pars compacta which causes striatal dopamine deficiency (review: Davie, 2008). Symptoms include bradykinesia, asymmetrical tremor, loss of circadian timing and in later stages delirium and dementia (review: Jankovic, 2008). The etiology of the disease is complex with both environmental factors and genetic predisposition to consider (Langston et al., 1983; Nuytemans et al., 2010; Ritz and Yu, 2000). However, the greatest risk factor for its development is age (Hindle, 2010). The neuropathological hallmark of PD and other synucleinopathies (e.g. dementia with Lewy bodies and multiple system atrophy) are Lewy Bodies and neurites that are positive for aggregated α-synuclein (Baba et al., 1998; Xia et al., 2008).

3.5.1 α-Synuclein

α-Synuclein is a small cytoplasmic membrane associated protein of 140 amino acids, encoded by the SNCA gene found mainly in pre-synaptic terminals and the cytosol throughout brain (Greten-Harrison et al., 2010; Murphy et al., 2000) but also in other cell types (Bartels et al., 2011). Three isoforms (α, β and ϒ) of synuclein derived from different genes with overlapping expression and 80 % sequence homology have been identified (Spillantini et al., 1995). α-Synuclein and β-synuclein play an essential role and can compensate for one another in the stabilisation of synaptic vesicles via interaction with cysteine string protein-α (Chandra et al., 2005) and SNAREs (SNAp REceptor) (Burre et al.,

2010). However, α-synuclein is the only member that aggregates to cause disease (Han et al., 1995; Polymeropoulos et al., 1997).

At neutral pH it is an unstructured and soluble protein capable of associating with membranes via highly conserved 11 amino acid repeats within its N-terminus (fig. 3.5). Furthermore, upon binding to acidic phospholipids in vesicles, its N-terminal region is thought to assume an α-helical secondary structure (Davidson et al., 1998). Three missense mutations within the helical membrane binding domain are associated with disease, A53T (Polymeropoulos et al., 1997), A30P (Kruger et al., 1998) and E46K (Zarranz et al., 2004) (fig. 3.5). A region initially identified as the non-amyloid-β component (NAC) in Alzheimer´s disease which is absent in β- and ϒ-synuclein (Periquet et al., 2007), is particularly prone to aggregation (Han et al., 1995; Ueda et al., 1993). Finally, the C-terminus (region 96-140) contains a proline rich region and has no defined secondary structure.

Oligomeric α-synuclein is thought to be the toxic intermediate in the pathogenesis of disease (Lashuel et al., 2002; Volles and Lansbury, 2002). Overexpression of variants that favour soluble oligomeric and not insoluble fibrillary forms cause significantly more neurotoxicity (Karpinar et al., 2009; Winner et al., 2011) by impeding ER exit of lysosomal destined proteins (Mazzulli et al., 2011) and the promotion of mitochondrial dysfunction (Hsu et al., 2000). Furthermore, α-synuclein may be phosphorylated on serines at positions 87 and 129 (Okochi et al., 2000) (fig. 3.5). In particular, phosphorylation of Ser129 leads to increased propensity to aggregate and phosphorylated α-synuclein is found in synucleinopathy lesions in PD brains (Fujiwara et al., 2002).

Interestingly, mutated forms but not wild-type α-synuclein have the potential to block CMA (Cuervo et al., 2004) thereby preventing degradation of related substrates such as the neuronal survival factor Myocyte-specific Enhancer Factor 2D (MEF2D) (Yang et al., 2009). Conversely sequestration of oligomers into insoluble amyloid structures (Lewy bodies) is thought to be a protective mechanism of the cell to prevent such toxic soluble species from permeabilisation of membranes and damaging interactions with other proteins (Lashuel and Lansbury, 2006).

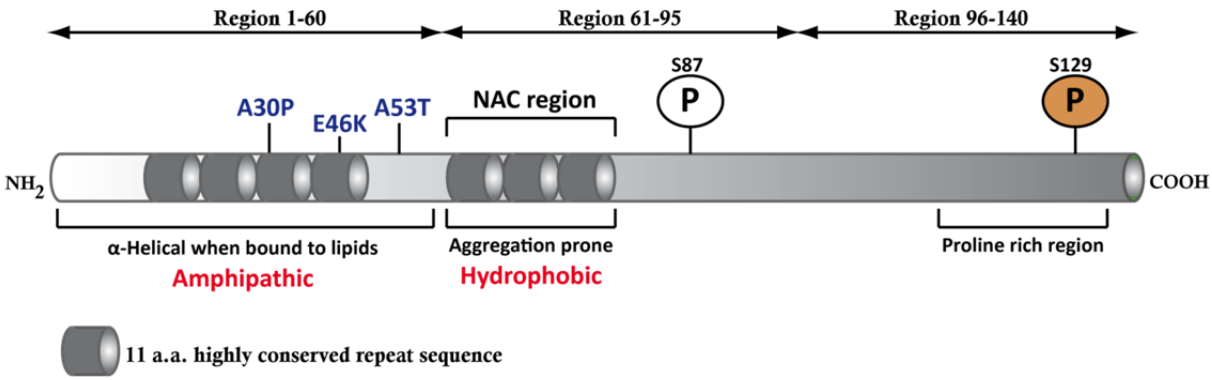

Figure 3.5 ***Model of α-synuclein.*** The α-helical prone C-terminus (region 1-60) with three known pathogenic mutations, a highly hydrophobic sequence (region 61-95) with a non-amyloid component region (NAC) responsible for aggregation and region 96-140 which contains a proline rich sequence that has no distinct structural tendency are highlighted. Two phosphorylation sites are also indicated. (Modified from: Bellucci et al., 2012).

3.5.2 Metabolism of α-synuclein within the cell

Both the ubiquitin-proteasomal-system (UPS) and the autophagy-lysosomal-pathway (ALP), mediated by CMA and macroautophagy, are suggested to be critical for α-synuclein degradation within the cell (Ebrahimi-Fakhari et al., 2011). A deubiquitinase USP9X was recently identified as a switch that elects whether α-synuclein is degraded by the UPS or the ALP via regulation of the number of ubiquitin molecules tagged to the protein (Rott et al., 2011). As a general rule monomeric wild-type α-synuclein is degraded by the proteasome and CMA whereas oligomeric and aggregated forms are degraded via macroautophagy (fig. 3.6) (Cuervo et al., 2004; Lamark and Johansen, 2010; Verhoef et al., 2002; Webb et al., 2003). Increased protein concentration of α-synuclein alone causes disease (Auluck et al., 2002; Masliah et al., 2000). Thus, dysfunction of either the UPS or ALP results in a synucleinopathy.

3.5.2.1 Proteasomal degradation of α-synuclein

With regard to the UPS, dysfunction as a result of mutations or perturbation of the function of some ubiquitin ligases and thus inefficient degradation of cytosolic α-synuclein ultimately results in a synucleinopathy. Many ubiquitin ligases have been identified for the tagging of α-synuclein for degradation by the proteasome including Ubiquitin Carboxy-terminal Hydrolase Like-1 (UCHL-1) (Leroy et al., 1998) and PARKIN/PARK2 (Kitada et al., 1998). When proteins form aggregates within the cytosol, they can no longer be degraded by the proteasome. In this case macroautophagy is responsible for its clearance (Verhoef et al., 2002; Yamamoto and Simonsen, 2011). Interestingly, PARKIN, among others, is reported to

play a crucial role in the polyubiquitination of aggregated proteins (Olzmann and Chin, 2008).

3.5.2.2 Lysosomal dependent metabolism of α-synuclein

Aggregated α-synuclein with polyubiquitinated tags is recognised by p62 for degradation by macroautophagy (Komatsu et al., 2007). Only wild-type, monomeric α-synuclein may be transported into the lysosome via CMA (Vogiatzi et al., 2008; Xilouri et al., 2009). In this way α-synuclein is recognised by the chaperone HSc70 before binding to the CMA transporter LAMP-2a at the lysosomal membrane (Cuervo et al., 2004). Regarding the degradation of α-synuclein within the lysosome, cathepsin D appears to be the major protease (fig. 3.6) as its expression correlates with both steady-state levels and toxicity of α-synuclein (Cullen et al., 2009; Qiao et al., 2008; Sevlever et al., 2008).

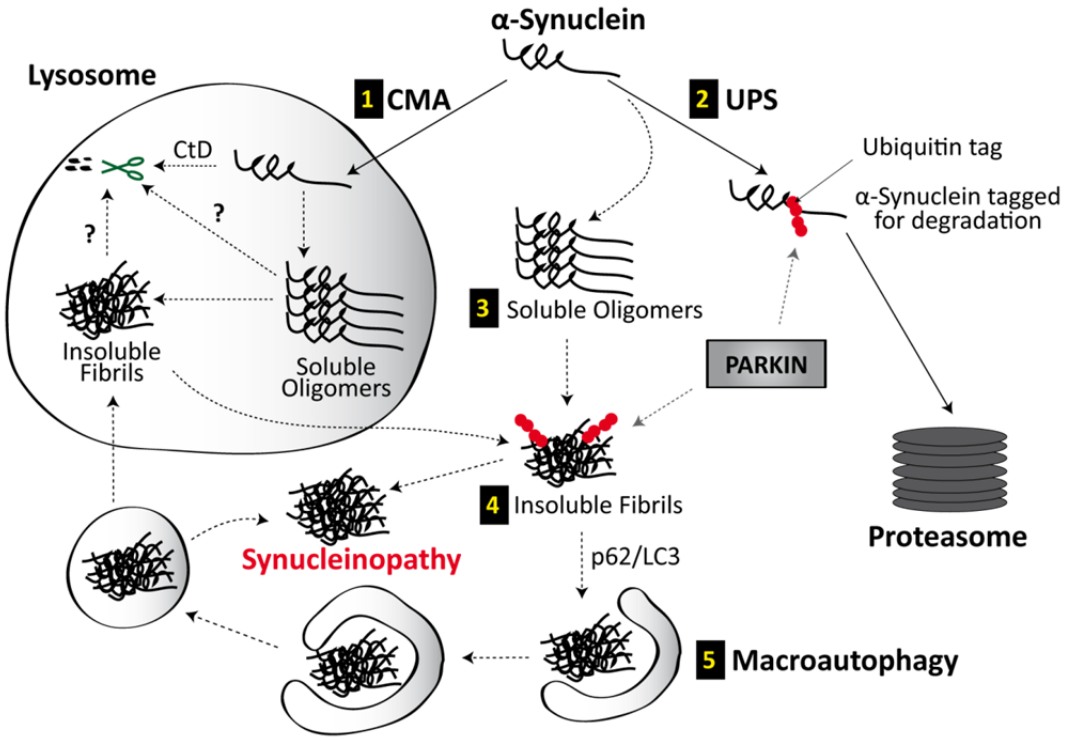

Figure 3.6 ***Metabolism of α-synuclein*****. (1)** Monomeric α-synuclein may be transported into the lysosome via CMA where it can be proteolytically cleaved by cathepsin D (CtD). **(2)** Alternatively, α-synuclein may be tagged with polyubiquitin, which is mediated by PARKIN, for degradation by the proteasome. **(3)** An elevation in the level of α-synuclein within the cytosol or lysosome causes its aggregation initially into soluble oligomers **(4)** and then insoluble fibrils. Cytosolic insoluble aggregated α-synuclein may be tagged with polyubiquitin and then **(5)** sequestered into double membrane vesicles for direction to the lysosome via p62 and LC3 in the process of macroautophagy. Soluble oligomers and insoluble fibrils are degraded by unknown means within the lysosome. Failure of any of these degradative pathways is hypothesised to result in the development of a synucleinopathy.

3.5.3 Causes and risk factors for the development of Parkinson´s disease

Both environmental and genetic factors are thought to contribute to the onset of the disease. While the disease predominantly affects the elderly, usually over 75 years, some early onset forms of the disease, termed juvenile PD, have been described. Duplications (Nishioka et al., 2006) and triplications (Singleton et al., 2003) of the SNCA gene as well as missense mutations (Kruger et al., 1998; Polymeropoulos et al., 1997; Zarranz et al., 2004) are linked to early onset PD. All mutants have a high potential to aggregate and are ineffectively degraded by the cell. Mutations and reduced catalytic activity within UCHL-1 (Leroy et al., 1998) and PARKIN/PARK2 (Kitada et al., 1998) as well as their reduced expression (Moran et al., 2007) have been identified as risk factors for the development of PD (fig. 3.7).

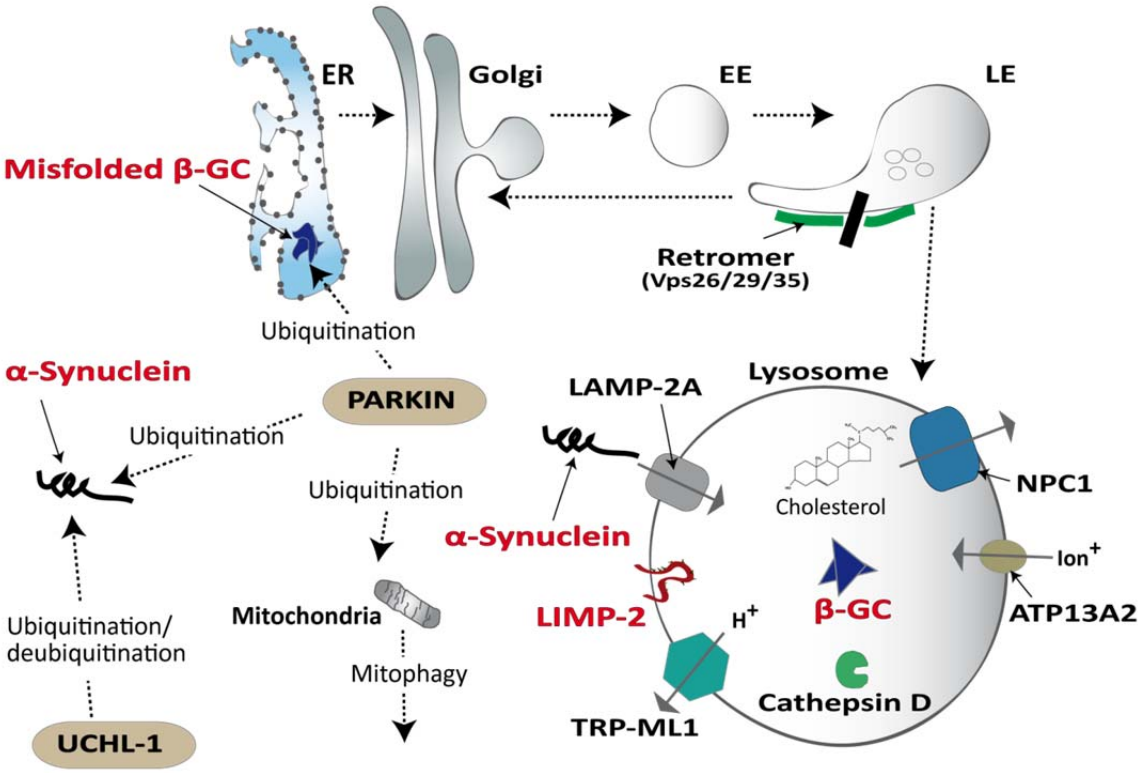

Figure 3.7 ***Lysosomal protein trafficking and function defects associated with PD.*** Proteins associated with ubiquitin mediated clearance (PARKIN and UCHL-1), retrograde transport of proteins to the Golgi (Vps35), a major lysosomal protease (cathepsin D), several lysosomal integral proteins and the soluble hydrolase β-GC are shown. Dysfunction, reduced function or misfolding of proteins involved in lysosome activity potentially perturb degradation of α-synuclein and thus cause Parkinson´s disease. Proteins such as β-GC, LIMP-2 and α-synuclein that are the main subject of this study are highlighted in red.

Deficits within proteins involved in trafficking or function of lysosomal proteins appear to affect greatly the capacity for degradation of α-synuclein by the cell (fig. 3.7). Mutations

within the vesicular protein Vps35, a subunit of the retromer complex responsible for retrograde transport of some transmembrane cargoes, such as the M-6-PR (Seaman et al., 1998) are associated with late-onset PD (Vilarino-Guell et al., 2011; Zimprich et al., 2011). Similarly, mutations within a cation transporter ATP13A2 lead to early-onset PD (Park et al., 2011; Ramirez et al., 2006; Usenovic et al., 2012) due to a reduction in acidification within the lysosome (Dehay et al., 2012). Additionally, single nucleotide polymorphisms of hydrolases such as β-GC (Gegg et al., 2012; Sidransky et al., 2009; Wong et al., 2004) and more recently LIMP-2 (Do et al., 2011; Michelakakis et al., 2012) have been associated with an increased risk for the development of PD. The importance of optimal lysosomal function is underlined by the occurrence of synucleinopathies alongside some lysosomal storage diseases in humans such as Niemann-Pick type C1 (Saito et al., 2004), Tay-Sachs disease and Sandhoff disease (Suzuki et al., 2007). Interestingly, mutations in β-GC are associated with the highest risk of developing PD (review: Westbroek et al., 2011).

3.5.4 Parkinson´s disease and β-GC

Several hypotheses have been proposed in order to establish a molecular and biochemical link between mutations in β-GC and aberrant α-synuclein degradation. Furthermore, the precise role of β-GC in regulating neuronal α-synuclein levels is still under debate. In PD patients carrying β-GC mutations α-synuclein positive Lewy bodies are found comparable with other synucleinopathies (Goker-Alpan et al., 2010; Tan et al., 2004; Wong et al., 2004). Mutant β-GC is thought to contribute to aggregation of α-synuclein and can be found localised in Lewy bodies (Goker-Alpan et al., 2010) suggesting direct interaction of both proteins (Yap et al., 2011). It has been speculated that mutated, misfolded β-GC either binds directly to α-synuclein, thereby promoting its aggregation, or indirectly affects α-synuclein levels by inhibiting proteasomal and lysosomal degradation in general (review: Westbroek et al., 2011).

One concept linked to mutant β-GC identifies impaired ERAD (Ron et al., 2010) or ineffective mitophagy (Narendra et al., 2008) as determining factors leading to PD. Both misfolded β-GC and α-synuclein are thought to share the same ubiquitin ligase (Shimura et al., 2000), PARKIN (fig. 3.7). Furthermore, PARKIN is thought to be critical for efficient clearance of mitochondria via macroautophagy in a process termed mitophagy. Interestingly,

mitochondrial dysfunction is also associated with the development of PD (Winklhofer and Haass, 2010).

However, such hypotheses do not describe the occurrence of PD in Gaucher patients with null mutations (Lesage et al., 2011). A general decrease in β-GC activity within PD brains appears to contribute to the pathogenesis of disease irrespective of whether GD mutations are simultaneously present or not (Gegg et al., 2012). Attenuation of β-GC activity in some neuronal cell lines leads to the accumulation of α-synuclein, mitochondrial dysfunction and damage caused by free radicals similar to the pathogenic state seen in PD (Cleeter et al., 2012; Manning-Bog et al., 2009). Additionally, reduced β-GC activity which conversely results in an increase in GluCer is thought to contribute to the stabilisation of oligomeric α-synuclein within the lysosome (Mazzulli et al., 2011) (fig. 3.8).

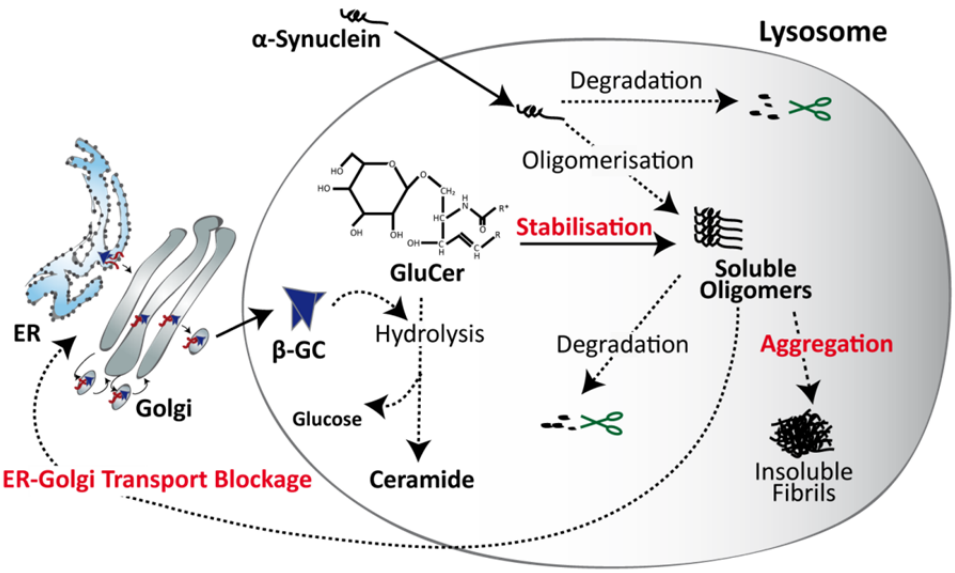

Figure 3.8 ***Pathogenic feed-forward loop of glucosylceramide and α-synuclein.*** An increase in α-synuclein causes its oligomerisation. Reduced activity of β-GC results in an increase in GluCer concentration within the lysosomal lumen. GluCer stabilises soluble α-synuclein oligomers, thus retarding its degradation. Soluble oligomers may form insoluble fibrils or block ER-Golgi trafficking of newly synthesised proteins causing an intensifying pathogenic loop. (Adapted from Mazzulli et al., 2011).

Furthermore, overexpression of α-synuclein is known to block ER-Golgi transport in both yeast and mammalian cells (Cooper et al., 2006; Thayanidhi et al., 2010). In this manner a pathogenic feed forward loop may be generated (fig. 7.8). That is, an increase in lysosomal lipids leads to the stabilisation of α-synuclein within the lysosome thereby reducing its effective clearance by proteases. α-Synuclein blocks trafficking of newly synthesised

lysosomal hydrolases and proteases from the ER leading to a further reduction in lysosomal enzymatic activity thereby exacerbating toxicity even further. Additionally, overexpression of α-synuclein was shown to disrupt the interaction between LIMP-2 and β-GC (Gegg et al., 2012) thus potentially leading to decreased transport of newly synthesised enzyme from the ER to the lysosome.

4 Objectives

The central aim of this project was the characterisation of the *in vivo* function of the Lysosomal Integral Membrane Protein type 2 (LIMP-2) within the central nervous system (CNS) of mice. Immunohistology as well as the preparation of primary neuronal and glial cultures were employed in order to elucidate the expression pattern of LIMP-2 in cells within the brain. Behavioural studies as well as an array of histological staining techniques, protein biochemistry, lysosomal enzyme activity assays and molecular biology preparations were used in order to explain the role LIMP-2 plays in the CNS.

Additionally, the potential mistrafficking of the lysosomal hydrolase β-Glucocerebrosidase (β-GC), the anticipated accumulation of its metabolic products and the putative accumulation of α-synuclein in neuronal cells was assessed using biochemical methods, immunological staining of histological sections and primary cell culture.

Finally, the therapeutic potential of LIMP-2 was analysed under the assumption that it is responsible for transportation of β-GC to the lysosome in neurons and reduction of enzymatic activity leads to accumulation of α-synuclein. Overexpression studies and glycosphingolipid synthesis inhibitor treatment of several cell lines and primary neurons coupled with biochemical and molecular biological analysis were employed. Additionally, using immunohistochemistry a possible change in the expression of LIMP-2 in human tissue from Parkinson´s disease patients was assessed.

5 Materials and Methods

5.1 Materials

Detailed lists from all machines, chemicals, kits, routine buffers and materials can be found in appendix 9.1.

5.1.1 Cell lines

Mouse embryonic fibroblasts (MEFs), HeLa and SHSY-5Y cells were used for overexpression experiments (table 5.1).

Table 5.1 ***Cell lines***.

Name	Description
HeLa	Cervical carcinoma cells (Henrietta Lacks) (DMSZ, Braunschweig, G)
SHSY-5Y	Human neuroblastoma cell (Biedler et al., 1978)
583-3 MEFs	LIMP-2 wild-type murine fibroblasts (Schröder, 2008)
583-2 MEFs	LIMP-2 knockout murine fibroblasts (Schröder, 2008)

5.1.2 Oligonucleotides

All primers for use in cloning, qRT-PCR and for genotyping were obtained from Sigma Aldrich (Steinheim, DE). A concentration of 100 µM was stored for 2-5 days at 4 °C or at -20 °C for longer periods of time.

5.1.3 Vectors

Two expression vectors, pFrog3 (Gunther et al., 1998) and pcDNA3.1 Hygro^{+} (Invitrogen, Darmstadt, DE), were used in the course of this study (table 5.2). The pFrog vector, derived from the pcDNA3 vector (Invitrogen, Darmstadt, DE), was originally designed for complementary RNA synthesis and has the 5'- and 3'-untranslated region of β-globin from *Xenopus laevis.* Within this vector the T7-promoter and cytomegalovirus (CMV) promoter controls transcription and a poly-adenylation signal from bovine growth hormone (BGH) helps to stabilise RNA after transcription. The Simian Virus 40 (SV40) promoter, that controls transcription of a neomycin resistance gene, permits selection in eukaryotic cells. Together with a CoIEI gene that allows replication in bacteria and an ampicillin resistance gene growth and selection of the vector in *E. coli* is also possible.

The vector pcDNA3.1 Hygro$^+$ has 3 promoters that allow a high expression rate of recombinant protein including the CMV-promoter and a T7-promoter and a poly-adenylation tail. Additionally, the presence of a SV40 promoter allows efficient transcription of hygromycin if selection of transfected cells is necessary. It also has an ampicillin resistance gene and pUC origin for selection and maintenance in *E. coli.*

Table 5.2 ***Vector description.***

Vector	Size (Kb)	Reference	Use	Resistance
pEGFP	4.7	Invitrogen, Darmstadt, DE	Estimation of transfection efficiency/ mock transfection	Kanamycin
pcDNA3.1 Hygro$^+$	5.4	Invitrogen, Darmstadt, DE	Transient and stable expression of desired cDNA	Ampicillin/ Hygromycin
pFrog3	5.7	(Gunther et al., 1998)	Transient expression of desired cDNA	Ampicillin/ Neomycin

5.1.4 Plasmids

The vector pFrog3 with human and murine LIMP-2 tagged at the carboxy-terminus (C-terminus) with myc (EQKLISEEDL) and the murine LIMP-2(DDD) mutant were generated by M. Schwake and J. Blanz, published in Blanz et al., 2010 and Reczek et al., 2007. Constructs of human α-synuclein (SNCA) were cloned (5.3.11) into the pcDNA3.1 Hygro$^+$ vector (5.1.3). All constructs used in overexpression experiments are outlined in table 5.3.

Table 5.3 ***Plasmids for overexpression in eukaryotic cells.*** MCS = multiple cloning site; h, human; m, mouse.

Vector	Size (kb)	Reference	Description
pFrog3	mLIMP-2-Myc	(Blanz et al., 2010; Reczek et al., 2007)	Murine LIMP-2 with C-terminal myc tag.
pFrog3	mLIMP-2(DDD)	(Blanz et al., 2010)	Murine LIMP-2 with mutation in helix known to be β-GC binding region.
pcDNA3.1 Hygro $^+$	SNCA	Self-produced	Human α-synuclein cDNA inserted into between HindIII/XhoI in the MCS.
pcDNA3.1 Hygro $^+$	SNCA-A53T	Self-produced	Human α-synuclein cDNA with disease mutation A53T inserted between HindIII/XhoI in the MCS.
pcDNA3.1 Hygro $^+$	SNCA-HA	Self-produced	Human α-synuclein cDNA with claI site followed by a C-terminal HA tag inserted between HindIII/XhoI in the MCS.

5.1.5 Mouse strains

LIMP-2-deficient mice from a mixed background of C57BL/6J x 129 SV/J were described previously (Berkovic et al., 2008; Gamp et al., 2003) and backcrossed at least 3 times into C57BL/6N from Charles River laboratories (Massachusetts, US). LIMP-2 deficient mice contain a neomycin (neo) cassette that disrupts transcription within exon 8 (Gamp et al., 2003). Embryos at gestation day 15.5 from sacrificed LIMP-2 heterozygote females terminally mated with LIMP-2 heterozygote males were used for neuronal cultures. Mice, 2-10 months old, were assessed for behavioural deficits. Sibling mice from either sex, 6-10 months old, were used for histological and biochemical analysis. Due to an increased mortality rate from 10 months onwards, mice were prepared at or before this age. LIMP-2 knockouts were always compared to their wild-type littermates.

Mice overexpressing human α-synuclein (S13) were acquired from Novartis (Novartis Pharma GmbH, Nürnberg, Germany). S13 transgene mice carry an inserted SNCA gene under the control of the THYmocyte differentiation antigen 1 (Thy-1) promoter leading to overexpression of α-synuclein in most neuronal populations. Embryos at gestation day 15.5 from sacrificed females carrying the α-synuclein transgene terminally mated with wild-type males were used for neuronal cultures. Mice overexpressing human α-synuclein with an aggregation prone mutation A53T, also under the control of the Thy-1 promoter (9813), were described previously (van der Putten et al., 2000).

Animals were maintained in a conventional animal facility. All experiments were carried out under guidelines set by the National Animal Care Committee of Germany.

5.1.6 Antibodies

Table 5.4 ***Antibodies used in this study*****.** (IF, immunofluorescence; WB, Western blot; IHC, immunohistochemistry; IH—F immunohistology – fluorescence).

Name	Source	Host	Dilutions			
			IF	WB	IHC	IH-F
α-Actin	Sigma Aldrich, Steinheim,DE	rabbit	--	1:2000	--	--
α-Alpha-synuclein (BD 610787)	Transduction Laboratories, Franklin Lakes, NJ, US	mouse	1:100	1:1000	1:1000	--
α-β-GC (4171)	Sigma Aldrich, Steinheim,DE	rabbit	--	1:2000	--	--
α-Calbindin	Abcam, Cambridge, UK	mouse	--	--	--	1:250
α-Cathepsin D (SII10)	(Hentze et al., 1984)	rabbit	--	1:1000	1:500	1:100
α-CD68	Serotec, Oxford, UK	rat	1:500	--	1:3000	1:200
α-GFAP	Sigma Aldrich, Steinheim, DE	mouse/ rabbit	1:200	--	1:3000	1:300
α-HA (3F10)	Roche, Penzberg, DE	rat	--	1:500	--	--
α-KDEL	Stressgen, Ann Arbor, MI, US	mouse	1:50	--	--	--
α-LAMP-1 (1D4B)	DSHB, Iowa City, US	rat	1:50	1:500	--	1:200
α-LAMP-2 (ABL93c)	DSHB, Iowa City, US	rat	1:100	1:500	--	1:200
α-LIMP-2	Pineda, Berlin, DE	rabbit	1:500	1:2000	1:3000	1:200
α-MAP-2	Sigma Aldrich, Steinheim, DE	mouse	1:300	--	--	--
α-MBP (MAB 386)	Chemicon, Billerica, US	rat	--	1:1000	--	--
α-NeuN (MAB 377)	Chemicon, Billerica, US	mouse	--	--	1:2000	--
α-p62 (PW9860)	Enzo Life Sciences, Lörrach, DE	rabbit	--	1:3000	1:3000	--
α-Polyubiquitin (FK1)	Biotrend, Cologne, DE	mouse	1:200	1:1000	1:1000	--
α-Tyrosine hydroxylase (Ab112)	Abcam, Cambridge, UK	rabbit	1:200	--	1:3000	--

Table 5.5 ***Secondary antibodies***. (IF, immunofluorescence; WB, Western blot; IHC, immunohistochemistry; IH—F immunohistology – fluorescence).

Name	Source	Host	Dilutions			
			IF	WB	IHC	IH -IF
α-Mouse Biotinylated	Abcam, Cambridge, UK	Goat	--	--	1:500	--
α-Rabbit Biotinylated	Abcam, Cambridge, UK	Goat	--	--	1:500	--
α-Rat Biotinylated	Abcam, Cambridge, UK	Goat	--	--	1:500	--
α-Mouse-HRP	Dianova GmbH, Hamburg, DE	Sheep	--	1:10,000	--	--
α-Rabbit-HRP	Dianova GmbH, Hamburg, DE	Sheep	--	1:10,000	--	--
α-Rat-HRP	Dianova GmbH, Hamburg, DE	Rabbit	--	1:10,000	--	--
α-Mouse-Alexa Fluor 488/594	Invitrogen, Darmstadt, DE	Goat	1:500	--	--	1:2000
α-Rabbit-Alexa Fluor 488/594	Invitrogen, Darmstadt, DE	Goat	1:500	--	--	1:2000
α-Rat-Alexa Fluor 488/594	Invitrogen, Darmstadt, DE	Goat	1:500	--	--	1:2000

5.1.7 Human tissue

Post-mortem brain tissue of patients diagnosed with PD and control tissue from individuals not suffering from neurodegenerative disease were obtained from the laboratory of Prof. Dr. Markus Glatzel, Institute of Neuropathology, University Medical Centre Eppendorf, Hamburg, DE. Samples from the midbrain/substantia nigra were from subjects outlined in table 5.6.

Table 5.6 ***Subject sample description***. Age, sex and neuropathology (if present) are indicated for each subject.

	Clinical internal number	Sex	Age	Pathology
Case 1	NP_17-2011	Male	74	Synucleinopathy
Case 2	NP_247-2007	Female	61	Synucleinopathy
Case 3	NP_94_12	Female	75	Synucleinopathy
Case 4	NP_120_12	Male	74	Synucleinopathy
Case 5	NP_224_08	Male	87	Synucleinopathy
Case 6	NP_96_10	Male	69	Synucleinopathy
Control 1	NP_246-2008	Male	61	Normal
Control 2	NP_368-2008	Male	68	Normal
Control 3	NP_251_2012 Bl.3	Female	82	Normal
Control 4	NP_252_2012 Bl.3	Male	68	Normal
Control 5	NP_253_2012 Bl.3	Female	72	Normal
Control 6	NP_255_2012 Bl.3	Female	88	Normal
Control 7	NP_256_2012 Bl.3	Female	82	Normal

5.2 Methods

5.2.1 Behavioural Testing

Behaviour was assessed in animals aged between 2 and 10 months. Each genotype had a minimum of 6 mice per age category. All behavioural observations were recorded with the operator blind to genotype of the animal tested.

5.2.1.1 Movement abnormalities

Mice were observed for approximately 1 minute at rest in a sterile box. General observation of movement at rest was scored 0/1 (0 = normal; 1 = movement abnormalities including resting tremors and jerking). Due to the difficulty in distinguishing between jerking and tremor only one category “movement abnormalities” was used to describe this phenotype.

5.2.1.2 Ataxia

Gait was observed in mice placed on the top or side of a holding cage and allowed to walk along the cage grid/side. Uncoordinated movement while walking along the cage cover or side was recorded as ataxia. Due to the difficulty in accurately assigning severity scoring of ataxia the presence and absence were designated 1 and 0 respectively.

5.2.1.3 Hind-limb clasping

Mice were suspended over a flat surface by the tail for approximately 30 seconds and the incidence of hind-limb clasping documented. Hind-limb clasping behaviour was scored 0/1 (0 = normal; 1 = clasps hind-limbs).

5.3 Molecular Biology

5.3.1 Mouse perfusion

Mice were perfused transcardially for histological preparation. Animals were anaesthetised with 10 µl/mg weight of a mixture of 1.2 % xylazin/0.16 % ketamine in phosphate buffered saline (PBS). Depth of anaesthesia was assessed by monitoring pinch withdrawal reflexes. After securing the mouse on a clean platform, the trunk was sterilised with 70 % ethanol and a lateral incision was made from the base of the torso to the neck. The diaphragm was cut and the rib-cage removed to allow access to the heart. A butterfly needle was inserted into

the left ventricle and the right atrium was cut. Vascular pressure was maintained at approximately 80 mm Hg. The mouse was perfused initially with 0.1 M phosphate buffer (PB) or PBS for 3 - 5 minutes or until the kidneys and liver were visibly pale followed by perfusion with 4 % paraformaldehyde (PFA) in PBS until the body was significantly rigid.

5.3.2 Isolation of the central nervous system (brain and spinal cord) from adult mice

Mice were perfused or sacrificed using a CO_2 chamber followed by cervical dislocation at the neck. The head was removed and sterilised briefly using 70 % ethanol. Skin was removed by cutting caudal to rostral along the midline of the head to behind the nose. Subsequently the skull was cut, again caudal-rostral, and removed carefully using forceps. Isolated brains intended for histological analysis were post-fixed at room temperature for 4 hours in 4 % PFA/ PBS. For separation of specific brain regions the entire brain was divided sagittally down the midline and areas were isolated with the aid of CX41 microscope (Olympus, Hamburg, DE) before freezing in liquid nitrogen and storage at -80 °C.

For isolation of the remaining CNS (the spinal cord), remaining organs were removed from the abdominal cavity. After careful removal of all outer skin and limbs the spine was fixed overnight in PBS/4 % PFA/1 % glutaraldehyde (EM fixative) for future experiments involving electron microscopy. Thereafter, fixed tissue was stored in fresh EM fixative at 4 °C until use.

Spinal cords were isolated from mice using a CX41 microscope (Olympus, Hamburg, DE). Mice were fixed to a styrofoam platform with the abdominal cavity facing down before removal of all muscle surrounding the spinal cord with a tweezers. Vertebrae of the spinal cord were cut carefully and removed individually. The spinal cord was then prepared as in section 5.3.4.

5.3.3 Tissue and section preparation

5.3.3.1 Paraffin embedding and sectioning of murine brain tissue

Fixed brain tissue was dehydrated in an ascending alcohol series (i.e. 30 minutes 50 % ethanol, 30 minutes 60 % ethanol, 30 minutes 70 % ethanol, 15 minutes 96 % ethanol, 30 minutes 96 % ethanol, 45 minutes 100 % ethanol, 60 minutes 100 % ethanol), cleared with

xylol (2 x 60 minutes) and incubated in Roti®Plast paraffin (Roth, Karlsruhe, DE) heated to approximately 60 °C (paraffin I 30 minutes, paraffin II overnight, paraffin III 30 minutes) before embedding in paraffin. Slices of 5 µm were cut using a Leica SM 2000R microtome (Leica, Wetzlar, DE) and transferred directly onto objectives.

5.3.3.2 Removal of paraffin and rehydration of histological sections

For all histological staining paraffin sections were cleared in Rotihistol® (Roth, Karlsruhe, DE) (2 X 10 minutes) before rehydration in an alcohol series (i.e. 5 minutes each in 100 % ethanol, 96 % ethanol, 70 % ethanol, 50 % ethanol) followed by rinsing in double-distilled H_2O (ddH_2O).

5.3.3.3 Sucrose embedding a preparation of free floating sections

Alternatively tissue was incubated in 30 % sucrose in 0.1 M PB at 4 °C for at least 24 hours. Free floating cryosections were cut on a Leica SM 2000R microtome (Leica, Wetzlar, DE) and placed in 0.1 M PB before immunological staining (section 5.3.5.7). In murine samples, sagittal sections were used for all analyses with the exception of sections that necessitated identification of the substantia nigra where coronal sections were used.

5.3.4 Histology

For general overviews of morphological changes within tissue histochemical staining may be utilised. Dyes are generally ionized compounds with the staining element located in one or more of the ions. The staining molecule is situated at the anion or cation for acidic and basic dyes, respectively. Neutral dyes have staining components in both anions and cations.

5.3.4.1 Nissl stain

This method of staining is used for the detection of Nissl substance, a large granular body found only in the cytoplasm of neurons. Both thin (5-10 µm) and free-floating (45 µm) sections can be stained using the Nissl technique. The Nissl body will be stained purple-blue. This stain is commonly used for identifying the basic neuronal structures in the CNS. Free floating sections were mounted on glass slides and allowed to dry for 48 hours at room temperature. Sections were dehydrated in 50 % ethanol for 5 minutes then incubated for 1 hour in 70 % ethanol. Slides were then stained for 2 minutes using 0.1 % cresyl violet with

approximately 300 µl of glacial acetic acid in 100 ml of ddH_2O. Slides were subsequently rinsed quickly in ddH_2O and differentiated for approximately 20 seconds in 96 % ethanol. Sections were dehydrated further in 100 % ethanol for 10 minutes, cleared and mounted as in section 5.3.5.8.

5.3.4.2 Luxol fast blue

Luxol fast blue is a staining method used for the detection of myelin/myelinated axons in fixed sections. The myelin, including phospholipids, will be stained blue-green. A 1 % luxol fast blue solution-L0294 (Sigma Aldrich, Steinheim, DE) was used to stain paraffin sections. Deparaffinised sections (5.3.3.2) were incubated overnight at 56 °C. Excess stain was rinsed off briefly in 95 % ethanol before rinsing thoroughly in ddH_2O. Slides were differentiated in 0.05 % lithium carbonate solution-62470 (sigma) for 30 seconds and a further 30 seconds in 70 % ethanol before rinsing in ddH_2O. Slides were differentiated further in 95 % ethanol and checked microscopically for staining intensity. Finally, sections were dehydrated completely in 100 % ethanol for 5 minutes each followed by two changes of RotiHistol® (Roth, Karlsruhe, DE) and mounted in Eukitt (Sigma Aldrich, Steinheim, DE) and visualised using a BX50 microscope (Olympus, Hamburg, DE).

5.3.4.3 Haematoxylin and Eosin

To allow for general morphological characterisation paraffin sections were stained using Haematoxylin and Eosin (H&E). Haematoxylin is a negatively charged basic stain that is attracted to the acidic phosphate groups of DNA, glycosaminoglycans and carboxyl groups of proteins and is therefore used to stain the nuclei of cells a deep purple at an acidic pH (to facilitate more specific nuclear staining). Conversely, Eosin is of acidic nature and is negatively charged. Thus, it is attracted to the basic, positively charged ammonium groups of proteins within the cytosol and therefore stains the cytosol of cells pink. Degenerated organelles within a cell tend to aggregate into spherical/elliptic structures. Eosin can be used to identify degenerating cells as these structures stain slightly darker and are known as eosinophilic spheroids. Staining of deparaffinised sections (5.3.3.2) from murine tissue was carried out using the protocol outlined in table 5.7.

Table 5.7 ***Protocols for histological staining H&E and PAS.***

H&E	**PAS**
Reagents: Haematoxylin Basic water (NaOH pH 7.8) Acid alcohol (1 % HCl in 70 % ethanol) 0.01 % Eosin / 95 % ethanol/ 0.5 % glacial acetic acid Alcohol dilution series (50 % - 100 %) Rotihistol®	Reagents: 0.05 % periodic acid Schiff's reagent Haematoxylin Basic water (NaOH pH 7.8) Acid Alcohol (1 % HCl in 70 % ethanol) Alcohol dilution series (50 % - 100 %) Rotihistol®
Protocol: • Haematoxylin 5 minutes. • Wash in running water 5 minutes. • Acid alcohol dunk 2-3 times until the sections turn pink. • Tap water rinse 3-5 minutes. • Basic water 5-6 slow dunks; the sections should darken noticeably. • Dehydrate in alcohol: 2 minutes 50 %, 70 %, 96 %. • Dip for 10-20 seconds in alcoholic eosin. • 2 more changes of 95 % ethanol, 100 % ethanol, 5 minutes each. • Clear in Rotihistol® and mount in Eukritt®.	Protocol: • 5 minutes periodic acid. • Rinse in ddH_2O. • Schiff's reagent 30 minutes. • Wash in running water 5 minutes. • Haematoxylin 5 minutes. • Wash in running water 5 minutes. • Acid alcohol dunk 2-3 times until the sections turn pink. • Tap water rinse 3-5 minutes. • Basic water 5-6 slow dunks; the sections should darken noticeably. • Dehydrate in alcohol: 2 minutes each - 50 %, 70 %, 96 %, 100 %. • Clear in Rotihistol® and mount in Eukritt®.

5.3.4.4 Periodic acid-Schiff

Periodic acid-Schiff (PAS) staining is a method to detect glycogen or accumulated carbohydrate-conjugates in tissue. The carbohydrate may be conjugated to a lipid or protein. Periodic acid selectively oxidises glucose/galactose residues to give aldehydes that react with Schiff´s reagent to produce a magenta staining. Increased staining in tissue may indicate metabolic disorders and thus storage of, for example, glycoprotein or glycolipid. Staining of deparaffinised sections (5.3.3.2) from murine tissue was carried out using the protocol outlined in table 5.7.

5.3.4.5 Golgi-Cox staining

A valuable tool in allowing the assessment of morphology within neurons is the Golgi-Cox staining method. Successful impregnation of brain tissue with this method provides a complete picture of neuronal morphology as a result of a metallic mercury deposit within the cytoplasm of neurons. However, for unknown reasons, irrespective of neuronal type, neurons are stained randomly allowing visualisation of individual neurons and their

processes (fig. 5.1). Of the visible neurons, virtually all areas can be seen including the cell body, all or part of the axon, dendrites and even dendritic substructures (spines).

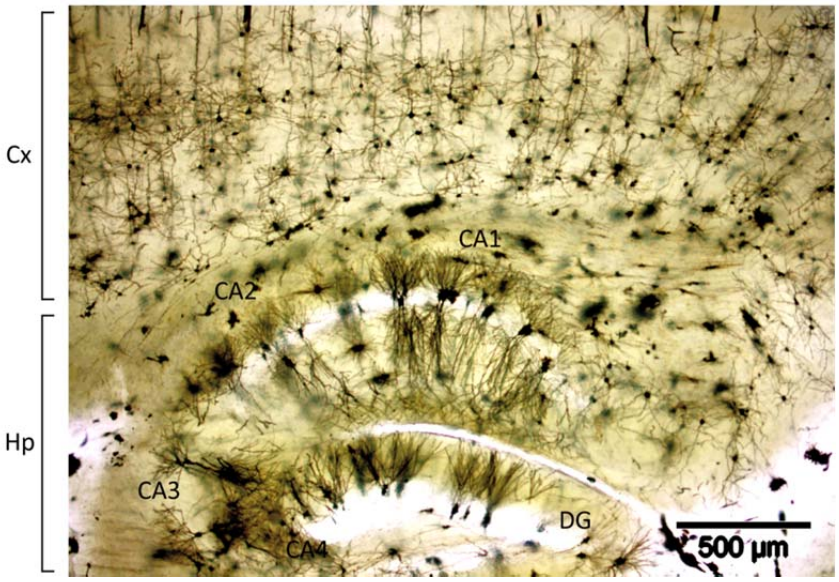

Figure 5.1 ***Golgi-Cox staining of a 240 µm thick sagittal section from murine brain.*** Staining allows morphological analysis of individual neurons in thick (100-240 µm) sections. Only a small percentage of neurons (1-10 %) are stained black using this technique. The cortex (Cx) and hippocampus (Hp) are shown including regions CA1-4 and part of the dentate gyrus (DG).

Golgi-Cox staining was carried out on 6-month-old mice using the FD Rapid GolgiStain™ Kit (FD Neurotechnologies, Columbia, US) according to the manufacturer´s instructions. Briefly, entire brains were excised from sacrificed mice and quickly rinsed in ddH_2O before placing in 5 ml of a 1:1 mixture of solution A:B and stored overnight in the dark. The mixture was replaced the next day and stored for a further 13 days at room temperature in the dark. The tissue was then transferred to a new tube with 5 ml solution C and stored in the dark at 4 °C. Buffer was replaced with fresh solution C the next day. All utensils used in staining were washed repeatedly in ddH_2O before use. Using a vibratome VT1200S (Leica, Wetzlar, DE), 240 µm sections were cut. Slices were transferred to glass slides with the aid of a brush and solution C before drying overnight at room temperature, protected from light. The next day sections were washed twice in ddH_2O before transferring to a mixture of 10 ml solution D, 10 ml solution E and 20 ml ddH_2O. Sections were incubated shaking gently for 10 minutes at room temperature before washing twice in ddH_2O for 5 minutes each. Tissue was then dehydrated in 50 %, 75 % and 95 % ethanol, 4 minutes each step followed by absolute ethanol, 4 times, 4 minutes each. Sample were then cleared in Rotihistol®, 3 times, 4 minutes each, and mounted in Eukitt®.

5.3.4.6 Immunohistology

An invaluable addition to morphological histological changes via histochemistry is the utilisation of antibodies in immunohistology. Indirect immunodetection differs from direct detection based on the use of an enzyme or fluorophore-coupled secondary antibody directed against the constant region (fragment crystallisable, Fc) of the primary antibody. As described in fig. 5.2, a primary antibody binds specifically to an epitope. In order to detect and quantify where the primary antibody has bound, a coupled secondary antibody is used. For amplification and extra sensitivity of the signal detectable from a streptavidin/biotin system may be used (ABC system) (fig. 5.2A). A biotinylated secondary antibody binds specifically to the Fc region of the bound primary antibody. Streptavidin binds to the biotin tag. Every streptavidin binds 3 other biotin molecules, each with a covalently attached enzyme (e.g. horse-radish peroxidase, HRP). Through these means the signal is amplified.

Using a chromogenic substrate a localised stain is produced in order to identify the presence of primary antibody binding. Two such chromogenic substrates are 3,3'-diaminobenzidine (DAB) and Fast-Red. HRP causes the reduction of DAB to an insoluble brown precipitate indicating exactly where antibody has bound. Fast-Red can be used as a chromogen in the presence of alkaline phosphatase enzyme to produce a red reaction product that can be seen using brightfield microscopy. Additionally, a fluorescently labelled secondary antibody may be used for detection of primary antibody bound epitope (fig. 5.2B).

Free floating murine sections from wild-type and knockout sibling pairs or epitope retrieved, rehydrated human paraffin sections were prepared for immunohistology either using DAB or fluorphore labelling. For paraffin sections epitopes were retrieved by boiling in citrate buffer pH 6 for 10 minutes. The sections were allowed to cool for 10 minutes in buffer before immunological staining.

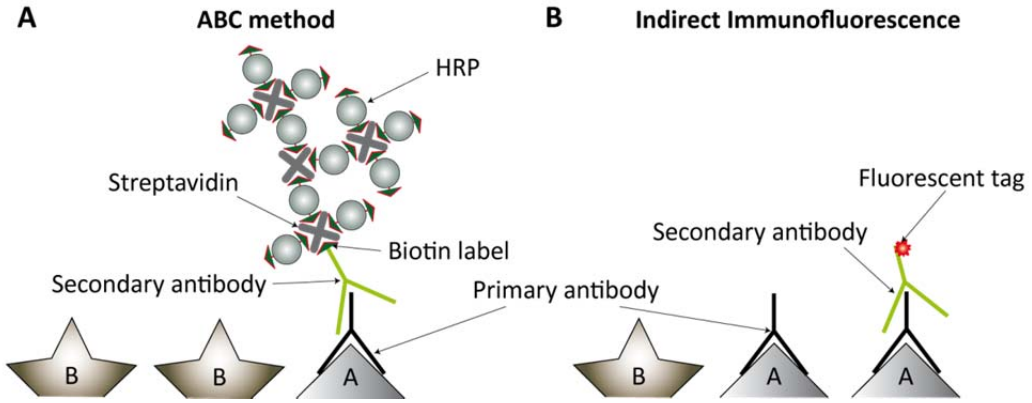

Figure 5.2 ***Immunological staining*****. A-/B-** A primary antibody recognises and binds to its epitope. **A-** The ABC method employs a secondary antibody with a biotin tag. A complex of biotinylated HRP and streptavidin is washed across the sample. To each biotinylated secondary antibody multiple complexes may bind thus amplifying the signal resulting from one bound primary antibody and increasing the sensitivity of the assay. **B-** The presence of bound primary antibody may be indirectly detected using a secondary antibody coupled to a fluorescent tag.

For immunohistochemistry staining endogenous peroxidase activity was stopped by incubating sections in 0.3 % H_2O_2/0.1M PB for 30 minutes. Sections were rinsed in 0.1 M PB and blocked in 0.1 M PB with 4 % normal goat serum, and 0.25 % Triton X-100 for 30 minutes at room temperature. After incubation with the first antibody overnight, sections were rinsed with 0.1 M PB/0.25 % Triton X-100 and incubated with secondary biotinylated antibodies (5.1.6 table 5.5). Sections were washed once with 0.1 M PB/0.25 % Triton X-100 then with 0.1M PB followed by 0.01 M PB and finally in ddH_2O before development using Vector Laboratories ABC kit followed by the elite DAB staining kit according to the manufacturer's instructions (Vector Laboratories, Enzo Life Sciences, Lörrach, DE). DAB sections were dehydrated and prepared for mounting as outlined in section 5.3.5.8 before microscopical analysis using a BX50 microscope (Olympus, Hamburg, DE). Sections for immunofluorescence were mounted in a mixture of 1, 4-diazabicyclo [2, 2, 2] octane (DABCO)/Mowiol (17 % Mowiol, 33 % Glycerol), 50 mg/ml DABCO, 1 µg/ml 4',6-diamidino-2-phenylindole (DAPI) and hardened in the dark at room temperature overnight. Sections were visualised using a confocal laser scanning microscope (CLSM) FV1000 (Olympus, Hamburg, DE).

5.3.4.7 TUNEL of histological sections

DNA fragmentation is associated with apoptotic events in the cell (Kerr et al., 1972). By labelling the ends of DNA fragments with nucleotides attached to a digoxigenin tag, cells

undergoing apoptosis can be identified (Gavrieli et al., 1992). Terminal deoxynucleotidyl Transferase (TdT) is an enzyme used for the transfer of deoxyuridine triphosphate (dUTP) onto the 3' end of a DNA strand. TdT dUTP Nick End Labeling (TUNEL) staining was used to detect the presence of apoptotic cells within brain tissue. This assay involves the addition of digoxigenin conjugated nucleotides to the 3' hydroxly ends of nicked DNA strands. A secondary antibody conjugated to a peroxidase reporter molecule. Using a chromogenic substrate the presence/absence and localisation of apoptosis may be assessed.

Paraffin sections (5.3.3.1) were stained using the ApopTag®Peroxidase *In situ* Apoptosis Detection Kit from Millipore (Schwalbach, DE) according to the manufacturer´s instructions. The entire procedure was carried out at room temperature unless otherwise stated. Briefly, paraffin sections were deparaffinised and rehydrated (5.3.3.2) before digestion in 20 µg/ml proteinase K diluted in PBS for 15 minutes. Endogenous peroxidase was quenched by incubating the sections in 3 % H_2O_2/PBS for 5 minutes. Samples were incubated with equilibration buffer before incubating with the TdT enzyme for an hour at 37 °C. In this step a digoxigenin label was conjugated to the ends of nicked DNA strands. The reaction was terminated with the "stop buffer". Sections were then washed repeatedly in PBS before incubating with an anti-digoxigenin antibody attached to a peroxidase for 30 minutes. The section was then washed in 4 changes of PBS for 2 minutes per wash. Colour development was carried out using the DAB staining kit according to the manufacturer's instructions (Vector Laboratories, Enzo Life Sciences, Lörrach, DE). Sections were dehydrated and prepared for mounting as outlined in section 5.3.5.8 before microscopical analysis using a BX50 microscope (Olympus, Hamburg, DE).

5.3.4.8 Dehydrating and mounting of histological sections

Sections were dehydrated in increasing concentrations of ethanol (5 minutes each; 50 % ethanol, 70 % ethanol, 96 % ethanol, 100 % ethanol). Alcohol was removed via 2 changes of RotiHistol® (Roth, Karlsruhe, DE) for 10 minutes each before mounting in Eukitt® (Sigma Aldrich, Steinheim, DE).

5.3.4.9 Electron microscopy of semi-thin sections

Electron microscopic analysis of spinal cords was carried out in collaboration with Michaela Schweizer, centre for molecular neurobiology, Hamburg, DE. Briefly, sections of spinal cord were embedded in gelatin before cutting 100 µm thick sections with a vibratome (Leica VT 1000S). The sections were rinsed three times in 0.1 M sodium cacodylate buffer (pH7.2–7.4) and osmicated using 1 % osmium tetroxide in cacodylate buffer. Following osmication, the sections were dehydrated using ascending ethyl alcohol concentration steps, followed by two rinses in propylene oxide. Infiltration of the embedding medium was performed by immersing the pieces in a 1:1 mixture of propylene oxide and Epon and finally in neat Epon and hardened at 60 °C. Semi-thin sections (0.5 µm) were prepared for light microscopy mounted on glass slides and stained for 1 minute with 1 % toluidine blue. Ultrathin sections (60 nm) were cut and mounted on copper grids. Sections were stained using uranyl acetate and lead citrate. Thin sections were examined and photographed using an EM902 electron microscope (Zeiss, Jena, DE).

5.3.5 Measurement of DNA/RNA concentration

The nucleic acid concentration was measured on a Synergy HT microplate reader (BioTec, Bad Friedrichshall, DE). Optical density (OD) was measured at a wavelength of 260 nm and 280 nm. OD at 260 nm correlates to the concentration of nucleic acids in solution and OD measured at 280 nm indicates contaminants such as protein or solvents. The ratio of OD 260/280 is therefore used to assess the purity of DNA. A generally accepted ratio for DNA is 1.8 and RNA 2.0.

5.3.6 Agarose gel electrophoresis

DNA and RNA may be separated based on size when run through an agarose gel in TAE buffer (appendix 9.1.5). Ethidium bromide (Roth, Karlsruhe, DE) is a dye that intercalates into nucleic acids and may thus be used to visualise DNA/RNA bands under UV light (312 nm). For all experiments agarose gel with a concentration of 1-1.5 %/ 0.03 % ethidium bromide solution (Roth, Karlsruhe, DE) was used. Desired DNA fragments were cut out of the gel and purified using the plasmid miniprep kit (Fermentas, St-Leon-Rot, DE) according to the manufacturer´s instructions or photographed with the aid of the Gel Jet Imager (Intas, Göttingen, DE).

5.3.7 Polymerase chain reaction

The polymerase chain reaction (PCR) is a method used to amplify a defined sequence of DNA in an exponential manner (Mullis et al., 1986). PCR is based on three steps necessary for correct amplification. Firstly, the double stranded DNA "melts" (becomes single stranded). Secondly, the temperature of the reaction is reduced to approximately 5 °C lower than the melting temperature of the primers (T_m) allowing "annealing" to take place. The T_m of a primer may be calculated based on the purine and pyrimidine content. Finally, "elongation" of DNA is carried out at an optimal temperature for the polymerase used where deoxyribonucleotides (dNTPs) are added 5´to 3´ to the growing DNA chain. These three steps are repeated several times. Each cycle results in double the amount of template. Therefore, a specific sequence of DNA may be amplified in an exponential manner. Usually such a reaction is preceded by a 3-5 minutes at 95 °C to allow complete melting of the template. Additionally, some enzymes require an initial, high temperature (hot-start) in order to become fully active. An extended period of approximately 5 minutes at the elongation temperature is also added at the end to allow complete exhaustion of all dNTPs. PCR reactions were used for amplification of cDNA for use in cloning of specific genes into a vector of choice (section 5.3.11), to assess the integrity of cDNA (section 5.3.9.2), for the quantification of gene expression (section 5.3.9.3) and in the genotyping of animals (section 5.3.10).

5.3.8 Quantitative RT-PCR

5.3.8.1 RNA extraction from tissue samples

The trizol method was used to isolate messenger RNA (mRNA) from whole brain according to the manufacturer's instructions. Briefly, tissue, from -80 °C, was placed directly onto a sterile petri-dish on dry-ice and cut into small pieces using a scalpel before transferring to a 5 ml screw-cap tube with 1 ml Trizol per 70 mg tissue. The sample was homogenised using a Xenox hand-mixer and further dissociated by passing through a 0.6 mm needle. The suspension was then incubated at room temperature for 5 minutes before adding 200 µl chloroform per 1 ml Trizol and shaken vigorously for 15 seconds. Again the mixture was incubated at room temperature for a further 10 minutes and centrifuged at 7,000 g (10,000 rpm) for 10 minutes at 4 °C.

The upper aqueous layer contains solubilised RNA for purification. Nucleospin RNA cleanup (Macherey-Nagel, Düren, DE) kit was used to purify RNA and DeoxyriboNuclease (DNase) treatment to eliminate any contaminating genomic DNA (gDNA) according to the manufacturer´s instructions. In a fresh 2 ml reaction tube 400 µl of the aqueous upper layer and 600 µl of RA1:ethanol mix (i.e. 1200 µl of RA1 + 1200 µl 96-100 % ethanol) from the Nucleospin kit were vortexed briefly. Subsequently, 700 µl of the mixture was pipetted onto a purification column and centrifuged at 8,000 g (11,000 rpm) for 30 seconds. The flow through was discarded and another 700 µl of the mix was pipetted onto the column and centrifuged as before placing in a new collecting tube.

Digestion of gDNA was carried out using 95 µl of DNase solution (10 µl Dnase + 90 µl DNase rnx buffer from the nucleospin RNA II kit). Tubes were incubated for 45 – 60 minutes at room temperature. Columns were then washed in the following order discarding the flow through after each centrifugation step:

- 250 µl of buffer RA2 followed by 1 minute centrifugation at 8,000 g.
- 700 µl of buffer RA3 followed by centrifugation at 8,000 g 1 minutes.
- 350 µl of Buffer RA3 followed by centrifugation at 8,000 g 4 minutes.

RNA was eluted with 60 µl of RiboNuclease free water (from the kit) and centrifuged at 8,000 g for 1 min. Integrity of RNA (messenger (mRNA) and ribosomal (rRNA)) was tested by running 1 µg on a 1 % agarose gel at 140 Volts (V) for 15 minutes. Clear, sharp bands representing the more abundant rRNA should be visible (fig. 5.3).

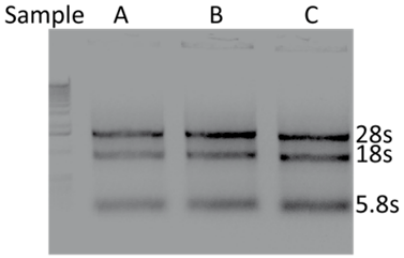

Figure 5.3 ***Intact RNA bands visualised on an agarose gel.*** RNA extractions run on a 1 % Agarose gel for 15 minutes at 140 V. The 28s, 18s and 5.8s rRNA bands are clearly visible for all 3 samples taken from murine brains indicating intact RNA.

5.3.8.2 Reverse transcription

Complementary DNA (cDNA) was synthesised from mRNA using the RevertAid^{TM}First Strand cDNA synthesis (Fermentas, St-Leon-Rot, DE) according to the manufacturer´s instructions. OligoDT primers were used in order to amplify mRNA only via binding to the 3´ poly-A tail. Synthesis of cDNA was carried out as outlined in table 5.8.

Table 5.8 ***cDNA synthesis pipetting and incubation scheme.***

Reagent/Incubation step	**Volume (µl)**
RNA	10.93
Primer (OligoDT)	2
DEPC H_2O	11.07
5 minutes at 70 °C	
5 X reaction buffer	8
RiboLock RNase inhibitor	2
10 mM dNTP	4
5 minutes at 37 °C	
Reverse transcriptase	2
60 minutes at 42 °C	
10 minutes at 70 °C	

A PCR reaction was used in order to assess the integrity of cDNA using GlycerAldehyde 3-phosphate DeHydrogenase (GAPDH) primers (forward: 5-CTG`CAC CAC CAA CTG CTT AG-3`, reverse: 5'-CAG TGA GCT TCC CGT TCA G-3`) (table 5.9). GAPDH is a gene expressed ubiquitously in all tissues. A product of the correct size indicates that the quality of cDNA is of an acceptable level for further analysis.

Table 5.9 ***PCR conditions for assessment of integrity of cDNA using GAPDH primers.***

Master Mix		**Programme**		
Reagent	**Volume (µl)**			
Primer Forward (10 µM)	2	95 °C	5 minutes	
Primer Reverse (10 µM)	2	95 °C	30 sec	x 40
10x Dream Taq Buffer	5	58 °C	30 sec	
Dream Taq 5U	1	72 °C	20 sec	
dNTP (2 mM)	4	72 °C	5 minutes	
DMSO	2.5	10 °C	∞	
cDNA (from 1 µg RNA)	1			
H_2O	32.5	**Amplicon size**: 237 bp		
Total volume	50			

5.3.8.3 Relative quantitative RT-PCR

Quantitative Real-Time PCR (qRT-PCR) is a sensitive technique used to quantify mRNA expression of specific genes. When compared to other methods of gene expression quantification such as northern blots and ribonuclease protection assays qRT-PCR is more sensitive and less labour intensive. A number of different methods of detection of cDNA derived from mRNA are available but all are based on the same principle. That is the measurememnt of DNA amplification in “real time”. These methods include TaqMan® probes, Molecular Beacons, Scorpions® and SyberGreen (SYBR®Green).

The most basic technique involves the use of SYBR®Green, a dye that only fluoresces when it intercalates into double stranded DNA. Primers designed to amplify one specific region within a sequence of cDNA are chosen. At the annealing temperature for each cycle the amount of double stranded DNA may be quantified relative to the signal emitted by SYBR® Green. Based on the amount of template available initially a certain number of cycles are needed before SYBR®Green signal may be detected above background called the threshold level. The number of cycles it takes to reach this value is the threshold value (C_t value). Therefore the amount of template is inversely proportional to the C_t value (fig. 5.4 sample A).

Amplification efficiency of primers may be calculating using a standard curve or may be assumed to be 100 % or 1 and therefore results in a fold increase of 2 with each cycle (Livak and Schmittgen, 2001). Due to the fact that SYBR®Green recognises all double stranded DNA it is important to run a melting curve after each reaction to eliminate the possibility of primer dimers in the reaction. The reaction is heated in a stepwise manner and the melting temperature of the products is measured. One clear peak of change in fluorescence relative to temperature should be visible indicating that all products melted at the same temperature (typically approximately 85 °C) and therefore only one product was amplified. The presence of primer dimers would show up as an extra peak at a lower temperature (approximately 80 °C or lower).

Expression of a house-keeping gene (HKG) such as GAPDH or actin is included for each cDNA sample that allows normalisation of samples. Abundance of gene expression in a test sample can therefore be expressed as a value relative to its level in a control sample using the formula:

$$2^{-\Delta\Delta Ct} = 2 \text{ ^ } -[(Ct_{test} - Ct_{control})_X - (Ct_{test} - Ct_{control})_{HKG}]$$

where X is the gene of interest and HKG is the house-keeping gene (Livak and Schmittgen, 2001).

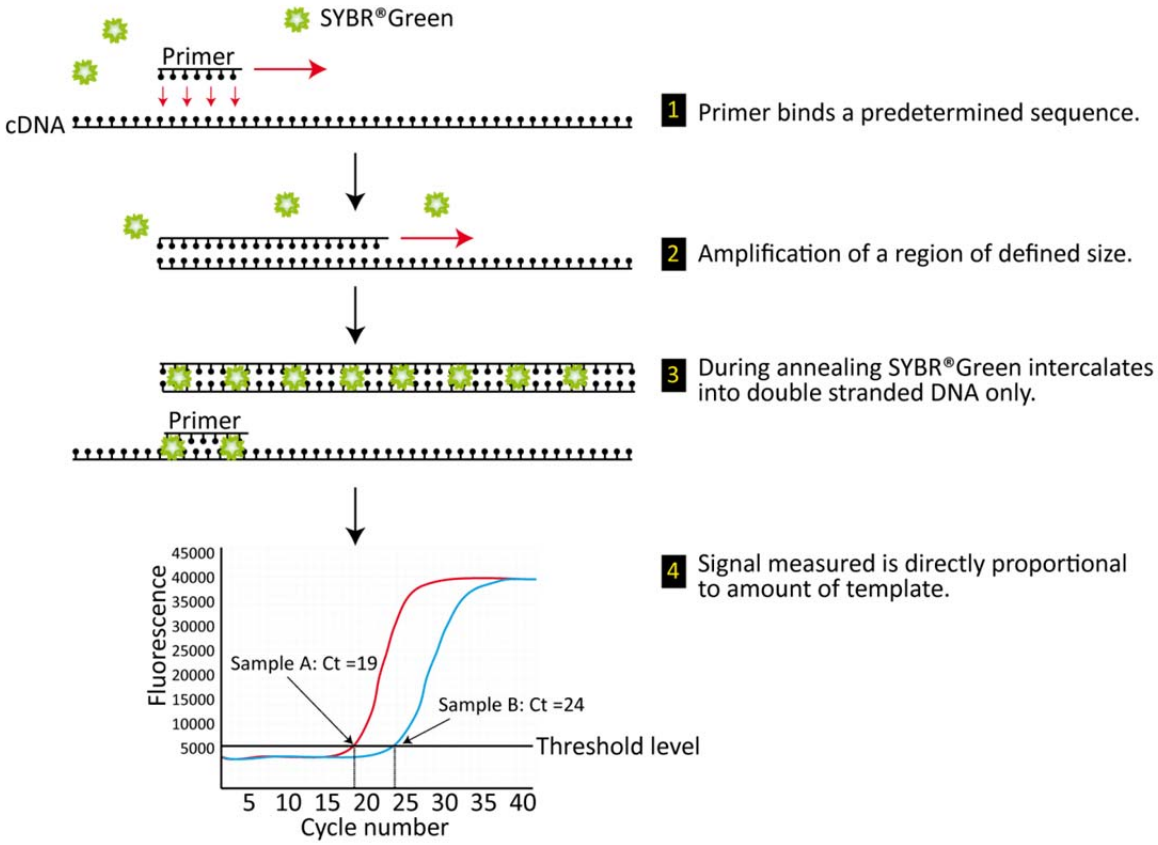

Figure 5.4 ***Overview of qRT-PCR.*** **1-** Primers bind to a specific sequence of DNA. **2-** The target sequence is elongated. **3-** Reduction in temperature results in annealing of double stranded complementary DNA and the intercalation of SYBR®Green. The signal detected is proportional to the amount of double stranded DNA present. **4-** The amount of template is relative to the cycle at which a threshold level of detection is reached (C_t value).

Primers for GAPDH (forward: 5'-CTG CAC CAC CAA CTG CTT AG-3', reverse: 5'-CAG TGA GCT TCC CGT TCA G-3'), LIMP-2 (forward: 5'-ACC TCT TCC CGT CAG ACT TG-3', reverse: 5'-CGT CGG CTT GGT AAA AGT GT-3') and β-GC (forward: 5'-GCT CAA CAT CCT TGC TTT GTC-3', reverse: 5'-CAT CTT CAG GGC TTG GTG A-3') were designed using Primer3 software. Quantitative RT-PCR was performed on a Roche thermocycler 1.5 using SYBR®Green (Takara, Shiga, Japan). The pipetting scheme for the master mix and programme used are outlined in

table 5.10. Relative expression was calculated using the $2^{-\Delta\Delta Ct}$ method (Livak and Schmittgen, 2001).

Table 5.10 ***Master mix and programme for qRT-PCR.***

Master Mix		**Programme**		
Reagent	**Volume (µl)**	94 °C	15 seconds	
Primer Forward (5 µM)	1	94 °C	15 seconds	x 35
Primer Reverse (5 µM)	1	58 °C	30 seconds	
SYBR®Green Master mix	10	72 °C	30 seconds	
H_2O	7			
cDNA	1	Melting curve to 94 °C.		
Total volume	20			

5.3.9 Genotyping

In order to determine whether an animal contained a wild-type allele and/or a knockout allele genotyping was carried out on tissue samples (approximately 0.5 cm tail biopsy) from all mice between 3 and 4 weeks of age. Additionally, mice were regenotyped in order to verify the genotype after sacrificing. Genomic DNA was isolated from tails and embryonic tissue via digestion in Direct PCR-lysis Kit (Peqlab, Erlangen, DE), incubated at 55 °C overnight or for 2 hours respectively. For each sample 200 µl lysis buffer and 2 µl 10 mg/ml proteinase K solution was pipetted onto tissue. Proteinase K was inactivated by heating to 85 °C for 45 minutes. Finally, the mixture was centrifuged at 11,000 g (13,000 rpm) for 5 minutes. Pups and embryos were genotyped using a PCR protocol as described previously (Gamp et al., 2003). Exon/Neo PCR was carried out with exon 8 spanning primers (Cx5, 5'-GGA TAC AGC AGG TGA CAG-3' and Cx3, 5'-ATA GGC TAC GGA CCA CAA-3') or Neo-specific primers (Neo_Kiel_3: 5'-GTT GTTC ACT GAA GCG GGA AGG GAC TGG CTG-3' and Neo_Kiel_4: 5'-GCG AAC AGT TCG GCT GGC GCG AGC CCC TGA-3') (fig. 5.5 and table 5.11). PCR reactions were run on a gel (1 % agarose/TAE buffer) for 30 minutes at 130 V and visualised under UV light with the aid of 0,03 % ethidium bromide.

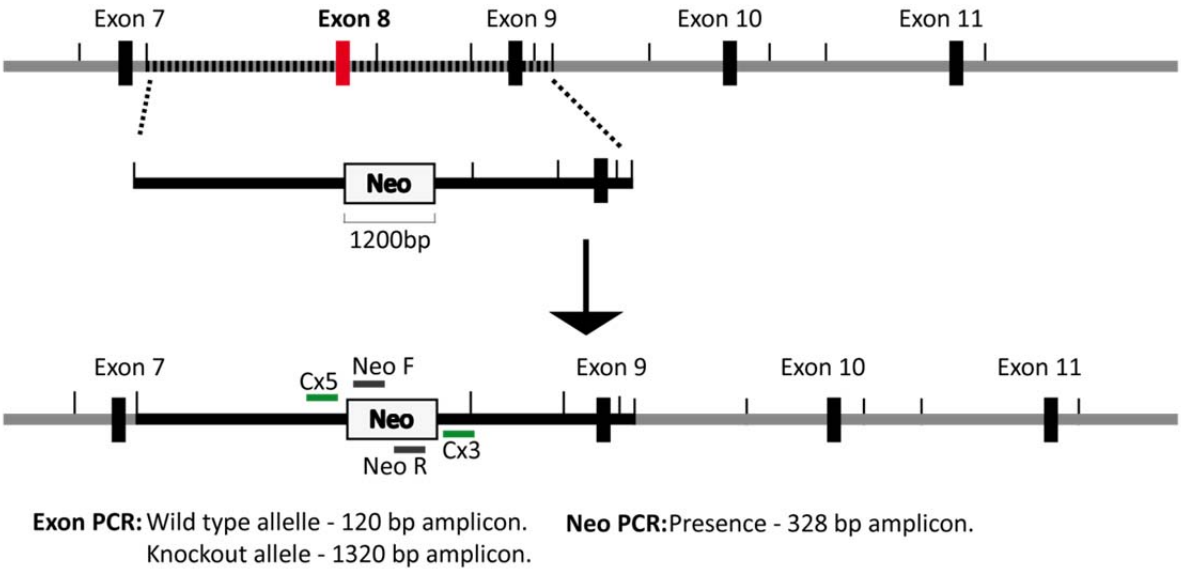

Figure 5.5 ***LIMP-2 gene knockout scheme*****.** Using homologous recombination a neomycin cassette is inserted into a region within the LIMP-2 gene (SCARB2) interrupting transcription at exon 8. Genotyping involves amplification of a sequence within the Neo casette to confirm its presence and amplification of a region around the Neo cassette/exon 8 to discriminate between wild-type and knockout alleles. The fragment amplified in the knockout allele is larger due to the presence of the Neo casette. (Adapted from: Gamp et al., 2003).

Table 5.11 ***PCR mix and programme conditions for LIMP-2 mouse genotyping.***

PCR Mix		**Programme**					
Reagent	**Volume (µl)**	**Neo**			**Exon**		
Primer Forward (10 µM)	2	96 °C	5 minutes		95 °C	5 minutes	
Primer Reverse (10 µM)	2	95 °C	15 seconds		95 °C	30 seconds	
10x Dream Taq Buffer	5	65 °C	30 seconds	x 40	58 °C	30 seconds	x 40
Dream Taq 5U	0.25	72 °C	1 minute		72 °C	2 minutes	
dNTP (10 mM)	1	72 °C	5 minutes		72 °C	5 minutes	
DMSO	2.5	10 °C	∞		10 °C	∞	
Template	3						
H_2O	32.5						
Total volume	50						

5.3.10 Cloning

Human α-synuclein cDNA (SNCA) was purchased from Thermo Fisher Scientific (Rockford, US) and cloned, using HindIII and XhoI restriction sites, into the pcDNA3.1 Hygro$^+$ vector (Invitrogen, Darmstadt, DE). The expression plasmids for SNCA were amplified using primers (forward: 5'-GTC TAA GCT TAT GGA TGT ATT CAT GA-3' and reverse: 5'-GTC TCT CGA GTT AGG CTT CAG GTT CG-3') and cloned into the pcDNA3.1 Hygro $^+$ vector between restriction sites HindIII and XhoI. Similarly, a HA tag (YPYDVPDYA) was added to the C-

terminus of SNCA using the reverse primer. The A53T mutant was created using the one-step quick mutagenesis kit (Stratagene/Agilent Technologies, Böblingen, DE) (primers: 166-SNCA-A53T_mutation_fwd: 5`-GTG GTG CAT GGT GTG ACA ACA GTG GCT GAG-3' and 167-SNCA-A53T_mutation_rev: 5'-CTC AGC CAC TGT TGT CAC ACC ATG CAC CAC-3') according to the manufacturer's instructions. All cloning PCR reactions were carried out using the protocol outlined in table 5.12. Pfu Polymerase (Fermentas, St-Leon-Rot, DE) was used for template amplification due to its inherent exonuclease activity and proof-reading capabilities. The elongation time is dependent on the expected amplicon. For the Pfu polymerase an elongation time of 2 minutes/kbp is recommended. All clones were verified by sequencing at GATC (www.gatc-biotech.com).

Table 5.12 ***PCR conditions for cloning of cDNA.*** X min = 2 minutes/1000 bp DNA.

Master Mix		**Programme**		
Reagent	**Volume (µl)**			
Primer Fwd (10 µM)	2	95 °C	5 minute	
Primer Rev (10 µM)	2	95 °C	30 sec	x 40
10x Pfu Buffer	5	56 °C	30 sec	
Pfu Polymerase 5U	0.5	72 °C	**X min**	
dNTP (2 mM)	4	72 °C	5 minute	
DMSO	2.5	10 °C	∞	
cDNA (from 10 ng RNA)	5			
H_2O	28			
Total volume	50			

The PCR product was then loaded on an agarose gel and run at approximately 120 V for 30 minutes. A clear band of the correct estimated size was then cut out of the gel using a scalpel and purified using the High Pure PCR product purification kit (Roche, Basel, CH) according to the manufacturer's conditions.

The purified PCR product and the vector were incubated with the appropriate restriction enzymes overnight and for 2 hours respectively. The vector was dephosphorylated via treatment with FastAP (Fermentas, St-Leon-Rot, DE) to prevent religation of the vector. The digested PCR product and fully treated vector were then again purified after running on a 1 % agarose gel as before. Both products were eluted in 40 µl autoclaved H_2O. Vector and PCR product were ligated using the T4 ligase (Fermentas, St-Leon-Rot, DE) overnight at 17 °C

as outlined in table 5.13. The ligase was deactivated by incubating it at 65 °C for 15 minutes before transfection (5.3.12).

Table 5.13 ***Ligation pipetting scheme.***

Reagent	Ligation (µl)	Control (µl)
PCR product	7	-
H_2O	-	7
Vector	1	1
T4 ligase buffer	1	1
T4 ligase	1	1
Total Volume	10	10

5.3.11 Amplification and purification of expression plasmids in Escherichia coli

For *in vitro* amplification of ligated plasmids from cloning or retransformation of established expression plasmids the bacterial strain XL1-Blue *Escherichia coli* (*E. coli*) was utilised (Bullock et al, 1987). Electrocompetent *E. coli* were thawed on ice. The bacteria were pipetted with 1 µl of the ligation mixture (table 5.13) or 1 µl plasmid stock into a cold electroporation cuvette followed by electroporation at 2.5 kV, 400 Ω and 25 µF in a Gene pulser (Biorad, Hercules, US). The electroporated cells were then incubated in 1 ml warm LB only for 30 minutes at 37 °C. Finally, ligation reactions were centrifuged for 1 minute at 5,000 rpm, 800 µl of the supernatant was discarded and the pellet resuspended before plating, with a sterile hockey-stick, onto LB-Agar plates with the appropriate antibiotic resistance (i.e 50 µg/ml ampicillin or 30 µg/mg kanamycin). Single positive clones were picked with a sterile toothpick and incubated in 3 ml of LB medium with the appropriate antibiotic resistance overnight at 37 °C. Plasmids were isolated from the expanded culture using the miniprep kit (Fermentas, St-Leon-Rot, DE) according to the manufacturer´s instructions. Retransformation reactions were added to 100 ml LB media with the appropriate antibiotic concentration. Plates/flasks were incubated overnight at 37 °C. Large quantities of plasmids were isolated for with the pure yield midi plasmid kit (Promega, Mannheim, DE).

5.4 Protein Biochemistry

5.4.1 Lysis of cells/tissue lysates

All preparations of protein lysates were carried out on ice to reduce protein degradation in conjunction with a cocktail of protease inhibitors (Complete^{TM}, Roche, Basel, CH). Cell pellets were lysed in Tris buffer (50 mM Tris-NaOH, 150 mM NaCl, 2 mM EDTA + complete^{TM} + 1 % Triton-X 100, 2 mM $MgCl_2$, pH 7.4), sonicated 2 x 15 seconds, placed for 30 minutes on ice then sonicated again 2 x 15 seconds. Lysates were then centrifuged at 11,000 g (13,000 rpm) for 15 minutes. The supernatant was used for protein concentration quantification, preparation of lysates for separation on a gel and β-GC enzyme activity assays.

5.4.2 Sequential detergent fractionation of mouse brain

In order to distinguish between soluble and insoluble aggregated protein within lysates from tissue samples a two buffer system was used. The triton-X-100 and Sodium-Dodecyl-Sulfate (SDS) fraction correspond to soluble and insoluble portions, respectively.

Sequential extraction of soluble and insoluble fractions was carried out as described previously (Mazzulli et al., 2006). Briefly, brains were lysed in 10 volumes of triton buffer (1 % triton x-100, 20 mM HEPES, 150 mM NaCl, 10 % glycerol, 1 mM $MgCl_2$, 50 mM NaF, 2 mM $NaVO_3$, protease inhibitors – pH 7.4). Lysates were then subjected to 4 freeze thaw cycles and ultracentrifuged (Optima^{TM} TLX ultracentrifuge, Beckman) at 100,000 g for 30 minutes. The two supernatants were pooled as the triton soluble fraction. The pellet was extracted as before in another 10 volumes of lysis buffer. The remaining pellet was extracted with 5 volumes of SDS buffer (2 % SDS, 50 mM Tris-HCl-pH7.4), boiled for 10 minutes, sonicated 4 times with 3 seconds pulses, at 50 % power, boiled for another 10 minutes and centrifuged at 20,000 g for 30 minutes. The supernatant is the SDS (insoluble) fraction.

5.4.3 Quantification of protein

Protein was quantified using a BCA kit (Thermo Fisher Scientific, Rockford, US) according to the manufacturer´s instructions. This method uses the reduction of Cu^{2+} to Cu^{+} by the chelation ability of peptides containing 3 or more amino acids. The generated Cu^{+} ion forms a coloured complex with the bicinchoninic acid (BCA) reagent. Absorbance can be measured

at 562 nm. The intensity of the blue complex is proportional to the amount of protein in the sample.

Lysates were diluted appropriately (generally 1:10 for lysed cell pellets and 1:100 for tissue lysates). Ten microlitres of standard or lysates was used for each reaction in a 96-well plate and 200 µl of a mixture from solutions A and B (50:1) and incubated at 37 °C for 20-30 minutes before measuring at 562 nm in a Synergy HT microplate reader (BioTec, Bad Friedrichshall, DE).

5.4.4 SDS-PAGE

Proteins were separated using a discontinuous SDS-polyacrylamide gel electrophoresis (SDS-PAGE) based on size (Laemmli, 1970). SDS is an anionic detergent that denatures proteins and binds to the polypeptide chain thereby exerting an evenly distributed charge. Protein samples are then heated to allow further denaturing of the protein and intercalation of SDS before loading on an acrylamide gel. Samples are pulled through the gel via the application of voltage across the gel. Thus the negatively charged SDS loaded polypeptides run towards the anode with smaller proteins running faster than larger ones. Depending on the separation of proteins desired (i.e. 10 % for greater separation of larger proteins, 12.5 % for more distinct bands of lower molecular weight) gels were prepared using components outlined in table 5.14.

Samples (20-30 µg), in 1 X Laemmli buffer with a reducing agent (100 mM DTT), were heated to 60 °C for 20 minutes. A standard marker (Fermentas, St-Leon-Rot, DE) was used for estimation of molecular mass. A voltage of 80 V was applied for the stacking gel and 100-140 V for the separating gel for the appropriate time (approximately 120 minutes).

Table 5.14 ***SDS-gel.***

Component	10 %	12,5 %	Stacking Gel (4,5 %)
Stacking gel buffer	-	-	1.35 ml
Separation gel buffer	2.6 ml	2.6 ml	-
Polyacryamide (30 %)	3.3 ml	4.2 ml	1.75 ml
ddH_2O	4.0 ml	3.1 ml	6.85 ml
10 % APS	60 µl	60 µl	60 µl
TEMED	30 µl	30 µl	30 µl
Total Volume	10 ml	10 ml	10 ml

5.4.5 Western Blotting

After electrophoresis of proteins the gel was prepared for transfer/"blotting" onto a membrane. Using the same SDS charged principle as in SDS-PAGE proteins were transferred onto a nitrocellulose membrane (Roth, Karlsruhe, DE) using current in tank-blot-transfer buffer in a chamber from Criterion™-System (BioRad, Munich, DE). Fig. 5.6A illustrates assembly of a gel and membrane in a tank blot holder. Membranes were blotted for 2 hours at 20 V on ice.

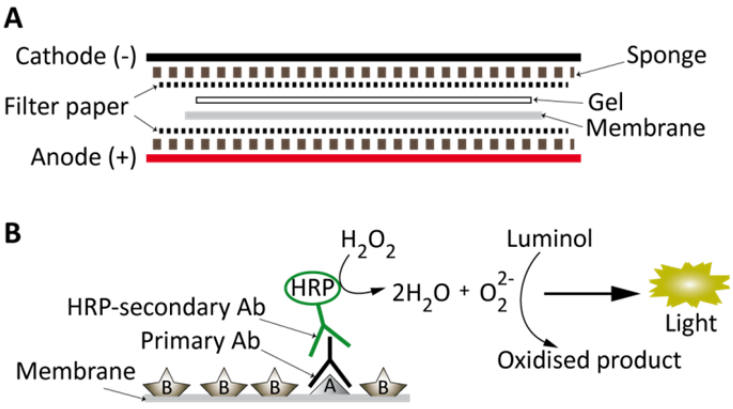

Figure 5.6 ***Western blotting principle.***
A- A Western blot is assembled as illustrated. Negatively loaded proteins are drawn to the anode after the application of voltage across the chamber. **B-** Sequential binding of the primary followed by HRP-labeled secondary antibodies allows identification of specific epitopes exposed on the membrane. Through HRP activity water and reactive oxygen are released from hydrogen peroxide. Light is then released through oxidation of luminol via reactive oxygen. (Ab, antibody).

5.4.5.1 Immunological detection

To prevent non-specific binding of antibodies, the membrane is "blocked" using a high concentration of proteins in solution washed over the surface in the form of 5 % milk solution. Primary antibodies recognise and bind specifically to epitopes exposed on the membrane. A secondary antibody against the constant chain (Fc-region) of the primary antibody is then used. The secondary antibody is coupled to a substance that will allow its

detection e.g. HRP. HRP uses H_2O_2 in the oxidation of luminol to give a chemiluminescent signal (fig. 5.6B).

Target proteins were detected using the relevant antibodies (5.1.6 table 5.4) incubated overnight at 4 °C in blocking solution consisting of 5 % milk powder dissolved in Tris-buffered saline/0.01 % Tween (TBS/T). After washing for 30 minutes in 3 changes of TBS/T and 1 hour in the secondary antibody (5.1.6 table 5.5) blots were imaged on a LAS4000-chemiluminescence detector (GE Healthcare, Munich, DE). Densitometric analyses were performed with ImageJ software (http://rsbweb.nih.gov/ij/) by dividing signal intensities of the appropriate band through signal intensities of the actin loading control.

5.4.5.2 Stripping of Western blots

In some cases it may be necessary to detect multiple proteins on a membrane. For this purpose the membrane was stripped of bound antibodies using a mixture of detergent and reducing agent (appendix 9.1.5) at 70 °C for 30 minutes – 1 hour. The membrane was subsequently washed 5 x 10 minutes in TBS/T. Consequently the membrane was blocked before exposing to new primary antibodies as in section 5.1.6.

5.4.6 Enzyme Activity Assays

Using a synthetic substrate, through a colour change reaction the activity of an enzyme (e. g. hydrolase) may be determined. 4-Nitrophenyl-conjugated to a specific sugar depending on the enzyme to be assayed is used as a synthetic substrate. Activity of the enzyme leads to hydrolytic cleavage of the carbohydrate group at acidic pH. Under basic conditions the enzyme is no longer active and cleaved p-nitrophenol becomes fully deprotonated and turns yellow allowing absorbance measurements at 405 nm (fig. 5.7).

Enzyme assays were performed in duplicates in 1.5 ml eppendorf cups. β-Glucocerebrosidase, β-hexosaminidase and α-mannosidase enzyme activity was measured using 10 mM 4-Nitrophenyl β-D-glucopyranoside, 10 mM p-nitrophenyl-a-D-mannopyranoside and 10 mM p-nitrophenyl-N-acetyl-ß-D-glucosaminide, respectively. Substrates were dissolved in citrate buffer (0.2 M Na-Citrate, 0.4 % BSA, pH 4.6). Approximately 10 µl (10 µg/µl protein) of brain/ cell lysates were incubated at 37 °C in 100 µl

solubilised substrate or citrate buffer only. All samples were carried out in duplicate. After 15 minutes-1 hour (for β-hexosaminidase), 2 hours (for β-glucocerebrosidase) or 5 hours (for α-mannosidase), 600-1000 µl glycine buffer (0.4 M, pH 10.4) was added. Samples were centrifuged for 5 minutes at full speed before pipetting 161 µl of the supernatant (corresponding to a path-length of 1 cm) onto a 96 well plate. Extinctions were measured at a wavelength of 405 nm on a Synergy HT microplate reader (BioTec, Bad Friedrichshall, DE). Absolute activities were calculated using the formula:

$$Activity\ \left[\frac{U}{mg}\right] = \left(\frac{\Delta E \times V_{end}}{t \times \varepsilon \times d \times V_{lysate}}\right) \div c_{lysate}$$

where U is the unit of enzyme activity µmol/minute, ΔE is the change in absorbance at 405 nm, V_{end} is the final volume in the reaction vessel, V_{lysate} is the volume of lysate used, d is the path length, t is time in minutes, ε is the molar absorption coefficient for p-nitrophenolate (18.5) and c_{lysate} is the concentration of the lysate.

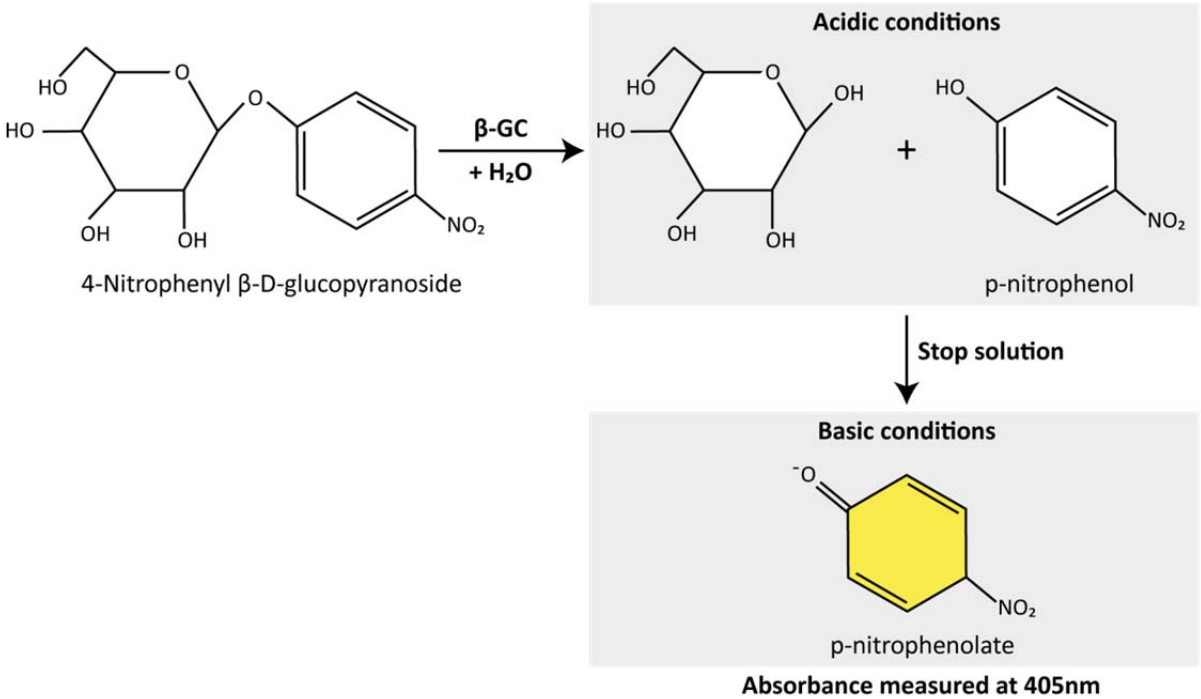

Figure 5.7 ***Basis of enzyme assay for* β-*glucocerebrosidase.*** 4-nitrophenyl, conjugated to a glucose ring, is used as a synthetic substrate for β-glucocerebrosidase (β-GC). Hydrolysis of the substrate under acidic conditions leads to cleavage of the sugar moiety leaving p-nitrophenol. Addition of a basic "stop solution" prevents further activity of the enzyme and results in isomerisation of p-nitrophenol into p-nitrophenolate whose presence can be detected at 405 nm.

5.5 β-Glucocerebrosidase specific enzyme activity assay

Cell lysates (approximately 30 µg/µl protein in 30 µl) were treated for 30 minutes at 37 °C with 100 nM Conduritol-B-Epoxide (CBE). Control samples were treated with PBS only. Lysates were then subjected to an enzyme activity assay using approximately 10 µl of the appropriate sample and 100 µl of the substrate 10 mM 4-nitrophenyl β-D-glucopyranoside. Absolute activity was calculated as described in 5.4.6. β-GC specific activity was calculated using the formula:

Specific Activity = ($Activity$ without treatment) - ($Activity$ CBE treated).

5.6 Cell biology

All work associated with primary cell culture and cell lines was performed under sterile conditions. All media components for general cell culture were purchased from PAA, Pasching, AU and all media components for primary cell culture from Invitrogen, Darmstadt, DE. A comprehensive list of media components can be found in the appendix 9.1.

5.6.1 Primary cell culture

Primary cells are cells taken directly from living tissue for growth *in vitro*. These cells more closely resemble the *in vivo* state of the tissue from which they are derived when compared to cancer or immortalised cell lines which have undergone several mitotic cycles. However, some cell types, such as post-mitotic neurons, are particularly sensitive and require specialised handling and media in order to allow their growth *in vitro.* Other cells such as astrocytes and microglia can be relatively easily isolated and cultured without difficulty.

5.6.1.1 Preparation and maintenance of primary neuronal culture

Primary cortical and mesencephalic neurons were prepared as described previously (Dobrenis et al., 2005) from the cortices and mesencephalons of gestational day 15.5 embryos from sacrificed terminally mated females (5.1.5).

On the day of embryo brain isolation, coverslips and plastic cell culture dishes were coated with 200 µg/ml sterile poly-D-lysine (Sigma Aldrich, Steinheim, DE) dissolved in ddH_2O for 4 hours at 37 °C and subsequently washed 5 times with sterile ddH_2O before drying

overnight under a sterile hood. Dissection buffer without sucrose was used for isolation of embryonic brain on day 1 and dissection buffer with sucrose was used only after removal of meninges on day 2 (table 5.15).

Table 5.15 ***Dissection buffer with or without sucrose.*** Ab/Am = Antibiotics/Antimycotics

Reagent	End concentration
NaCl	138 mM
KCl	5.4 mM
Na_2HPO_4	0.17 mM
KH_2PO_4	0.22 mM
D-glucose	5.5 mM
Ab/Am (100x) (Invitrogen, Darmstadt, DE)	1 mM
Gentamicin (50 mg/ml) (Invitrogen, Darmstadt, DE)	25 µg/ml
*Sucrose (19.99 g in 1L)	58 mM

pH 7.3 - 7.35 at room temperature.

For the preparation of primary neurons a female mouse was sacrificed using a CO_2 chamber followed by cervical dislocation at the neck. All buffers used throughout the preparation were maintained on ice. The uterus, containing embryos, was surgically removed and immediately placed in cold dissection buffer (table 5.15). The embryo/uterus "string" was briefly dipped in 70 % ethanol and immediately placed in ice-cold 20-30 ml dissection buffer. Subsequently, the uterus was transferred to a sterile hood where each embryo, still within its amniotic sac, was removed from the uterus and placed in a 6 cm dish with isolation buffer on ice. Each embryo was then transferred to a fresh individual 6 cm dish where the amniotic sac and umbilical cord were removed. The embryo was then washed 4-5 times in buffer, each time changing the forceps and buffer. Finally, the head was removed and placed in a fresh 6 cm plate with approximately 500 µl buffer. Tissue was removed from the remaining embryo for genotyping (section 5.3.10).

Using 2 forceps, the skin and skull were removed thereby exposing the brain with the aid of a CX41 microscope (Olympus, Hamburg, DE). The embryonal brain was then transferred to a 50 ml falcon tube with 15-20 ml "hibernating media" (table 5.16) and placed, with the cap tightly sealed, on its side in the dark overnight at 4 °C.

Table 5.16 ***Hibernating media.*** (300ml)

Reagent	Volume
Hibernate E	150 ml
B27	6 ml
L-15 media	60 ml
CO_2 independent media	90 ml

The next day "hibernating media" was decanted off. Wild-type brains were pooled in a 6 cm plate with ice-cold dissection buffer (with sucrose) as were knockout samples. Heterozygote or undefined samples were discarded. Each brain was sagittally divided (fig. 5.8A). The olfactory bulb was used as an orientation point. Mesencephalon (midbrain), diencephalon and telencephalon (cortex) (fig. 5.8B) were separated before removal of meninges (fig. 5.8C). Brains were cut into small pieces using forceps and transferred with dissection buffer to a 50 ml conical tube and allowed to settle for 1 minute. The supernatant containing dissociated cells was transferred to a new 50 ml tube with one quarter volume of fetal bovine serum (FBS) (Invitrogen, Darmstadt, DE) on ice.

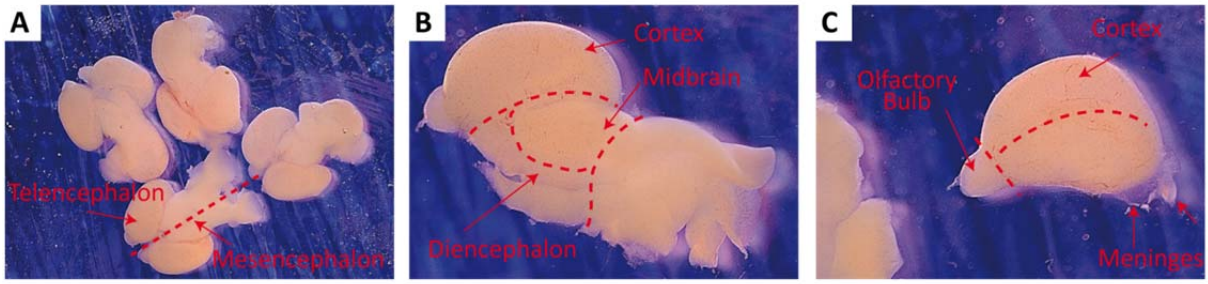

Figure 5.8 ***Brain dissection.*** **A-** Isolated brains were divided rostral to caudal. **B-** The midbrain (mesencephalon) and diencephalon were then removed from the cortical shell (telencephalon). **C-** Finally, the olfactory bulb was separated. Cortices were then transferred to fresh buffer before removal of the meninges.

Table 5.17 ***Dissociation buffer.***

Reagent	Volume/concentration
DNase Buffer	50 ml
Trypsin	0.05 %

pH 7.3 - 7.35 on ice.

Table 5.18 ***DNase buffer.***

Reagent	Volume/concentration
Isolation Buffer	100 ml
$MgSO_4$	6mM
DNase	0.05 %

pH 7.3 - 7.35 on ice.

Prewarmed dissociation buffer (table 5.17) (0.5 ml per brain, minimum of 3 ml) was added to the cell pellet and swirled/tapped gently for 30 seconds before transferring to the 37 °C shaking waterbath for 3 minutes. Half the volume of FBS was then added before titurating, slowly, 5 times with a clean 1 ml pipette without the addition of air bubbles. The cell suspension was allowed to settle and the supernatant pooled with the cells on ice. 1 ml of DNase buffer (table 5.18) was added to the cell pellet, titurated 7 times and allowed to settle for 1 minute. The supernatant was pooled with the cells on ice. The pooled cell suspension was now kept at room temperature. DNase buffer treatment was repeated twice. The tube was then flicked several times before adding 1 ml DNase buffer and titurating 7 times. The supernatant was added to the pooled cells.

Cell suspensions were then centrifuged at 210 g in a table top centrifuge (Universal 32, Typ 1605, Hettich, Tuttlingen, DE) for 11 minutes at room temperature before resuspension in fresh isolation buffer (1 ml per cortex/midbrain). Viable cells were counted using a C-chip™ heamocytometer (PAA, Pasching, AU) and trypan blue (Invitrogen, Darmstadt, DE) to identify dead cells. That is 100 µl of cell suspension was added to 20 µl of trypan blue and 80 µl of isolation buffer. The number of cells counted in each large box is multiplied by 10,000 cells/cm^3, and by the dilution factor used.

Table 5.19 ***Plating media*** (100 ml)

Reagent	Volume
$C_3H_3NaO_3$ (22 g/ml)	500 µl
B27	2 ml
Glucose (6 g/ml)	2 ml
Glutamax (100x)	3 ml
FBS	10 ml
Gentamicin (50 mg/ml)	50 µl
Ab/Am (100x)	250 µl

Fill to 100 ml with DMEM/F12.

Table 5.20 ***Pure *N media*** (100 ml)

Reagent	Volume
B27	2 ml
Glucose (6 g/ml)	1 ml
Glutamax (100x)	1 ml
Gentamicin (50 mg/ml)	25 µl
Ab/Am (100x)	250 µl

Fill to 100 ml with neurobasal.

*N, neuronal media.

Table 5.21 ***Mixed *N media*** (100 ml)

Reagent	Volume
B27	2 ml
Glucose (6 g/ml)	1 ml
Glutamax (100x)	1 ml
Gentamicin (50 mg/ml)	25 µl
Ab/Am (100x)	250 µl
FBS	10 ml

Fill to 100 ml with neurobasal.

*N, neuronal media.

Note: All media components were purchased from Invitrogen, Darmstadt, DE.

Samples were centrifuged again at 210 g and resuspended in the appropriate volume of "plating media" (table 5.19) before seeding at a concentration of 2 X 10^6 cells per 6 cm plate. Plates and coverslips were pre-coated with poly-D-lysine. Cells were grown at 37 °C, 95 % humidity and 5 % CO_2. After 1 day half the media was replaced with "pure neuronal media" (table 5.20) or "mixed neuronal media" (table 5.21). It is essential that the neurons are never exposed to air.

For the culturing of pure neuronal cultures it was necessary to prevent the overgrowth of mitotic cells (glial cells and some contaminating fibroblasts). Therefore, after 3 days *in vitro* half of the conditioned media was harvested, cleared of debris via centrifugation and stored in the fridge. To prevent the growth of mitotic cells cytosine arabinoside (Fluka, Buchs, CH) was added to cultures, with an end concentration of 10 µM, overnight. The next day half the media was changed three times. Each time a mixture of 1:1 conditioned:fresh media was used. Half the media was changed every 3 days.

For mixed neuronal cultures half the media was changed every 3 days for the first 2 weeks and every two days or when the media was yellow thereafter.
Neuronal cultures at 7-21 days in vitro (DIV) and mixed cultures from 14-24 DIV were used for immunofluorescence, Bodipy®493/503 staining and Western blots as indicated.

5.6.1.2 Preparation and maintenance of primary mixed glial culture

Single cell suspensions were achieved using the same method as used for neuronal cultures after hibernation. Cells were seeded at a density of 2 x 10^6 cells per 6 cm dish. Mixed glial cultures were grown for 14 days on coverslips and plastic cell culture dished in DMEM-high glucose with 10 % FBS and antibiotics at 37 °C, 95 % humidity and 5 % CO_2. Fresh media was added at 1 DIV. Half the media was changed every 3-4 days. Glial cells were harvested at 28 DIV.

5.6.2 Passaging of cells

In order to plate out cell lines for overexpression experiments, confluent cells were washed twice with sterile PBS. Proteins responsible for the adherence of cells and their metabolic cofactors were cleaved/chelated using a solution of trypsin/EDTA solution. The mixture was

added to washed cells (1 ml per 10 cm dish or 500 µl per 6 cm dish) and incubated for 5-10 minutes at 37 °C. DMEM-high glucose with 10 % FCS and antibiotics (complete media) was used to stop trypsinisation. Resuspended cells were split appropriately before seeding on plastic culture dishes and grown at 37 °C, 95 % humidity and 5 % CO_2.

5.6.3 Transient and stable transfection of cells

HeLa, MEFs or SHSY-5Y cells (5.1.1) were transfected with Turbofect (Fermentas, St. Leon-Rot, DE) for transient and stable transfection of cells according to the manufacturer's instructions. Transiently transfected cells were harvested 48 hours later in ice-cold PBS/complete. The pcDNA3.1 hygro$^+$ vector (5.1.3) was used for stable transfection of LIMP-2 MEF cells. Two days after transfection, 100 ug/ml hygromycin (PAA, Pasching, AU) was added to the media. Every second day the concentration was raised by 100 ug/ml until all cells in the control (non-transfected) plate were dead or a maximum of 500 ug/ml hygromycin was reached. Cells were maintained thereafter at the maximum concentration. Following positive results for stable expression of the protein of interest, confluent plates were split 1:100. After 5-7 days individual colonies were scraped using a sterile pipette tip and transferred for culturing to a fresh dish.

5.6.4 Cryopreservation and thawing of cell lines

Due to the potential of cell lines to undergo genetic drift in continuous culture and the necessity to maintain a bacteria free sample of stably transfected cells of a low passage number, cells may be cryopreserved in liquid nitrogen. Adherent cells are trypsinised (5.6.2) and resuspensed in complete medium in the presence of a cryoprotective agent such as dimethylsulfoxide (DMSO). Cryoprotective agents reduce the freezing point of the medium and slow the rate at which samples are cooled thereby greatly reducing the risk of ice crystal formation, which can damage or kill cells.

Trypsinised cells from a 10 cm plate with approximately 80 % confluency were resuspended in complete media, centrifuged at 200 g for 5 minutes in a tabletop centrifuge (Universal 32, Typ 1605, Hettich, Tuttlingen, DE). The supernatant was discarded and the pellet resuspended in 1 ml complete media and cooled for 10 minutes on ice. Subsequently 1 ml of ice cold freezing media (20 % dimethylsulfoxide + complete media) was added to the cell

suspension which was mixed gently and quickly divided into aliquots in cryotubes. Frozen tubes were then stored at -80 °C overnight before long-term storage in liquid nitrogen.

To thaw out samples, frozen ampules were removed from the liquid nitrogen tank and opened briefly under the sterile hood. The cryotube was closed and thawed shortly in a 37 °C water bath until only a small amount of frozen cells remains in the tube. The cell suspension was quickly transferred to 5 ml of complete media and centrifuged at 200 g for 5 minutes. The pellet was resuspended in fresh complete media and seeded on a 10 cm plate for culturing at 37 °C, 95 % humidity and 5 % CO_2. The next day cells were briefly washed with PBS and fed with fresh complete media.

5.6.5 Harvesting of cells

Cells were harvested on ice in PBS in a cocktail of protease inhibitors (Complete™, Roche, Basel, CH). Cells were washed twice with PBS and scraped using a policeman's rubber with 1ml $PBS_{complete}$. Samples were then pelleted at 1,700g (5000 rpm) for 10 minutes. Pellets were further processed for enzyme assays/SDS-PAGE or frozen at -20 °C until use.

5.6.6 Substrate reduction of cultured cells

The synthesis of glycosphingolipids may be inhibited within the cell using N-butyldeoxynojirimycin (miglustat) an inhibitor of glucosylceramide synthase (Platt et al., 1994). Sterile miglustat (Tocris, Bristol, UK) was diluted in DMEM at a concentration of 1 mM. Aliquots were frozen at -20 °C until use. A final concentration of 10 µM was added once to the media of cells 4 hours post transfection. Neurons were treated every other day after 4 days in culture with a final concentration of 10 µm for 10 days.

5.6.7 Indirect immunofluorescence and Bodipy®493/503 staining

In order to assess the expression and localisation of certain proteins within the cell antibodies directed against specific cellular compartments or cell types may be utilized. A similar indirect system to that used for immunohistology is employed (section 5.3.5.6 fig. 5.2B). For immunofluorescence, mixed glia, mixed neuronal cultures, Bodipy®493/503 treated cells were quickly washed once with PBS before fixation for 20 minutes in 4 % PFA/PBS solution at room temperature and permeabilisation for 5 minutes in 0.2 %

saponin/PBS (washing solution). This was followed by masking of aldehyde groups with 0.12 % glycine washing buffer for 10 minutes. Cells were then blocked with 10 % FCS in 0.2 % saponin/PBS (blocking solution). The primary antibody (5.1.6), diluted in blocking solution, was pipetted onto parafilm in a dark, wet chamber and the coverslip with fixed cells placed top-down. After at least 2 hours incubation at room temperature each coverslip was dipped 5 times in washing solution before application of the appropriate secondary antibody (5.1.6) for 1 hour at room temperature. Finally, coverslips were again dipped initially in washing solution and then once in water before mounting in mowiol containing 4', 6-diamidino-2-phenylindole (DAPI) to stain nuclei and 1,4-Diazobicyclo[2.2.2]octane (Dabco) (Sigma Aldrich, Steinheim, DE) as an antifading agent (DAPI/Mowiol/Dabco) and hardened overnight in the dark.

Due to the unavailability of a working antibody for the detection of glucosylceramide in cells an indirect method of staining general lipids was employed. Bodipy®493/503 is a lipophilic dye previously used to quantify accumulation of glucosylceramide in neurons (Mazzulli et al., 2011). A stock solution of Bodipy®493/503 (Invitrogen, Darmstadt, DE), diluted in ethanol, was prepared and stored at -20 °C until use. At day 14 DIV live neurons were incubated with Bodipy®493/503 to a final concentration of 10 µg/ml in neuronal culture media @ 37 °C/5 % CO_2 for 30 minutes, washed 5 times in PBS and fixed for 20 minutes in 4 % PFA and finally washed 3 times in PBS before embedding in DAPI/Mowiol/Dabco. Cells were visualised using a confocal laser scanning microscope (CLSM) FV1000 (Olympus, Hamburg, DE).

5.6.8 Computer software

Table 5.22 ***Software used for data analysis.***

Programme	Supplier
Adobe Illustrator	Adobe Systems Inc., San Jose, US
Adobe Photoshop	Adobe Systems Inc., San Jose, US
DNASTAR Lasergene 8	Lasergene, Madison, US
EndNoteX4	Thomson Reuters, Carlsbad, CA, US
Fluo View 1000 ASW 3.0	Olympus, Hamburg, DE
Image J	http://rsbweb.nih.gov/ij/
MS-Office	Microsoft Corporation, Redmond, US
CellA	Olympus, Hamburg, DE
GraphPad	Graphpad Incorporated, LaJolla CA, US

5.6.9 Statistical analysis

For the identification of statistically significant differences between knockout and wild-type samples or treated and untreated samples p-values were determined via a two-tailed, unpaired Student *t* test using Microsoft Excel software. In order to determine a significant difference between more than two groups a one-way ANalysis Of VAriance (ANOVA) followed by Student-Newman-Keul's multiple comparison test were calculated using GraphPad software (Graphpad Incorporated). Samples were considered significantly different when $p < 0.05$.

6 Results

Deafness, ataxia, slight hyperactivity but no cognitive decline have been reported in LIMP-2-deficient mice that were maintained in a mixed genetic background (SVJ129_C57BL/6J Harlan) (Berkovic et al., 2008). The recent discovery that accumulation of glucosylceramide (GluCer), the substrate of β-glucocerebrosidase (β-GC), directly influences the accumulation and aggregation of α-synuclein necessitated a more thorough analysis of the central nervous system (CNS) of LIMP-2-deficient mice for signs of neuropathology and more specifically synucleinopathy. However, chromosomal deletion of the α-synuclein locus was reported for the C57BL/6J strain from Harlan (Specht and Schoepfer, 2001) used for backcrossing in previous reports of phenotypes in LIMP-2-deficient mice. Therefore, mice were backcrossed into the wild-type C56BL/6N strain from Charles River. All animals were genotyped according to the protocol outlined in methods 5.3.9 and were backcrossed at least 3 times before behavioural, histological or biochemical analysis.

6.1 LIMP-2 deficiency leads to abnormal behaviour and reduced weight

Mice lacking LIMP-2 expression bred in the C56BL/6N background show a severe phenotype. LIMP-2 deficient mice were significantly smaller than their wild-type littermates (fig. 6.1A) and failed to thrive beyond 4 months of age (fig. 6.1B). Furthermore, when suspended from the tail for approximately 30 seconds over a flat surface wild-type mice display a splayed appearance (fig. 6.1C left panel). In contrast, LIMP-2 deficiency led to hind-limb clasping (fig. 6.1C middle panel), a general indication of central nervous system dysfunction, with onset at 3-5 months (table 6.1), which progressed to partial paralysis (fig. 6.1C right panel) in approximately 59 % of mice at 10 months. Additionally, mice lacking LIMP-2 presented with progressive kyphosis (fig. 6.1D lower panel and table 6.1) and ataxia (table 6.1) as previously reported (Gamp et al., 2003).

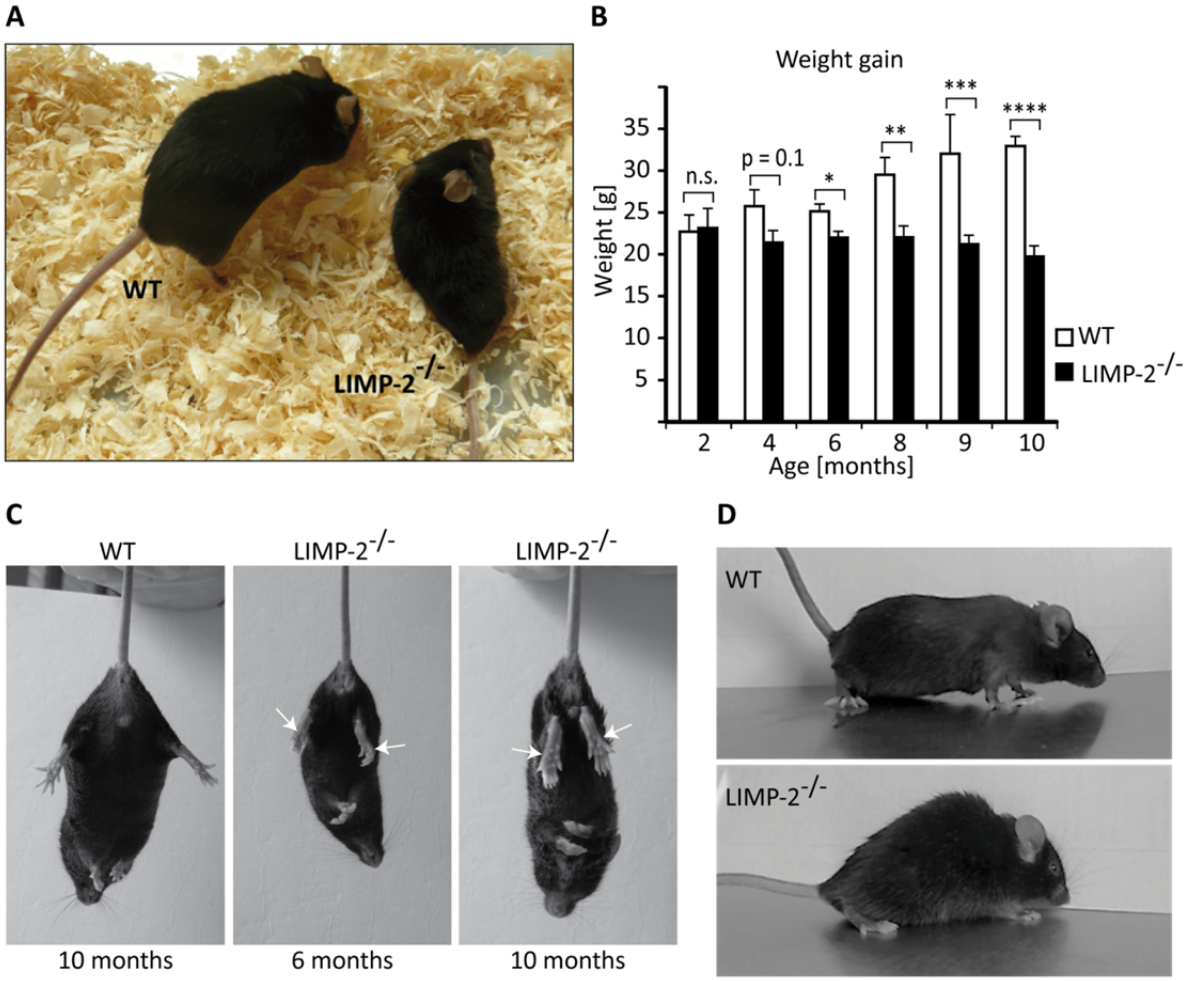

Figure 6.1 ***Macroscopical anomalies in LIMP-2-deficient mice.*** **A-** LIMP-2 knockout mice (LIMP-$2^{-/-}$) are smaller than their wild-type (WT) littermates. Mice depicted are 10-month-old males. **B-** LIMP-2-deficient mice fail to gain weight beyond 4 months of age when compared to their WT littermates. (Data are given as means ± SE and are considered not significant (n.s.) when $p > 0.05$, * $p = 0.03$, ** $p = 0.02$, *** $p = 0.002$, **** $p = 0.0001$, $n \geq 3$ for each genotype per age category). **C-** Hind-limbs of WT mice are splayed when suspended by the tail whereas LIMP-$2^{-/-}$ mice exhibit hind-limb clasping (middle panel, arrows) which progresses to partial paralysis of the hind-limbs at 10 months (right panel, arrows). **D-** LIMP-$2^{-/-}$ mice exhibit kyphosis. Mice depicted are 10-month-old males.

Lack of LIMP-2 expression as seen in AMRF patients (Berkovic et al., 2008) causes, among other symptoms, action myoclonus (Badhwar et al., 2004). Interestingly, in LIMP-2-deficient mice myoclonic jerking (data not shown) and tremor where observed at rest, which increased in prevalence in older mice (table 6.1). Increased mortality was observed from 9 months of age and knockout mice did not survive beyond 10 months (data not shown). In addition to previously reported phenotypes in LIMP-2 knockout mice, reduction in size and symptoms indicative of neurological impairment could be observed when LIMP-2 is absent.

Table 6.1 ***Behavioural analysis of wild-type (WT) and LIMP-2-deficient (LIMP-2$^{-/-}$) mice.*** Incidence of hind-limb clasping (HLC), ataxia, kyphosis and tremor. N value corresponds to number of mice.

Symptom	Age (months)	Genotype	Incidence (%)	n =	Symptom	Age (months)	Genotype	Incidence (%)	n =
HLC	3-5	WT	0	6	***Ataxia***	3-5	WT	0	6
	7	WT	0	6		7	WT	0	6
	10	WT	0	10		10	WT	0	10
	3-5	LIMP-2$^{-/-}$	33	9		3-5	LIMP-2$^{-/-}$	56	9
	7	LIMP-2$^{-/-}$	44	8		7	LIMP-2$^{-/-}$	67	8
	10	LIMP-2$^{-/-}$	41	17		10	LIMP-2$^{-/-}$	65	17
Kyphosis	3-5	WT	0	6	***Tremor***	3-5	WT	0	6
	7	WT	0	6		7	WT	0	6
	10	WT	0	10		10	WT	0	10
	3-5	LIMP-2$^{-/-}$	38	9		3-5	LIMP-2$^{-/-}$	0	9
	7	LIMP-2$^{-/-}$	67	8		7	LIMP-2$^{-/-}$	56	8
	10	LIMP-2$^{-/-}$	88	17		10	LIMP-2$^{-/-}$	82	17

6.2 Neuropathological symptoms due to loss of LIMP-2 expression

To determine the cause of behavioural symptoms, brain sections from 6- and 10-month-old littermates were analysed for signs of neuroinflammation, brain lesions, regional degeneration and alterations in the expression of lysosomal markers.

6.2.1 Astrogliosis and neuroinflammation

Glial cells often become reactive in response to CNS insult (Kreutzberg, 1996; O'Callaghan and Jensen, 1992). Extensive astrogliosis (fig. 6.2B) and microgliosis (fig. 6.2D) was observed in LIMP-2-deficient brain using immunohistochemisty of free-floating sections (methods 5.3.5.6) from 6-month-old LIMP-2 knockout brains using Glial Fibrillary Acid Protein (GFAP) and the activated macrophage specific antibody *Cluster of Differentiation* 68 (CD68) as markers for astrogliosis and microgliosis, respectively (Holness and Simmons, 1993). Reactive astrogliosis may be identified through an increase in GFAP positive glial cells as well as cellular morphological changes (review: Sofroniew, 2009). Activated astrocytes have larger soma and star shaped appearance with an increased number of extending processes (fig. 6.2B') when compared to non-activated glia (fig. 6.2A').

Astrogliosis was quite widespread, affecting all regions of the CNS with the exception of the molecular layer of the cerebellum and the outer layer of the cortex. Extensive microgliosis was observed throughout the CNS of LIMP-2-deficient mice and was particularly acute within

myelinated regions including the corpus callosum, anterior commissure and white matter of the cerebellum (fig. 6.2C/D and C'/D'). Additionally, significant CD68 immunostaining was detected in the fornix and pons. Microgliosis, although not as pronounced as within heavily myelinated regions, was also prominent within other regions affected in Parkinson´s disease, specifically the midbrain, including the substantia nigra, of LIMP-2-deficient mice (fig. 6.2B). Similar results were obtained for 10-month-old mice with more severe microgliosis detected in white matter (data not shown). Histological analysis suggests that deficiency in LIMP-2 causes severe astrogliosis and microgliosis in mice.

6.2.2 Upregulation of lysosomal proteins in LIMP-2-deficient murine brain

In cases where a lysosomal protein is impaired as well as in neurodegenerative diseases such as Parkinson´s disease changes in lysosomal protein expression is often observed (reviews: Butler et al., 2006; Parente et al., 2012). In fact, immunohistochemical analysis of the CNS of LIMP-2-deficient mice revealed a marked increase in cathepsin D expression (fig. 6.3A) but no change in its maturation in the lysosome (fig. 6.3B). Elevated levels of cathepsin D were mainly in microglial cells as indicated by colocalisation with the microglial marker CD68 in immunohistological sections from LIMP-2-deficient mice (fig. 6.3C). Similarly, a slight increase in the steady-state level of LAMP-1 in LIMP-2-deficient whole brain lysates could be observed via Western blot (fig. 6.4C) which was particularly obvious in myelinated regions visualised via immunohistochemistry (fig. 6.4A). Interestingly, whereas no increase in LAMP-2 could be detected in an immunoblot of whole brain lysates (6.4D), a region specific increase was detected via immunohistochemistry (fig. 6.4B).

Increased expression of all three lysosomal proteins was particularly noticeable in myelinated regions including the corpus callosum, white matter tracts of the cerebellum and the anterior commissure (data not shown) in LIMP-2-deficient brain which can probably be attributed to increased numbers of activated microglial cells. In fact, using double immunofluorescence of histological sections, elevated expression of LAMP-1 and LAMP-2 colocalised in the same cell type as cathepsin D (data not shown). Therefore, LIMP-2 deficiency leads to an increase in lysosomal protein expression within the CNS of mice that is particularly concentrated in myelinated regions.

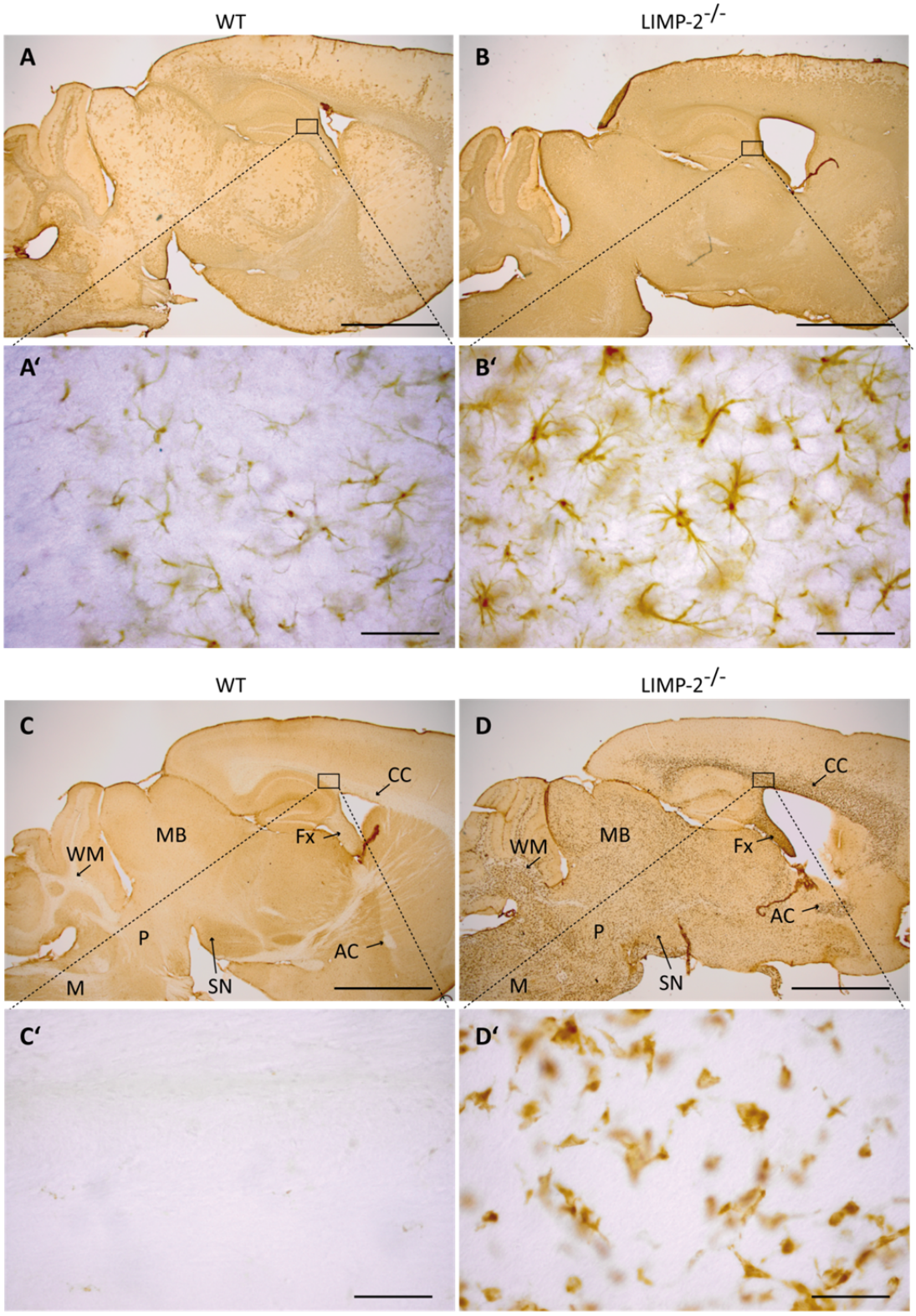

Figure 6.2 ***Gliosis in LIMP-2-deficient brain.*** Representative immunohistochemically stained sections of 6-month-old wild-type (WT) and LIMP-2 knockout (LIMP-$2^{-/-}$) littermates (n= 3 per genotype). **A/B-** Astrogliosis (GFAP) and **C/D-** microgliosis (CD68) was observed in the brains of LIMP-$2^{-/-}$ mice but not in WT littermate controls. (Scale bar = 2 mm; CC, corpus callosum; WM, white matter; AC, anterior commissure; Fx, fornix; MB, midbrain; SN, substantia nigra; P, pons; M, medulla). **A'/B'-** Higher magnification image of CA3 region stained for GFAP showing significant morphological changes in astrocytes (scale bar = 50 µm). **C'/D'-** Higher magnification image of corpus callosum stained for CD68 revealing dramatic increase in microglial population numbers when LIMP-2 is deficient.

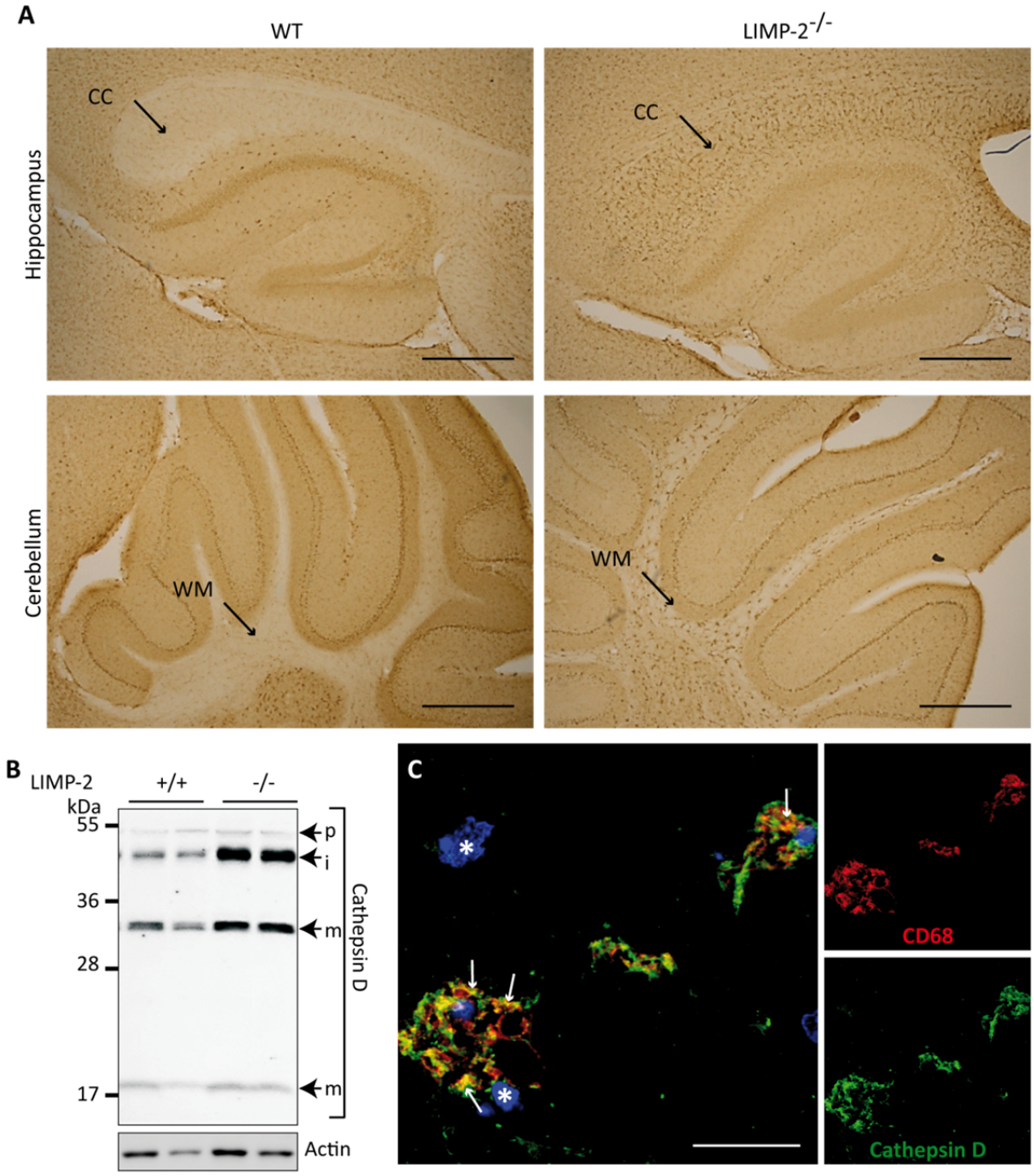

Figure 6.3 ***Elevation of cathepsin D in LIMP-2-deficient brain.*** **A-** Representative immunohistological sections of 6-month-old wild-type (WT) and LIMP-2 knockout (LIMP-$2^{-/-}$) littermates. Cathepsin D immunostaining shows a significant increase in detectable protein in LIMP-$2^{-/-}$ mice when compared to WT littermate controls. (Arrows indicate white matter regions; CC, corpus callosum; WM, white matter of the cerebellum; n = 3 per genotype; scale bar = 500 µm). **B -** Western blot analysis comparing wild-type (+/+) and LIMP-2 knockout (-/-) whole brain lysates show an increase in detectable cathepsin D but no change in its maturation in LIMP-$2^{-/-}$ samples (p, pro-form; i, immature form; m, mature form). **C-** Double immunofluorescence labelling of sections from LIMP-2-deficient mice with cathepsin D (green) and the microglial marker CD68. Colocalisation (arrows) indicates that cathepsin D levels are mainly elevated in microglia. (Image is from the white matter of the cerebellum of a 10-month-old LIMP-2-deficient mouse; scale bar = 10 µm; asterisks indicate non-microglial cells).

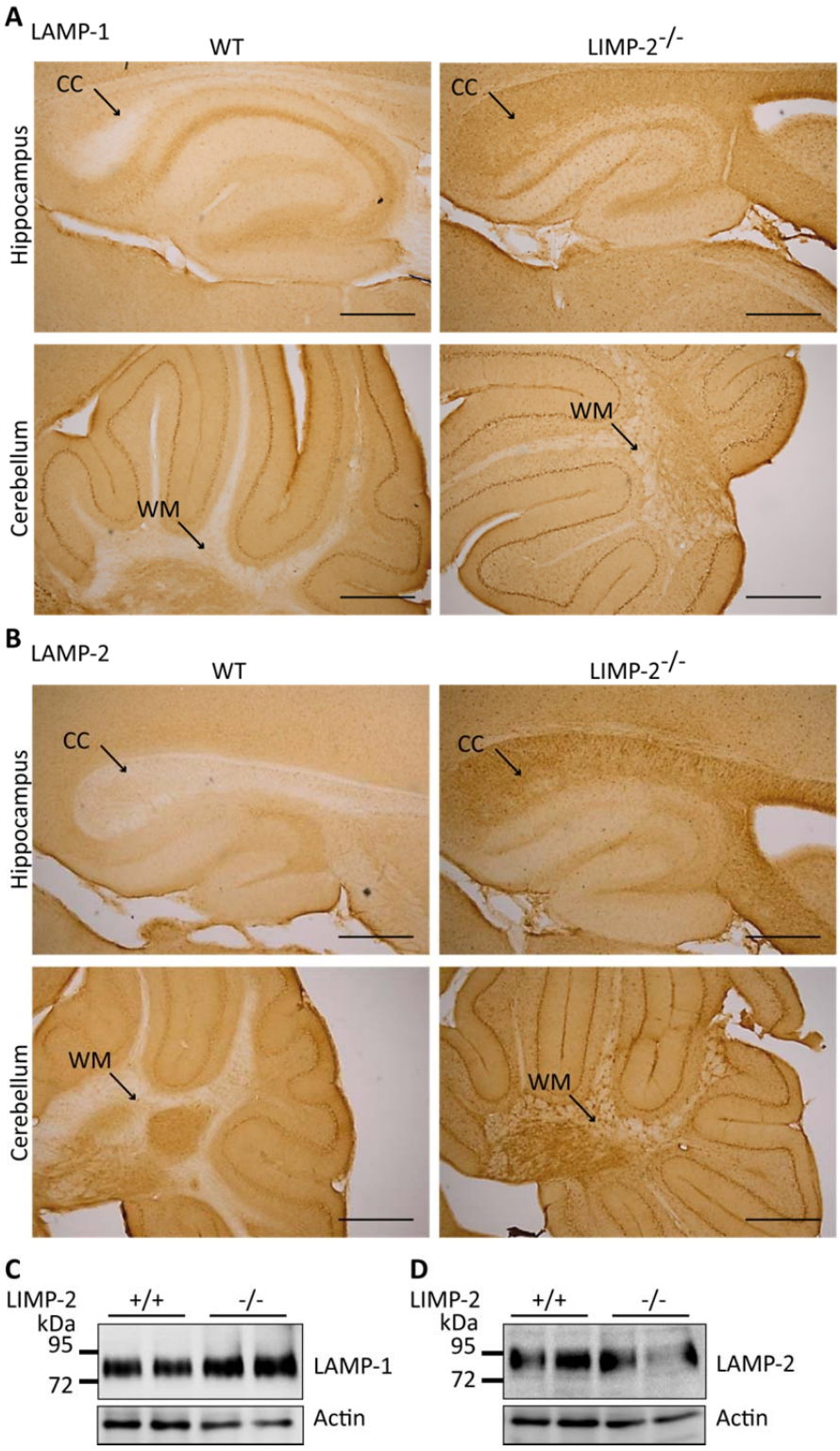

Figure 6.4 ***Upregulation of lysosomal membrane proteins in LIMP-2-deficient brain.*** Representative immunohistological sections of 6-month-old wild-type (WT) and LIMP-2 knockout (LIMP-2$^{-/-}$) littermates. (Arrows indicate white matter regions; CC, corpus callosum; WM, white matter of the cerebellum; n = 3 per genotype; scale bar = 500 µm). **A-** Immunostaining for LAMP-1 revealed increased protein particularly in the corpus callosum and white matter tracts of LIMP-2$^{-/-}$ brain. **B-** Similarly, increased LAMP-2 expression was evident in LIMP-2$^{-/-}$ brain. **C-** Western blot analysis of whole brain lysates shows a slight increase in LAMP-1 levels in LIMP-2-deficient (-/-) mice when compared to wild-type (+/+). **D-** No differences in LAMP-2 levels were observed in lysates from wild-type and LIMP-2-deficient mice.

6.2.3 Loss of LIMP-2 does not cause demyelination within the CNS

Due to excessive neuroinflammation indicated by microgliosis observed within myelinated regions of the brain and previous reports of peripheral nerve demyelination in LIMP-2-deficient mice (Gamp et al., 2003) the presence of irregularities in CNS myelination was assessed. Immunohistochemistry, using myelin basic protein (MBP), revealed no differences in myelination between wild-type and knockout brains (fig. 6.5A-D). Furthermore luxol fast blue (methods 5.3.5.2), a dye attracted to myelin's high lipid content, showed no aberrations in the corpus callosum or white matter tracts of the cerebellum when LIMP-2 was absent (fig. 6.5E-H). Therefore, it appears that no obvious demyelination defects within the CNS are caused by deficiency in LIMP-2.

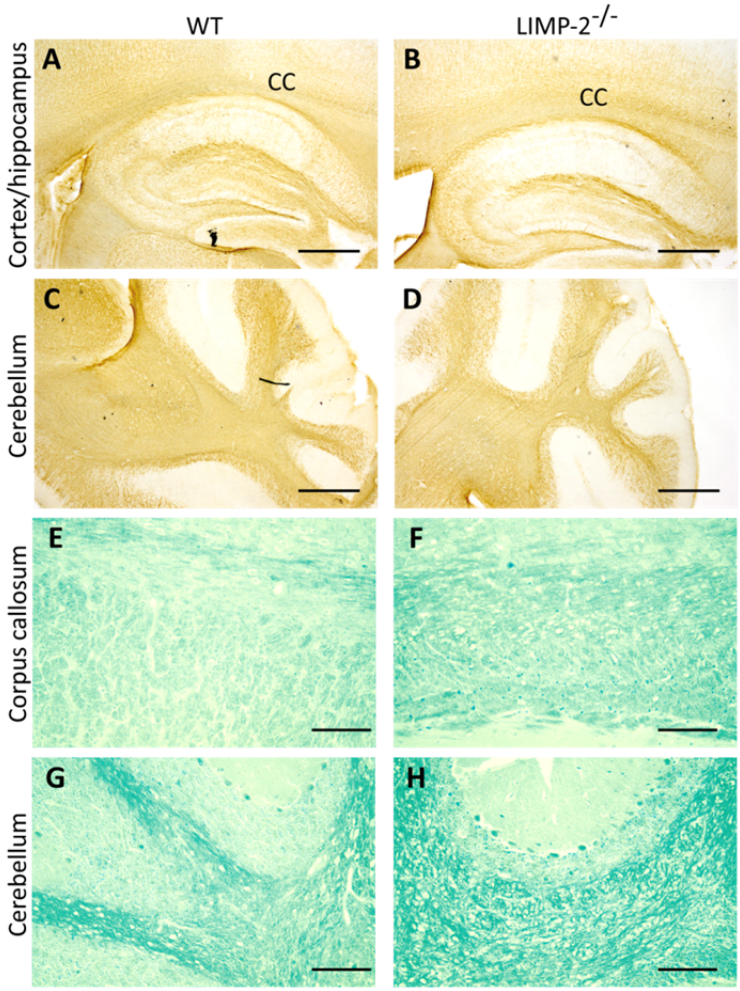

Figure 6.5 ***No difference in CNS myelination when LIMP-2 is absent.*** **A to H-** Representative histological sections of 6-month-old wild-type (WT) and LIMP-2 knockout (LIMP-$2^{-/-}$) littermates (n ≥ 2 per genotype; CC, corpus callosum; scale bars **A-D** = 500 µm, **E-H** = 100 µm). **A/B-** Immunohistological staining of free floating sections using the myelin marker MBP reveals no discernable differences in myelination of the corpus callosum or **C/D-** the white matter of the cerebellum in LIMP-$2^{-/-}$ mice. **E/F-** Similarly, no deficiencies in myelination were detected in the corpus callosum or **G/H-** white matter of the cerebellum in LIMP-$2^{-/-}$ brain paraffin sections stained with luxol fast blue.

6.2.4 Morphological changes in LIMP-2-deficient brain

The overall effect of astrogliosis and microgliosis on the general morphology of LIMP-2-deficient brain was assessed using hematoxylin and eosin (H&E) staining of paraffin sections (methods 5.3.5.3). Eosinophilic spheroids (fig. 6.6B/B') and cellular shrinkage (fig. 6.6B/D), which is suggestive of dystrophic axons and cellular injury, were visible in brain sections from LIMP-2-deficient mice in the cortex and the substantia nigra (fig. 6.6) but not in wild-type littermates.

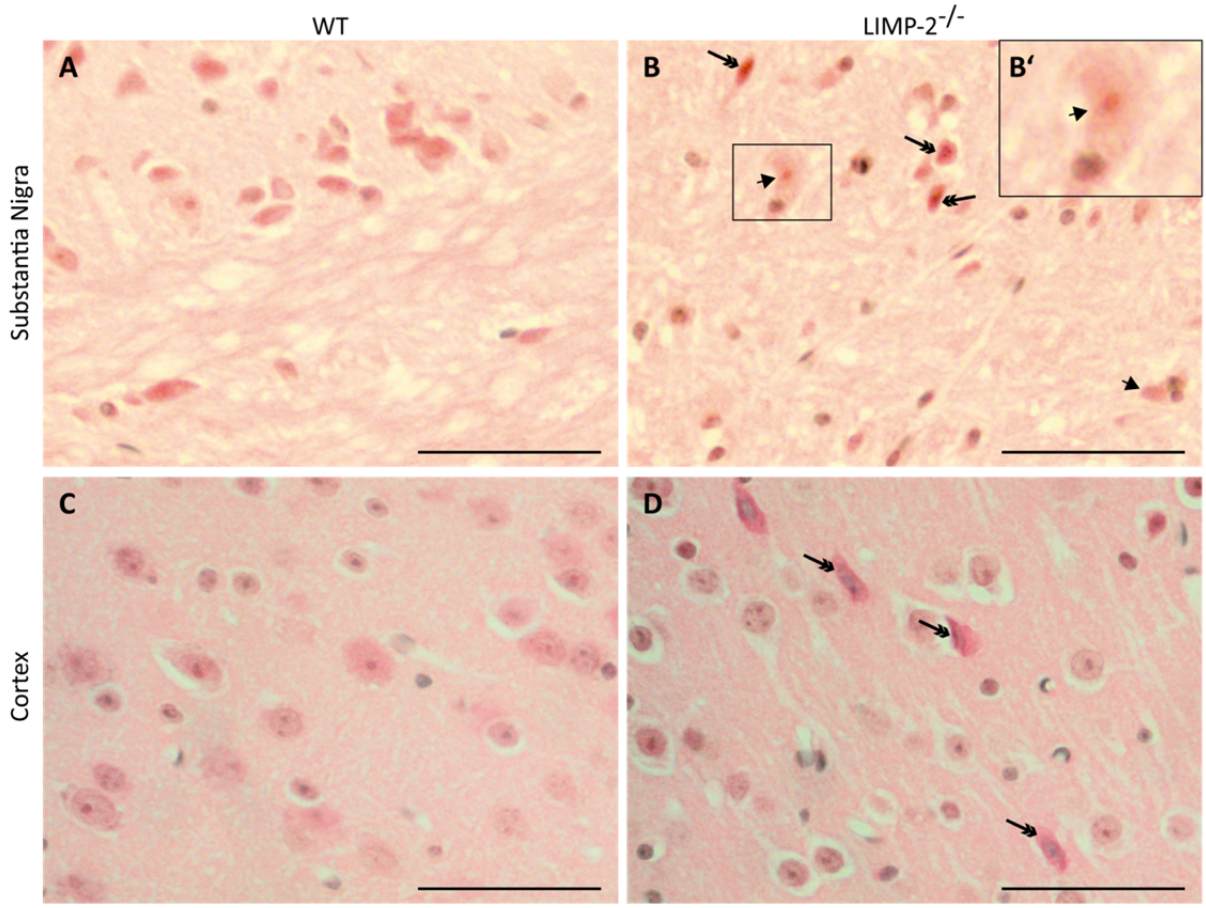

Figure 6.6 ***H&E staining reveals cellular shrinkage and eosinophilic spheroids in LIMP-2-deficient brain.*** Representative histological sections of 6-month-old wild-type (WT) and LIMP-2 knockout (LIMP-2$^{-/-}$) littermates. **A/B-** Cellular shrinkage (double arrows) is observed within the substantia nigra and **C/D-** the cortex. **B-** Additionally, eosinophilic spheroids (arrows) can be observed within the substantia nigra (n = 2 per genotype; scale bar = 500 µm). **B'**- Digitally zoomed image of an eosinophilic spheroid from the region outlined in B.

6.2.5 General alterations in neuronal populations due to LIMP-2 deficiency

The presence of astrogliosis and neuroinflammation throughout several regions of LIMP-2-deficient brain and morphological disparities within the CNS necessitated the evaluation of abnormalities in neuronal populations, which may coincide with gliosis and cellular injury. Thus, to assess whether neuronal loss occurs in LIMP-2-deficient brain, immunostaining using the neuronal marker NeuN (Neuronal Nuclei transcription factor) (Mullen et al., 1992) was carried out. No apparent difference in neuronal density was observed in the cortex or cerebellum (fig. 6.7A-D). Additionally, while no obvious alterations in the density of neurons within the striatum could be detected, the striatal region appeared to be reduced in area. Potential dystrophy was highlighted by an excessively large diameter of the lateral ventricle in LIMP-2 knockout brains (fig. 6.7E/F). However, quantification of striatal area in 10-month-old wild-type and LIMP-2 knockout littermates revealed no significant differences (data not shown).

Interestingly, a loss of approximately 25 % in NeuN positive neurons within the Cornu Ammonis 2 (CA2) and CA3 accompanied by a decrease in neurons within the CA4 region of the hippocampus was evident (fig. 6.8A/B). Similarly, a dye used to identify neuronal populations via staining of the Nissl bodies within the soma with cresyl violet (methods 5.3.5.1) revealed a clear reduction in pyramidal neurons within the CA2, CA3 and CA4 regions of the hippocampus (fig. 6.8C/D). Potential dystrophy of neurons within the CA2-4 regions of the hippocampus was evident in LIMP-2-deficient murine brain.

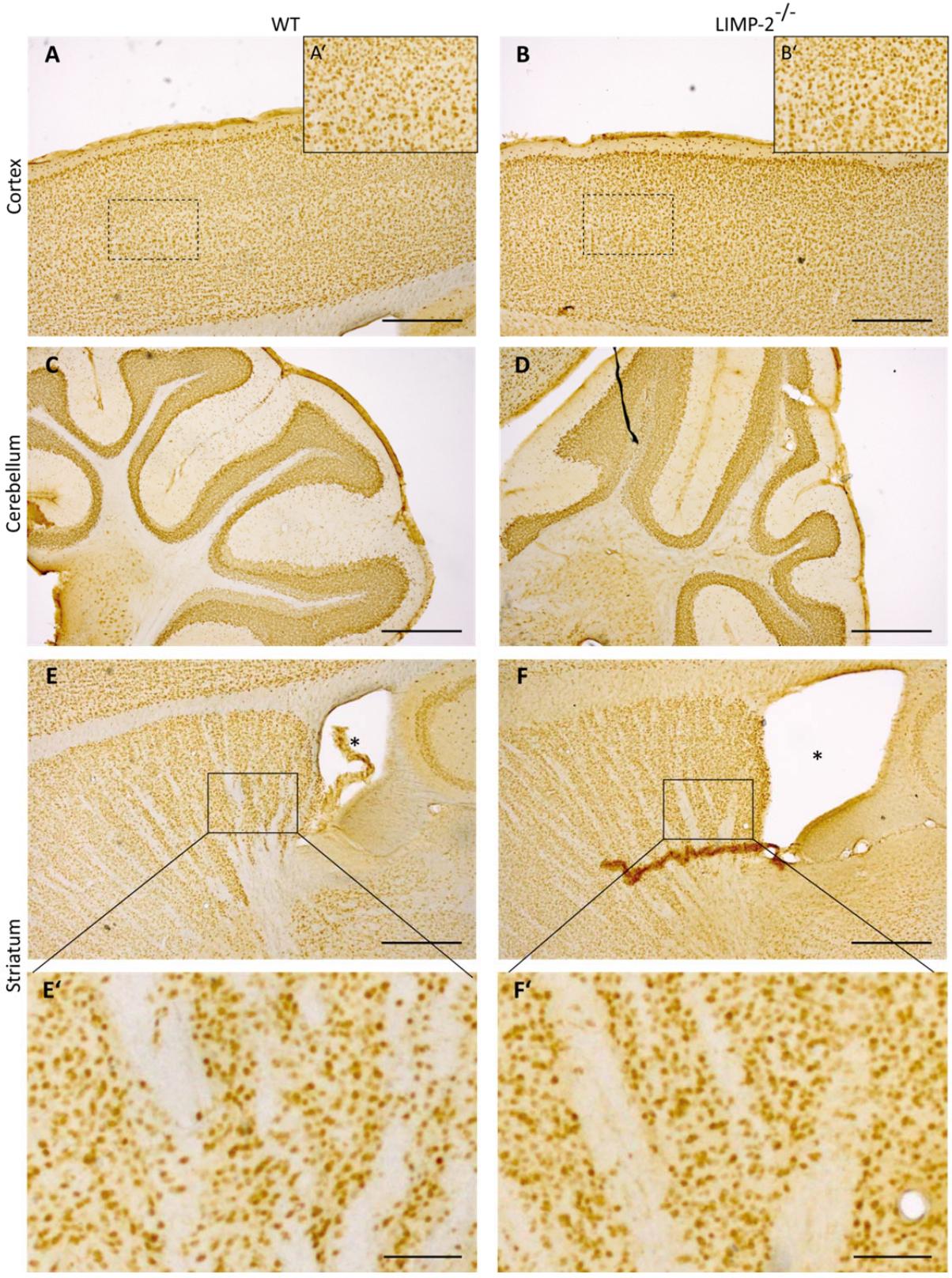

Figure 6.7 ***Immunohistological staining using the neuronal marker NeuN.*** **A to F-** Representative histological sections of 6-month-old wild-type (WT) and LIMP-2 knockout (LIMP-$2^{-/-}$) littermates. **A to D-** No difference in neuronal density was observed within the cortex or cerebellum due to LIMP-2 deficiency. **E/F** Enlarged lateral ventricle but no difference in neuronal density in the striatum of LIMP-$2^{-/-}$ mice. **E'/F'** Digitally zoomed picture of region outlined in **E/F** (n = 3 per genotype; large scale bar = 500 µm, digital zoom scale bar = 100 µm, asterisk indicates lateral ventricle).

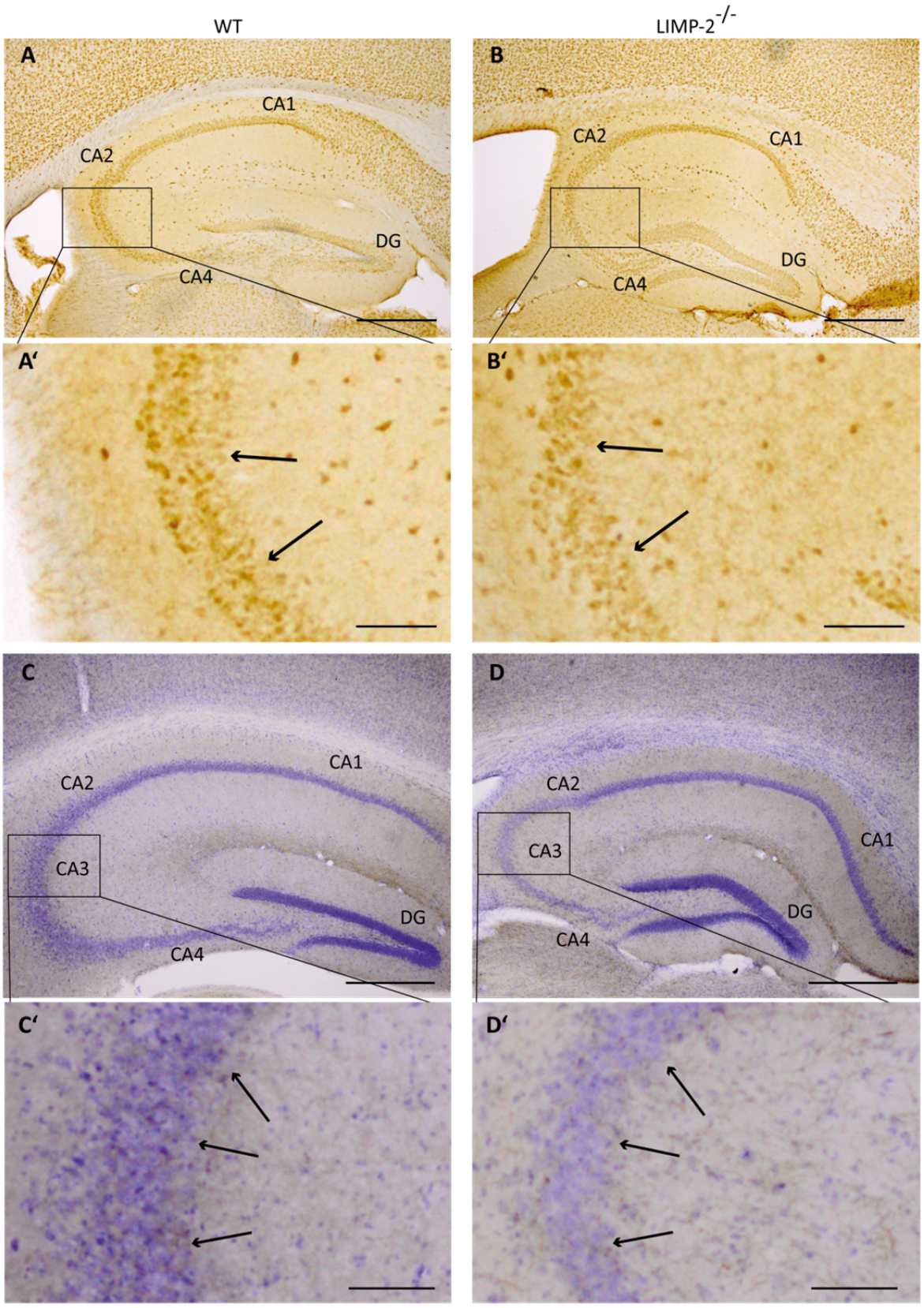

Figure 6.8 NeuN and Nissl staining of murine brain highlighting degeneration of neurons within the hippocampus. A/B- Representative histological sections of 6-month-old wild-type (WT) and LIMP-2 knockout (LIMP-$2^{-/-}$) littermates. Reduced density of neurons is observed in the Cornu Ammonis 2 (CA2), CA3 and CA4 regions of the hippocampus. **A'/B'-** Digitally zoomed image of the CA3 region of hippocampus. Arrows point to pyramidal neurons. **C/D-** Histological sections of 10-month-old WT and LIMP-$2^{-/-}$ littermates. The CA3 regions were digitally zoomed. Arrows point to pyramidal neurons. A dramatic reduction of Nissl positive neurons was observed within regions CA2-4. (N = 3 per genotype; large scale bar = 500 µm, digital zoom scale bar = 100 µm).

6.2.6 LIMP-2-deficiency leads to apoptosis in murine brain

Loss of neurons as well as the presence of eosinophilic spheroids and marked gliosis throughout the CNS may be a result of cellular death. Therefore, Terminal deoxynucleotidy transferase (deoxyuridine triphosphate) dUTP Nick End Labelling (TUNEL) staining (methods 5.3.5.7) was used to detect the presence of apoptotic cells within brain tissue. TUNEL is a method used to detect DNA degradation in apoptotic cells. This assay exploits the fact that fragmentation of nuclear chromatin during apoptosis leads to the exposure of 3'-hydroxyl termini of DNA. The nicks in DNA can be identified by terminal deoxynucleotidyl transferase which catalyses the addition of dUTPs that are labelled with a marker (Gavrieli et al., 1992).

Interestingly, a clear presence of apoptotic cells was observed within the white matter of the cerebellum, substantia nigra, and pons, of 6-month-old LIMP-2-deficient brain (fig. 6.9B, D and H). Apoptosis was also apparent in older mice which was particularly acute in the cerebellum (fig. 10B/H and table 6.2). No clear increase in the prevalence of apoptosis in the cerebellum or substantia nigra was observed in older mice (fig. 6.10). Whereas no apoptosis was observed in the midbrain of 6-month-old mice (fig. 6.9F), a clear increase in apoptotic cells was detected in older mice (fig. 6.10F). Additionally, the occurrence of apoptotic cells within the pons increased slightly in older mice (fig. 6.10H and table 6.2). With the exception of the corpus callosum (data not shown), no apoptosis was observed in other regions of the CNS due to LIMP-2 deficiency in 6- or 10-month-old mice. No apoptotic cells were observed in wild-type control mice. Loss of LIMP-2 expression appears to cause apoptosis within the cerebellum, pons, substantia nigra and midbrain of mice.

Table 6.2 ***Quantification of apoptosis in LIMP-2-deficient mice.*** Incidence of apoptotic cells per region in LIMP-2-deficient mice at 6 and 10 months of age identified by TUNEL staining. (Cells were counted in each regional picture taken at 20 X magnification; N value corresponds to number of mice analysed).

Region	6 months (n = 1)	10 months (n = 3)
White matter cerebellum	16	16±1
Substantia Nigra	5	2±2
Midbrain	0	5±2
Pons	3	6±1

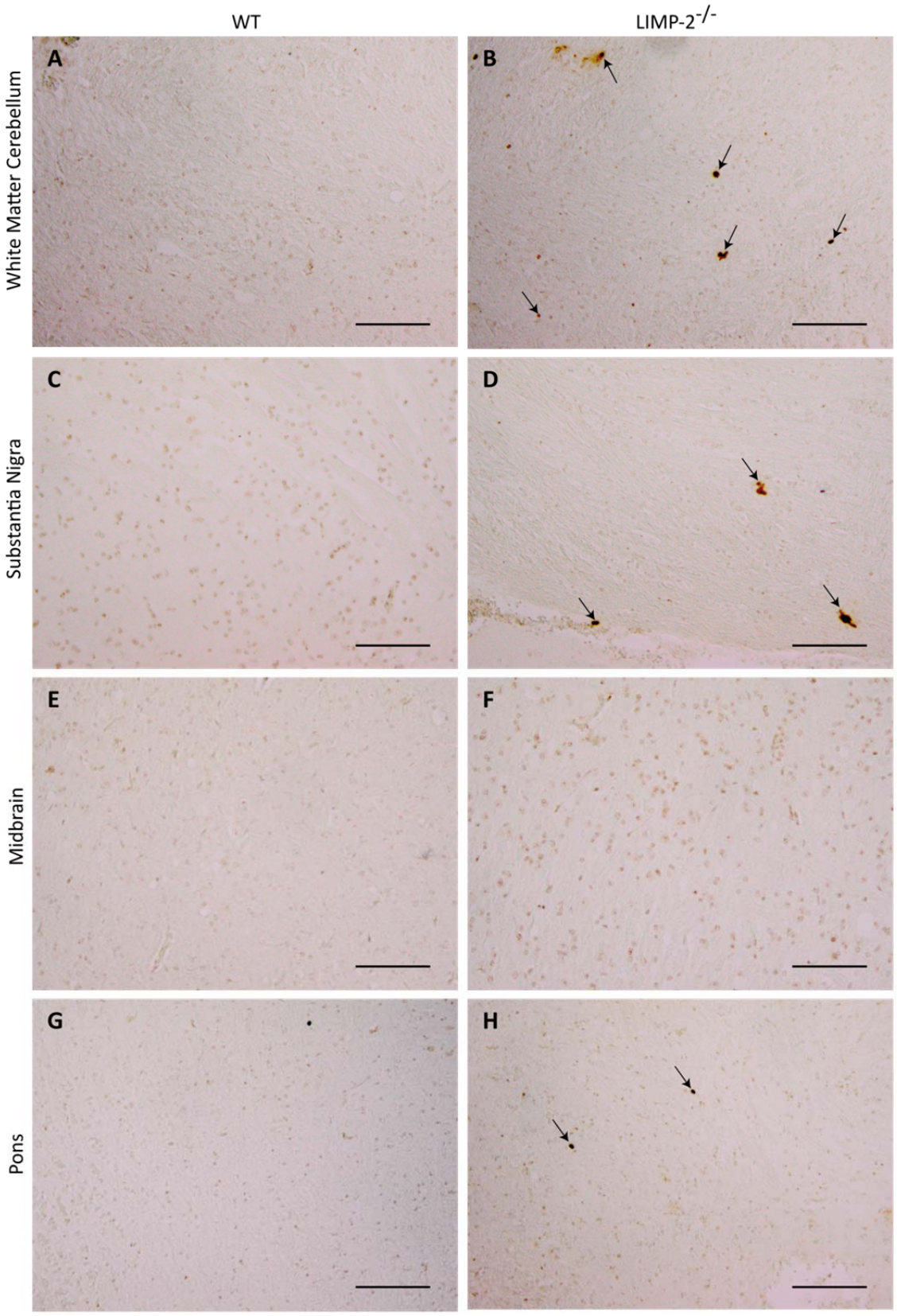

Figure 6.9 ***Apoptosis is observed in brains of 6-month-old LIMP-2-deficient mice*****. A-** Representative histological sections of 6-month-old wild-type (WT) and LIMP-2 knockout (LIMP-$2^{-/-}$) littermates stained using the TUNEL method (arrows indicate apoptotic cells; n = 1 per genotype; scale bar = 100 µm).

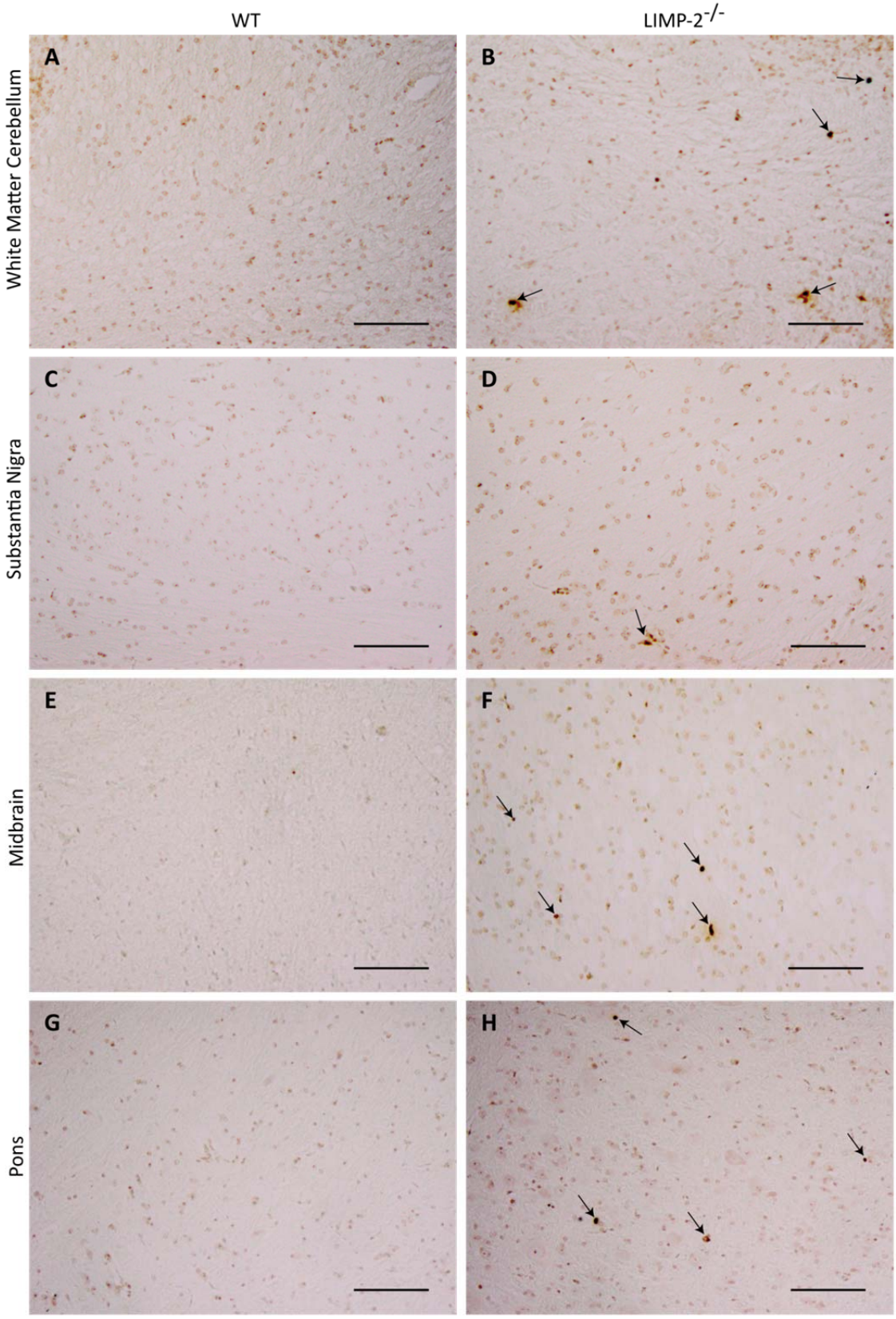

Figure 6.10 ***Apoptosis is observed in brains of 10-month-old LIMP-2-deficient mice.*** **A-** Representative histological sections of 10-month-old wild-type (WT) and LIMP-2 knockout (LIMP-$2^{-/-}$) littermates stained using the TUNEL method (arrows indicate apoptotic cells; n = 3 per genotype; scale bar = 100 µm).

6.3 Characterisation of LIMP-2 expression pattern in the CNS

Neuropathological symptoms observed in LIMP-2 knockout mice raised the question whether distribution of LIMP-2 in different brain areas correlates with severity of neuroinflammation and neuronal damage. LIMP-2 is known to be expressed in murine fibroblasts (Reczek et al., 2007) and brain (Gamp et al., 2003). Furthermore, enriched expression of LIMP-2 has been reported within the Purkinje cell layer (Berkovic et al., 2008). However, an in-depth analysis of its exact cellular distribution within the CNS has not been evaluated.

Immunohistological staining of murine brain using an antibody directed against LIMP-2 showed ubiquitous expression with enrichment in the 4th layer of the cerebral cortex and within the CA2 and CA3 regions of the hippocampus (fig. 6.11A/A'). Enrichment of LIMP-2 expression was also observed in the Purkinje cell layer of the cerebellum (fig. 6.11B/B'). A similar distribution of LIMP-2 was seen in human cerebellum (fig. 6.11C). LIMP-2 also appeared to be expressed in cells within the pars compacta and pars reticulata of the substantia nigra (fig. 6.11D). No LIMP-2 signal was detected in LIMP-2-deficient brains (fig. 6.11A/B inset). Furthermore, no significant difference in regional expression of LIMP-2 was observed in Western blot analysis of lysates from individual brain regions (fig. 6.11E/F).

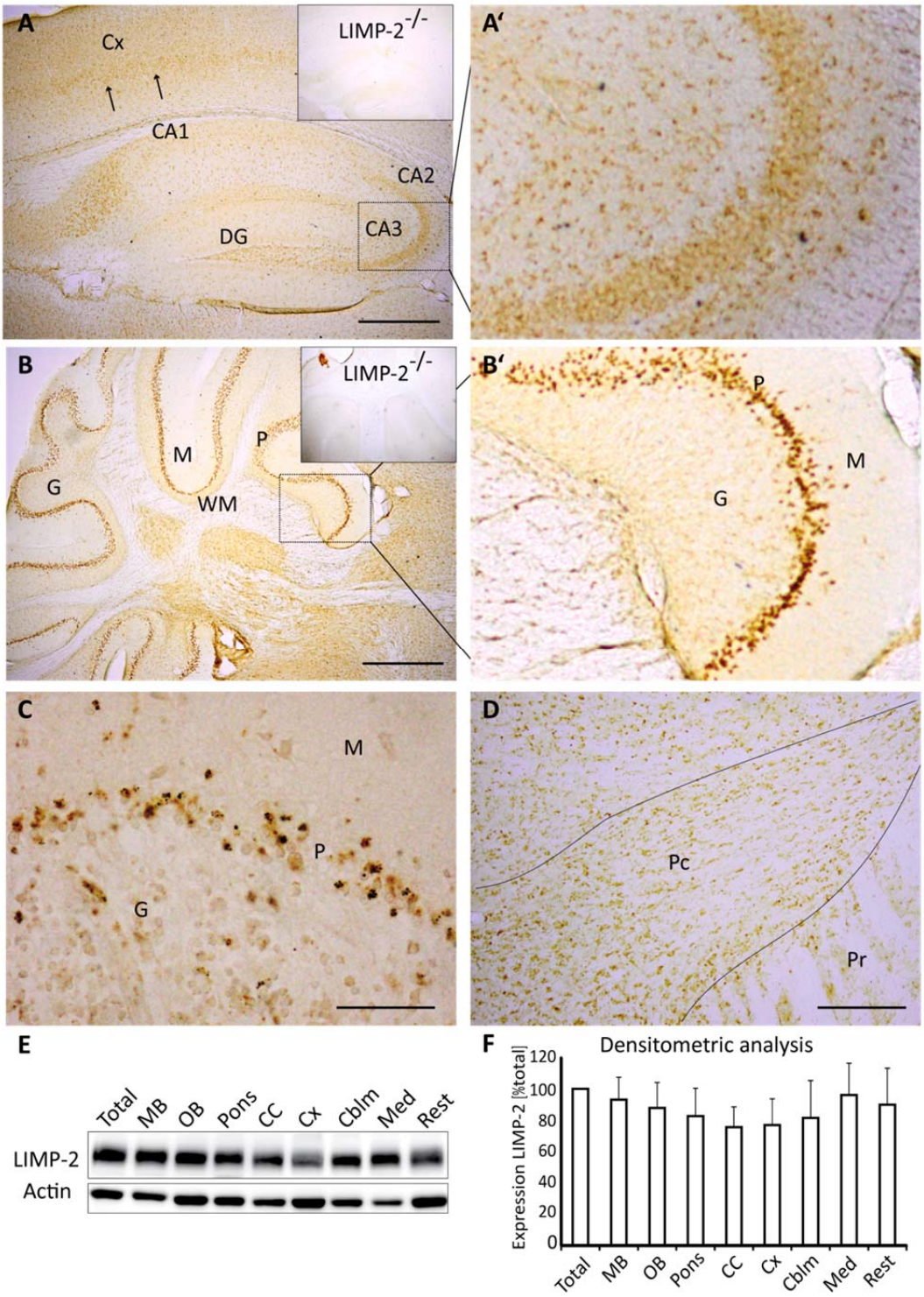

Figure 6.11 ***Expression profile of LIMP-2 in brain.*** **A to D-** Immunohistochemistry of murine brain **(A, B, D)** and human cerebellum **(C)** using an antibody directed against LIMP-2. No staining was observed in LIMP-2 knockout (LIMP-$2^{-/-}$) samples (inset). (Murine sections are from 6-month-old mice; n = 3 per genotype; C- scale bar = 50 µm: A, B, D- scale bar = 200 µm). **A-** Enriched LIMP-2 expression was observed within the 4th cortical layer (arrows) and the Cornu Ammonis 2 (CA2) and CA3 regions (Cx, cortex; DG, dentate gyrus). **A'**- Digitally zoomed image outlined in A. **B-** Enriched expression of LIMP-2 was seen within the Purkinje cell layer of the cerebellum (WM, white matter; M, molecular cell layer; G, granular cell layer; P, Purkinje cell layer). **B'**, digitally zoomed image of area outlined in B. **C-** High expression of LIMP-2 was observed within the Purkinje cell layer of human cerebellum. **D-** LIMP-2 appears to be expressed within the substantia nigra (Pc, pars compacta; Pr, pars reticulata). **E-** Western blot analysis of lysates from regions of murine brain. (Total, total brain; MB, midbrain; OB, olfactory bulb; CC, corpus callosum; Cx, cortex; Cblm, cerebellum; Med, medulla; Rest, remaining brain). **F-** Densitometric analysis of Western blots from brain regions normalised to actin showed no significant difference in LIMP-2 expression (values normalised to total brain and presented as mean values ± SEM; n = 3).

Similarly, immunofluorescence staining of LIMP-2 (methods 5.3.5.7) within the murine CNS revealed ubiquitous expression in wild-type brain whereas no signal was detected in LIMP-2-deficient sections (fig. 6.12 and fig. 6.13). Furthermore, LIMP-2 is expressed in astrocytes as indicated by co-staining with the astrocyte marker Glial Fibrillary Acidic Protein (GFAP) (fig. 6.12A/C/E and fig. 6.13A). Additionally, in agreement with neuropathological observations obtained via immunohistochemistry (results 6.2.1), a significant increase in astrocytes could be observed in LIMP-2-deficient brains (fig. 6.12B/D/F and fig. 6.13B/D). Enriched LIMP-2 expression was again observed within the Purkinje cell layer of the cerebellum (fig. 6.13C). Purkinje cells were identified using the cellular marker calbindin (fig. 6.13E/F). Strikingly, enriched LIMP-2 expression was detected in cells dispersed between Purkinje cells. From their size and position these cells resemble Bergmann glia.

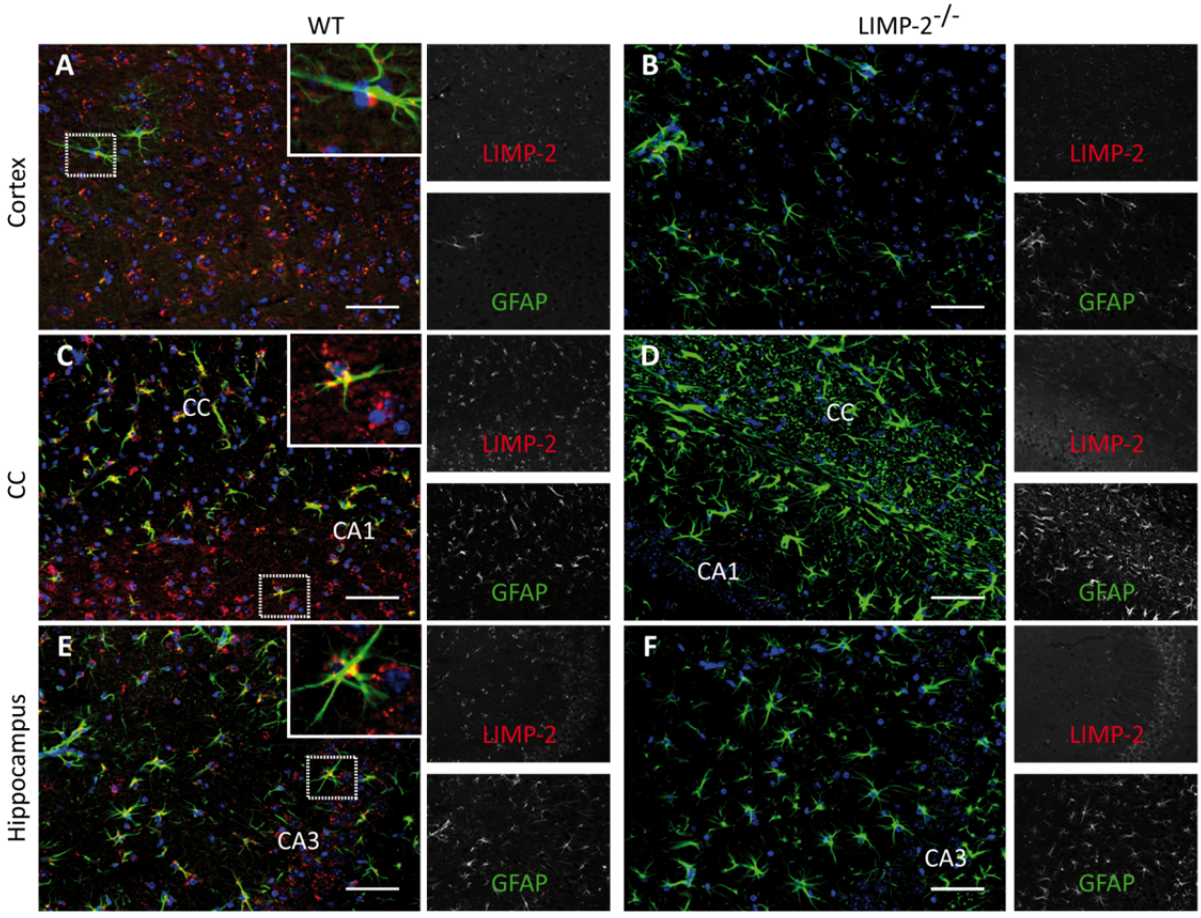

Figure 6.12 ***Expression profile of LIMP-2 in neurons and astrocytes.*** **A to F-** Representative histological sections showing ubiquitous LIMP-2 (red) expression in different brain regions from wild-type (WT) and LIMP-2 knockout (LIMP-$2^{-/-}$) littermates. No LIMP-2 signal was detected in LIMP-$2^{-/-}$ tissue. LIMP-2 expression was detected in GFAP (green) positive astrocytes. Additionally, an increased number of GFAP positive astrolial cells were observed in LIMP-$2^{-/-}$ brain sections (scale bar = 50 µm; inset, digitally zoomed image of area outlined with dotted line; nuclei stained with DAPI blue; CC, corpus callosum; Cornu Ammonis, CA).

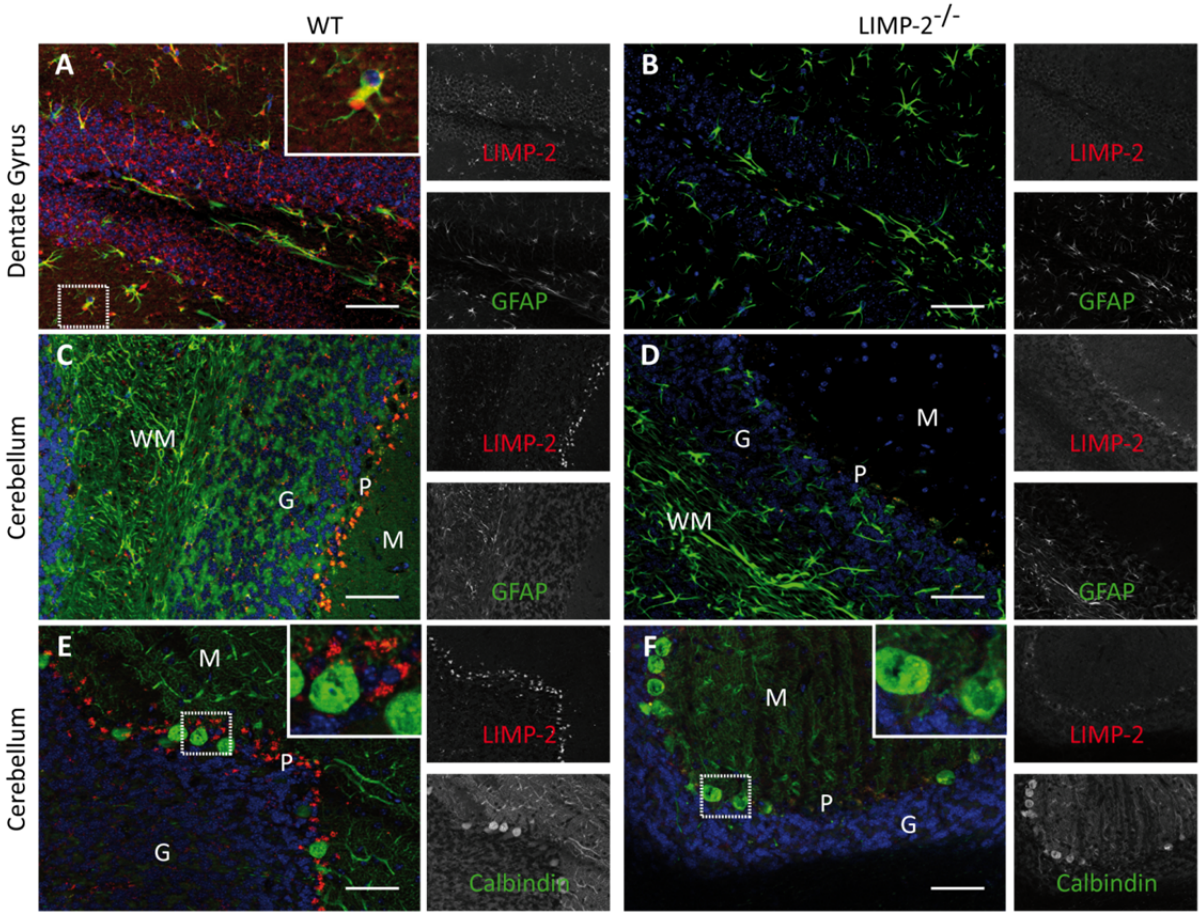

Figure 6.13 ***Expression profile of LIMP-2 in neurons and astrocytes.*** Representative histological sections showing ubiquitous LIMP-2 (red) expression in brain section from LIMP-2 knockout (LIMP-$2^{-/-}$) and their wild-type (WT) littermates. No LIMP-2 signal was detected in LIMP-$2^{-/-}$ tissue**. A/B-** LIMP-2 expression was detected in GFAP (green) positive astrocytes. **C/D-** Enriched expression of LIMP-2 is observed in the Purkinje cell layer of the cerebellum. **E/F-** LIMP-2 expression was increased in cells found between Purkinje cell soma indicated by calbindin staining (green) (inset shows digitally zoomed image of area within dotted line; WM, white matter; G, granular cell layer; P, Purkinje cell layer; M, molecular cell layer; scale bar = 50 µm; inset, digitally zoomed image of area outlined with dotted line; nuclei stained with DAPI blue).

LIMP-2 appears to be ubiquitously expressed in astrocytes as well as other cell types throughout the CNS. Neuropathological indications were particularly severe within myelinated regions of the CNS. However, astrogliosis, neuroinflammation or increased lysosomal protein expression did not correlate with regions where enriched LIMP-2 expression was detected.

6.4 LIMP-2 expression in astrocytes, microglia and neurons

LIMP-2 appears to be ubiquitously expressed throughout the central nervous system and double immunofluorescence of LIMP-2 with GFAP has shown that LIMP-2 is expressed in

astrocytes *in vivo*. Similarly, vesicular LIMP-2 staining was identified within NeuN positive neurons in histological sections from wild-type mice (fig. 6.14A/B).

Due to the presence of multiple cell types and the difficulty in visualisation of individual cells with cellular markers within thick histological sections, primary neurons or glia were cultured (methods 5.5.1). Matrix-Associated Protein type 2 (MAP-2), a protein that specifically stains the soma and dendrites of neurons, and the neuronal marker NeuN were used to identify neurons in culture. Costaining of LIMP-2 with neuronal markers was carried out on pure primary cultures, fixed after 14 days *in vitro* (DIV). Neuronal LIMP-2 expression, with the majority of signal detected close to the soma (fig. 6.15A/A'), could be observed. This correlates with previous studies that report the majority of lysosomes to be within neurons clustered in the perikarya (Overly and Hollenbeck, 1996; Parton et al., 1992).

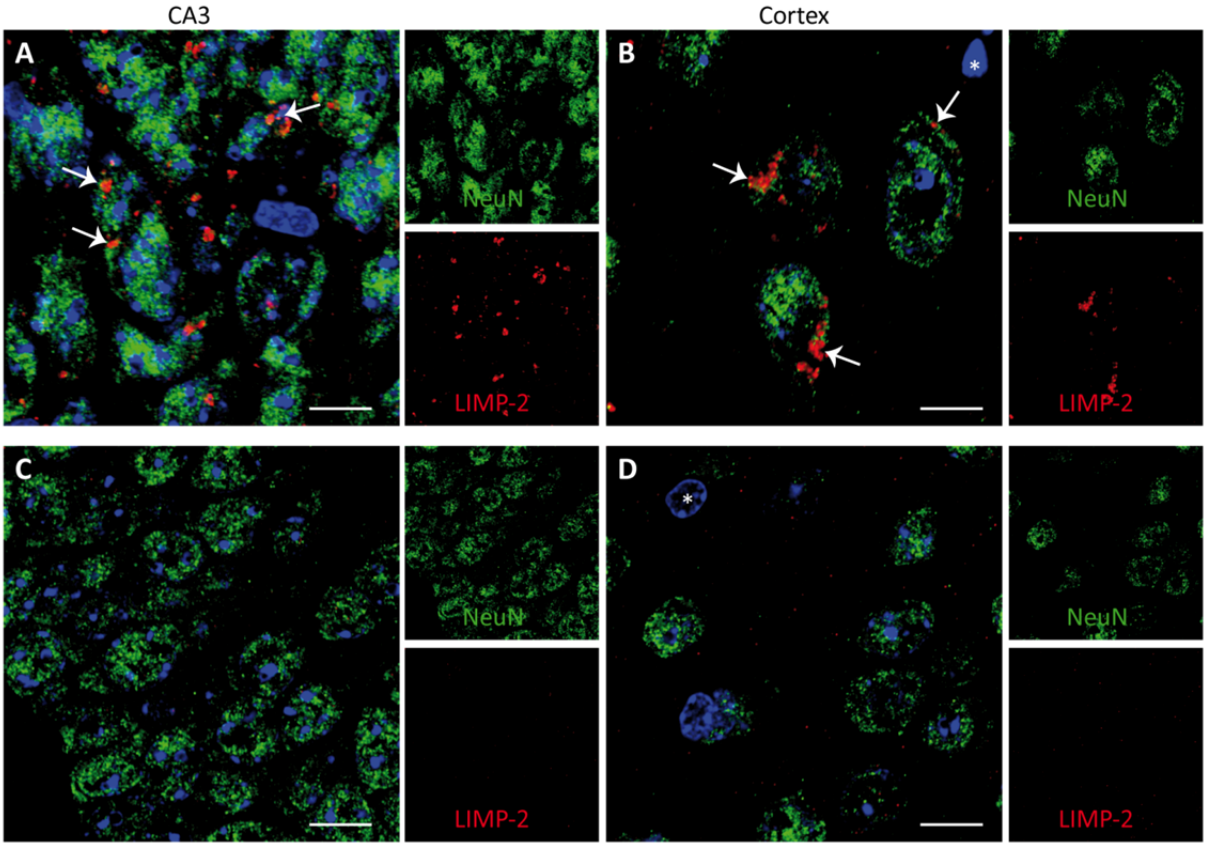

Figure 6.14 ***LIMP-2 is expressed in neurons.*** **A/B-** Representative histological sections showing ubiquitous LIMP-2 (red) expression in neurons identified using the neuronal marker NeuN (green) from the Cornu Ammonis 3 (CA3) region if the hippocampus and the cortex of wild-type mice. **C/D-** No LIMP-2 signal was detected in LIMP-2 knockout tissue**.** (Asterisks indicate unidentified non-neuronal cells; arrows points to vesicular staining of LIMP-2; scale bar = 10 µm).

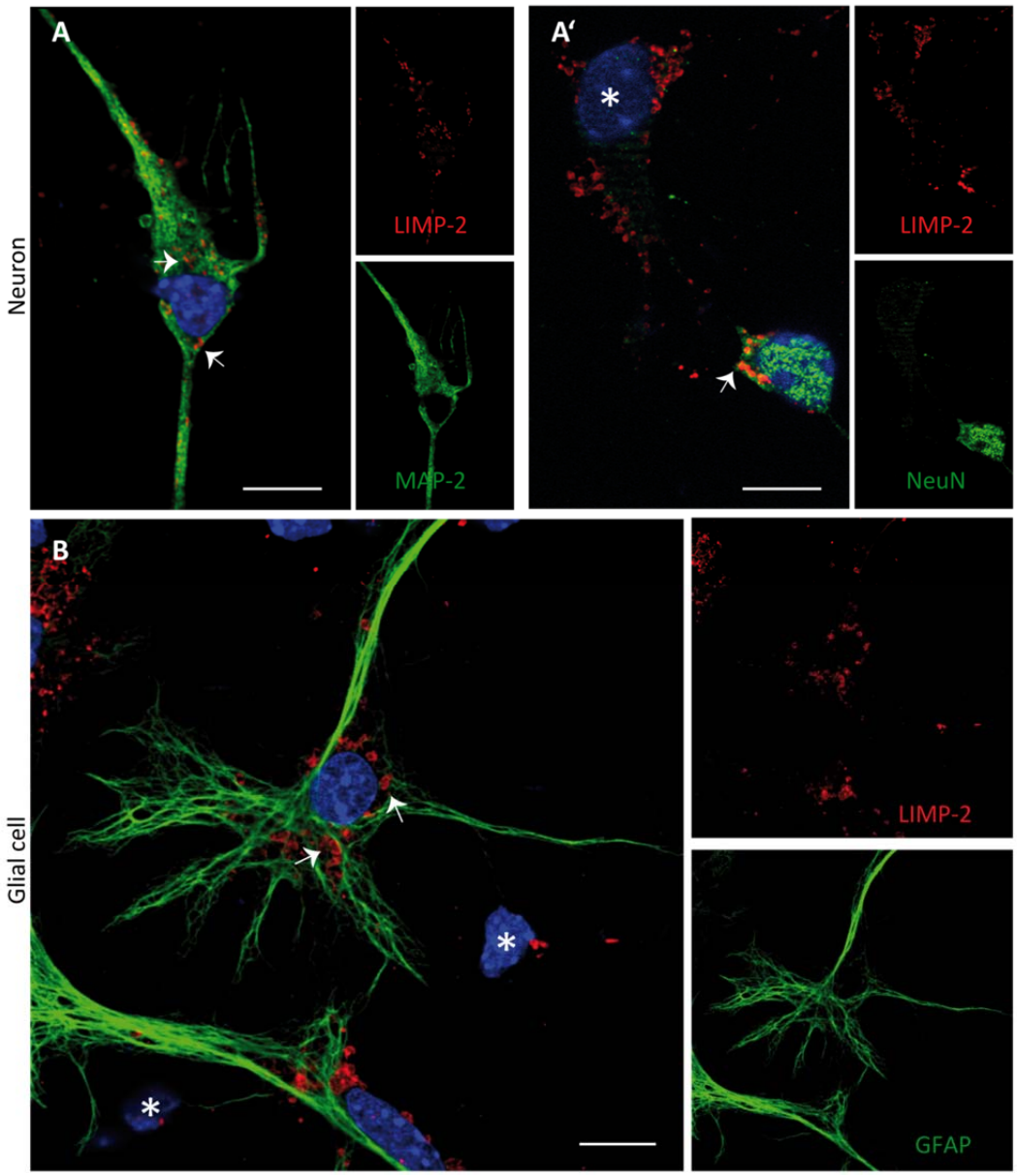

Figure 6.15 ***Expression of LIMP-2 in different cell types of the murine central nervous system.*** **A/A'-** Immunfluorescence of pure primary neuronal cultures shows LIMP-2 (red) positive vesicles clustered around the soma of neurons (NeuN/MAP-2 (green) are neuronal markers; arrows indicate LIMP-2 positive vesicles; asterisk indicate non-neuronal cells; scale bar = 10 µm). **B-** Immunofluorescence of primary astrocytes show clear staining of LIMP-2 (red) in cells positive for the astrocyte marker GFAP (green) (arrows indicate LIMP-2 positive vesicles; asterisk indicate non-astrocyte cells; scale bar = 10 µm).

In mixed glial cultures, the presence of astrocytes and microglial cells in culture was validated via immunofluorescence. In agreement with immunological staining using the astrocyte marker GFAP, vesicular expression of LIMP-2 could be detected in astrocytes (fig. 6.15B). Strikingly, no LIMP-2 could be detected in activated microglial cells identified using the cellular marker CD68 (fig. 6.16 upper panel). Whereas clear vesicular LIMP-2 may be detected in cells negative for CD68 (fig. 6.16 asterisk), no LIMP-2 signal was detected in activated microglial cells. No LIMP-2 signal was detected in cultures from knockout embryos

(fig. 6.16 lower panel). LIMP-2 is expressed in astrocytes and in neurons but not in activated microglial cells.

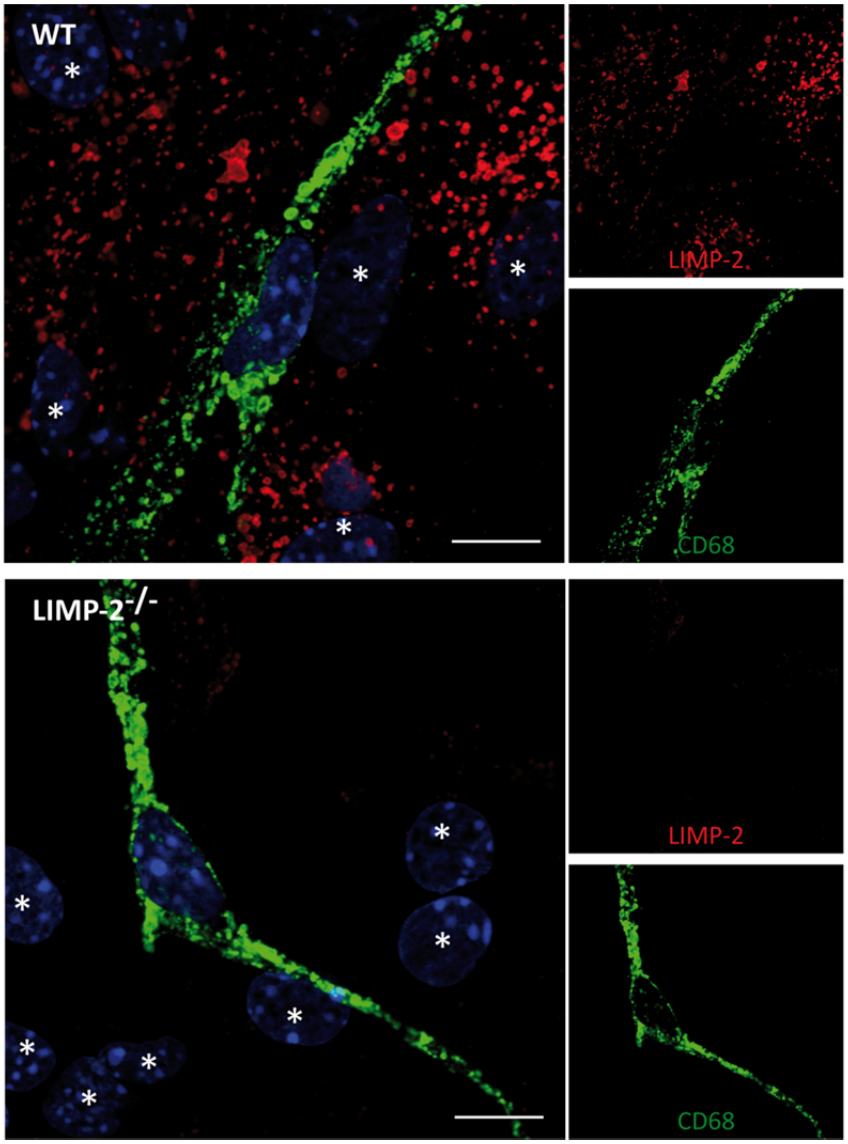

Figure 6.16 ***LIMP-2 is undetectable in activated microglial cells.*** Immunofluorescence of primary mixed glial cultures from wild-type and LIMP-2-deficient (LIMP-$2^{-/-}$) animals. Using the cellular marker CD68 (green), microglial cells were identified in a mixed glial culture containing astrocytes and microglial cells. Whereas LIMP-2 (red) positive vesicles were observed in non-microglia, no signal was evident in CD68 positive cells (asterisk indicate non-microglial cells; scale bar = 10 µm).

6.5 β-GC mistrafficking in LIMP-2-deficient brain, primary neurons and astrocytes

The absence of LIMP-2 in fibroblasts is known to lead to mistrafficking of β-GC. Therefore, the next step was to assess whether mistrafficking of the enzyme occurs in neuronal tissue. Firstly, changes in transcription of β-GC was assessed using relative quantitative RT-PCR of cDNA derived from mRNA of brain material from wild-type and LIMP-2 knockout brains

(methods 5.3.8). Whereas transcription levels remain unchanged (fig. 6.17A), a dramatic reduction in β-GC protein was detected in murine brain deficient in LIMP-2 (fig. 6.17B/C) and mouse embryonic fibroblasts (MEFs) as previously reported (Reczek et al., 2007). A significant decrease in β-GC enzymatic levels was observed in lysates from midbrains of LIMP-2-deficient mice which was reduced even further in the pons. However, due to the discrepancy between Western blot analysis and β-GC enzyme activity assays an alternative assay was used in order to discriminate between lysosomal β-GC hydrolytic activity and a related enzyme, β-Glucosidase 2 (GBA2). GBA2 is responsible for metabolism of GluCer outside of the lysosome (Boot et al., 2007) and is reported to be dysregulated in Gaucher disease mouse models and patients (Burke et al., 2012; Korschen et al., 2013). Thus changes in GBA2 activity may interfere with the general β-GC activity assay used. Therefore, lysates were pretreated with Conduritol-B-Epoxide (CBE), an inhibitor specific for β-GC reported to not cross react with GBA2 (Boot et al., 2007). Therefore, loss of activity due to treatment with CBE is solely due to activity of β-GC. After incubation with the inhibitor, lysates were subjected to an enzyme activity assay as before. Strikingly, in agreement with reduced levels of β-GC detected via Western blot, only 32 % of wild-type activity was measured in LIMP-2-deficient lysates (fig. 6.17E). Additionally, an increase in other lysosomal hydrolase activity was observed in the midbrain of LIMP-2-deficient mice but this was not significant. Interestingly, a significant increase in the activity of α-mannosidase and β-hexosaminidase was observed in the pons of mice when LIMP-2 was not expressed (fig. 6.17D).

In agreement with analysis of brain tissue, reduced levels of detectable β-GC were observed in Western blots from both primary glial cultures (which include mostly astrocytes with a minor number of microglial cells) (fig. 6.18A/C) and primary neuronal cultures (fig. 6.18B/C) where LIMP-2 is not expressed. Moreover, vesicular staining of β-GC was observed in wild-type neurons but was absent in LIMP-2-deficient cultures (fig. 6.18D). Loss of LIMP-2 in brain, isolated glia and neurons leads to altered trafficking of β-GC and thus a dramatic reduction of the hydrolytic activity of the enzyme within lysosomes.

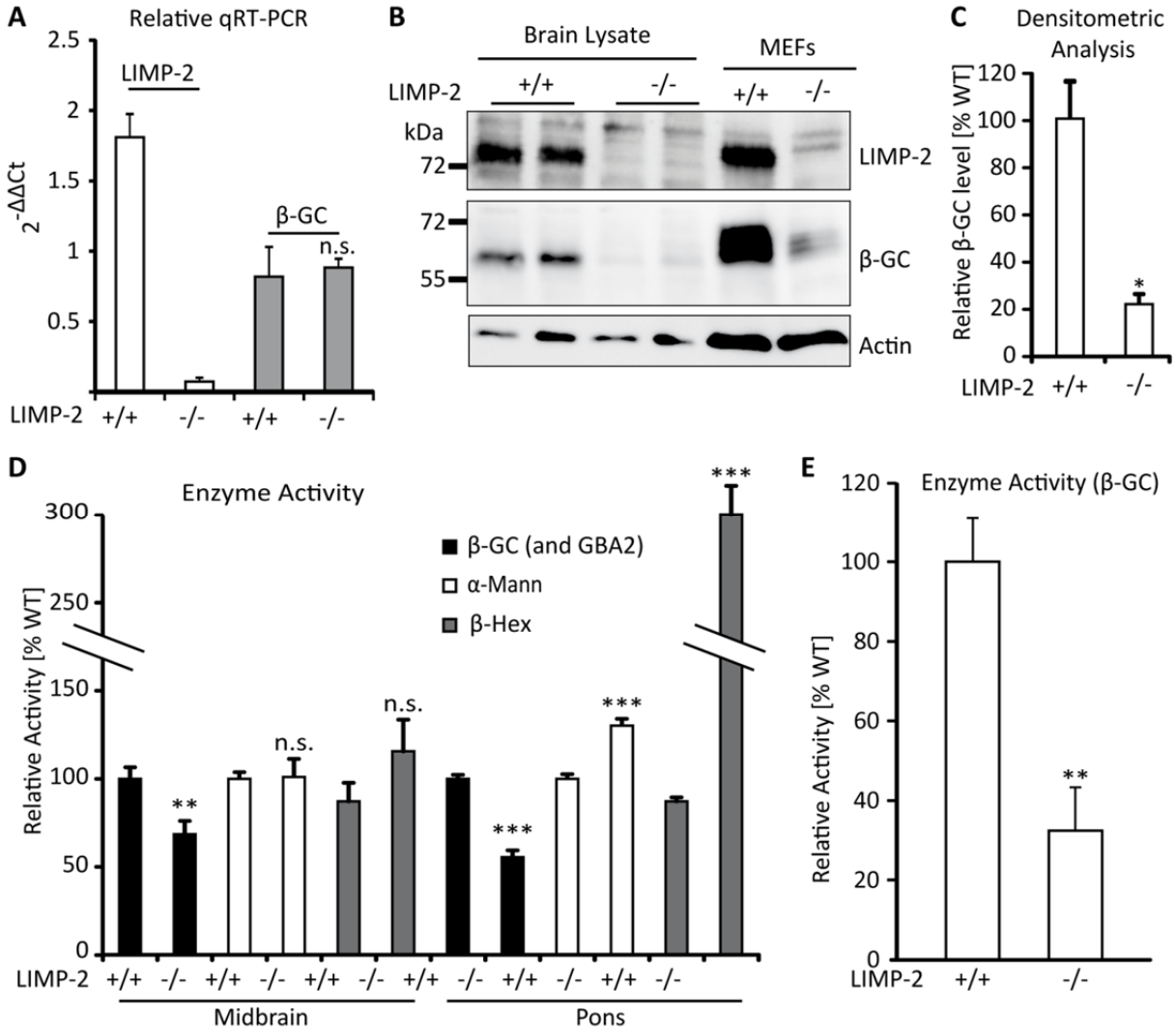

Figure 6.17 β-*GC mistrafficking in LIMP-2-deficient brain tissue.* **A-** Relative quantitative RT-PCR of LIMP-2 and β-GC cDNA from whole brains of wild-type (+/+) and LIMP-2-deficient (-/-) littermates. (Relative values calculated using the $\Delta\Delta C_t$ method normalised to GAPDH and presented as mean values ± SEM; n = 3 per genotype; **p < 0.0005; n.s. = not significant, p < 0.05). **B-** Western blot of whole brain lysates and mouse embryonic fibroblasts (MEFs) from wild-type (+/+) and LIMP-2-deficient (-/-) littermates. When LIMP-2 is missing, a dramatic reduction in detectable β-GC is observed. Actin was used as a loading control. **C-** Densitometric analysis of brain lysates from wild-type (+/+) and LIMP-2-deficient (-/-) littermates from the immunoblot shown in B (values normalised to wild-type are presented as mean ± SEM; *p < 0.05). **D-** Enzymatic actvity of β-GC (including GBA2 activity), β-hexosaminidase (β-Hex) and α-mannosidase (α-Mann) in midbrain and pons from 10-month-old mice. In midbrain samples a significant reduction in β-GC activity was observed in LIMP-2 knockout (-/-) mice when compared to wild-type (+/+) whereas other lysosomal enyzme activities remain unchanged. β-GC activity is reduced even further in the pons and other lysosomal enzyme activities are significantly increased. **E-** Enzymatic actvity of β-GC only. Activity measured in lysates from the pons, treated with the β-GC specific inhibtor, CBE, was subtracted from activity measured in non-treated samples. A significant reduction in β-GC activity was observed in LIMP-2 knockout (-/-) mice when compared to wild-type (+/+) (values normalised to percentage activity wild-type and presented as mean ± SEM; n > 5 per genotype; **p = 0.002).

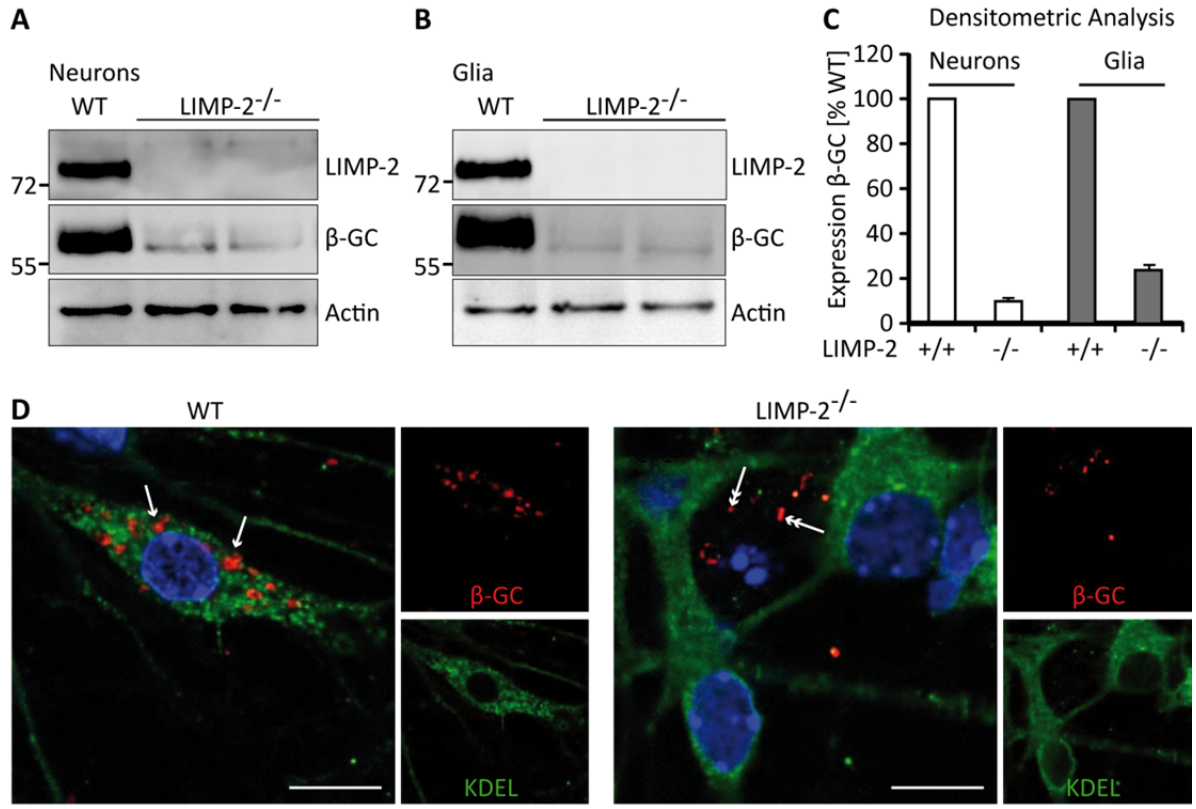

Figure 6.18 β-*GC mistrafficking in primary neurons and glia deficient in LIMP-2.* **A-** Western blot of lysates from primary pure neuronal cell cultures derived from wild-type (WT) and LIMP-2-deficient (LIMP-2$^{-/-}$) mice. A significant reduction in β-GC was observed in LIMP-2$^{-/-}$ samples (LIMP-2 antibody was used to verify genotype and actin was used as a loading control). **A-** Western blot of lysates from primary glial cell cultures derived from WT and LIMP-2$^{-/-}$ mice. A dramatic reduction in β-GC was observed in LIMP-2$^{-/-}$ samples (LIMP-2 antibody was used to verify genotype and actin was used as a loading control). **C-** Densitometric quantification of β-GC from immunoblots in A/B. A reduction of 10-20 % in β-GC levels were observed in lysates from LIMP-2-deficient neuronal and glial cultures. (Values normalised to wild-type presented as mean ± SEM**). D-** Immunofluorescence of primary neurons derived from WT and LIMP-2$^{-/-}$ mice fixed at 14 DIV. Intracellular vesicular staining (arrows) of β-GC (red) is clearly visible in WT but is absent from LIMP-2$^{-/-}$ neurons. Extracellular unspecific staining (double arrows) was observed in LIMP-2$^{-/-}$ neurons (KDEL (green) was used as an ER marker; scale bar = 10 µm).

6.6 Accumulation of lipids and carbohydrate-conjugates due to LIMP-2 deficiency

6.6.1 Increase of lipid content in LIMP-2-deficient neurons

Due to the reduction in β-GC activity, it would be logical to surmise that this would result in an increase in the enzyme's substrate, GluCer, in neurons. However, no working antibody for the detection of GluCer is available. Therefore, a general lipid stain, Bodipy®493/503, previously used to assess GluCer accumulation (Mazzulli et al., 2011) was used to stain primary neurons (methods 5.6.7). This non-specific lipid stain is attracted to the fatty acid component of GluCer and thus may be used to indirectly assess its accumulation. When compared to primary neurons derived from wild-type littermates, neuronal cells from embryos deficient in LIMP-2 show a clear increase in intracellular vesicular lipid staining

(fig. 6.19A/B). Similarly, accumulation of droplets within the soma of MAP-2 positive neurons in a mixed culture (containing neurons, astrocytes and microglial cells) was observed (fig. 6.19C single arrows). Additionally, lipid accumulation was observed in other unidentified cell types in mixed cultures of LIMP-2-deficient primary mixed neuronal cultures (fig. 16.9C double arrows). Deficiency in LIMP-2 leads to the accumulation of Bodipy®493/503 positive lipid droplets in neurons grown in culture.

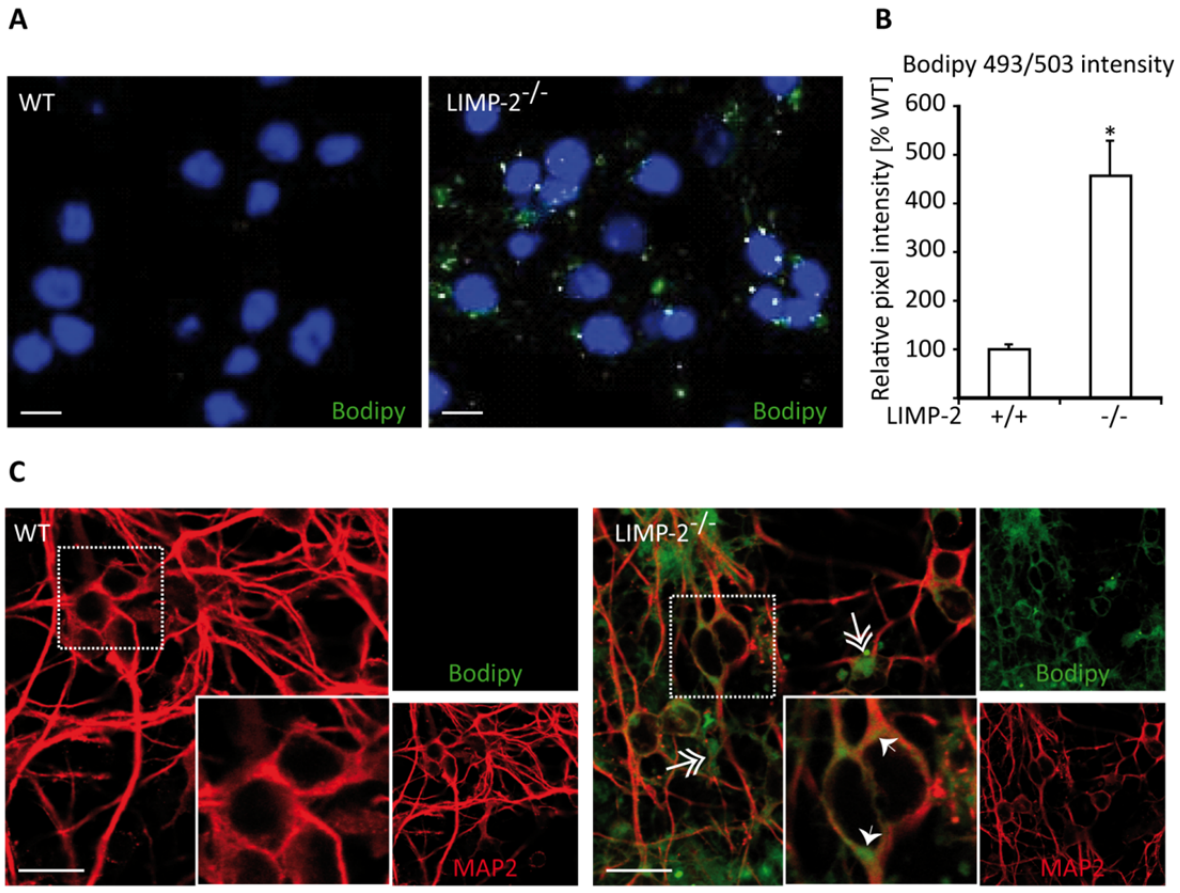

Figure 6.19 ***Lipid accumulation in LIMP-2-deficient primary neurons.*** **A-** Bodipy®493/503 staining (green) of neurons grown in pure primary neuronal cultures derived from LIMP-2 knockout (LIMP-2$^{-/-}$) and wild-type (WT) littermate embryos. (Nuclei are stained blue with DAPI; scale bar = 10 µm). **B-** Densitometric quantification of Bodipy®493/503 signal normalised to DAPI intensity in LIMP-2 knockout (-/-) and wild-type (+/+) neurons from primary pure neuronal cultures. A significant accumulation of lipids was observed in LIMP-2-deficient neurons (Values normalised to percentage activity wild-type and presented as mean ± SEM; $p < 0.0001$). **C-** Bodipy®493/503 staining (green) of neurons grown in mixed primary neuronal cultures derived from wild-type (WT) and LIMP-2 knockout (LIMP-2$^{-/-}$) littermate embryos. Single arrows point to lipid droplets within the soma of MAP-2 (red) positive neurons. Double arrows indicate non-neuronal cells positive for Bodipy®493/503 accumulation (scale bar = 10 µm; area outlined is digitally zoomed and shown in the inset).

6.6.2 PAS positive deposits are observed throughout LIMP-2-deficient brain

Equally, due to the absence of a working antibody to identify the accumulation of GluCer in histological sections an indirect method of detection was employed. The periodic acid-Schiff

(PAS) stain may be used to detect the presence of pathological accumulation of carbohydrate-conjugates thereby potentially detecting the glucose component of GluCer. Interestingly, PAS positive accumulation was found throughout the CNS of 6-month-old LIMP-2-deficient mice but was completely absent from their wild-type littermates (fig. 6.20). Similar accumulation, with equal severity, was detected in mice at 10 month (data not shown).

Myelinated areas such as the white matter of the cerebellum (fig. 6.20E/F), corpus callosum (fig. 6.20G/H) and the anterior commissure (data not shown) showed the most severe PAS positive accumulation relative to other areas also observed to have pathological deposits such as the substantia nigra, pons, other parts of the cerebellum and the cortex (fig. 6.20A-D and I/J). Additionally, PAS positive accumulation was observed within the midbrain and fornix and in some areas of the hippocampus (data not shown). Accumulation of a carbohydrate-conjugate was observed throughout the CNS of LIMP-2-deficient mice which may suggest the deposition of GluCer or one of its catabolic products.

6.7 Storage and neuronal degeneration in the spinal cord of LIMP-2-deficient mice

Accumulation of PAS positive deposits throughout LIMP-2-deficient brain and increased levels of Bodipy®493/503 positive lipid droplet within neurons coupled with the presence of partial paralysis of the hind-limbs of 10-month-old mice prompted further investigation into potential anomalies present in the spinal cord of knockout mice. Electron microscopy of semi-thin sections from the ventral horn of lumbar spinal cord revealed the presence of degenerating neurons (fig. 6.21B/B(i) red arrows). Large electron dense inclusions and lipid-like droplets within both healthy (fig. 6.21B(ii)) and degenerating (fig. 6.21B(iii)) motor neurons were observed in LIMP-2 knockout mice only.

An accumulation of unidentified storage material and other unidentified lipids as well as degeneration of motor neurons was evident in the spinal cord of mice deficient in LIMP-2.

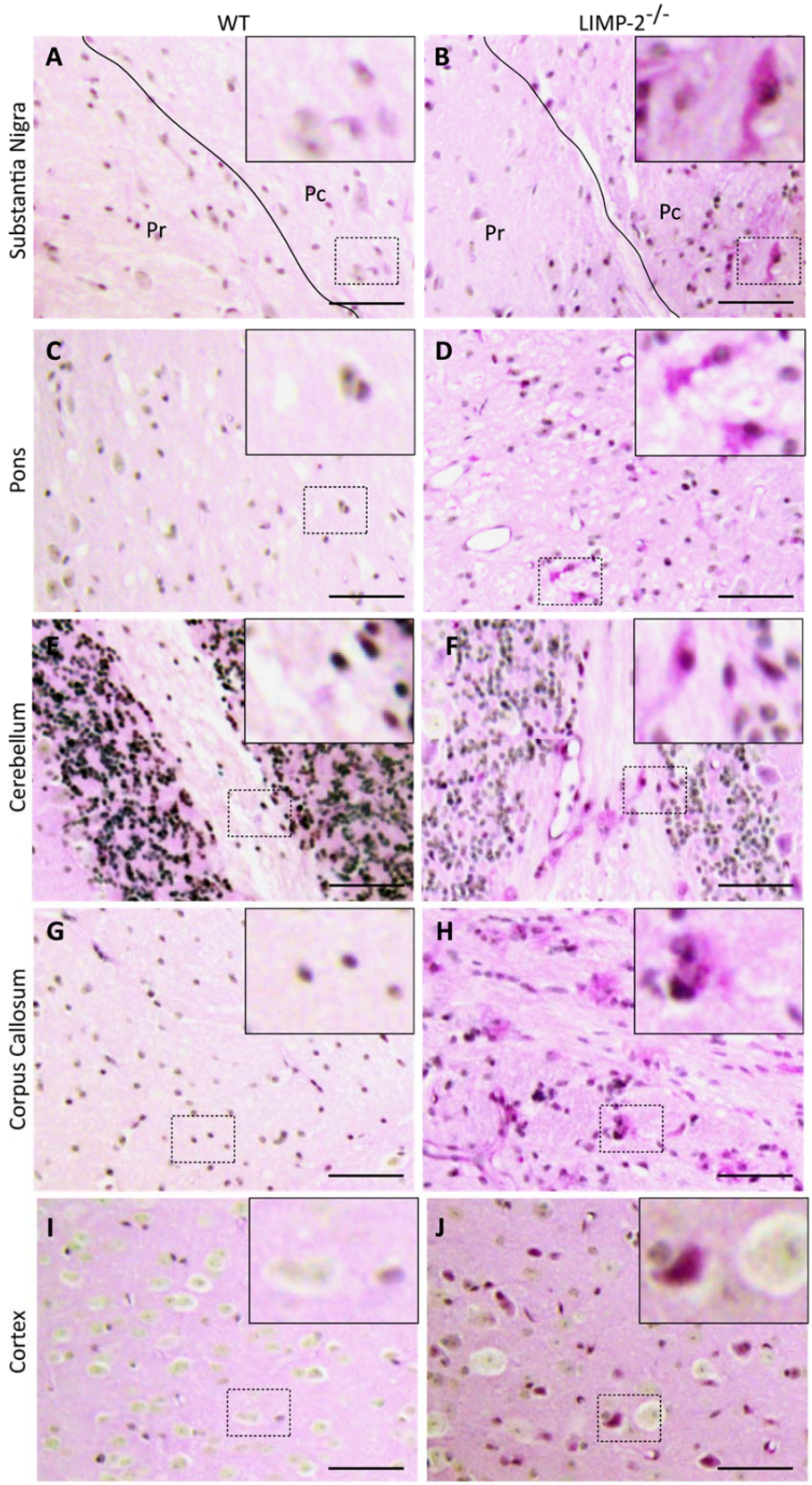

Figure 6.20 ***Carbohydrate-conjugate accumulation throughout the CNS of LIMP-2-deficient mice.*** **A to J-** The presence of PAS positive substance indicates the existence of accumulated carbohydrate-conjugates throughout the CNS of 6-month-old LIMP-2-deficient (LIMP-$2^{-/-}$) mice. No accumulation was detected in wild-type (WT) littermates. Paraffin sections were stained using the PAS method (Periodic acid-Schiff stain, dark pink; nuclear staining, haematoxylin, blue; insets indicate digitally zoomed image of area outlined in dotted box; Pc, pars compacta; Pr, pars reticulata; scale bar = 50 µm; n = 4 per genotype).

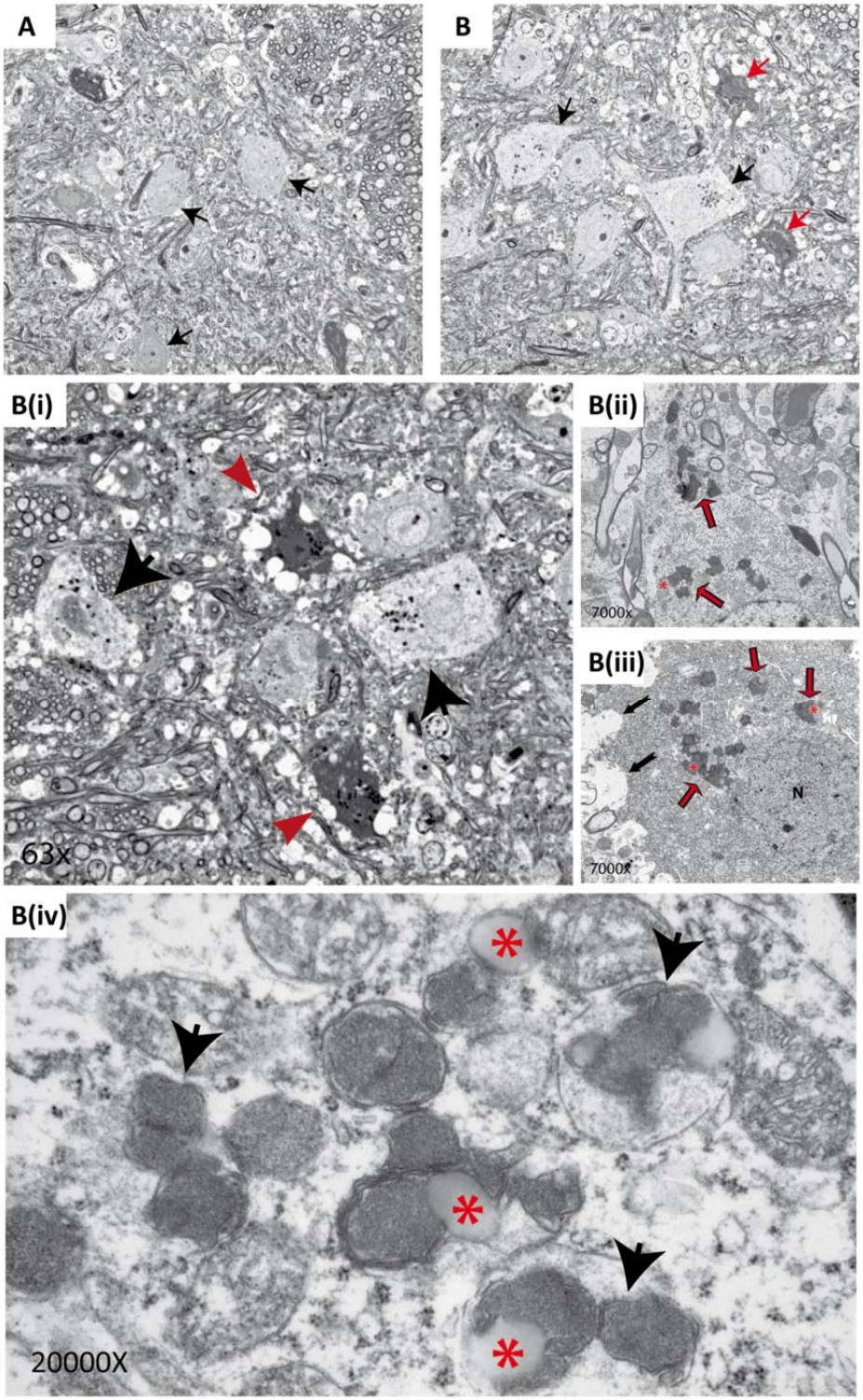

Figure 6.21 ***Degeneration of motor neurons and presence of inclusions within the spinal cord of LIMP-2-deficient mice.*** (Electron micrographs of spinal cord sections from the lumbar region of **A-** wild-type and **B-** LIMP-2-deficient mice; in collaboration with M. Schweizer, Centre for Molecular Neurobiology, Hamburg). **A-** Motor neurons of wild-type mice show no inclusions and normal morphology (arrows). **B-** Several motor neurons in LIMP-2-deficient mice indicate signs of degeneration highlighted by their shrunken appearance and dark cytoplasm (red arrows). **B(i)** The presence of dark electron dense inclusions was observed in both degenerating (red arrows) and otherwise morphologically normal neurons (black arrows). Higher magnification of a **B(ii**) non-degenerating and **B(iii)** degenerating neuron reveals the storage of electron dense inclusions and lipid-like droplets (asterisk). Furthermore, the ruffled boarder of the dying motor neurons (black arrows) can be clearly seen. **B(iv)** 20000X magnification shows storage of cytosolic membrane bound dark, dense material (arrows) and unidentified lipid-like droplets (asterisks).

6.8 α-Synuclein accumulation in LIMP-2-deficient brain and primary neurons

Accumulation of GluCer was recently discovered to potentially directly influence α-synuclein accumulation (Mazzulli et al., 2011). This suggestion, coupled with evidence of mistrafficking and reduced activity of the enzyme as well as a potential accumulation of its substrate in LIMP-2-deficient mice, prompted investigation of pathological accumulation of α-synuclein within the CNS. Immunohistological investigation revealed accumulation of α-synuclein in brains lacking LIMP-2 which was particularly acute in the pars compacta but also observed in the pars reticulata of the substantia nigra and even more pronounced in the pons (fig. 6.22B/D). Furthermore, accumulation was detected in the midbrain (fig. 6.22F) and corpus callosum (data not shown) as well as the granular cell layer of the cerebellum (fig. 6.22H) in LIMP-2-deficient mice.

Moreover, in pure primary cortical neurons, cultured from LIMP-2-deficient embryos, a notable accumulation of vesicular α-synuclein is evident already after only 7 DIV (fig. 6.23B) which persisted until the oldest cultures were harvested at 21 DIV (fig. 6.24B). Accumulated α-synuclein was particularly concentrated in the soma and proximal neurites of LIMP-2-deficient primary neurons (fig. 6.23B/D). Similar accumulation was observed in mixed cortical cultures (fig. 6.24C/D) and in dopaminergic neurons from primary mixed mesencephalic cultures (fig. 6.24E/F). Loss of LIMP-2 appears to promote the aggregation of α-synuclein in cultured neuronal cells as well as within the substantia nigra, pons, midbrain and cerebellum in mice.

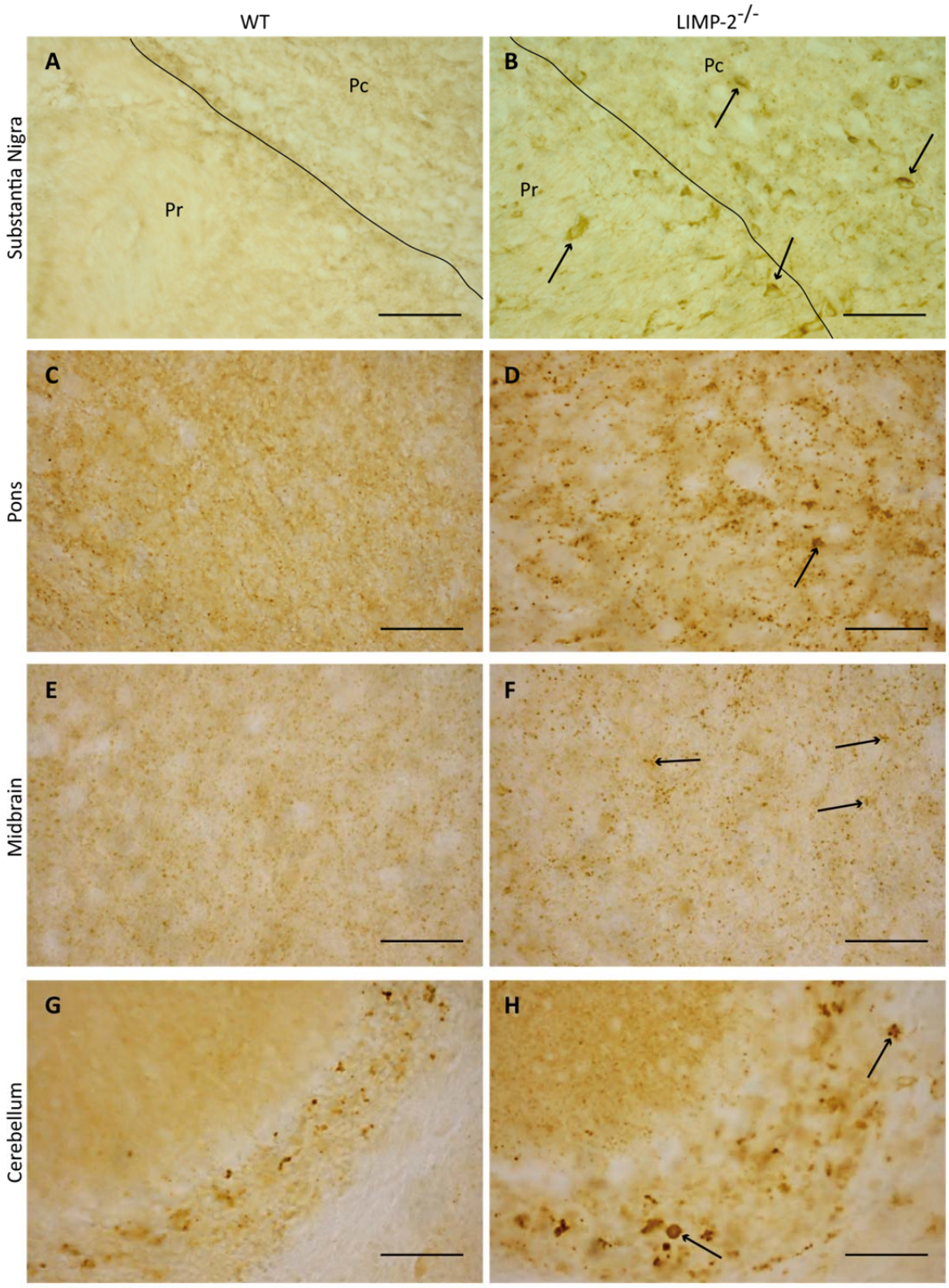

Figure 6.22 ***Accumulation of α-synuclein in several regions of murine brain deficient in LIMP-2.*** Representative free-floating histological sections of 6-month-old LIMP-2-deficient (LIMP-$2^{-/-}$) and wild-type (WT) mice stained for α-synuclein. **A/B-** Pathological aggregation of α-synuclein is observable within the pars compacta (Pc) and pars reticulata (Pr) in the substantia nigra of LIMP-$2^{-/-}$ mice. **C/D-** Accumulation of α-synuclein is evident within the pons as well as **E/F-** the midbrain of LIMP-$2^{-/-}$ mice. **G/H-** Accumulation of α-synuclein, while reduced in severity relative to other areas of the CNS, was also evident within the granular cell layer of the cerebellum. (Larger deposits of aggregated protein are indicated by arrows; scale bar = 50 µm).

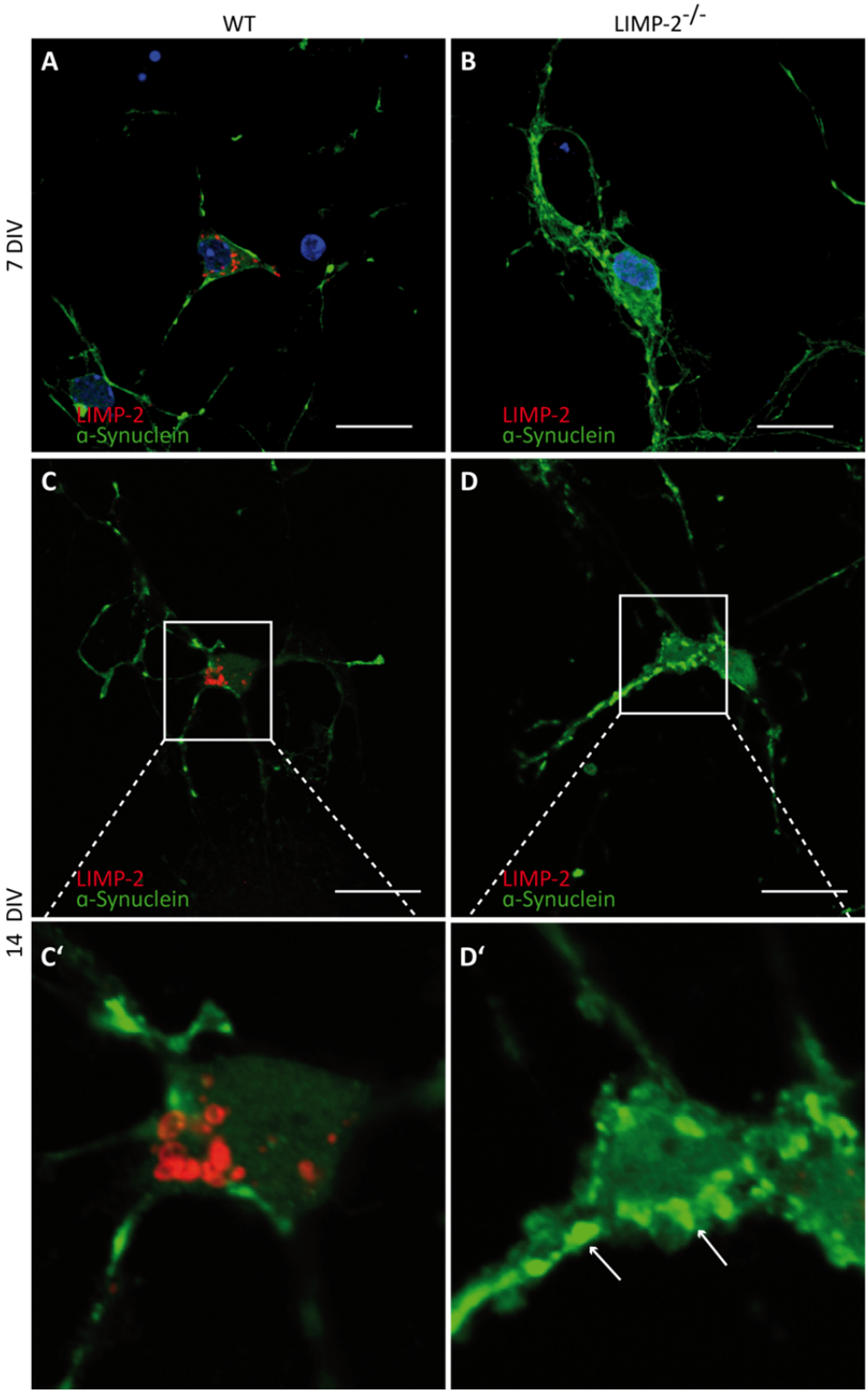

Figure 6.23 ***Accumulation of α-synuclein in primary cortical neurons.*** Immunofluorescence staining of α-synuclein (green) and LIMP-2 (red) in pure primary neuronal cultures, derived from the cortices of wild-type (WT) and LIMP-2-deficient (LIMP-$2^{-/-}$) littermates (scale bar = 20 µm). **A/B-** After 7 days *in vitro* (DIV) LIMP-$2^{-/-}$ neurons show large aggregates of α-synuclein. A substantial aggregation of α-synuclein within the soma and proximal dendrites could be observed (scale bar = 20 µm). **C/D-** Considerable accumulation of α-synuclein was also seen after 14 DIV. **C'/D'**- Digitally zoomed images; arrows indicate α-synuclein aggregates.

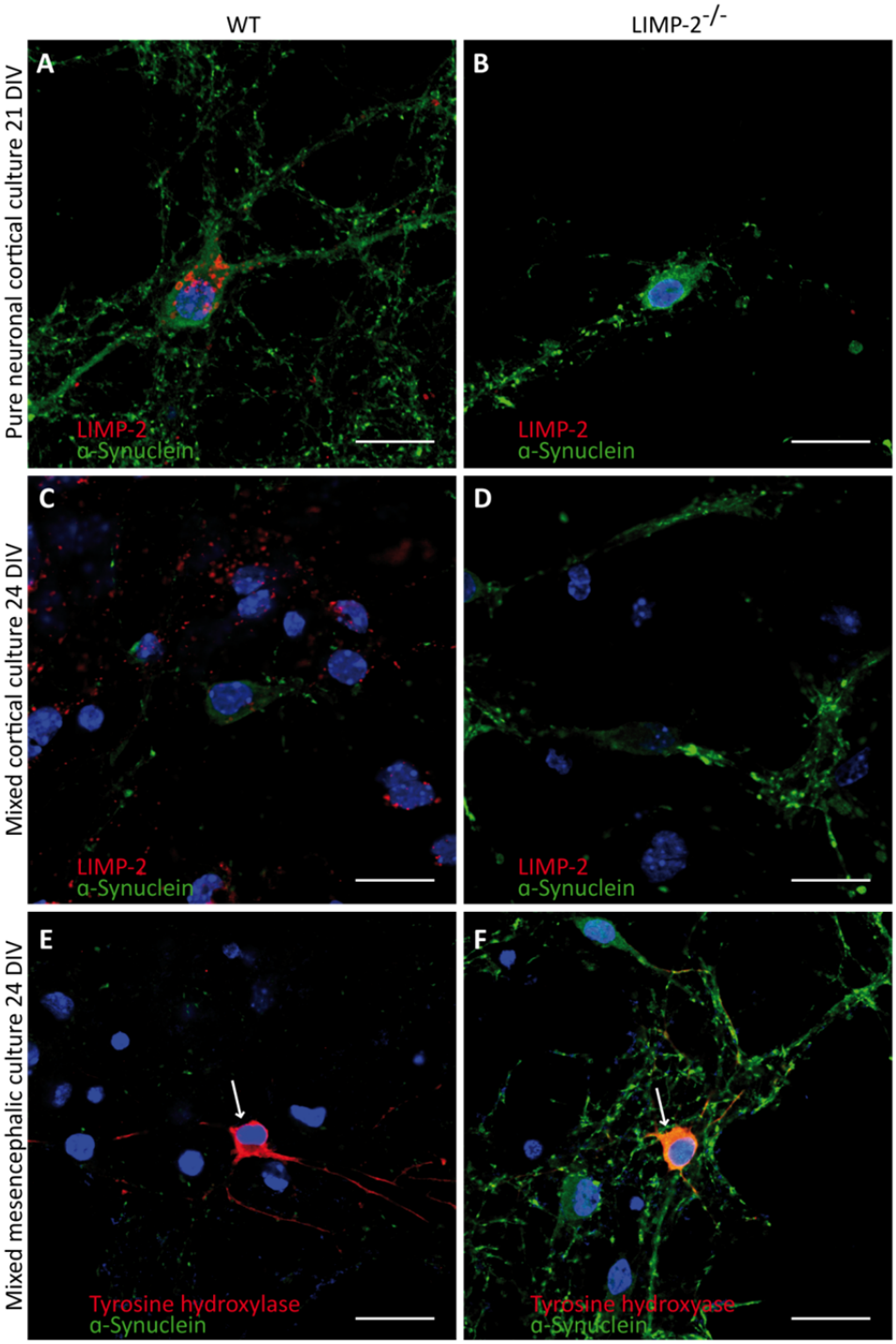

Figure 6.24 ***Accumulation of α-synuclein in older pure and mixed primary cultures.*** Primary neurons derived from the cortices or mesencephalons of wild-type (WT) and LIMP-2-deficient (LIMP-2$^{-/-}$) littermates were fixed after 21 or 24 days *in vitro* (DIV) as indicated. Immunofluorescence demonstrates the presence of α-synuclein (green) and LIMP-2 (red) vesicular staining. **A/B-** After 21 DIV significant neurite degeneration in surviving neurons as well as persistent somatal α-synuclein accumulation could be observed in pure neuronal cultures from LIMP-2$^{-/-}$ mice. **C/D**- Similarly, after 24 DIV aggregated α-synuclein was also evident in LIMP-2$^{-/-}$ mixed neuronal/glial cultures. **E/F-** Dopaminergic neurons from mixed mesencephalic cultures were identified by immunofluorescence staining with tyrosine hydroxylase (red). Some punctated staining of α-synuclein (green) is evident in WT neurons whereas mesencephalic neurons, particularly dopaminergic neurons, show larger aggregates of α-synuclein (arrows indicate the soma of dopaminergic neurons; scale bar = 20 µm).

6.8.1 Accumulation of soluble α-synuclein in LIMP-2-deficient brains

To examine the biochemical nature of the accumulated α-synuclein visualised in sections, sequential extraction of proteins using a triton-X 100 buffer for the extraction of soluble proteins and an SDS buffer for insoluble aggregates (methods 5.4.2) was employed. Using an antibody directed against wild-type α-synuclein LIMP-2-deficient mice show a tendency towards a decrease in soluble monomeric α-synuclein in the midbrain (fig. 6.25A/B). Furthermore, approximately 50 % of LIMP-2-deficient mice showed an accumulation of soluble oligomeric α-synuclein (fig. 6.25A, soluble fraction and 6.25B). No aggregation of insoluble α-synuclein was detected in LIMP-2-deficient mice (fig. 6.25A, insoluble fraction). Similar results were observed for lysates prepared from the pons from wild-type and LIMP-2-deficient mice (data not shown). A tendency towards a decrease in monomeric α-synuclein and conversely an accumulation of soluble oligomeric α-synuclein is observed when LIMP-2 is missing in murine brain.

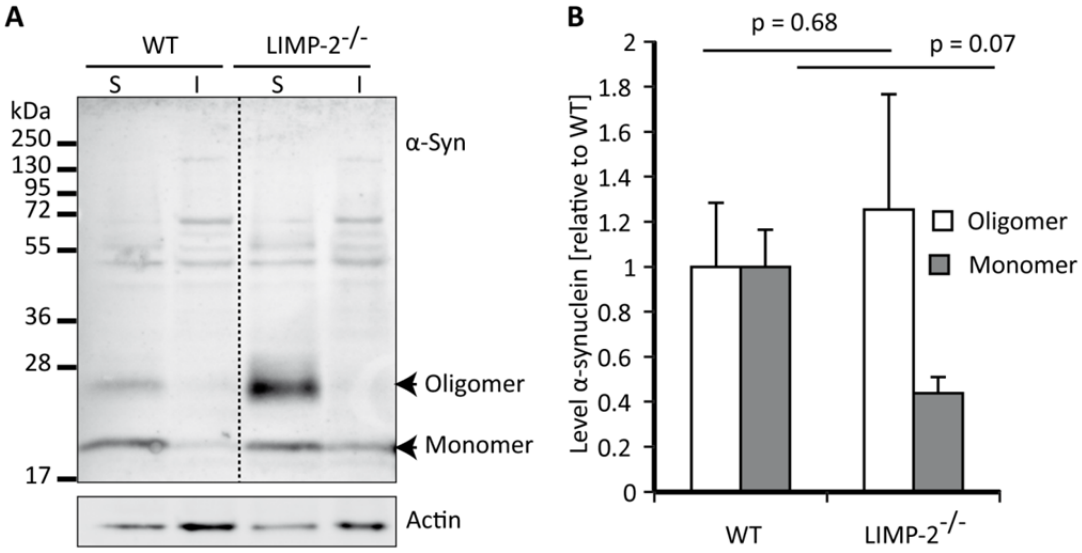

Figure 6.25 ***Sequential biochemical extraction reveals α-synuclein accumulation in LIMP-2-deficient midbrain.*** **A/B-** A representative immunoblot of brain lysates from wild-type (WT) and LIMP-2 knockout (LIMP-$2^{-/-}$) mice, subjected to biochemical extraction to separate soluble (S) and insoluble (I) aggregates. Western blot analysis using an antibody directed against α-synuclein (α-Syn) revealed a slight reduction in the monomeric form in the triton-X-100 fraction (soluble) of knockout samples, whereas an oligomeric form of α-synuclein was present in approximately 50 % of LIMP-$2^{-/-}$ samples. No changes in levels of monomeric or higher molecular weight aggregates were observed in insoluble fractions (arrows points to oligomeric and monomeric forms of α-synuclein; actin was used as a loading control). **B-** Quantification of soluble monomeric and oligomeric α-synuclein accumulated in WT and LIMP-$2^{-/-}$ midbrains. LIMP-$2^{-/-}$ mice show a tendency to have a decrease in levels of monomeric α-synuclein and conversely an increase in oligomeric α-synuclein (values normalised to actin are shown relative to expression in wild-type and presented as mean ± SEM; n ≥ 7 per genotype).

6.9 α-Synuclein associated neuropathology in LIMP-2-deficient brain

6.9.1 Shrinkage of dopaminergic neurons and neurites in the substantia nigra

Accumulation of soluble oligomers of α-synuclein was observed within the midbrain which has been shown to be particularly toxic to dopaminergic neurons (Lashuel et al., 2002; Volles and Lansbury, 2002). Additionally, immunohistological anaylsis revealed a significant amount of accumulated α-synuclein within the substantia nigra. Furthermore, medial levels of microgliosis and the presence of cellular shrinkage as well as eosinophilic spheroids within the substantia nigra indicate that dopaminergic neurons, the primary neuronal type within this region, may be affected in LIMP-2-deficient mice. Using immunohistochemical staining with a marker for dopaminergic neurons, tyrosine hydroxylase, the rate-limiting enzyme in catecholamine biosynthesis, shrinkage of perikarya within the substantia nigra pars compacta (fig. 6.26B) as well as a tendency towards an overall reduction in dopaminergic neurons within the substantia nigra (fig. 6.26C) was observed in LIMP-2-deficient murine brain. Interestingly, staining of the ventral tegmentum, a region also innervated by dopaminergic neurons, showed degeneration of neurites extending from the soma of shriveled neurons with condensed soma in LIMP-2-deficient mice (data not shown). Loss of LIMP-2 expression appears to dramatically affect the general health and morphology of dopaminergic neurons in murine brain.

6.9.2 Dendritic spine degeneration in LIMP-2-deficient mice

The accumulation of α-synuclein is known to cause degeneration of dendritic spines (Kramer and Schulz-Schaeffer, 2007). Build-up of α-synuclein oligomers was observed within the midbrain of LIMP-2-deficient mice. Therefore, using the Golgi-Cox staining method (methods 5.3.5.5), which randomly stains entire neurons, dendrites from the midbrain of wild-type and LIMP-2 knockout mice were identified. Analysis of dendritic processes revealed a potential reduction in spines on LIMP-2-deficient midbrain neurons (fig. 6.27A).

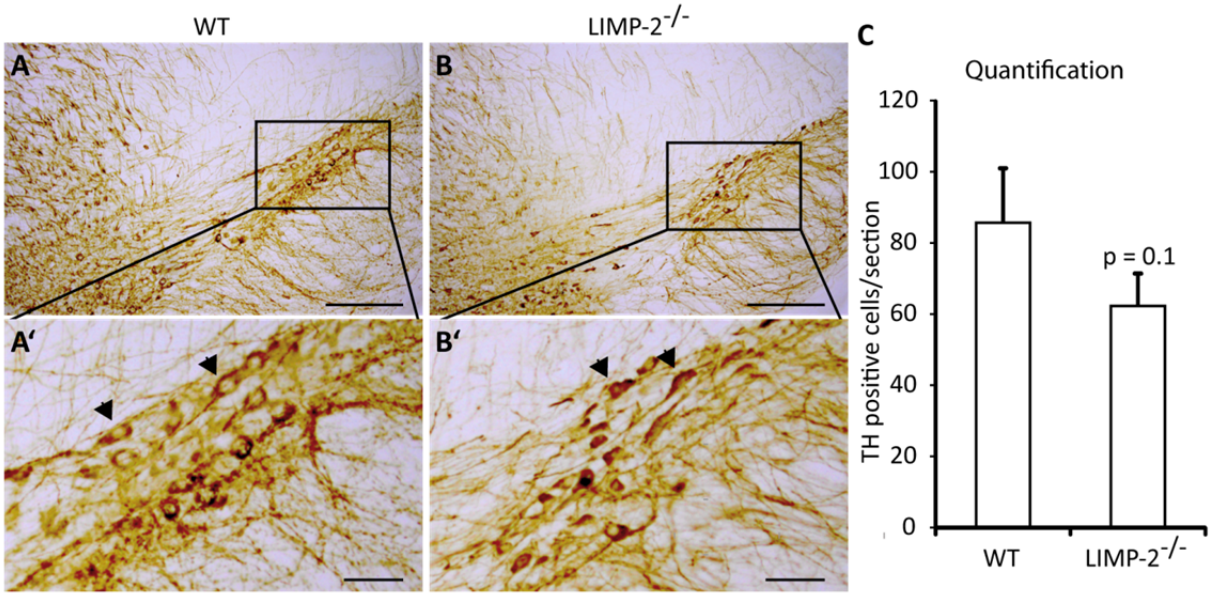

Figure 6.26 ***Shrinkage and degeneration of dompaminergic neurons in LIMP-2-deficient brain.*** **A/B-** Representative histological sections stained with the dopaminergic neuronal marker tyrosine hydroxylase showing the substantia nigra of 10-month-old wild-type (WT) and LIMP-2 knockout (LIMP-$2^{-/-}$) littermates. Arrows point to the somas of dopaminergic neurons within the pars compacta (outlined in black box). Cellular shrinkage was only evident in LIMP-$2^{-/-}$ sections. **A'/B'-** digitally zoomed pictures from regions outlined with black boxes (scale bars: **A/B** = 200 µm; **A'/B'** = 50 µm). **C-** Quantification of TH positive cells within the substantia nigra revealed a tendency towards a reduction in dopaminergic neurons in LIMP-$2^{-/-}$ mice when compared to their WT littermates (values shown are mean ± SEM; n = 3 per genotype, 5 sections per animal quantified. Quantification of samples was carried out in collaboration with H. Altmeppen, Institute of Neuropathology, University medical centre Eppendorf, Hamburg, DE].

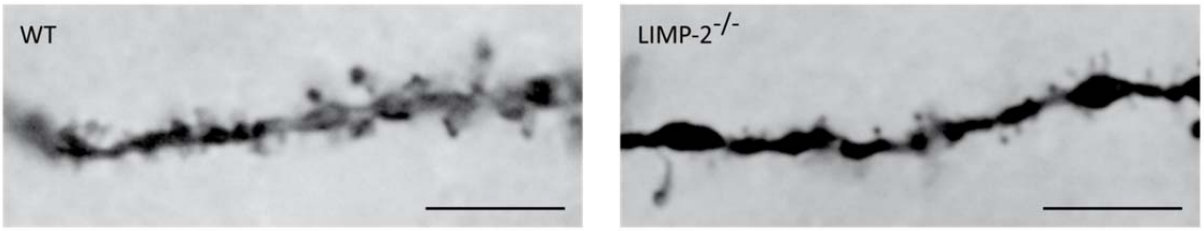

Figure 6.27 ***Golgi-Cox staining of midbrains showing potential dendritic spine degeneration in mice lacking LIMP-2 expression.*** Representative images of dendrites from the midbrain of a wild-type (WT) and LIMP-2-deficient (LIMP-$2^{-/-}$) mice showing a potential decrease in dendritic spine number (scale bar = 5 µm; n = 2 per genotype).

6.10 LIMP-2 deficiency causes anomalies in ubiquitin tagged proteins

The accumulation of α-synuclein in several regions of the murine CNS suggests that degradative mechanisms may be perturbed due to LIMP-2 deficiency. Monomeric proteins destined for degradation by the proteasome are tagged with a polyubiquitin chain (Thrower et al., 2000). However, aggregated proteins such as α-synuclein are also polyubiquitinated and then recognised by p62 for degradation by macroautophagy (Komatsu et al., 2007; Watanabe et al., 2012). Since α-synuclein is degraded both by the lysosome and the

ubiquitin proteasomal system and dysfunction of one usually leads to upregulation of the other (Ebrahimi-Fakhari et al., 2011), the accumulation of proteins tagged with polyubiquitin for degradation was assessed in the brains of LIMP-2 knockout mice. No significant changes in levels of polyubiquitinated proteins were detected in the triton soluble fraction from pons of LIMP-2-deficient mice when compared to their wild-type littermates (fig. 6.28A/C). Soluble lysates from other regions of the CNS showed similar results (data not shown). Additionally, no increase in insoluble high molecular weight tagged proteins was detected in LIMP-2-deficient pons lysates (fig. 6.28B/C) or in lysates from the midbrain, cerebellum and cortex (data not shown). However, a significant increase in polyubiquitination of a triton insoluble protein was observed at approximately 60 kDa (fig. 28B/C). A band of similar intensity was observed in the insoluble fraction from Parkinson´s disease mouse models overexpressing mutated human α-synuclein (A53T) and in another mouse model where wild-type murine α-synuclein (SNCA) is overexpressed (fig. 6.28B, SNCA and A53T). This increase in ubiquitination observed in immunoblots was supported by an increase in polyubiquitin staining within several regions of LIMP-2-deficient brains including the substantia nigra and pons (fig. 6.29). LIMP-2 deficiency leads to significant changes in the level of an unidentified insoluble polyubiquitinated protein within the CNS.

Due to the fact that insoluble protein may only be degraded by macroautophagy (Verhoef et al., 2002; Yamamoto and Simonsen, 2011) and not the proteasome it was necessary to assess if autophagy is affected within the CNS when there is a deficiency of LIMP-2. In fact, within the pons a significant increase in soluble p62 was detected via Western blot of approximately 20 % (fig. 6.30A/B), whereas no clear differences in p62 were observed in soluble lysates from the midbrain of the same mice (data not shown). Within histological sections, accumulation of p62 was observed in the cortex and substantia nigra. However, the most dramatic accumulation was observed in the pons (fig. 6.30C).

This evidence suggests that a deficiency in LIMP-2 causes the accumulation of aggregated insoluble protein that is tagged by chains of ubiquitin but cannot be effectively degraded by macroautophagy despite upregulation of p62.

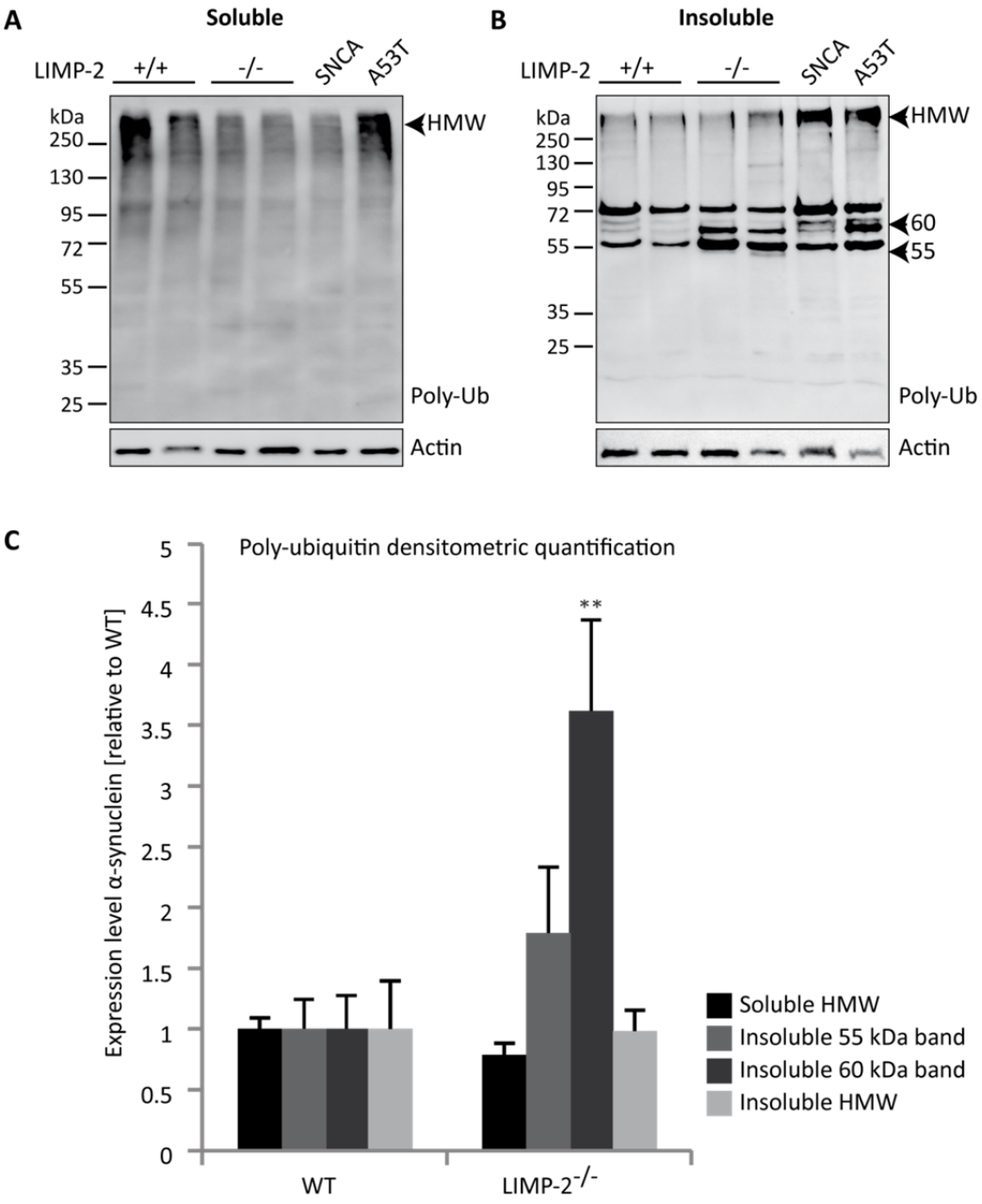

Figure 6.28 ***Anomalies in polyubiquitin labelled proteins in LIMP-2-deficient brain.*** **A/B-** Representative Western blot of lysates from the pons of wild-type (+/+) and LIMP-2 knockout (-/-) pons seperated into triton soluble (soluble) and triton insoluble (insoluble) fractions. Positive controls for α-synuclein mediated effects on polyubiquitination were lysates from the pons of a mouse overexpressing wild-type murine α-synuclein (SNCA) and a mouse overexpressing the mutated form of α-synuclein (A53T) (blots were stained for polyubiquitin, Poly-Ub. Actin was used as a loading control. HMW; high molecular weight smear of proteins; 60, 60 kDa band; 55, 55 kDa band). **A-** No changes were observed in the soluble fraction when comparing wild-type and LIMP-2-deficient lysates. A potential increase was observed in the lysate of A53T producing mice. **B-** No differences were observed in high molecular weight tagged proteins when comparing wild-type and LIMP-2 knockout lysates. However, a marked increase of larger polyubiquitin tagged proteins was noticable in lysates from SNCA and A53T overexpressing mice. Strikingly, a peculiar ubiquitination pattern of smaller proteins was noticable in LIMP-2 knockout lysates and in mutant (A53T) α-synuclein mice (arrow heads). **C-** Quantification of soluble and insoluble polyubiquitinated proteins in the pons of LIMP-2-deficient (LIMP-2-/-) and wild-type (WT) mice. A significant increase in an unidentified polyubiquitinated protein running at 55 KDa (**$p < 0.009$) was observed in LIMP-2-deficient mice when compared to their wild-type age matched controls ($n \geq 7$ per genotype).

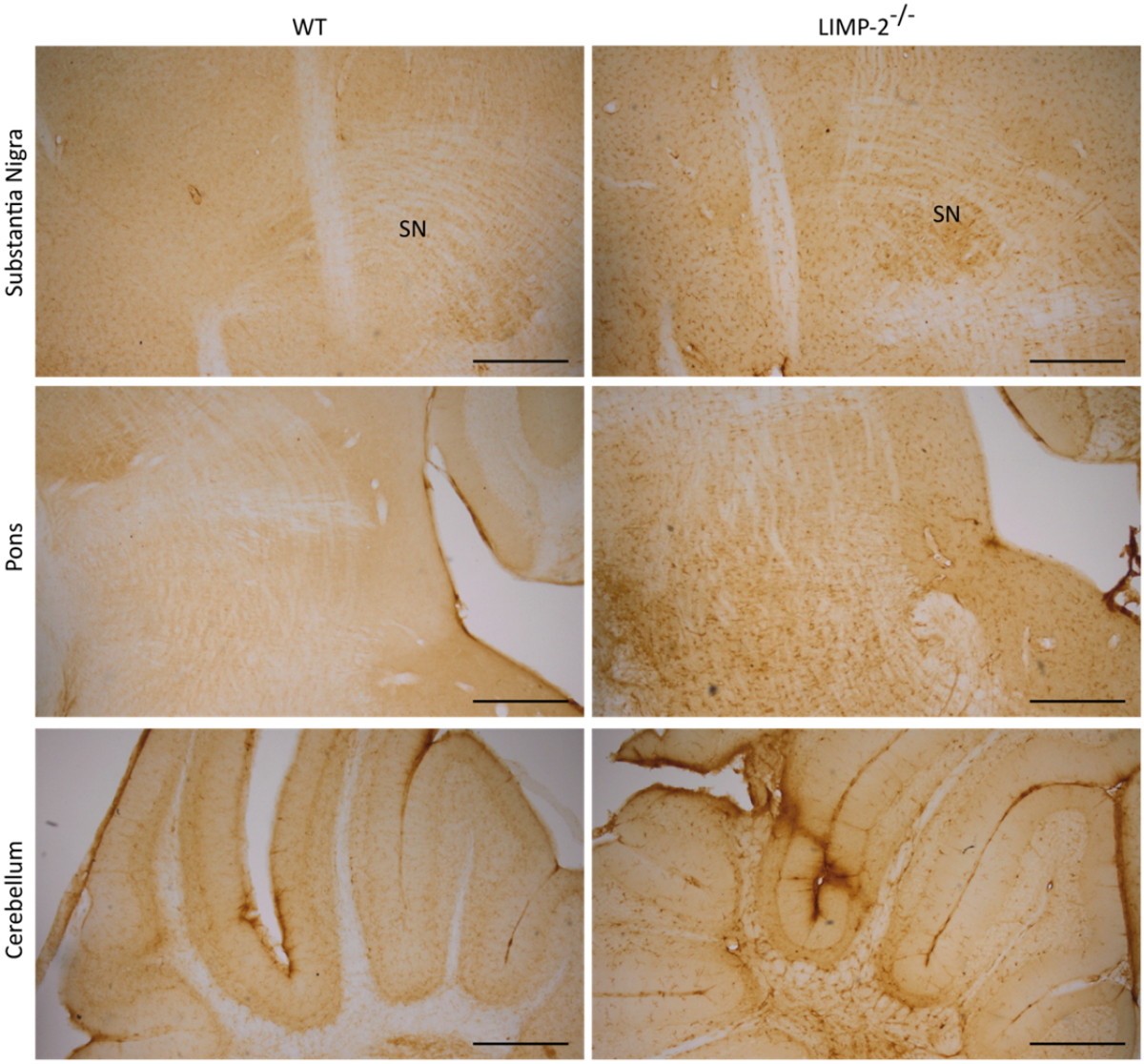

Figure 6.29 ***Accumulation of polyubiquitin labelled proteins in LIMP-2-deficient brain.*** Representative sections from 6-month-old wild-type (WT) and their LIMP-2-deficient (LIMP-$2^{-/-}$) littermates. Sections were subjected to immunohistological staining with a polyubiquitin antibody. Significant staining was observed throughout the central nervous system of LIMP-$2^{-/-}$ mice (n = 3 per genotype; SN, substantia nigra; scale bar = 500 µm).

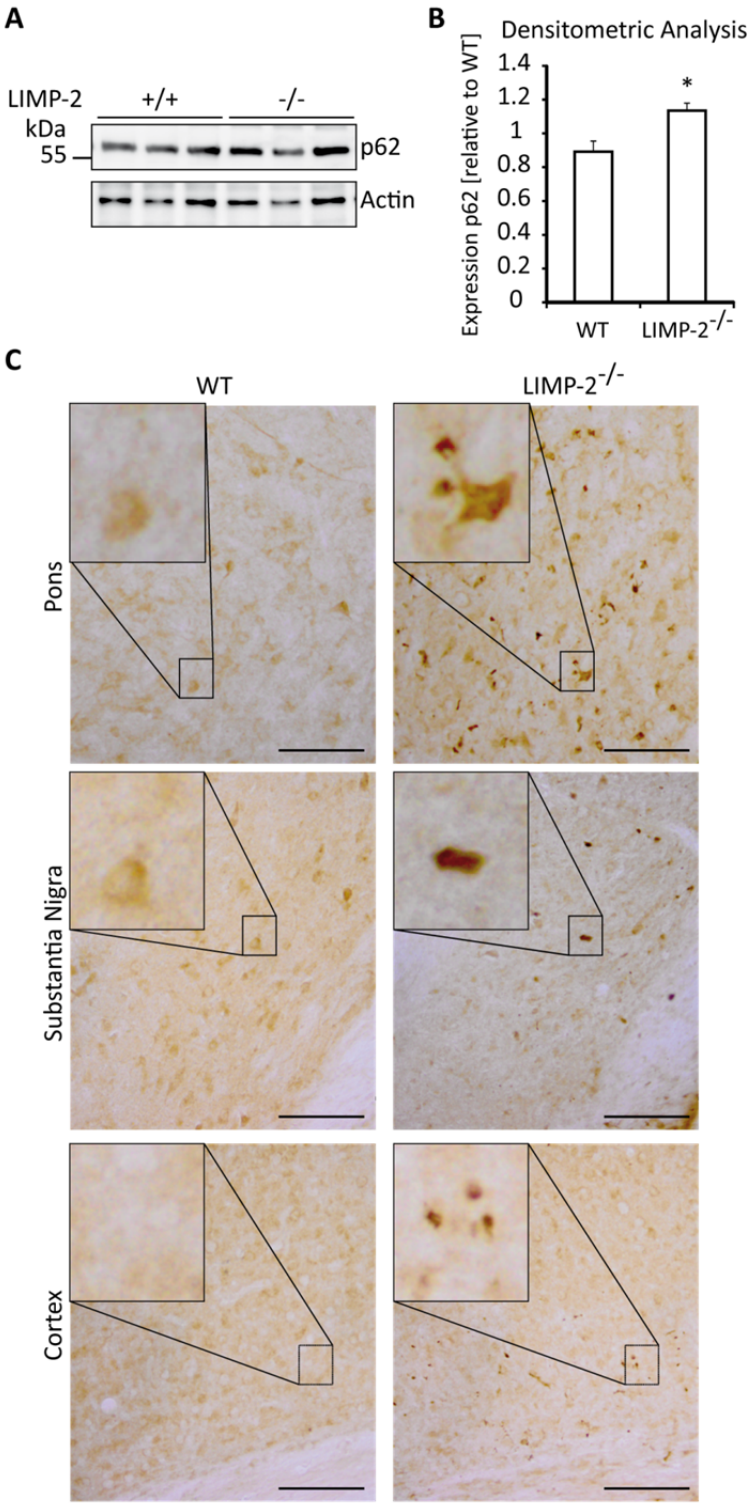

Figure 6.30 ***Upregulation of p62 in LIMP-2-deficient brains.*** **A-** Representative Western blot of soluble lysates from the pons of wild-type (+/+) and LIMP-2 knockout (-/-) mice. A significant increase in p62 signal was observed in LIMP-2 knockout animals (n = 3 per genotype). **B-** Densitometric analysis of lysates from the pons of wild-type and LIMP-2-deficient mice. A significant difference in the quantity of p62 was observed in knockout mice. (Values shown are relative to expression in wild-type samples expressed as mean ± SEM, normalised to actin, n = 3 per genotype, *p < 0.05). **C-** Representative immunohistological section from 10-month-old mice stained for p62. A substantial increase in p62 positive aggregates was visible in LIMP-2-deficient (LIMP-$2^{-/-}$) brains when compared to their wild-type (WT) littermates (scale bar = 100 µm; n ≥ 4 per genotype).

6.11 Summary of neuropathology in the CNS of LIMP-2-deficient mice

The absence of LIMP-2 causes an array of neuropathological symptoms in mice. In an attempt to assess if there is a correlation between the occurrences of pathology in numerous assays presented in this study sections were quantified relative to their perceived severity. Results of the analysis are outlined in table 6.3.

Table 6.3 ***Summary of pathological observations in the brain of LIMP-2-deficient mice when compared to wild-type littermates*** (n.d. = not defined; the number of plus symbols indicate the severity of pathology where '+' signifies its presence and '+++' denotes severe disease, whereas '-' specifies absence of any abnormalities).

Age (months)	*Region*	*GFAP*	*CD68*	*TUNEL*	*PAS*	*p62*	*α-Synuclein*
6	Cerebellum	++	+++	++	+++	n.d.	+
	Hippocampus	+	+	-	+	n.d.	-
	Pons	++	+++	+	++	n.d.	++
	Substantia Nigra	++	++	+	+	n.d.	+
	Cortex	+	+	-	+	n.d.	-
	Corpus Callosum	++	+++	+	++	n.d.	+
10	Cerebellum	++	+++	++	+++	+	+
	Hippocampus	+	+	-	+	-	-
	Pons	++	+++	++	++	+++	+++
	Substantia Nigra	++	++	-	+	++	++
	Cortex	+	+	-	+	+	-
	Corpus Callosum	+++	++++	+	++	+	++

6.12 LIMP-2 as a therapeutic target for Parkinson´s disease

Evidence from histological analysis, immunoblot analysis and primary neuronal cultures show that loss of LIMP-2 results in the accumulation of α-synuclein. Additionally, a reduction in activity of β-GC is thought to be responsible for the build-up of GluCer within the cell leading to retarded degradation of α-synuclein (Mazzulli et al., 2011; Sardi et al., 2011). To elucidate if an increased expression of LIMP-2 also affects the homeostasis of α-synuclein overexpression experiments were employed (methods 5.6.3 and 5.4.1).

LIMP-2 and α-synuclein were transiently expressed in HeLa cells. Overexpression of wild-type LIMP-2 led to a significant reduction of the steady-state level of endogenous and overexpressed α-synuclein (fig. 6.31A/B) and increased the ratio of post ER:ER forms of β-GC (fig. 6.31A lanes 3 and 5) when compared to overexpression of α-synuclein alone (fig. 6.31A lane 2). Furthermore, overexpression of LIMP-2 significantly increased the activity of β-GC (fig. 6.31C). Interestingly expression of a LIMP-2 mutant (LIMP-2(DDD)) incapable of binding β-GC (Blanz et al., 2010) also led to a slight reduction of α-synuclein (fig. 6.31A/B) while no changes could be observed in the post ER:ER β-GC ratio (fig. 31A lane 6) or enzyme activity (fig. 6.31C). Additionally, overexpression of LIMP-2 in conjunction with α-synuclein led to a significant increase in β-GC enzyme activity when compared to overexpression of LIMP-2 alone (fig. 6.31C).

The ability of overexpression of LIMP-2 to reduce the steady-state level of α-synuclein in HeLa cells was similar to results obtained from overexpression experiments in human dopaminergic neuroblastoma cells (SHSY-5Y), a frequently used cell culture model for research on α-synuclein metabolism. Overexpression of LIMP-2 led to an increase in β-GC activity in SHSY-5Y cells (fig. 6.32A/B). Additionally, overexpression of LIMP-2 (fig. 6.32C lanes 5 and 6) and LIMP-2(DDD) (fig. 6.31C lanes 7 and 8) also led to a reduction in the steady-state levels of coexpressed α-synuclein.

Likewise, increasing amounts of transfected LIMP-2 cDNA led to a decrease in both the wild-type (fig. 6.33A, lane 2 compared to lanes 6, 8, 10, 12) and a pathologically mutated form of α-synuclein (A53T) (fig. 6.33A, lane 3 compared to lanes 7, 9, 11, 13) when coexpressed in MEFs. A significant reduction in steady-state levels of wild-type α-synuclein may be achieved via overexpression of LIMP-2 (fig. 6.33B). Similar to results obtained in HeLa cells, increasing amounts of LIMP-2, when overexpressed in LIMP-2-deficient MEFs, led to an increased post-ER form of β-GC and a decreased level of α-synuclein (fig. 6.32C lanes 2 and 3).

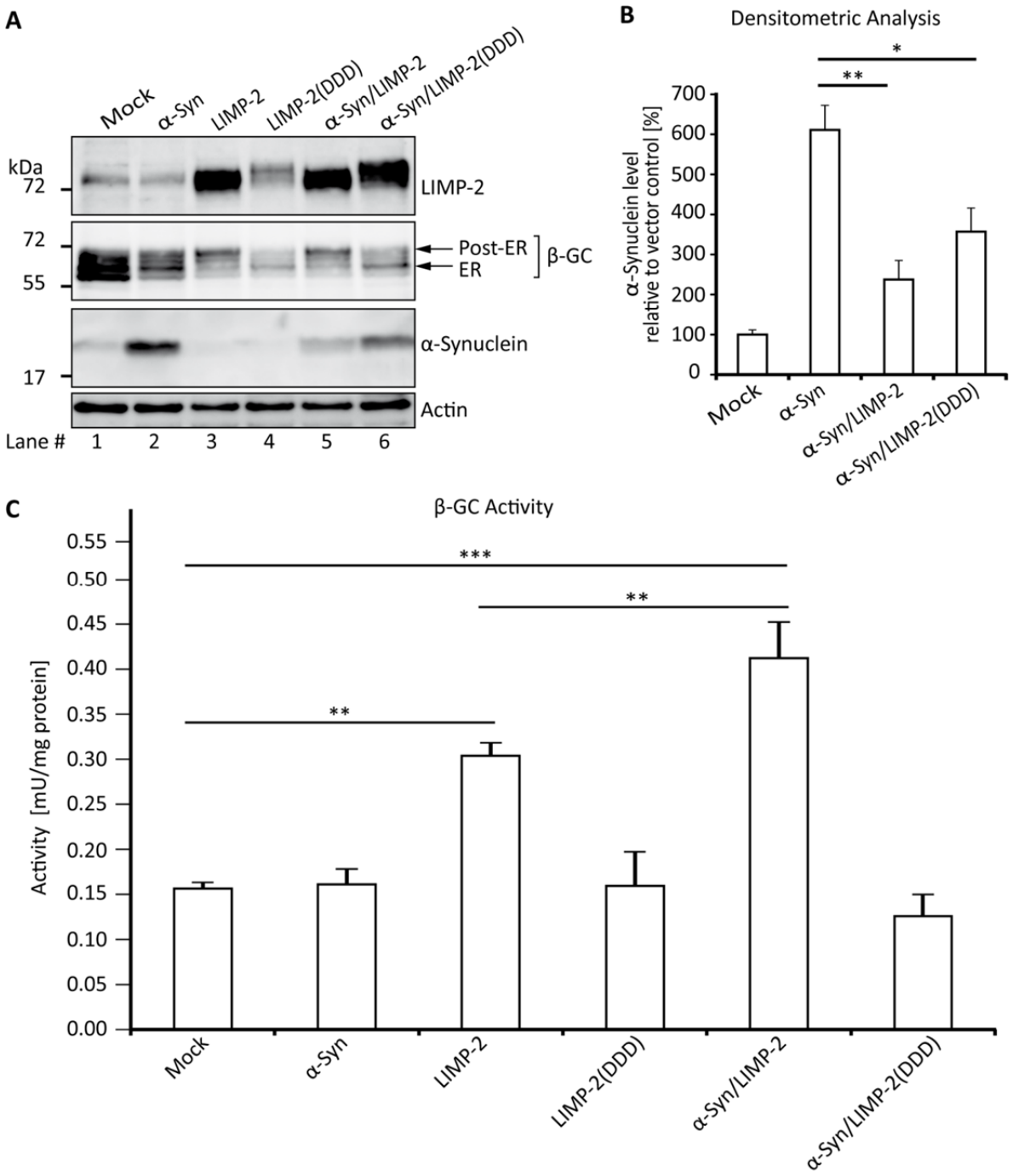

Figure 6.31 ***Increased expression of LIMP-2 modulates the activity and trafficking of β-GC resulting in a reduction in steady-state levels of α-synuclein.*** **A-** Western blot analysis of α-synuclein (α-syn) expression after coexpression with LIMP-2 or LIMP-2(DDD) in HeLa cells. Overexpression of LIMP-2 but not LIMP-2 (DDD) led to a decrease in ER β-GC. Both LIMP-2 and LIMP-2(DDD) were capable of decreasing the level of α-synuclein. (In order to keep the amount of transfected cDNA constant, reactions where α-synuclein, LIMP-2 or LIMP-2(DDD) should be expressed alone, an equal amount of a plasmid expressing eGFP was cotransfected). **B-** Overexpression of LIMP-2 led to a significant reduction in the detectable amount of α-synuclein. Although the effect was not as pronounced, a reduction in α-synuclein levels was also achieved via overexpression of LIMP-2(DDD). (Values are normalised to expression in vector control and presented as the mean ± SEM; n = 3; $^{**}p < 0.01$; $^{*}p < 0.05$). **C-** Activity assay for β-GC in HeLa cells. A significant increase in enzyme activity is achieved when LIMP-2 but not LIMP-2(DDD) is overexpressed. An even more dramatic increase in activity of β-GC is observed when LIMP-2 is coexpressed with α-synuclein (α-syn). (Values shown are actual activity units presented as the mean ± SEM; n = 6; $^{***}p < 0.001$ $^{**}p < 0.01$).

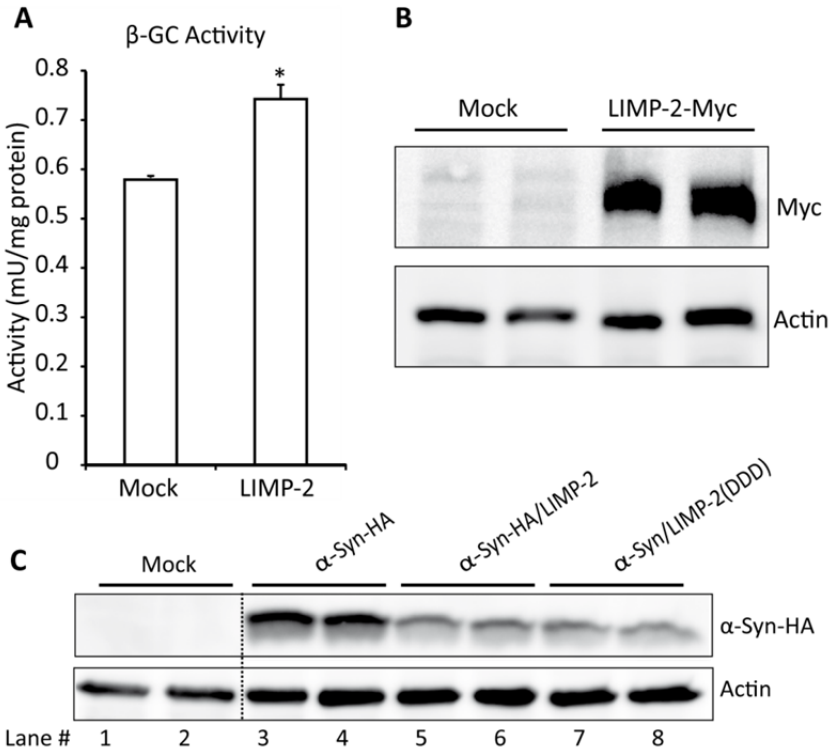

Figure 6.32 ***Overexpression of LIMP-2 increases the activity of β-GC and reduces the steady-state of α-synuclein in human SHSY-5Y cells.*** **A-** A β-GC activity assay indicated a significant increase in the activity of β-GC after overexpression of LIMP-2 (values shown are actual activity units presented as mean ± SEM; n = 2; *$p < 0.05$). **B-** Overexpression of myc tagged LIMP-2 was detected in lysates from duplicate transfections. Actin was used as a loading control. **C-** Overexpressed α-synuclein with a HA tag (α-syn-HA) is reduced when both LIMP-2 and LIMP-2(DDD) are coexpressed. Each transfection was performed in duplicate. Actin was used as a loading control (in order to keep the amount of transfected cDNA constant reactions where α-synuclein, LIMP-2 or LIMP-2(DDD) should be expressed alone, an equal amount of a plasmid expressing eGFP was cotransfected).

An increase of GluCer concentration is thought to directly influence the degradation of α-synuclein. Furthermore, in a pathogenic loop, increased concentration of α-synuclein is thought to decrease activity of β-GC in the lysosome leading to further build-up of GluCer in the cell (Mazzulli et al., 2011). Therefore, by decreasing the synthesis of GluCer within the cell, the clearance of α-synuclein may be potentially enhanced. Thus, MEFs overexpressing wild-type α-synuclein (fig. 6.33A lane 2) or a construct carrying the A53T pathogenic mutation (fig. 6.33A lane 3) were treated once for 48 hours with the glucosyltransferase synthase inhibitor miglustat. A slight increase in the steady-state level of both wild-type and mutated α-synuclein was observed after treatment with miglustat (fig. 6.33 lanes 4 and 5) However, repitition of treatment in MEFs did not show any significant differences in the steady state levels of α-synuclein after miglustat treatment.

In a similar experiment, endogenous α-synuclein levels within primary neurons from wild-type and mice overexpressing murine α-synuclein (α-syn-Tg) were measured with or without treatment over a 10 day period. Immunofluorescence showed, as expected, an increase in α-synuclein levels in neurons from α-syn-Tg mice when compared to wild-type mice (fig. 6.34A/C). However, treatment of neurons with miglustat did not change the steady-state levels of α-synuclein in wild-type (fig. 6.34B) or α-syn-Tg mice (fig. 6.34D).

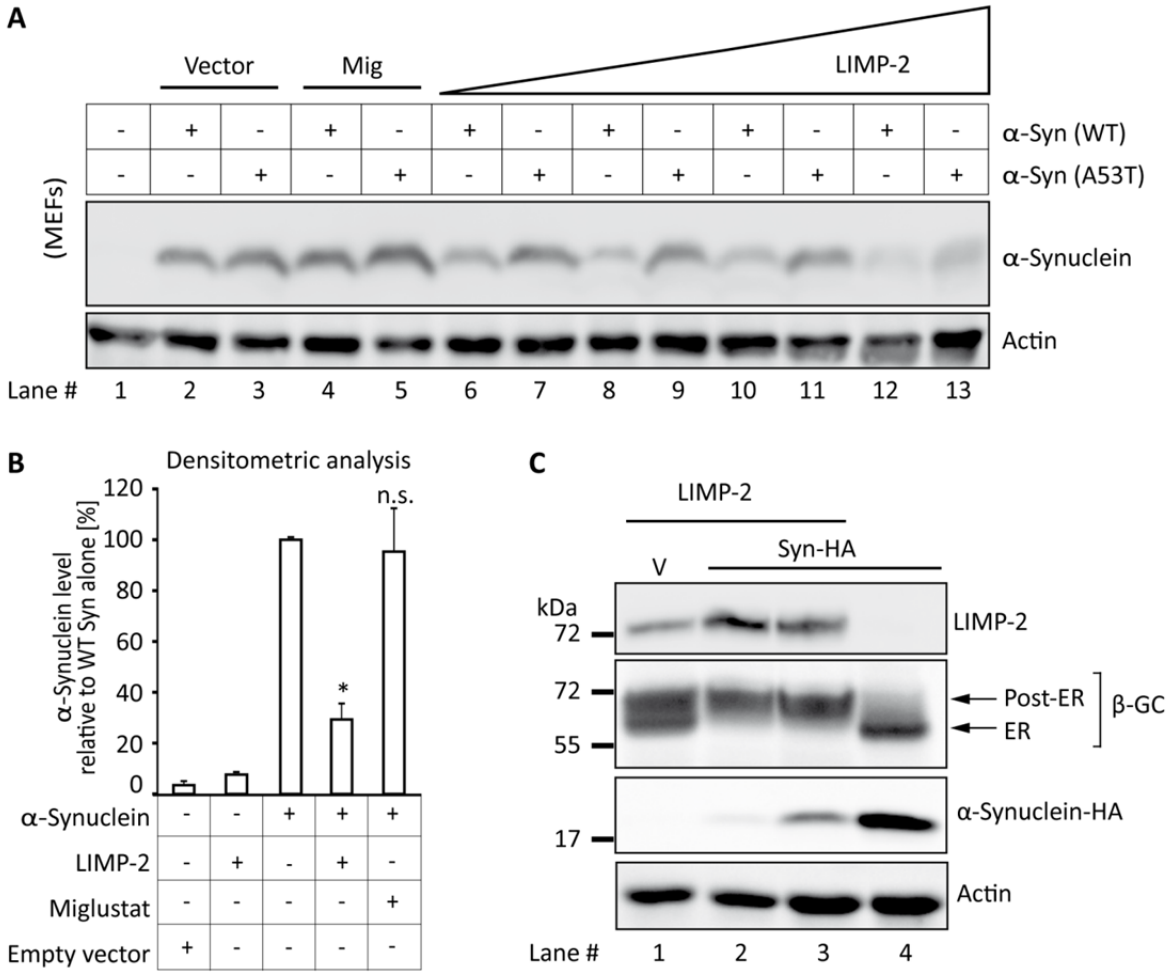

Figure 6.33 ***Increased expression of LIMP-2 but not short term treatment with miglustat directly affects the steady-state levels of α-synuclein.*** **A-** Western blot analysis of overexpression of wild-type α-synuclein (α-syn(WT)) and mutated (α-syn(A53T)) in MEFs after treatment with 10 µm miglustat or coexpression with increasing amounts of LIMP-2 (1, 2, 3, 5 ug cDNA). Miglustat had no effect on the steady-state of α-synuclein. Increasing amounts of LIMP-2 cDNA led to decreasing levels of both α-syn(WT) and α-syn(A53T). (In order to keep the amount of transfected cDNA constant reactions where α-synuclein, LIMP-2 or LIMP-2(DDD) should be expressed alone, an equal amount of a plasmid expressing eGFP was cotransfected; actin was used as a loading control; Mig, miglustat). **B-** Densitometric analysis of α-synuclein levels in MEFs after coexpression with LIMP-2 or treatment with miglustat (Values normalised to expression in wild-type and presented as mean values ± SEM; n = 3 per sample; n.s. = not significant, $p < 0.05$). **C-** Western blot analysis of α-synuclein tagged with HA (α-synuclein-HA) in individual MEF clones expressing differential levels of LIMP-2. Cells were stably transfected with α-synuclein-HA. Single clones were picked and tested for LIMP-2 and α-synuclein-HA expression. An increased amount of α-synuclein was detected in cells with lower LIMP-2 expression. ER and post-ER forms of GBA are highlighted with arrows. Actin was used as a loading control. (V, vector only).

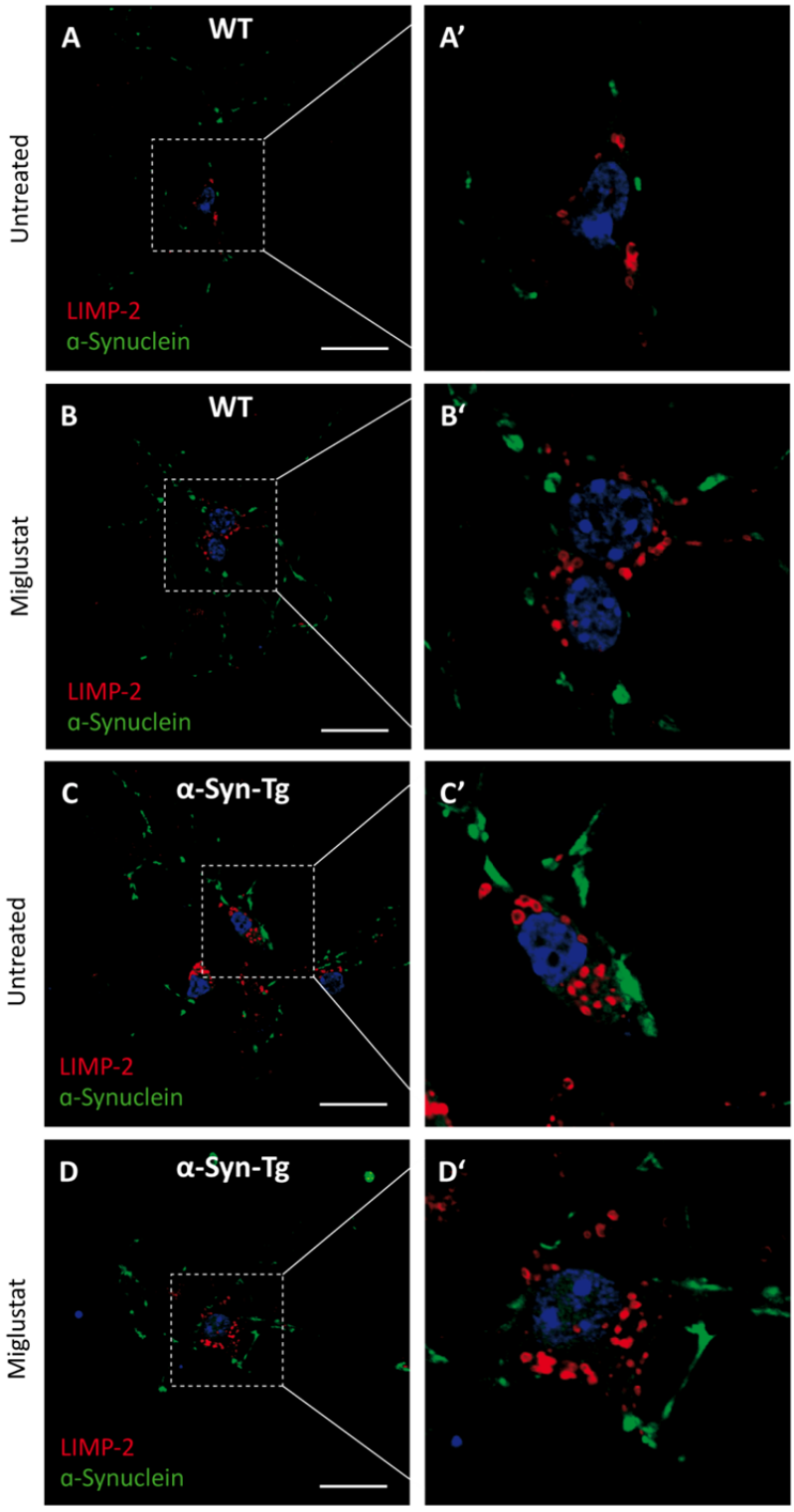

Figure 6.34 ***Short term treatment with miglustat does not affect the steady-state levels of α-synuclein in primary neurons.*** Primary neurons treated for 10 days with 10 µM miglustat every second day followed by fixation after 14 days *in vitro.* **E/G-** Immunofluorescence showed an increase in α-synuclein (green) punctate staining after miglustat treatment in wild-type neurons (WT). **F-** Increased amount of α-synuclein staining was observed in primary neurons from mice overexpressing a transgene of α-synuclein (α-Syn-Tg). **H-** However, miglustat treatment did not influence α-synuclein levels after treatment with miglustat (DAPI stains nuclei blue; scale bar = 10 µm).

The reduction of α-synuclein levels appears to be proportional to the expression of LIMP-2. By increasing the delivery of β-GC to the lysosome, via overexpression of LIMP-2, the intralysosomal degradation of α-synuclein appears attenuated. LIMP-2 expression directly affects the steady-state expression of α-synuclein. However, short-term reduction of GluCer levels in MEFs or neurons using miglustat treatment did not succeed in reducing α-synuclein levels.

6.13 LIMP-2 expression in Parkinson`s disease

The pathogenic loop created as a consequence of reduced trafficking of β-GC to the lysosome caused by α-synuclein may be overcome via overexpression of LIMP-2. This may prove to be a successful compensatory mechanism through which the cell could cope with α-synuclein overloading. Therefore, midbrains from healthy and PD patients were assessed for changes in levels of LIMP-2 using immunohistochemistry. LIMP-2 is expressed in dopaminergic neurons within the substantia nigra (fig. 6.35A). However, while LIMP-2 staining appears more condensed within the midbrain of PD patients when compared to healthy brain (fig. 6.35B), quantification of total LIMP-2 levels in the substantia nigra revealed no descernable differences in expression (data not shown).

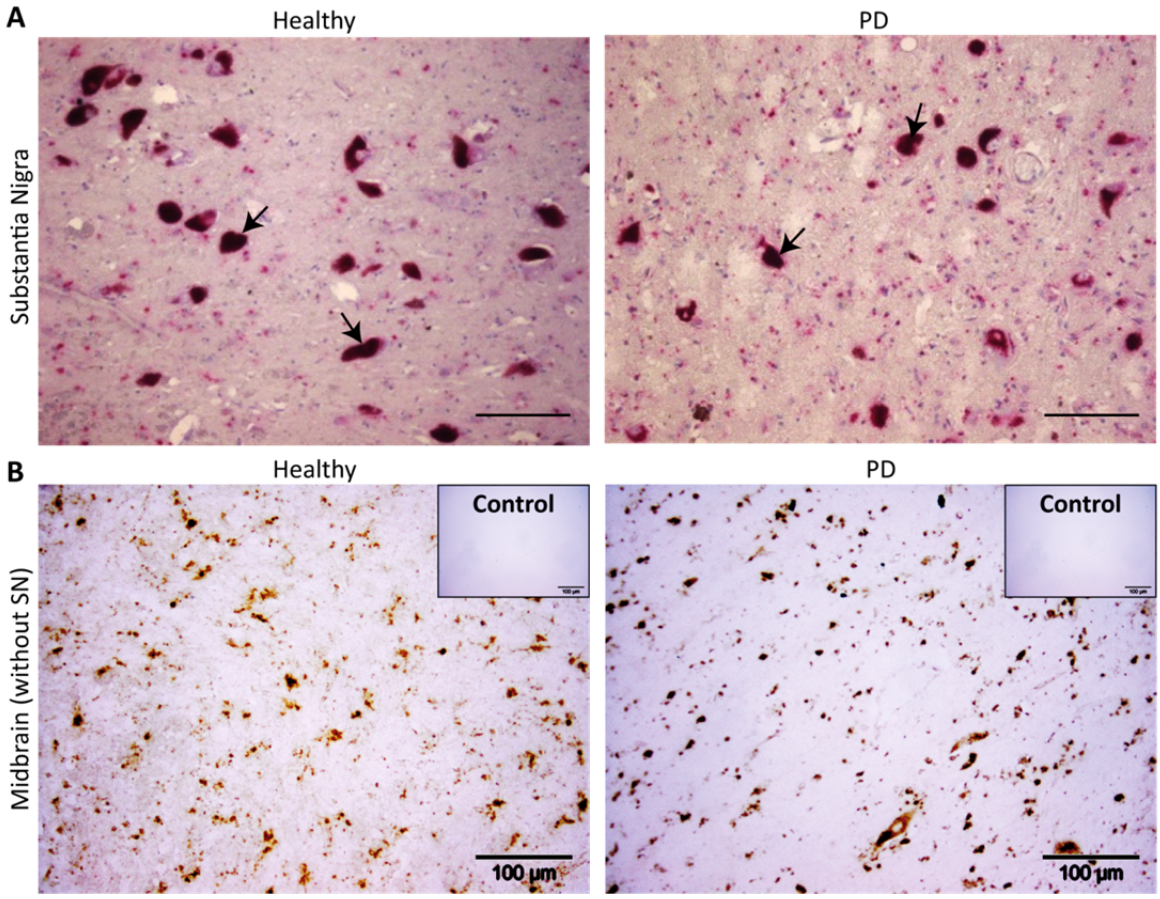

Figure 6.35 ***LIMP-2 immunological staining in the substantia nigra of Parkinson's disease and control brains.*** Representative immunohistological staining from human midbrain/substantia nigra sections from a healthy person with no history of neurological disorders (healthy) and patients diagnosed with Parksinson`s disease (PD) (n = 7 controls and n = 6 diseased brains; scale bar = 100 µm). **A-** LIMP-2/ FastRed labelling of substantia nigra. Dopaminergic neurons (arrows) express LIMP-2 (red) in healthy and PD brain. Cells surrounding dopaminergic neurons also express LIMP-2 (Fast red labelling was carried out in collaboration with H. Altmeppen, Institute of Neuropathology, University medical centre Eppendorf, Hamburg, DE9. **B-** LIMP-2/DAB labelling of midbrain. LIMP-2 positive staining appears to be more concentrated and darker in PD brain. The image shown was obtained from a region directly adjacent to the substantia nigra (inset: control staining showing no non-specific binding of the secondary antibody; scale bar = 100 µm).

7 Discussion

Despite the well-known role of LIMP-2 as a receptor for delivery of β-GC to lysosomes little is known about its function in the CNS. The data presented in this work reveal a distinct relationship between the level of LIMP-2 expression and the clearance of α-synuclein intimately connected to the trafficking and hydrolytic activity of β-GC within the lysosomes of neurons. Dysfunction of β-GC causes Gaucher disease (Brady et al., 1966), the most frequent lysosomal storage disorder that is genetically linked to PD (Westbroek et al., 2011) and other synucleinopathies such as Lewy body disease (Clark et al., 2009; Goker-Alpan et al., 2006). A reduction in β-GC activity was previously reported in spleen, liver and MEFs deficient in LIMP-2 (Reczek et al., 2007). Interestingly, loss of β-GC hydrolytic activity as well as accumulation of its substrate GluCer is associated with the development of PD (Gegg et al., 2012; Mazzulli et al., 2011). Based on this hypothesis, the mistrafficking and loss of β-GC activity due to deficiency of LIMP-2 in murine brain and its putative role in the development of synucleinopathy was determined.

A knockout mouse of LIMP-2 (Gamp et al., 2003) was used in order to characterise its *in vivo* function in brain. An appreciable advantage of using mice deficient in a single protein is the possibility to elucidate critical functions of a protein within an organism. The connection between β-GC and LIMP-2 coupled with the distinct relationship between the enzyme's activity and the development of PD prompted reanalysis of LIMP-2-deficient mice for signs of a neurological phenotype and more specifically irregularities in α-synuclein levels. However, LIMP-2 mice were previously backcrossed into the C57BL/6J strain from Harlan which are reported to have a spontaneous deletion of the α-synuclein gene and thus are incapable of showing signs of synucleinopathy (Specht and Schoepfer, 2001). In this study, the effect of LIMP-2 deficiency in murine brain from mice backcrossed into the C57BL/6N strain from Charles River was analysed.

7.1 β-GC is mistrafficked in neurons and astrocytes deficient in LIMP-2

The lysosomal hydrolase β-GC is clearly missorted in cells of the CNS when LIMP-2 is missing. Gaucher type 2/3 patients (Sidransky et al., 1992; Sidransky et al., 1996) as well as mouse models for the disease (Enquist et al., 2007; Tybulewicz et al., 1992; Xu et al., 2003) exhibit

severe neurological symptoms attributed to reduction in β-GC activity (Brady et al., 1966). Secretion and thus low tissue levels of β-GC was previously reported in fibroblasts and macrophages deficient in LIMP-2 (Reczek et al., 2007). In this study a significant reduction in the activity of β-GC was observed in cells of the CNS from LIMP-2-deficient mice. In Western blots of lysates from brain as well as primary glial and neuronal cultures, where LIMP-2 was absent, the enzyme itself was barely measurable. Additionally, no β-GC was detected in immunofluorescence studies of LIMP-2-deficient neurons. The absence of LIMP-2 led to a dramatic decrease in activity and steady-state levels of β-GC in the CNS of mice.

Strikingly, in this study LIMP-2 was not detectable in cultured activated wild-type microglial cells positive for CD68, whereas clear vesicular staining was detected in both astrocytes and neurons. It remains uncertain whether LIMP-2 is expressed in resting microglia. Double immunofluorescence of LIMP-2 with a general microglial marker, such as Ionized calcium-Binding Adapter molecule 1 (Iba1), in histological sections is necessary to clarify this point. Interestingly, previous studies have reported reduced β-GC protein levels in lysates from cultured macrophages which was not as pronounced as in fibroblasts (Reczek et al., 2007). Such findings point to a cell type specific transport route of β-GC, independent of LIMP-2, particularly in cells of monocytic origin. Since data presented in this thesis indicate that LIMP-2-deficient brains show dramatic microglial activation in histological sections one could speculate that the residual β-GC activity observed in activity assays is due to significant microglia activation in brain observed via immunohistochemistry. However, further studies on β-GC trafficking in isolated brain cells are needed to clarify the cell type specific role of LIMP-2 within this process. Experiments with pure microglial cultures would help in the elucidation of other trafficking mechanisms/players employed by β-GC. Using a fluorescent probe (Inhibody®), designed to detect active β-GC (Witte et al., 2010), microglial cells isolated from brain or from cultures may be assessed for their enzyme content via flow cytometry or fluorescent microscopy. A pull-down assay of β-GC with lysates from pure cultures of microglial cells would help in the identification of other transporter molecules involved in LIMP-2 independent transport of the enzyme.

7.2 Changes in lysosomal function in the CNS of LIMP-2 knockout mice

Several factors relating to lysosomal function were altered in the brains of LIMP-2-deficient mice. A slight elevation of LAMP-1 and a more dramatic increase in levels of cathepsin D observed in immunoblots and immunohistochemistry correlates with previous studies in neuronopathic Gaucher mouse models (Vitner et al., 2010). The observed elevated levels of cathepsin D can be attributed to activation of microglial cells. Increased lysosomal proteolytic activity in response to pathological processes in surrounding tissue but not as a result of decreased β-GC activity is observed when microglial cells are activated (Vitner et al., 2010). Elevated levels of LAMP-1 and LAMP-2 can probably also be attributed to the increase in number of activated microglial cell in LIMP-2-deficient brain, as double immunofluorescence studies of both proteins with cathepsin D showed high levels of both proteins in the same cell type (data not shown). Cathepsin D is thought to be a protease responsible for degradation of α-synuclein (Cullen et al., 2009; Qiao et al., 2008; Sevlever et al., 2008) and LAMP-2, specifically isoform LAMP-2a, plays a major role in the transport of α-synuclein into the lysosome (Cuervo et al., 2004). Interestingly, oligomeric forms of α-synuclein are known to be exocytosed from neurons and taken up by microglial cells thereby activating them (Kim et al., 2013). Furthermore, activated microglia have been shown to sequester extracellular toxic α-synuclein into their lysosomes thereby potentially enhancing its clearance (Bae et al., 2012). However, while the increase in cathepsin D observed in microglia cells of LIMP-2-deficient mice may help in the clearance of α-synuclein, it is unlikely that LAMP-2 plays a critical role. This is due to the fact that LAMP-2a transports monomeric α-synuclein across the lysosomal membrane and not its oligomeric form (Cuervo et al., 2004).

Additionally, LIMP-2-deficient mice showed a significant increase in lysosomal hydrolytic activity which is similar to findings in mice deficient in other lysosomal proteins such as the chloride/proton transporter CLC-7 (Kasper et al., 2005) and alpha-mannosidase (Blanz et al., 2008). More specifically, activity of α-mannosidase and β-hexosaminidase were significantly increased in pons of mice lacking LIMP-2 but only slightly elevated in the midbrain. Furthermore, total β-glucosidase activity (β-GC and GBA2) was significantly less in the pons when compared to the midbrain of LIMP-2-deficient mice. Interestingly, higher levels of α-synuclein accumulation and p62 deposits were observed in the pons when compared to

the midbrain which signifies a relationship between perturbed lysosomal function and neuropathological changes in LIMP-2-deficient mice. Further experiments including enzyme activity assays of other regions of LIMP-2-deficient mice are necessary in order to establish if a general connection between neuropathology and lysosomal dysfunction occurs as a result of LIMP-2 deficiency. Finally, immunofluorescence of lysosomal hydrolases in conjunction with neuronal and glial markers is necessary in order to determine in which cell type(s) lysosomal hydrolytic function is altered.

7.3 Lipid and carbohydrate-conjugate accumulation in LIMP-2-deficient brains

This study shows that mistrafficking of β-GC in LIMP-2-deficient murine brain and primary neurons results in a significant decrease in active enzyme causing accumulation of PAS positive carbohydrate-conjugates and elevated levels of Bodipy®493/503 stained lipids in brain and primary neurons, respectively. Even though Bodipy®493/503 has been used to stain for accumulated GlcCer in primary cultured neurons (Mazzulli et al., 2011) further detailed lipid analysis should be carried out in order to identify the causative lipids accumulating in LIMP-2-deficient brains.

PAS staining of carbohydrate-conjugates was used to indirectly assess the presence of GluCer accumulation in the CNS of LIMP-2-deficient mice. Extensive accumulation of PAS positive storage material was observed throughout the brain of knockout mice. This was particularly acute within the myelinated regions such as the corpus callosum and the white matter tracts of the cerebellum where the highest concentration of activated microglial cells was observed. Incidentally, in a knockout mouse of β-GC that shows severe neuropathology which led to premature death around post-natal day 21, loss of the enzyme was not crucial for activation of microgliosis. However, accumulation of material within microglia cells resulted in a decrease in their number and exacerbated the severity and progression of the disease (Enquist et al., 2007). Therefore, microglia cells probably engulf storage material exocytosed from cells and in some cases dead cells that have potentially accumulated GluCer. Interestingly, previous studies have outlined the ability of both wild-type and LIMP-2 knockout fibroblasts and macrophages to engulf extracellular β-GC, thereby restoring a small percentage of enzyme to the lysosome (Reczek et al., 2007). Therefore, in addition to the possible LIMP-2-independent trafficking of β-GC to the lysosome, activated microglial cells,

that are phagocytic in nature (review: Banati et al., 1993), may take up secreted enyzme from the parenchymal space. Furthermore, similar to microglial cells engineered to have normal levels of β-GC activity in a type 2 Gaucher disease model (Enquist et al., 2007), LIMP-2-deficient microglial cells may still play a crucial protective role in the diseased tissue by engulfing and degrading exocytosed GluCer from surrounding tissue. Such a theory would help explain the differences in severity of presentation of neurological symptoms between Gaucher mice completely deficient in β-GC (Enquist et al., 2007; Tybulewicz et al., 1992) and LIMP-2-deficient mice where the enzyme is mistrafficked.

In order to clarify in which cell population(s) carbohydrate-conjugate storage occurs within the LIMP-2-deficient CNS, PAS staining combined with a Nissl stain would prove useful for the identification of accumulation within neurons. Additionally, the severity of carbohydrate storage within the CNS did not intensify between 6 and 10 months of age in LIMP-2-deficient mice. The analysis of younger animals is necessary to pinpoint if there is a common onset of storage as well as neuropathology and behavioural anomalies resulting from the absence of LIMP-2 expression.

Whereas PAS is used for the identification of glycosphingolipid storage material in other lysosomal diseases (Jeyakumar et al., 2003) one can only speculate as to the nature and identity of the substance accumulated in brain material. One clear problem in this study was the uncertainty of whether GluCer levels are elevated in LIMP-2-deficient brain. This was due to high levels of galactosylceramide (GalCer) in the myelin of brain tissue and the inability of LC-MS (liquid chromatography mass spectrometry) to distinguish between this lipid and GluCer. Therefore, a clear solution to this problem would be the analysis of glycosphingolipid levels in pure neuronal cultures with reduced contamination of GalCer.

Finally, glucosylsphingosine (GluSph) is a neurotoxic metabolic product of GluCer (Schueler et al., 2003). In fact, GluSph is a second substrate for β-GC, although it is less efficiently cleaved than GluCer (Pentchev et al., 1973). Whereas not all Gaucher mice exhobot elevated levels of GluCer within the CNS (Enquist et al., 2007; Sun et al., 2010a), GluSph levels have been shown to be elevated in most Gaucher mouse models that exhibit neurological symptoms (Enquist et al., 2007; Sardi et al., 2011; Sun et al., 2010a; Tybulewicz et al., 1992).

Elevated levels of GluSph are hypothesised to be predominantly responsible for neurological impairment in the most severe of Gaucher cases (Orvisky et al., 2002). Additionally, GluSph is proposed to reduce the activity of β-GC (Schueler et al., 2003). Furthermore, GluSph cannot be contained within lipid bilayers and is found circulating in plasma of Gaucher diseased patients (Dekker et al., 2011) and has therefore unlimited destructive potential in the CNS. It remains however elusive whether levels of GluSph are substantially elevated in LIMP-2 mice.

7.4 Pathological changes within the spinal cord of mice when LIMP-2 is missing

LIMP-2-deficient mice exhibit partial hind-limb paralysis towards the last weeks of their shortened life (10 months) and advancing kyphosis which can be attributed to degeneration of motor neurons within the spinal cord. This is similar to symptoms observed in mouse models for type 2/3 Gaucher disease (Sun et al., 2010a) and PD (Lee et al., 2002). Neurodegeneration was accompanied by the accumulation of lipid-like droplets and electron dense material in the majority of neurons. However, it is not clear if degeneration is a direct result of accumulation as not all neurons appeared to be affected. Electron microscopy (EM) analysis of the spinal cord from a mouse model of type 2 Gaucher disease reported the presence of what was assumed to be GluCer. The authors report accumulation of “lipid tubules present in lysosomes” (Willemsen et al., 1995). However, due to the poor quality of pictographs presented in this publication it is difficult to draw any parallels between observations in LIMP-2-deficient mice and this Gaucher mouse model. In another mouse model of Gaucher disease type 3, storage of unidentified material was reported in axonal processes of neurons within the spinal cord of mutant animals (Sun et al., 2010a). However, one should be cautious in drawing parallels in relation to the nature of the stored substances in spinal cord as the accumulated lipid-like droplets or dense material have not been definitively identified in Gaucher or LIMP-2-deficient mice. Additional studies involving EM coupled with immunostaining of lysosomal markers are necessary in order to determine if the storage material observed in LIMP-2-deficient mice is within lysosomes or not.

Furthermore, in some AMRF cases peripheral nerve neuropathy has been reported (Chaves et al., 2011) and LIMP-2 deficiency is known to cause peripheral nerve demyelination in mice (Gamp et al., 2003) which may also contribute to paralysis (Huxley et al., 1996). Furthermore, kyphosis, demonstrated progressively in LIMP-2 knockout mice, is common in

mouse models of motor-system and spinocerebellar neurodegeneration and is caused by loss of muscle tone in the spinal region secondary to neurodegeneration (Guyenet et al., 2010).

Further EM analysis of semi-thin sections from murine brain, particularly from older mice, is necessary to determine if similar lipid accumulation also results from LIMP-2 deficiency in brain. Previous EM studies have identified osmiophilic inclusions in the Purkinje cells of the cerebellum in LIMP-2 knockout mice (Berkovic et al., 2008). However, no other areas of the CNS were analysed. Additionally, identification of neuronal shrinkage and death via EM analysis of brain material from LIMP-2 knockout mice would complement neuropathological characterisation in this study. Preliminary data indicated that dendritic spines may be affected in LIMP-2-deficient mice. However, visualisation of individual spines and their quantification as well as sample preparation using the Golgi-Cox method is quite challenging and prone to bias. Using EM, individual spines and any deficit they may have in the formation of synapses can be visualised and quantified more readily at higher resolution.

7.5 Severe behavioural and neuropathological anomalies due to LIMP-2 deficiency

LIMP-2-deficient mice were significantly smaller than their wild-type littermates and failed to gain weight beyond 4 months of age. Similar observations have been made in quite a number of mice engineered to be deficient in a specific protein and it is a general indication that the organism is in a diseased state (review: Reed et al., 2008). Some examples where reduced size and failure to gain weight is observed in genetically engineered animals include mice deficient in LAMP-2 (Tanaka et al., 2000), phosphotransferase knockout mice (Kollmann et al., 2012) and in mouse models for PD (Rieker et al., 2011). Such a severe weight phenotype was not reported in LIMP-2-deficient mice that were bred in the C57BL/6J background indicating that this phenotype is dependent on the strain used for breeding.

LIMP-2-deficient mice exhibited clear symptoms of CNS impairment, indicated by hind-limb clasping, similar to other mice with neuropathological symptoms due to lysosomal storage (Kasper et al., 2005; Sun et al., 2010b). Despite the fact that LIMP-2 appears to be ubiquitiously expressed in neurons and astrocytes throughout the CNS, several distinct areas appear to be affected differentially in murine knockout brain. With the exception of the

outer cortical layers and the molecular layer in the cerebellum, severe widespread astrogliosis was observed throughout the CNS in LIMP-2-deficient mice. Additionally, reactive microgliosis, an indication of neuroinflammation, was observed in LIMP-2-deficient brain which was particularly acute within myelinated areas and regions involved in PD such as the midbrain and pons. Furthermore, significant CD68 immunostaining was detected in the fornix, a region associated with "excessive daytime sleepiness" in PD patients (Matsui et al., 2006). Astrogliosis and microglial activation are seen as a non-specific pathological indication of neuronal lesions/abnormalities and are also observed in acute mouse models of Gaucher disease (Enquist et al., 2007; Sun et al., 2010a; Wong et al., 2004; Xu et al., 2003) as well as in PD patients and mouse models (Gomez-Isla et al., 2003; Wilms et al., 2007). Such severe gliosis has not been observed in LIMP-2 knockout mice bred in the α-synuclein deficient background. Therefore, it is highly likely that the neuropathological symptoms now observed in LIMP-2-deficient mice are a direct result of α-synuclein expression. It is unknown whether activation of microglia and the proliferation of astrocytes aggrevates disease or is merely in response to foreign or toxic accumulated products within the CNS. However, general gliosis remains a common denominator linking Gaucher disease, synucleinopathies and LIMP-2 deficiency (fig. 7.1).

In LIMP-2-deficient mice, pathology including apoptosis and carbohydrate storage correlated with the pattern of microgliosis, indicating that neuroinflammation and cell death is particularly acute in storage regions of the brain. A similar response to storage of glycosphingolipids has been observed in a Gaucher type 2 mouse model (Enquist et al., 2007; Jeyakumar et al., 2003). In this study no increase in severity of carbohydrate storage was seen in LIMP-2-deficient mice between 6 and 10 months of age. Similarly, with the exception of the corpus callosum, no changes in severity in microglial activation were observed due to LIMP-2 deficiency when comparing 6- and 10-month-old mice. Histological analysis of younger mice is necessary to determine the age of onset of neurological disease and define if there is a common onset of storage, microgliosis and apoptosis.

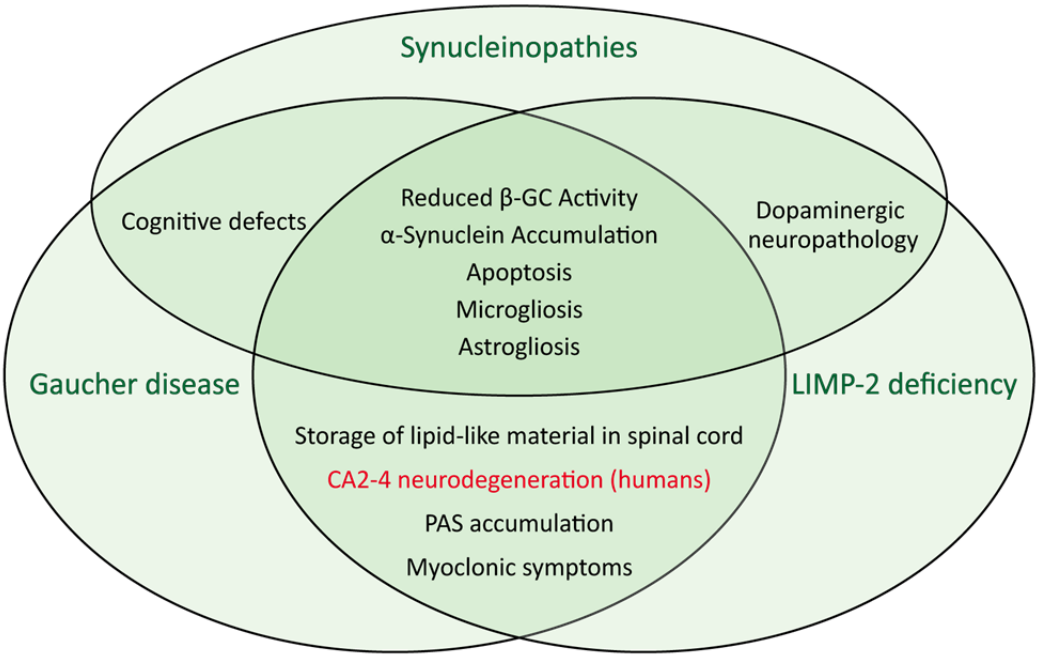

Figure 7.1 Overview of commonality in neuropathology between what is known about synucleinopathies, Gaucher disease and LIMP-2 deficiency in mice. Neurodegeneration observed in human Gaucher patients and LIMP-2-deficient mice but not in Gaucher mouse models is highlighted in red. Microgliosis and astrogliosis are only observed in severe Gaucher disease mouse models, synucleinopathies and when LIMP-2 is deficient in mice.

Strikingly, activation of CD68 positive microglial cells in myelinated regions did not appear to be linked to demyelination within the corpus callosum, anterior commissure or white matter of the cerebellum. Deficiency in LIMP-2 was previously shown to affect the myelination of peripheral nerves in mice. It appears that LIMP-2 plays a more critical role within the myelination mechanisms of the peripheral nervous system (PNS) due to an apparently increased degradation of myelin proteins (Gamp et al., 2003). Additionally, there are several differences between myelination of axons within the CNS and PNS. Schwann cells are responsible for myelination of peripheral nerves whereas oligodendrocytes wrap axons of neurons within the CNS with myelin sheaths. Furthermore, while one Schwann cell is responsible for the myelination of one axon in the peripheral nervous system a single oligodendrocyte spirally ensheathes numerous axons at once in a much more complex process within the CNS (Taveggia et al., 2010). Further research is necessary in order to clarify the effects of such progressive acute microgliosis within the myelinated regions of LIMP-2-deficient mice. Ultrastructural analysis may unveil more subtle morphological changes in myelination within the brain of mice deficient in LIMP-2.

Neuronal damage, indicated by eosinophilic spheroids and cellular shrinkage as well as neuronal loss, observed in the hippocampus may account for some behavioural changes observed in LIMP-2-deficient mice. While the CA1 appears to be spared, extensive loss of neurons in the CA2-4 regions in the hippocampus of Gaucher patients has been reported in individuals suffering from myoclonic symptoms. Additionally, loss of neurons occurs in areas where normally the highest expression of β-GC is observed within the hippocampus (Wong et al., 2004). Similarly, in this study, increased expression of LIMP-2 was detected in the CA2/CA3 region of the hippocampus. Interestingly, LIMP-2-deficient mice show neuronal loss in CA2-4. Furthermore, LIMP-2 knockout mice exhibit myoclonic jerking-like behaviour (data not shown) which may be attributed to hippocampal pathology similar to that seen in Gaucher patients (fig. 7.1). Due to the loss of neurons observed within the hippocampus LIMP-2-deficient mice should show deficits in spatial orientation and memory. No cognitive decline was reported in LIMP-2-deficient mice bred in the C57BL/6J background (Berkovic et al., 2008). Both Gaucher mouse models reported to suffer from synucleinopathy (Sardi et al., 2011; Sardi et al., 2013) and mouse models for PD (Pham et al., 2010; Zhu et al., 2007) have cognitive difficulties. It would be interesting to see if LIMP-2-deficient mice from this study have such abnormalities. Tests such as the Morris water maze (Morris, 1981) or the radial arm maze (Brown et al., 2007), two of the most widely used models to assess memory and hippocampal function could be used.

Interestingly, loss of LIMP-2 expression resulted in tremor in mice similar to that observed in some PD mouse models (Lee et al., 2002; Martin et al., 2006). The exact cause of tremor in LIMP-2-deficient mice is difficult to determine. Generally, tremor can be attributed to dopaminergic neuronal damage within the nigrostriatal system both in PD patients (review: Braak et al., 2003) and in mouse models (Ittner et al., 2008). Behavioural symptoms coupled with loss as well as shrinkage of dopaminergic neurons within the pars compacta of the substantia nigra in knockout animals observed in this study points out a clear connection between PD and LIMP-2-deficiency in mice (fig. 7.1).

Several other overlapping symptoms are common to neuropathic Gaucher disease, synucleinopathies and LIMP-2 deficiency (fig. 7.1). Enzymatic activity of β-GC is significantly reduced in Gaucher mouse models (Enquist et al., 2007; Sun et al., 2010a; Tybulewicz et al.,

1992) and in LIMP-2-deficient mice. This may be the cause of carbohydrate storage observed within histological sections which could indicate storage of GluCer. Storage of this lipid can therefore influence the clearance of α-synuclein (Mazzulli et al., 2011), thus leading to a common pathological synucleinopathy. An increased concentration of α-synuclein is known to perturb the autophagic system (Cuervo et al., 2004; Huang et al., 2012; Winslow et al., 2010) similar to observations in this study indicated by an increase in p62 staining in several regions of the CNS and in lysates from the pons of LIMP-2-deficient mice. Further analysis of LIMP-2-deficient mice concerning changes in levels of other proteins involved in macroautophagy such as LC3 (Kabeya et al., 2000) and beclin-1 (Russo et al., 2011) in conjunction with quantitative RT-PCR to rule out changes in transcription of autophagic genes would help to validate these results.

7.6 The absence of LIMP-2 causes perturbation in the metabolism of α-synuclein

The synucleinopathies encompass a large group of neurodegenerative disorders characterised by intracellular accumulation of α-synuclein in neurons and glial cells (Galvin et al., 2001; Xia et al., 2008). Dysfunction of lysosomal degradation through perturbation of the acidification (Usenovic et al., 2012), loss of protease activity (Cullen et al., 2009) or due to accumulation of lipids (Suzuki et al., 2007), especially GluCer (Mazzulli et al., 2011), has been shown to cause α-synuclein accumulation. Moreover, α-synuclein accumulation *in vitro* and *in vivo* has been linked to reduced β-GC activity using the inhibitor conduritol β-epoxide (CBE) or siRNA directed against the enzyme and in Gaucher mouse models (Manning-Bog et al., 2009; Mazzulli et al., 2011; Xu et al., 2011) reflecting disturbed lipid metabolism that could account for α-synuclein accumulation.

Previous findings and results reported in this study point to an essential role for LIMP-2 in the trafficking and activity of β-GC in neurons and astrocytes and therefore the clearance of GluCer. In fact elevated levels of GluCer, probably as a consequence of reduced β-GC activity, were previously detected in LIMP-2-deficient mouse liver and lung but not in brain (Reczek et al., 2007). However, it should be noted that this data reflects the situation in non-backcrossed mice. The recent discovery that perturbation of β-GC activity and thus accumulation of its substrate GluCer can directly cause the aggregation of α-synuclein through stabilisation of its oligomeric form (Mazzulli et al., 2011) raised the question

whether dysfunction of the enzyme and subsequently elevated levels of lipids may also cause α-synuclein accumulation and PD-like symptoms in backcrossed LIMP-2-deficient mice.

Clear evidence indicating progressive accumulation of α-synuclein was observed within the CNS in the absence of LIMP-2. Deposits of α-synuclein were particularly concentrated in the pons, midbrain, substantia nigra and the granular cell layer of the cerebellum in LIMP-2-deficient mice. A dramatic reduction in total enzyme levels was observed in Western blots as well as a significant decrease in enzyme activity using an enzyme assay for specific measurement of β-GC within LIMP-2-deficient brain. Furthermore, 56 % of total β-glucosidase activity (β-GC and GBA2) was observed in the pons of LIMP-2-deficient mice whereas approximately 70 % was recorded in the midbrain. Interestingly, α-synuclein accumulation was also more severe in the pons when compared to the midbrain. This evidence points to a potential link between reduced enzymatic clearance of GluCer and neuropathological consequences. Enzyme activity measurement of lysates from the cortex and cerebellum is necessary to validate if there is a connection between lysosomal activity and neuropathology in other regions of the CNS.

Accumulation of α-synuclein can assume many forms. Generally an increase in monomeric α-synuclein, due to retardation of its degradation either by the lysosome or proteasome leads to an increase in its concentration which alone causes its assembly into soluble ordered fibrils (Lashuel et al., 2002; Volles and Lansbury, 2002). Biochemical analysis of soluble and insoluble fractions revealed a tendency towards a decrease in monomeric α-synuclein in LIMP-2-deficient brains. Nonetheless, this result contradicts immunohistochemical analysis which did not suggest a decrease in the quantity of α-synuclein in brain when LIMP-2 was missing. However, an inclination towards accumulation of soluble oligomeric α-synuclein but no evidence of aggregated insoluble α-synuclein was noted in LIMP-2-deficient brain. Due to the aggregation of protein the epitope recognised by the antibody used in this study (syn-1) may be masked. Therefore, in order to eliminate the possibility that α-synuclein forms insoluble aggregates when LIMP-2 is missing another commercially available antibody against α-synuclein (4D6) was used. However, no aggregated α-synuclein was observed in the insoluble fraction of LIMP-2 knockout brains

(data not shown). Furthermore, the majority of α-synuclein is phosphorylated at serine 129 when aggregated (Fujiwara et al., 2002). Therefore, an antibody directed against the pathogenic, phosphorylated form of α-synuclein was used. However, no evidence of α-synuclein aggregation was evident in knockout lysates (data not shown).

Several mouse models for Gaucher disease are reported to accumulate α-synuclein that are summarised in table 7.1. On a biochemical level few research groups have attempted to analyse the accumulation of α-synuclein Gaucher mouse models. Mice have been created that have hypomorphic expression of prosaposin (PSNA), a beta subunit necessary for optimal activity of β-GC (table 7.1(2)). Both studies describe PSNA mice crossed with those expressing Gaucher causing mutations in β-GC. The β-GC$^{V394L/PSNA}$ mouse (table 7.1(3)) was reported to accumulate α-synuclein in two separate publications (Mazzulli et al., 2011; Xu et al., 2011). Xu *et al*. reported a similar increase in an oligomeric form of α-synuclein in β-GC$^{V394L/PSNA}$ mice to that observed in LIMP-2-deficient mice. However, using different biochemical extraction coupled with an array of different antibodies dissimilar aggregation patterns of α-synuclein were reported by Mazzulli *et al*. for the β-GC$^{V394L/PSNA}$ mouse. Other publications reporting accumulation of α-synuclein in Gaucher mouse models have not examined the biochemical nature via immunoblot of the histologically accumulated deposits. Furthermore, antibodies used by Mazzulli *et al.* are not commercially available making a direct comparison between this study and previous publications difficult.

7.7 Synucleinopathy in Gaucher mouse models and LIMP-2-deficient mice

Besides the hypothesis that suggests accumulation of α-synuclein is a result of the stabilisation effect of GluCer, several other theories exist in an attempt to explain the link between β-GC and PD. One theory describes the toxic gain of function exerted by mutated β-GC by directly promoting α-synuclein accumulation suggesting a mutant specific phenotype. In fact, the majority of β-GC was found to be localised in α-synuclein positive Lewy bodies in PD patients carrying mutations in the enzyme (Goker-Alpan et al., 2010) suggesting direct interaction of both proteins (Yap et al., 2011). In support of this theory, α-synuclein accumulation was reported in an older Gaucher mouse model where heterozygote expression of β-GC^{D409V} was enough to cause disease (table 7.1(4)) (Sardi et al., 2011). Thus, the expression of disease associated mutants of β-GC is enough to perturb

metabolism of α-synuclein. However, such hypotheses do not describe the occurrence of PD in Gaucher patients with null mutations resulting in absent β-GC (Lesage et al., 2011) or the accumulation of α-synuclein in LIMP-2-deficient mice. Therefore, it is highly unlikely that misfolding of β-GC alone is responsible for the occurrence of synucleinopathies.

Gaucher disease mouse models should be cautiously compared to LIMP-2-deficient mice when considering presentation of neurological symptoms and particularly when discussing the development of synucleinopathy with regard to the hypothesis describing GluCer´s role in the stabilisation of α-synuclein. Complete deletion of the β-GC gene is lethal leading to death shortly after birth due to skin barrier defects (Tybulewicz et al., 1992). Furthermore, β-GC knockout mice, where the skin phenotype was rescued (Enquist et al., 2007), as well as other mouse models of severe neuronopathic Gaucher disease such as the β-GC$^{L444P/A459P}$ and β-GC$^{L444P/A459P}$ (Liu et al., 1998), die soon after birth before any synucleinopathy has time to develop (table. 7.1(5)).

Misfolded proteins within the endoplasmatic reticulum (ER) are destroyed by the cells` internal quality control system in a process known as ER associated degradation (ERAD) (Vembar and Brodsky, 2008). In fact, evidence pointing to additive toxic gain of function effects caused by ERAD of β-GC mutants as well as reduction in enzyme activity is suggested to cause accumulation of α-synuclein (Sardi et al., 2011). ERAD is activated when disease-causing mutants of β-GC are expressed in the cell (Ron and Horowitz, 2005). Furthermore, overexpression of mutated β-GC has been shown to directly cause the accumulation of α-synuclein (Cullen et al., 2011) potentially through the monopolisation of the ubiquitin ligase PARKIN (Ron et al., 2010) for the degradation of accumulated enzyme in the ER. Interestingly, in this study β-GC could not be detected in the ER of LIMP-2-deficient primary neurons and is therefore probably exocytosed from the cell similar to reports in fibroblasts (Reczek et al., 2007). It is thus likely that, due to the fact that β-GC is no longer retained within the ER but is merely transported out of the cell, the potential disturbance on the homeostasis of α-synuclein is not as severe as that seen in the presence of Gaucher associated mutants where the synergistic effects of reduced enzymatic activity and ERAD are proposed to cause synucleinopathy (Sardi et al., 2011)(Sardi et al., 2011).

Table 7.1 Overview of Gaucher disease mouse models and analysis of synucleinopathies. Increased accumulation of glucosylceramide (GluCer) or glycoslysphingosine (GluSph) in brain are indicated with an arrow and regions where synucleinopathy was reported are outlined (GD, Gaucher disease; ~ = no change; N.D. = not determined).

	Neurological phenotype	Accumulation	Synucleinopathy
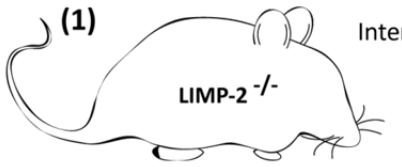 Gamp et al., 2003; This study	Intermediate.	GluCer N.D. GluSph N.D.	Pons Substantia Nigra Midbrain Cerebellum Corpus Callosum
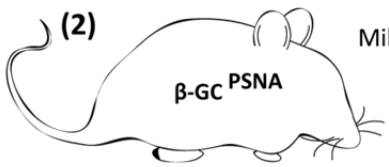 Sun et al., 2005; Xu et al., 2011	Mild neurodegeration.	GluCer ~ GluSph ~	Cortex
 Mazzulli et al., 2011; Sun et al., 2010; Xu et al., 2011	Severe. Reminescent of GD type 3.	GluCer ↑ GluSph ↑	Cortex Hippocampus Substantia Nigra
 Sardi et al., 2011; Xu et al., 2003	Cognitive impairment.	GluCer ~ GluSph ↑	Cortex Hippocampus
 Enquist et al., 2007; Liu et al., 1998; Tybulewicz et al., 1992	Severe. Reminescent of GD type 2/3.	GluCer ↑ GluSph N.D.	N.D.
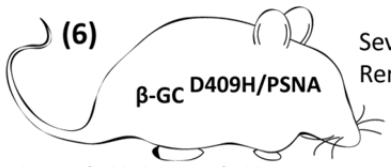 Sun et al., 2010; Xu et al., 2011	Severe. Reminescent of GD type 3.	GluCer ↑ GluSph ↑	Hippocampus Midbrain Cerebellum Striatum Substantia Nigra Cortex
 Sun et al., 2010; Xu et al., 2011	No overt impairment noted.	GluCer ~ GluSph N.D.	Cerebellum Brain stem (Pons)

A similar pattern of synucleinopathy to that observed in LIMP-2-deficient mice was previously reported in a mouse model for severe Gaucher disease type 3 (table 7.1(6)) where expression of mutated β-GC in conjunction with low expression levels of prosaposin, referred to as β-GC$^{D409H/PSNA}$, resulted in a significant reduction in enzyme activity and storage of GluCer within the CNS. The authors reported accumulation in the same regions as observed in LIMP-2-deficient mice in this study with the exception of the pons which was not assessed in the publication (Xu et al., 2011). Additionally, α-synuclein deposits have been reported in the cortex and hippocampus of the β-GC$^{D409H/PSNA}$ mouse (Xu et al., 2011) as well as many other Gaucher disease mouse models including β-GC$^{V394L/PSNA}$ (Xu et al., 2011, Mazzulli et al., 2011) and mice with Gaucher disease causing point mutations (β-GC^{D409H} and β-GC^{D409V}) (Sardi et al., 2011; Xu et al., 2011) (table 7.1(4 and 7)). Unfortunately, due to the high level of endogenous α-synuclein superficial detection of differences in accumulation of α-synuclein within the cortex and hippocampus was not possible in LIMP-2-deficient mice.

Several other explanations may account for discrepancies between neuropathology observed in Gaucher mouse models and LIMP-2-deficient mice. In mouse models believed to recapitulate the symptoms of type 2 and 3 Gaucher disease in humans mutated forms of β-GC as well as dramatically reduced expression of prosaposin were used (Xu et al., 2011). Saposins A-D are derived from a common precursor, prosaposin. Each saposin is involved in the degradation pathway of a specific sphingolipid. PSNA mice express prosaposin at a subnormal level, thus leading to deficiency in all saposins A-D and an accumulation of a concert of sphingolipids (Sun et al., 2002). Thus, crossing this mouse with mice expressing Gaucher disease mutants, in an attempt to perturb specifically the activity of β-GC, is intrinsically flawed. In fact, whether these mice are an appropriate model for Gaucher disease is under debate (review: (Farfel-Becker et al., 2011). Therefore, Gaucher models´ effects on reduction in the activity of β-GC and the development of synucleinopathy are clouded through the dampening of several other lysosomal enzymes and the resulting accumulation of other sphingolipids in addition to GluCer.

Accumulation of α-synuclein was shown to be approximately twice as severe in the presence of both mutated β-GC and reduction in activity when compared to the heterozygotes expressing mutated enzyme on one allele. Interestingly, injection of mice with CBE mimic

some aspects of neuronopathic Gaucher disease (Xu et al., 2008) but only showed limited accumulation of α-synuclein in brain stem, olfactory bulb and hypothalamus after treatment for 24-36 days (Xu et al., 2011). Additionally, treatment of mice with CBE once was reported to raise α-synuclein levels within the substantia nigra but no aggregation was reported (Manning-Bog et al., 2009). However, no other *in vivo* studies in mice assessing the direct influence of reducing β-GC activity without the necessity of overexpressing mutants of hypomorphic expression of prosaposin are possible as knockout mice for β-GC are embryonically lethal (Tybulewicz et al., 1992).

LIMP-2-deficient mice provide a unique means of assessing what influence a significant reduction of β-GC activity has on the accumulation of α-synuclein in neurons without affecting ERAD via the expression of toxic mutants, reducing the activity of several hydrolases through hypomorphic expression of prosaposin or lethal knockout of the enzyme. An interesting aspect that should be analysed in the future would be the parallels of α-synuclein accumulation between primary neurons derived from neuronopathic Gaucher (Tybulewicz et al., 1992) and LIMP-2-deficient mice.

Further studies on transgenic mice such as those overexpressing mutant LIMP-2 that is targeted to the lysosomes correctly but incapable of binding β-GC (Blanz et al., 2010) could help to elucidate the specific role of LIMP-2 and lipid metabolism in the development of synucleinopathies. Any phenotype uncovered in these mice should be only due to defects in β-GC trafficking thereby minimise any confusion with other yet unknown functions of LIMP-2. Similarly, analysis of recently reported mice that overexpress LIMP-2 (Lin et al., 2013) may prove useful in the interpretation of its potential to augment the clearance of α-synuclein through increasing the activity of β-GC. Conversely, crossing of LIMP-2-deficient mice with those overexpressing wild-type or a pathological form of α-synuclein, two scenarios known to increase the progression of PD (Rieker et al., 2011; van der Putten et al., 2000), should result in an earlier and more severe onset of disease. Finally, crossing of LIMP-2 overexpressing mice (Lin et al., 2013) with PD mouse models (Rieker et al., 2011; van der Putten et al., 2000) would add strength to the hypothesis that influencing LIMP-2 levels can potentially impact α-synuclein levels. Furthermore, even though several PD mouse models describe accumulation of α-synuclein within the spinal cord in addition to other

regional analysis of the CNS, the occurrence of α-synuclein was not yet assessed within the spinal cords of Gaucher mice or LIMP-2-deficient mice.

7.8 Changes in ubiquitination and macroautophagy due to LIMP-2 deficiency

Selective macroautophagy, mediated by p62, is recognised as a mechanism employed by the cell in the removal of protein aggregates (Bjorkoy et al., 2005; Filimonenko et al., 2010) and damaged organelles (review: Cuervo et al., 2005). Efficient clearance of damaged organelles, proteins and protein aggregates is crucial for cellular homeostasis.

The adapter protein p62 mediates autophagic degradation of ubiquitinated proteins and is itself degraded by autophagy. Therefore, its accumulation usually signifies a disruption in the autophagolysosomal system. Some Gaucher mouse models exhibit deficiency in autophagic clearance (Sun et al., 2010a). Accumulation of p62 was observed throughout the CNS of LIMP-2-deficient mice suggesting the impairment of autophagosome/lysosome function. Interestingly, Western blot analysis showed significant changes in soluble p62 levels in lysates from the pons, a region observed to have more dramatic reduction in β-GC activity and the most significant accumulation of α-synuclein. This correlated with immunohistology that showed a significant increase in p62 deposits in the pons when compared to other regions of the CNS also shown to have such deposits in LIMP-2-deficient material. However, it is possible that p62 may be also retained by insoluble proteins. Further analysis of insoluble fractions for the accumulation of p62 is necessary in order to determine if there is a difference in its abundance via Western blot of other areas of the brain due to LIMP-2 deficiency.

Proteins of an aggresome and exposed proteins on the surface of damaged organelle are normally ubiquitinated (Arrasate et al., 2004; Kopito, 2000). However, no increase in insoluble high molecular weight proteins was detected in LIMP-2-deficient brains pointing to the absence of aggresomes. This is not surprising as no indication of accumulation of insoluble aggregated α-synuclein was observed in LIMP-2-deficient brains. Bands detected by polyubiquitin (FK1) that failed to react with the antibody directed against α-synuclein (syn-1), such as the 60 kDa band may be ubiquitinated forms of α-synuclein. In this case some additional posttranslational modifications may have masked the epitope recognised by

syn-1. UCHL-1 can deubiquitinate α-synuclein (Liu et al., 2002) and could thus be used to treat lysates (Sampathu et al., 2003). A reduction in the 60 kDa band in lysates treated *in vitro* with UCHL-1 would establish if this band corresponds to ubiquitinated α-synuclein.

Upregulation of macroautophagy in immunohistological sections could indicate a potential dysfunction in clearance of organelles due to LIMP-2 deficiency. An unidentified polyubiquitinated band was significantly increased in insoluble fractions of LIMP-2-deficient brains which could be a target of macroautophagy that has not been degraded. For instance, mitochondrial dysfunction is associated with an increase in concentration of oligomeric fibrils of α-synuclein and autophagy is impaired in cells harbouring mitochondrial dysfunction which also causes the accumulation of p62 (Arduino et al., 2012). Furthermore, accumulation of undegraded mitochondrial components is found in electron dense material within a mouse model for neuronal ceroid lipofuscinosis (Kasper et al., 2005) similar to that found in the spinal cord of LIMP-2-deficient mice.

Additionally, it is not clear if p62 accumulation is within neurons, astrocytes or microglia. Further experiments involving immunofluorescence of neuronal, astrocytes and microglial markers in conjunction with p62 are necessary to determine the location of deposits in LIMP-2-deficient brain.

7.9 LIMP-2 knockout mice represent a valid mouse model for AMRF

Whereas renal problems reported for AMRF patients are dissimilar to LIMP-2-deficient mice many aspects of their behavioural and neuropathological criteria are comparable. Both human patients and mice lacking LIMP-2 expression suffer from ataxia (Badhwar et al., 2004; Berkovic et al., 2008) and deafness (Perandones et al., 2012). Furthermore, LIMP-2-deficient mice show signs of tremor and myoclonic jerking. However, more specialised analysis involving electroencephalography measurement is required to establish if they suffer from myoclonic seizures similar to symptoms observed in patients (Balreira et al., 2008; Berkovic et al., 2008; Chaves et al., 2011; Dardis et al., 2009).

Ultrastructural studies have shown an accumulation of electron dense material within the cerebellum of both AMRF patients (Badhwar et al., 2004) and in LIMP-2-deficient mice

(Berkovic et al., 2008). In this study, loss of LIMP-2 expression in mice causes PAS positive deposits throughout the CNS. Similar accumulation has been reported in the cortex (Badhwar et al., 2004) and cerebellum (Berkovic et al., 2008) of AMRF patients. Acute storage of PAS positive material in the myelinated regions of the CNS was observed in LIMP-2-deficient mice. Such accumulation has not been reported in AMRF material. However, neuropathological data concerning AMRF is sparse with the cortex, cerebellum and striatum mentioned in publications describing patient material. Consequently, extensive reanalysis of AMRF post mortem material is warranted in order to validate LIMP-2-deficient mice as a mouse model for human disease. Such examinations should include assessement of PAS positive accumulation, microgliosis, astrogliosis, disturbed lysosomal function, α-synuclein accumulation and neurodegeneration. The parallel between CNS anomalies in AMRF patients and LIMP-2-deficient mice is an important aspect that should be assessed in the future.

7.10 LIMP-2 may provide a novel target in the treatment of PD

The activity of β-GC is significantly reduced in PD brain irrespective of whether the patients carry Gaucher mutations or not (Gegg et al., 2012). Reduction in enzymatic activity correlates with reports that increased α-synuclein levels impede trafficking of proteins out of the ER (Cooper et al., 2006; Mazzulli et al., 2011) (fig. 7.2-4). Furthermore, an increase in the level of α-synuclein is proposed to interrupt the interaction of LIMP-2 with β-GC (Gegg et al., 2012), thus disrupting correct trafficking of the enzyme to the lysosome. Due to the ability of GluCer to stabilise α-synuclein, thereby promoting the formation of toxic oligomers (fig. 7.2-3) and retarding its degradation (Mazzulli et al., 2011), it is feasible that reduction of lipid accumulation within the lysosome may improve clearance of the protein. It is therefore plausible that LIMP-2 expression can directly influence whether a patient develops PD or not.

A reduction in β-GC activity was previously shown to decrease proteolysis within the lysosome (Mazzulli et al., 2011). Therefore, initial degradation of α-synculein may also be affected due to a decrease in enzyme activity and the resulting increase in GluCer or its metabolic products. The reintroduction of active β-GC into Gaucher mouse models ameliorated CNS impairment and synucleinopathies (Sardi et al., 2011). Even more

interesting is that the overexpression of β-GC in murine PD models leads to a decrease in monomeric α-synuclein (Sardi et al., 2013) pointing to the significance of β-GC activity for maintenance of α-synuclein levels. It has been reported that functional loss of β-GC leads to α-synuclein accumulation that itself further inhibits β-GC`s lysosomal activity (Mazzulli et al., 2011). Due to the progressive nature of the pathogenic loop described by Mazzulli *et al.*, methods that increase targeting of β-GC to the lysosome have been suggested as a promising therapeutic approach to counteract impaired trafficking of the enzyme as a result of increased concentrations of α-synuclein.

Recently, single nucleotide polymorphisms (SNPs) associated with the LIMP-2 gene (SCARB2) were identified as genetic risk factors for the development of PD. One SNP (rs6812193) was located 64 Kb upstream (Do et al., 2011) and the other (rs6825004) within the second intron of the SCARB2 (Michelakakis et al., 2012). Other studies have confirmed the connection between the SNP rs681293 and PD (Hopfner et al., 2013). Disease associated SNPs are commonly located outside the coding regions of a gene and thus are proposed to exert their effects by influencing transcription factor binding or gene splicing. While genetic deviation in the transcriptional level of LIMP-2 is an attractive candidate for the developments of PD, further studies involving the characterisation of transcription factors and effects on splicing of LIMP-2 in the presence of PD associated SNPs are necessary to verify its validity as a risk factor gene.

Due to the negative effects of the accumulation of GluCer on the degradation of α-synuclein (Mazzulli et al., 2011) a direct means of preventing the generation of the lipids within the cell may be a useful target in combatting the disease (fig. 7.2A). Miglustat, identified as a potential drug for the treatment of several lysosomal storage diseases (Accardo et al., 2010), inhibits the glucoslyceramide synthase (Platt et al., 1994) thus leading to a significant reduction in GluCer within the cell. However, in this study miglustat treatment of mouse embryonic fibroblasts (MEFs) overexpressing wild-type or aggregation prone, mutated (A53T) α-synuclein did not have a significant effect on the clearance of the pathogenic protein. It should be pointed out that, whether or not a reduction in GluCer levels was achieved was not assessed in these experiments. Furthermore, MEF cells were treated for 2 days. Perhaps a longer period of treatment with the inhibitor is necessary for the effects

on α-synuclein levels to be noticeable. Finally, neurons are known to have high levels of glycosphingolipids (Yu et al., 2009). Primary neuronal cultures from wild-type mice or those overexpressing α-synuclein were treated every second day with miglustat for a total of 10 days. Optimisation of the experimental setup including length of treatment and assessment of the effects of miglustat treatment on GluCer levels via liquid-chromatography mass spectrometry would help elucidate the potential effects on α-synuclein levels after treatment.

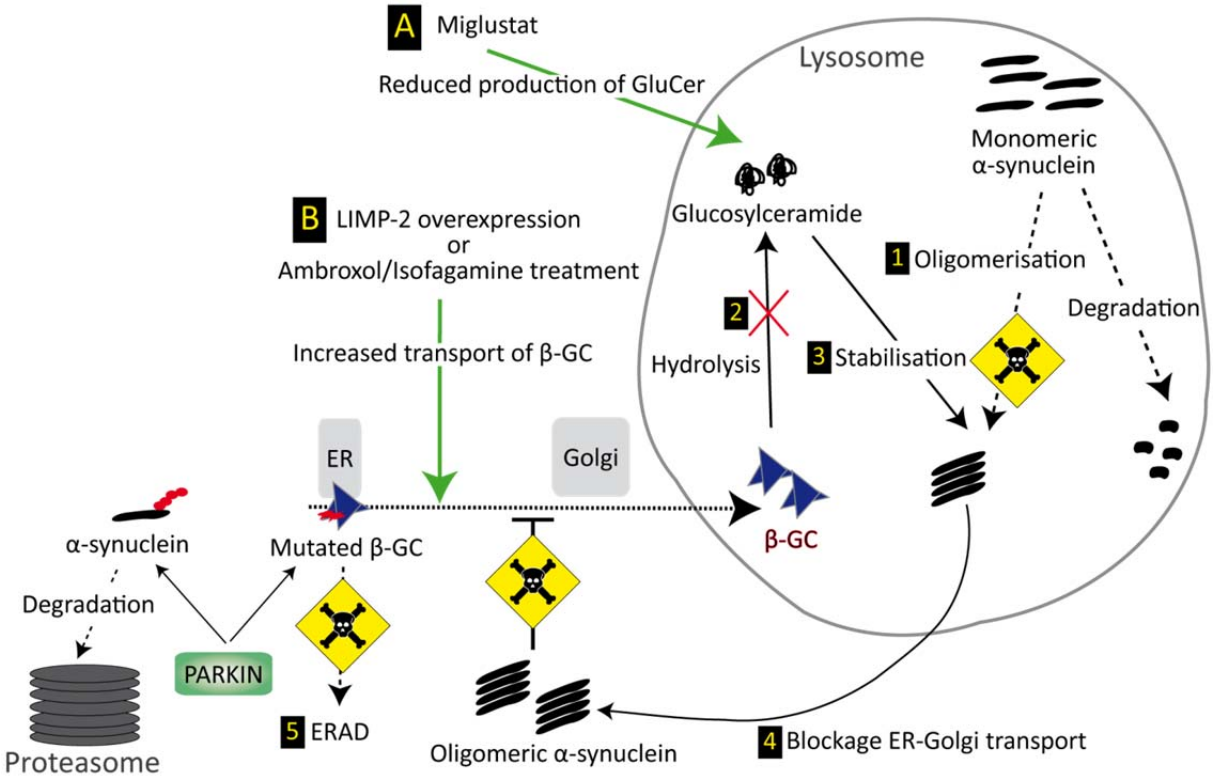

Figure 7.2 Model outlining an array of strategies aimed at reducing the accumulation of glucosylceramide and α-synuclein in the cell. **1-** Increased levels of α-synuclein within the lysosome lead to its oligomerisation. **2-** A decrease in β-GC activity leads to elevated concentrations of glucosylceramide (GluCer) **3-** which can stabilise α-synuclein oligomers thereby impeding their degradation. **4-** Soluble oligomeric fibrils may permeate the lysosome and block trafficking of newly synthesised proteins from the ER to the Golgi. **5-** Expression of mutated β-GC results in activation of ER associated degradation (ERAD) using the ubiquitin ligase PARKIN causing a reduction in ubiquitination of α-synuclein and thus reducing its degradation by the proteasome. **A-** Miglustat directly reduces levels of GluCer by blacking its synthesis in the Golgi. **B-** Chemical chaperones shown to increase transfer of mutated β-GC from the ER may help in the transport of wild-type enzyme thereby overcoming the blockage created by α-synuclein oligomers and alleviating the toxic effects of ERAD on proteasomal dependent clearance of α-synuclein.

To date no *in vivo* analysis has linked mutations in LIMP-2 to the development of a synucleinopathy. Furthermore, ample brain tissue from AMRF diseased brain is not available.

An interesting circumvent to the problem of establishing whether α-synuclein accumulates in human LIMP-2-deficient dopaminergic neurons would be the use of a relatively new technology that creates inducible pluripotent stem cells (iPSCs) from fibroblasts (Takahashi et al., 2007). Subsequently, the AMRF patient-derived-iPSCs can be differentiated into neurons (Seibler et al., 2011). Analysis of β-GC mistrafficking in conjunction with measurement of GluCer and GluSph levels would help in the clarification of LIMP-2´s role in the development of synucleinopathies. Stable transfection of human dopaminergic neuroblastoma cells (SHSY-5Y) with α-synuclein, or α-synuclein with the mutation A53T, known to cause aggregation, followed by transfection of these cells with siRNA against LIMP-2 and known AMRF disease causing mutants of LIMP-2 may prove useful in elucidating whether heterozygote or homozygote mutations affect susceptibility to the accumulation of PD.

While β-GC levels are known to be reduced in PD brain (Gegg et al., 2012) and the enzyme is found co-aggregated in Lewy bodies with α-synuclein (Goker-Alpan et al., 2010; Sidransky and Lopez, 2012), limited information is available describing LIMP-2 levels in PD patients. Two recent publications reported no change in LIMP-2 protein in brain lysates from patients suffering from sporadic PD or Lewy body disease (Gegg et al., 2012; Kurzawa-Akanbi et al., 2012). However, the level of LIMP-2, specifically within dopaminergic neurons, has never been assessed. To date, no study has analysed changes in LIMP-2 expression in response to disease within the substantia nigra. Unfortunately, due to the high quantity of neuromelanin in dopaminergic neurons it was not possible to determine accurately if there were any differences in LIMP-2 expression with this neuronal type as a result of disease. Immunofluorescence with a dopaminergic marker and LIMP-2 would help to reveal whether any changes occur in PD brain. More interestingly, immunofluorescence studies with antibodies directed against α-synuclein and LIMP-2 would aid in determining whether there is a difference in the steady-state level and localisation of LIMP-2 in neurons positive for Lewy bodies.

An increased expression of α-synuclein was previously reported to cause ER retention of β-GC (Mazzulli et al., 2011). One measure that one could take to increase β-GC activity within the lysosome would be manipulation of the transcription level of the enzyme`s

transporter, LIMP-2 (fig. 7.2B). Interestingly, overexpression of LIMP-2 has already been shown to enhance trafficking and rescue lysosomal activity of the L444P mutant of β-GC (Reczek et al., 2007). In this study the ER retention of β-GC, caused by increased levels of α-synuclein, could be overcome in HeLa cells by overexpressing LIMP-2. Furthermore, increased levels of LIMP-2 led to an increase in the activity of β-GC in both HeLa and SHSY-5Y cells. In this way, it is probable that more lysosomal β-GC, when trafficked correctly, results in an increase in activity and thus reduced lysosomal GluCer therefore abolishing the stabilising effects of this lipid on α-synuclein. Additionally, the reduction of α-synuclein levels via overexpression of a LIMP-2 mutant incapable of binding β-GC may indicate a direct influence of LIMP-2 on α-synuclein metabolism. Such an influence on α-synuclein steady-state levels would thus be independent of LIMP-2´s function as a lysosomal transport receptor that has not been previously considered.

While analysis of the promoter region of LIMP-2 may prove an interesting measure to uncover new therapeutic targets for the treatment of PD, no pharmaceuticals have been identified capable of enhancing LIMP-2 levels on a transcriptional basis. However, a recent report indicated that LIMP-2, but not LAMP-1 or LAMP-2, mRNA and protein levels may be increased in specialised cells within the kidney of mice after a low salt challenge (Schmid et al., 2012) indicating that LIMP-2 transcription can potentially be influenced. The evaluation of changes in LIMP-2 transcription in a high-throughput screen with small molecules may prove useful in the discovery of novel effectors for the treatment of PD. Additionally, increased expression of β-GC alone may prove useful in combatting the toxicity caused by augmented levels of α-synuclein. In fact viral transfection of β-GC was recently shown to reduce monomeric levels of α-synuclein in a PD mouse model (Sardi et al., 2013). The master regulator of lysosomal/autophagy protein expression, TFEB is known to increase transcriptional levels of β-GC but not LIMP-2 (Sardiello et al., 2009). Furthermore, TFEB activation is intimately connected to autophagy (Settembre et al., 2011) and was previously shown to influence the clearance of Huntingtin in cultured cells (Sardiello et al., 2009). In fact starvation leads to TFEB nuclear translocation and increased activity (Settembre et al., 2011). Therefore, enhancing lysosomal function, particularly the activity of β-GC is an interesting therapeutic strategy for the treatment of PD.

Another means of increasing trafficking of β-GC to the lysosome would be the use of well-established chemical chaperones (fig. 7.2B). Isofagamine and ambroxol have been shown to increase lysosomal targeting and activity of the β-GC mutant L444P (Bendikov-Bar et al., 2011; Khanna et al., 2010) which is associated, when homozygous, with severe neuronopathic cases of type 3 Gaucher disease. The β-GC mutant D409V, associated with synucleinopathy in mice (Sardi et al., 2011), was previously shown to reverse α-synuclein deposits in cell culture via treatment with isofagamine (Cullen et al., 2011). Of course the question remains whether such chaperones would have a pronounced effect on correctly folded wild-type β-GC and still increase its trafficking from the ER to the lysosome to overcome the blockage in ER-Golgi trafficking caused by increased levels in α-synuclein (Cooper et al., 2006; Thayanidhi et al., 2010). Manipulation of the trafficking and activity of β-GC via its interaction with LIMP-2 or chemical chaperones may prove to be attractive targets in the treatment of synucleinopathies. Whether application of chaperones or influencing of LIMP-2 expression would have a measurable effect on wild-type β-GC retained within the ER due to blockage of trafficking caused by α-synuclein toxicity is not known.

7.11 LIMP-2, β-GC and α-synuclein interactions en route to and within the lysosome

While overexpression of LIMP-2 in cultured cells led to a significant increase in hydrolytic activity of β-GC an unexpected synergistic effect of coexpression with α-synuclein was observed in activity assays. LIMP-2 and β-GC are thought to interact at neutral pH and dissociate from one another in the acidic environment of the lysosome (Zachos et al., 2012). Thus, overexpression of LIMP-2 leads to an increased level of lysosomal β-GC. Additionally, overexpression of α-synuclein leads to an increase of its transport into the lysosome for degradation. However, α-synuclein is thought to interact with β-GC (fig. 7.3-2) which is favoured at an acidic pH (Yap et al., 2011) thereby inhibiting enzyme activity (Yap et al., 2013) and potentially preventing its degradation. Cells are lysed in a buffer at neutral pH. Thus, α-synuclein can dissociate from the enzyme allowing it to become again active. In support of this hypothesis overexpression of LIMP-2, which leads to increased lysosomal delivery of β-GC, resulted in an enhanced increase in lysosomal activity of β-GC when coexpressed with α-synuclein (fig. 7.3-3) when compared to overexpression of LIMP-2 alone.

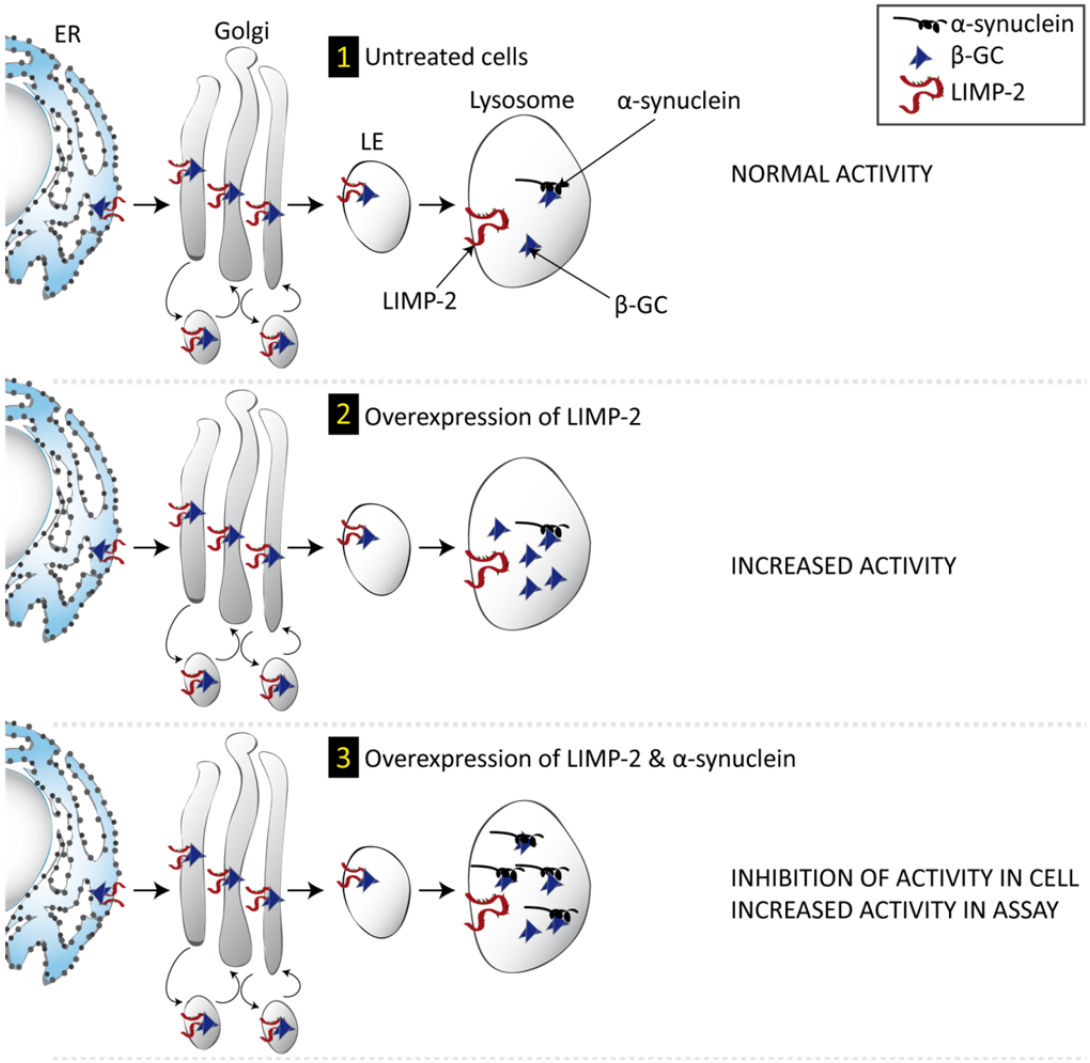

Figure 7.3 Model of the effects of overexpression of LIMP-2 and α-synuclein on activity of β-GC. 1- Untreated cells show normal β-GC activity. **2-** Overexpression of LIMP-2 leads to an increase in delivery of β-GC to the lysosome and increased activity as measured via an enzyme activity assay. **3-** Overexpression of LIMP-2 leads to an increase in delivery of β-GC to the lysosome. However, overexpression of α-synuclein may also lead to its increase in concentration within the acidic environment of the lysosome where it can bind and potentially stabilise β-GC and inhibit its activity. After lysis of cells in neutral buffer, β-GC is no longer bound to α-synuclein and thus an increase in activity is observed using an enzyme activity assay. (LE, late endosome).

7.12 Conclusion

This study underlines the importance of LIMP-2 as a β-GC transporting protein in neurons and its potential role in the development of PD and other synucleinopathies. From the data presented it can be speculated that accumulating lipids caused by reduced β-GC activity initiate α-synuclein accumulation which correlates with previous studies linking accumulation of lipids due to lysosomal dysfunction with the development of synucleinopathies. One of the fundamental questions is whether LIMP-2 may influence α-synuclein levels independently of its trafficking functions for β-GC.

In this work LIMP-2 deficiency in neurons within the CNS of mice led to mistrafficking of β-GC and an accumulation of α-synuclein, an unidentified polyubiquitinated protein as well as several unknown substances in primary neurons, spinal cord and histological sections of a lipid/carbohydrate nature. Probably as a result of lysosomal dysfunction, as highlighted by an accumulation in the macroautophagic marker p62 and significant changes in lysosomal hydrolase and cathepsin D levels, evidence of neurodegeneration and apoptosis and severe astrogliosis and neuroinflammation were observed (fig. 7.4).

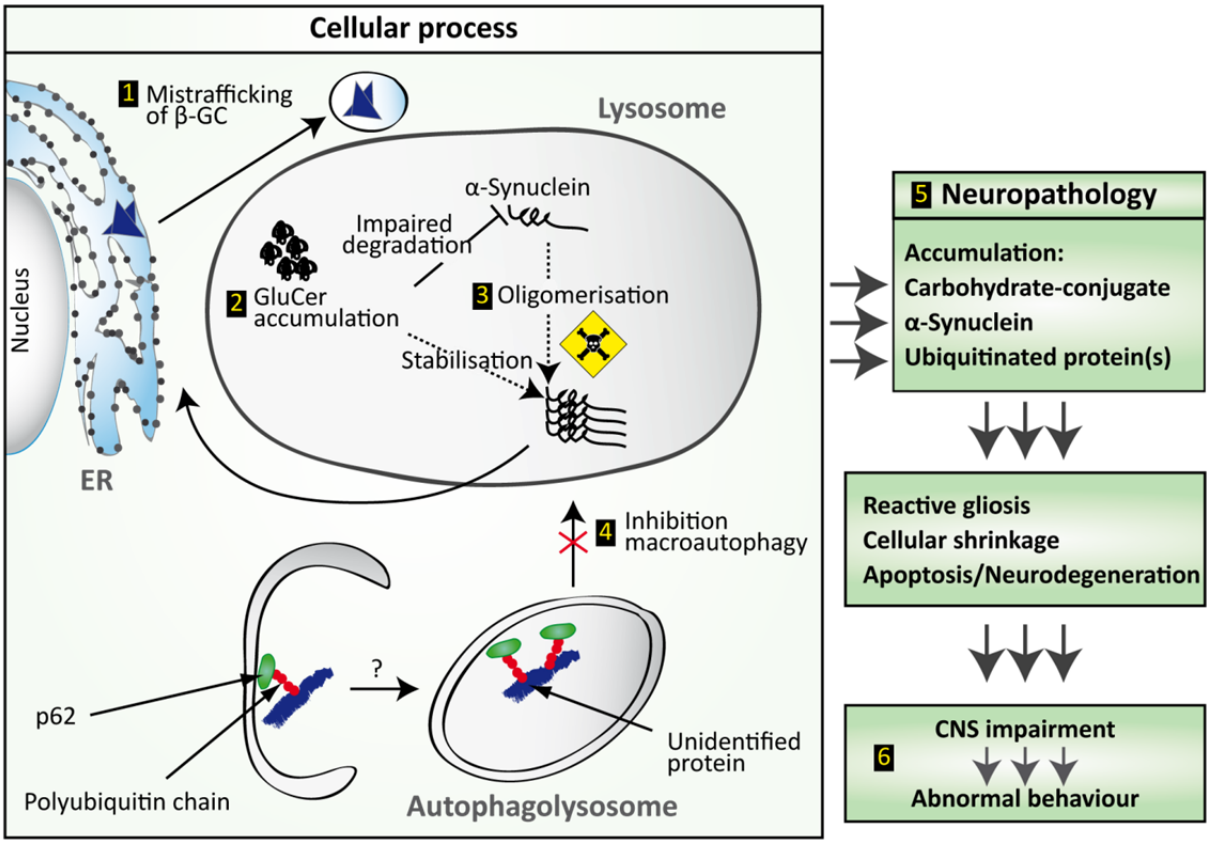

Figure 7.4 Model of molecular processes due to LIMP-2 deficiency. 1- β-GC does not reach the lysosome in the absence of LIMP-2. **2-** This in turn potentially leads to the accumulation of glucosylceramide (GluCer) within the lysosome which may lead to a reduction of degradation of α-synuclein. **3-** Consequently an increase in α-synuclein`s concentration ultimately results in its oligomerisation. **4-** Reduced lysosomal function due to storage within the cell may cause the blockage of macroautophagic clearance of certain substrates**. 5-** Accumulation of several potentially toxic substances probably eventually leads to apoptosis, neurodegeneration and reactive gliosis **6-** causing central nervous system (CNS) impairment manifesting as behavioural abnormalities in mice.

8 References

Accardo, A., Pensiero, S., Ciana, G., Parentin, F., and Bembi, B. (2010). Eye movement impairment recovery in a Gaucher patient treated with miglustat. Neurol Res Int *2010*, 358534.

Alfonso, P., Pampin, S., Estrada, J., Rodriguez-Rey, J.C., Giraldo, P., Sancho, J., and Pocovi, M. (2005). Miglustat (NB-DNJ) works as a chaperone for mutated acid beta-glucosidase in cells transfected with several Gaucher disease mutations. Blood cells, molecules & diseases *35*, 268-276.

Altarescu, G., Hill, S., Wiggs, E., Jeffries, N., Kreps, C., Parker, C.C., Brady, R.O., Barton, N.W., and Schiffmann, R. (2001). The efficacy of enzyme replacement therapy in patients with chronic neuronopathic Gaucher's disease. J Pediatr *138*, 539-547.

Arduino, D.M., Esteves, A.R., Cortes, L., Silva, D.F., Patel, B., Grazina, M., Swerdlow, R.H., Oliveira, C.R., and Cardoso, S.M. (2012). Mitochondrial metabolism in Parkinson's disease impairs quality control autophagy by hampering microtubule-dependent traffic. Human molecular genetics *21*, 4680-4702.

Arrasate, M., Mitra, S., Schweitzer, E.S., Segal, M.R., and Finkbeiner, S. (2004). Inclusion body formation reduces levels of mutant huntingtin and the risk of neuronal death. Nature *431*, 805-810.

Auluck, P.K., Chan, H.Y., Trojanowski, J.Q., Lee, V.M., and Bonini, N.M. (2002). Chaperone suppression of alpha-synuclein toxicity in a Drosophila model for Parkinson's disease. Science (New York, NY *295*, 865-868.

Baba, M., Nakajo, S., Tu, P.H., Tomita, T., Nakaya, K., Lee, V.M., Trojanowski, J.Q., and Iwatsubo, T. (1998). Aggregation of alpha-synuclein in Lewy bodies of sporadic Parkinson's disease and dementia with Lewy bodies. Am J Pathol *152*, 879-884.

Badhwar, A., Berkovic, S.F., Dowling, J.P., Gonzales, M., Narayanan, S., Brodtmann, A., Berzen, L., Caviness, J., Trenkwalder, C., Winkelmann, J.*, et al.* (2004). Action myoclonus-renal failure syndrome: characterization of a unique cerebro-renal disorder. Brain *127*, 2173-2182.

Bae, E.J., Lee, H.J., Rockenstein, E., Ho, D.H., Park, E.B., Yang, N.Y., Desplats, P., Masliah, E., and Lee, S.J. (2012). Antibody-aided clearance of extracellular alpha-synuclein prevents cell-to-cell aggregate transmission. J Neurosci *32*, 13454-13469.

Bainton, D.F. (1981). The discovery of lysosomes. The Journal of cell biology *91*, 66s-76s.

Balreira, A., Gaspar, P., Caiola, D., Chaves, J., Beirao, I., Lima, J.L., Azevedo, J.E., and Miranda, M.C. (2008). A nonsense mutation in the LIMP-2 gene associated with progressive myoclonic epilepsy and nephrotic syndrome. Human molecular genetics *17*, 2238-2243.

Banati, R.B., Gehrmann, J., Schubert, P., and Kreutzberg, G.W. (1993). Cytotoxicity of microglia. Glia *7*, 111-118.

Bartels, T., Choi, J.G., and Selkoe, D.J. (2011). alpha-Synuclein occurs physiologically as a helically folded tetramer that resists aggregation. Nature *477*, 107-110.

Bellucci, A., Navarria, L., Zaltieri, M., Missale, C., and Spano, P. (2012). alpha-Synuclein synaptic pathology and its implications in the development of novel therapeutic approaches to cure Parkinson's disease. Brain Res *1432*, 95-113.

Bendikov-Bar, I., Ron, I., Filocamo, M., and Horowitz, M. (2011). Characterization of the ERAD process of the L444P mutant glucocerebrosidase variant. Blood cells, molecules & diseases *46*, 4-10.

Berkovic, S.F., Dibbens, L.M., Oshlack, A., Silver, J.D., Katerelos, M., Vears, D.F., Lullmann-Rauch, R., Blanz, J., Zhang, K.W., Stankovich, J.*, et al.* (2008). Array-based gene discovery

with three unrelated subjects shows SCARB2/LIMP-2 deficiency causes myoclonus epilepsy and glomerulosclerosis. American journal of human genetics *82*, 673-684.
Biedler, J.L., Roffler-Tarlov, S., Schachner, M., and Freedman, L.S. (1978). Multiple neurotransmitter synthesis by human neuroblastoma cell lines and clones. Cancer Res *38*, 3751-3757.
Bjorkoy, G., Lamark, T., Brech, A., Outzen, H., Perander, M., Overvatn, A., Stenmark, H., and Johansen, T. (2005). p62/SQSTM1 forms protein aggregates degraded by autophagy and has a protective effect on huntingtin-induced cell death. The Journal of cell biology *171*, 603-614.
Blanz, J., Groth, J., Zachos, C., Wehling, C., Saftig, P., and Schwake, M. (2010). Disease-causing mutations within the lysosomal integral membrane protein type 2 (LIMP-2) reveal the nature of binding to its ligand beta-glucocerebrosidase. Human molecular genetics *19*, 563-572.
Blanz, J., Stroobants, S., Lullmann-Rauch, R., Morelle, W., Ludemann, M., D'Hooge, R., Reuterwall, H., Michalski, J.C., Fogh, J., Andersson, C*., et al.* (2008). Reversal of peripheral and central neural storage and ataxia after recombinant enzyme replacement therapy in alpha-mannosidosis mice. Human molecular genetics *17*, 3437-3445.
Block, M.L., and Hong, J.S. (2005). Microglia and inflammation-mediated neurodegeneration: multiple triggers with a common mechanism. Prog Neurobiol *76*, 77-98.
Boot, R.G., Verhoek, M., Donker-Koopman, W., Strijland, A., van Marle, J., Overkleeft, H.S., Wennekes, T., and Aerts, J.M. (2007). Identification of the non-lysosomal glucosylceramidase as beta-glucosidase 2. The Journal of biological chemistry *282*, 1305-1312.
Braak, H., Del Tredici, K., Rub, U., de Vos, R.A., Jansen Steur, E.N., and Braak, E. (2003). Staging of brain pathology related to sporadic Parkinson's disease. Neurobiol Aging *24*, 197-211.
Brady, R.O., Kanfer, J.N., Bradley, R.M., and Shapiro, D. (1966). Demonstration of a deficiency of glucocerebroside-cleaving enzyme in Gaucher's disease. The Journal of clinical investigation *45*, 1112-1115.
Brown, M.F., Farley, R.F., and Lorek, E.J. (2007). Remembrance of places you passed: social spatial working memory in rats. J Exp Psychol Anim Behav Process *33*, 213-224.
Buccoliero, R., Bodennec, J., and Futerman, A.H. (2002). The role of sphingolipids in neuronal development: lessons from models of sphingolipid storage diseases. Neurochemical research *27*, 565-574.
Bullock et al, W.O., Fernandez J M, Short J M. (1987). XL1-blue: a high efficiency plasmid transforming recA Escherichia coli strain with beta-galactosidase selection. BioTechniques *5*, 376–379.
Burke, D.G., Rahim, A.A., Waddington, S.N., Karlsson, S., Enquist, I., Bhatia, K., Mehta, A., Vellodi, A., and Heales, S. (2012). Increased glucocerebrosidase (GBA) 2 activity in GBA1 deficient mice brains and in Gaucher leucocytes. J Inherit Metab Dis.
Burre, J., Sharma, M., Tsetsenis, T., Buchman, V., Etherton, M.R., and Sudhof, T.C. (2010). Alpha-synuclein promotes SNARE-complex assembly in vivo and in vitro. Science (New York, NY *329*, 1663-1667.
Butler, D., Nixon, R.A., and Bahr, B.A. (2006). Potential compensatory responses through autophagic/lysosomal pathways in neurodegenerative diseases. Autophagy *2*, 234-237.
Canuel, M., Korkidakis, A., Konnyu, K., and Morales, C.R. (2008). Sortilin mediates the lysosomal targeting of cathepsins D and H. Biochemical and biophysical research communications *373*, 292-297.

Capablo, J.L., Franco, R., de Cabezon, A.S., Alfonso, P., Pocovi, M., and Giraldo, P. (2007). Neurologic improvement in a type 3 Gaucher disease patient treated with imiglucerase/miglustat combination. Epilepsia *48*, 1406-1408.

Chandra, S., Gallardo, G., Fernandez-Chacon, R., Schluter, O.M., and Sudhof, T.C. (2005). Alpha-synuclein cooperates with CSPalpha in preventing neurodegeneration. Cell *123*, 383-396.

Chaves, J., Beirao, I., Balreira, A., Gaspar, P., Caiola, D., Sa-Miranda, M.C., and Lima, J.L. (2011). Progressive myoclonus epilepsy with nephropathy C1q due to SCARB2/LIMP-2 deficiency: clinical report of two siblings. Seizure *20*, 738-740.

Clark, L.N., Kartsaklis, L.A., Wolf Gilbert, R., Dorado, B., Ross, B.M., Kisselev, S., Verbitsky, M., Mejia-Santana, H., Cote, L.J., Andrews, H.*, et al.* (2009). Association of glucocerebrosidase mutations with dementia with lewy bodies. Archives of neurology *66*, 578-583.

Cleeter, M.W., Chau, K.Y., Gluck, C., Mehta, A., Hughes, D.A., Duchen, M., Wood, N.W., Hardy, J., Mark Cooper, J., and Schapira, A.H. (2012). Glucocerebrosidase Inhibition Causes Mitochondrial Dysfunction And Free Radical Damage. Neurochem Int.

Cooper, A.A., Gitler, A.D., Cashikar, A., Haynes, C.M., Hill, K.J., Bhullar, B., Liu, K., Xu, K., Strathearn, K.E., Liu, F.*, et al.* (2006). Alpha-synuclein blocks ER-Golgi traffic and Rab1 rescues neuron loss in Parkinson's models. Science (New York, NY *313*, 324-328.

Cosma, M.P., Pepe, S., Annunziata, I., Newbold, R.F., Grompe, M., Parenti, G., and Ballabio, A. (2003). The multiple sulfatase deficiency gene encodes an essential and limiting factor for the activity of sulfatases. Cell *113*, 445-456.

Cox, T., Lachmann, R., Hollak, C., Aerts, J., van Weely, S., Hrebicek, M., Platt, F., Butters, T., Dwek, R., Moyses, C.*, et al.* (2000). Novel oral treatment of Gaucher's disease with N-butyldeoxynojirimycin (OGT 918) to decrease substrate biosynthesis. Lancet *355*, 1481-1485.

Cox, T.M., and Cachon-Gonzalez, M.B. (2012). The cellular pathology of lysosomal diseases. J Pathol *226*, 241-254.

Cuervo, A.M., Bergamini, E., Brunk, U.T., Droge, W., Ffrench, M., and Terman, A. (2005). Autophagy and aging: the importance of maintaining "clean" cells. Autophagy *1*, 131-140.

Cuervo, A.M., and Dice, J.F. (2000). When lysosomes get old. Exp Gerontol *35*, 119-131.

Cuervo, A.M., Stefanis, L., Fredenburg, R., Lansbury, P.T., and Sulzer, D. (2004). Impaired degradation of mutant alpha-synuclein by chaperone-mediated autophagy. Science (New York, NY *305*, 1292-1295.

Cullen, V., Lindfors, M., Ng, J., Paetau, A., Swinton, E., Kolodziej, P., Boston, H., Saftig, P., Woulfe, J., Feany, M.B.*, et al.* (2009). Cathepsin D expression level affects alpha-synuclein processing, aggregation, and toxicity in vivo. Mol Brain *2*, 5.

Cullen, V., Sardi, S.P., Ng, J., Xu, Y.H., Sun, Y., Tomlinson, J.J., Kolodziej, P., Kahn, I., Saftig, P., Woulfe, J.*, et al.* (2011). Acid beta-glucosidase mutants linked to Gaucher disease, Parkinson disease, and Lewy body dementia alter alpha-synuclein processing. Annals of neurology *69*, 940-953.

Dardis, A., Filocamo, M., Grossi, S., Ciana, G., Franceschetti, S., Dominissini, S., Rubboli, G., Di Rocco, M., and Bembi, B. (2009). Biochemical and molecular findings in a patient with myoclonic epilepsy due to a mistarget of the beta-glucosidase enzyme. Molecular genetics and metabolism *97*, 309-311.

Davidson, W.S., Jonas, A., Clayton, D.F., and George, J.M. (1998). Stabilization of alpha-synuclein secondary structure upon binding to synthetic membranes. The Journal of biological chemistry *273*, 9443-9449.

Davie, C.A. (2008). A review of Parkinson's disease. Br Med Bull *86*, 109-127.

de Duve, C. (1959). Lysosomes, a new group of cytoplasmic particles. Subcellular Particles Ed, 128-159.
De Duve, C., and Beaufay, H. (1959). Tissue fractionation studies. 10. Influence of ischaemia on the state of some bound enzymes in rat liver. The Biochemical journal *73*, 610-616.
Dehay, B., Ramirez, A., Martinez-Vicente, M., Perier, C., Canron, M.H., Doudnikoff, E., Vital, A., Vila, M., Klein, C., and Bezard, E. (2012). Loss of P-type ATPase ATP13A2/PARK9 function induces general lysosomal deficiency and leads to Parkinson disease neurodegeneration. Proceedings of the National Academy of Sciences of the United States of America *109*, 9611-9616.
Dekker, N., van Dussen, L., Hollak, C.E., Overkleeft, H., Scheij, S., Ghauharali, K., van Breemen, M.J., Ferraz, M.J., Groener, J.E., Maas, M.*, et al.* (2011). Elevated plasma glucosylsphingosine in Gaucher disease: relation to phenotype, storage cell markers, and therapeutic response. Blood *118*, e118-127.
Del Bigio, M.R., Chudley, A.E., Booth, F.A., and Pacin, S. (2004). Late infantile onset krabbe disease in siblings with cortical degeneration and absence of cerebral globoid cells. Neuropediatrics *35*, 297-301.
Desmond, M.J., Lee, D., Fraser, S.A., Katerelos, M., Gleich, K., Martinello, P., Li, Y.Q., Thomas, M.C., Michelucci, R., Cole, A.J.*, et al.* (2011). Tubular proteinuria in mice and humans lacking the intrinsic lysosomal protein SCARB2/Limp-2. American journal of physiology *300*, F1437-1447.
Dibbens, L.M., Michelucci, R., Gambardella, A., Andermann, F., Rubboli, G., Bayly, M.A., Joensuu, T., Vears, D.F., Franceschetti, S., Canafoglia, L.*, et al.* (2009). SCARB2 mutations in progressive myoclonus epilepsy (PME) without renal failure. Annals of neurology *66*, 532-536.
Dittmer, F., Ulbrich, E.J., Hafner, A., Schmahl, W., Meister, T., Pohlmann, R., and von Figura, K. (1999). Alternative mechanisms for trafficking of lysosomal enzymes in mannose 6-phosphate receptor-deficient mice are cell type-specific. Journal of cell science *112 (Pt 10)*, 1591-1597.
Do, C.B., Tung, J.Y., Dorfman, E., Kiefer, A.K., Drabant, E.M., Francke, U., Mountain, J.L., Goldman, S.M., Tanner, C.M., Langston, J.W.*, et al.* (2011). Web-based genome-wide association study identifies two novel loci and a substantial genetic component for Parkinson's disease. PLoS Genet *7*, e1002141.
Dobrenis, K., Chang, H.Y., Pina-Benabou, M.H., Woodroffe, A., Lee, S.C., Rozental, R., Spray, D.C., and Scemes, E. (2005). Human and mouse microglia express connexin36, and functional gap junctions are formed between rodent microglia and neurons. J Neurosci Res *82*, 306-315.
Dong, X.P., Cheng, X., Mills, E., Delling, M., Wang, F., Kurz, T., and Xu, H. (2008). The type IV mucolipidosis-associated protein TRPML1 is an endolysosomal iron release channel. Nature *455*, 992-996.
Duncan, J.R., and Kornfeld, S. (1988). Intracellular movement of two mannose 6-phosphate receptors: return to the Golgi apparatus. The Journal of cell biology *106*, 617-628.
Dvir, H., Harel, M., McCarthy, A.A., Toker, L., Silman, I., Futerman, A.H., and Sussman, J.L. (2003). X-ray structure of human acid-beta-glucosidase, the defective enzyme in Gaucher disease. EMBO reports *4*, 704-709.
Ebrahimi-Fakhari, D., Cantuti-Castelvetri, I., Fan, Z., Rockenstein, E., Masliah, E., Hyman, B.T., McLean, P.J., and Unni, V.K. (2011). Distinct roles in vivo for the ubiquitin-proteasome system and the autophagy-lysosomal pathway in the degradation of alpha-synuclein. J Neurosci *31*, 14508-14520.

Enquist, I.B., Lo Bianco, C., Ooka, A., Nilsson, E., Mansson, J.E., Ehinger, M., Richter, J., Brady, R.O., Kirik, D., and Karlsson, S. (2007). Murine models of acute neuronopathic Gaucher disease. Proceedings of the National Academy of Sciences of the United States of America *104*, 17483-17488.

Eskelinen, E.L., Tanaka, Y., and Saftig, P. (2003). At the acidic edge: emerging functions for lysosomal membrane proteins. Trends in cell biology *13*, 137-145.

Farfel-Becker, T., Vitner, E.B., and Futerman, A.H. (2011). Animal models for Gaucher disease research. Dis Model Mech *4*, 746-752.

Filimonenko, M., Isakson, P., Finley, K.D., Anderson, M., Jeong, H., Melia, T.J., Bartlett, B.J., Myers, K.M., Birkeland, H.C., Lamark, T*., et al.* (2010). The selective macroautophagic degradation of aggregated proteins requires the PI3P-binding protein Alfy. Mol Cell *38*, 265-279.

Forgac, M. (1998). Structure, function and regulation of the vacuolar (H+)-ATPases. FEBS letters *440*, 258-263.

Fujita, H., Ezaki, J., Noguchi, Y., Kono, A., Himeno, M., and Kato, K. (1991). Isolation and sequencing of a cDNA clone encoding 85kDa sialoglycoprotein in rat liver lysosomal membranes. Biochemical and biophysical research communications *178*, 444-452.

Fujiwara, H., Hasegawa, M., Dohmae, N., Kawashima, A., Masliah, E., Goldberg, M.S., Shen, J., Takio, K., and Iwatsubo, T. (2002). alpha-Synuclein is phosphorylated in synucleinopathy lesions. Nature cell biology *4*, 160-164.

Fukuda, T., Ewan, L., Bauer, M., Mattaliano, R.J., Zaal, K., Ralston, E., Plotz, P.H., and Raben, N. (2006). Dysfunction of endocytic and autophagic pathways in a lysosomal storage disease. Annals of neurology *59*, 700-708.

Furst, W., and Sandhoff, K. (1992). Activator proteins and topology of lysosomal sphingolipid catabolism. Biochimica et biophysica acta *1126*, 1-16.

Futerman, A.H., and Pagano, R.E. (1991). Determination of the intracellular sites and topology of glucosylceramide synthesis in rat liver. The Biochemical journal *280 (Pt 2)*, 295-302.

Galvin, J.E., Lee, V.M., and Trojanowski, J.Q. (2001). Synucleinopathies: clinical and pathological implications. Archives of neurology *58*, 186-190.

Gamp, A.C., Tanaka, Y., Lullmann-Rauch, R., Wittke, D., D'Hooge, R., De Deyn, P.P., Moser, T., Maier, H., Hartmann, D., Reiss, K*., et al.* (2003). LIMP-2/LGP85 deficiency causes ureteric pelvic junction obstruction, deafness and peripheral neuropathy in mice. Human molecular genetics *12*, 631-646.

Gavrieli, Y., Sherman, Y., and Ben-Sasson, S.A. (1992). Identification of programmed cell death in situ via specific labeling of nuclear DNA fragmentation. The Journal of cell biology *119*, 493-501.

Gegg, M.E., Burke, D., Heales, S.J., Cooper, J.M., Hardy, J., Wood, N.W., and Schapira, A.H. (2012). Glucocerebrosidase deficiency in substantia nigra of parkinson disease brains. Annals of neurology *72*, 455-463.

Gelfman, C.M., Vogel, P., Issa, T.M., Turner, C.A., Lee, W.S., Kornfeld, S., and Rice, D.S. (2007). Mice lacking alpha/beta subunits of GlcNAc-1-phosphotransferase exhibit growth retardation, retinal degeneration, and secretory cell lesions. Invest Ophthalmol Vis Sci *48*, 5221-5228.

Ginzburg, L., Kacher, Y., and Futerman, A.H. (2004). The pathogenesis of glycosphingolipid storage disorders. Semin Cell Dev Biol *15*, 417-431.

Goker-Alpan, O., Giasson, B.I., Eblan, M.J., Nguyen, J., Hurtig, H.I., Lee, V.M., Trojanowski, J.Q., and Sidransky, E. (2006). Glucocerebrosidase mutations are an important risk factor for Lewy body disorders. Neurology *67*, 908-910.

Goker-Alpan, O., Stubblefield, B.K., Giasson, B.I., and Sidransky, E. (2010). Glucocerebrosidase is present in alpha-synuclein inclusions in Lewy body disorders. Acta neuropathologica *120*, 641-649.

Goldblatt, J., Szer, J., Fletcher, J.M., McGill, J., Rowell, J.A., and Wilson, M. (2005). Enzyme replacement therapy for Gaucher disease in Australia. Intern Med J *35*, 156-161.

Gomez-Isla, T., Irizarry, M.C., Mariash, A., Cheung, B., Soto, O., Schrump, S., Sondel, J., Kotilinek, L., Day, J., Schwarzschild, M.A*., et al.* (2003). Motor dysfunction and gliosis with preserved dopaminergic markers in human alpha-synuclein A30P transgenic mice. Neurobiol Aging *24*, 245-258.

Gonzalez-Noriega, A., Grubb, J.H., Talkad, V., and Sly, W.S. (1980). Chloroquine inhibits lysosomal enzyme pinocytosis and enhances lysosomal enzyme secretion by impairing receptor recycling. The Journal of cell biology *85*, 839-852.

Grabowski, G.A., Leslie, N., and Wenstrup, R. (1998). Enzyme therapy for Gaucher disease: the first 5 years. Blood Rev *12*, 115-133.

Graves, A.R., Curran, P.K., Smith, C.L., and Mindell, J.A. (2008). The Cl-/H+ antiporter ClC-7 is the primary chloride permeation pathway in lysosomes. Nature *453*, 788-792.

Greten-Harrison, B., Polydoro, M., Morimoto-Tomita, M., Diao, L., Williams, A.M., Nie, E.H., Makani, S., Tian, N., Castillo, P.E., Buchman, V.L*., et al.* (2010). alphabetagamma-Synuclein triple knockout mice reveal age-dependent neuronal dysfunction. Proceedings of the National Academy of Sciences of the United States of America *107*, 19573-19578.

Gunther, W., Luchow, A., Cluzeaud, F., Vandewalle, A., and Jentsch, T.J. (1998). ClC-5, the chloride channel mutated in Dent's disease, colocalizes with the proton pump in endocytotically active kidney cells. Proceedings of the National Academy of Sciences of the United States of America *95*, 8075-8080.

Guyenet, S.J., Furrer, S.A., Damian, V.M., Baughan, T.D., La Spada, A.R., and Garden, G.A. (2010). A simple composite phenotype scoring system for evaluating mouse models of cerebellar ataxia. J Vis Exp.

Han, H., Weinreb, P.H., and Lansbury, P.T., Jr. (1995). The core Alzheimer's peptide NAC forms amyloid fibrils which seed and are seeded by beta-amyloid: is NAC a common trigger or target in neurodegenerative disease? Chem Biol *2*, 163-169.

Hentze, M., Hasilik, A., and von Figura, K. (1984). Enhanced degradation of cathepsin D synthesized in the presence of the threonine analog beta-hydroxynorvaline. Archives of biochemistry and biophysics *230*, 375-382.

Hindle, J.V. (2010). Ageing, neurodegeneration and Parkinson's disease. Age Ageing *39*, 156-161.

Holness, C.L., and Simmons, D.L. (1993). Molecular cloning of CD68, a human macrophage marker related to lysosomal glycoproteins. Blood *81*, 1607-1613.

Honing, S., Sandoval, I.V., and von Figura, K. (1998). A di-leucine-based motif in the cytoplasmic tail of LIMP-II and tyrosinase mediates selective binding of AP-3. The EMBO journal *17*, 1304-1314.

Hopfner, F., Schormair, B., Knauf, F., Berthele, A., Tolle, T.R., Baron, R., Maier, C., Treede, R.D., Binder, A., Sommer, C*., et al.* (2011). Novel SCARB2 mutation in action myoclonus-renal failure syndrome and evaluation of SCARB2 mutations in isolated AMRF features. BMC Neurol *11*, 134.

Hopfner, F., Schulte, E.C., Mollenhauer, B., Bereznai, B., Knauf, F., Lichtner, P., Zimprich, A., Haubenberger, D., Pirker, W., Brucke, T.*, et al.* (2013). The role of SCARB2 as susceptibility factor in Parkinson's disease. Mov Disord.

Horowitz, M., and Zimran, A. (1994). Mutations causing Gaucher disease. Human mutation *3*, 1-11.

Hsu, L.J., Sagara, Y., Arroyo, A., Rockenstein, E., Sisk, A., Mallory, M., Wong, J., Takenouchi, T., Hashimoto, M., and Masliah, E. (2000). alpha-synuclein promotes mitochondrial deficit and oxidative stress. Am J Pathol *157*, 401-410.

Huang, Y., Chegini, F., Chua, G., Murphy, K., Gai, W., and Halliday, G.M. (2012). Macroautophagy in sporadic and the genetic form of Parkinson's disease with the A53T alpha-synuclein mutation. Transl Neurodegener *1*, 2.

Huxley, C., Passage, E., Manson, A., Putzu, G., Figarella-Branger, D., Pellissier, J.F., and Fontes, M. (1996). Construction of a mouse model of Charcot-Marie-Tooth disease type 1A by pronuclear injection of human YAC DNA. Human molecular genetics *5*, 563-569.

Huynh-Ba, G., Friedberg, J.R., Vogiatzi, D., and Ioannidou, E. (2008). Implant failure predictors in the posterior maxilla: a retrospective study of 273 consecutive implants. J Periodontol *79*, 2256-2261.

Infante, R.E., Wang, M.L., Radhakrishnan, A., Kwon, H.J., Brown, M.S., and Goldstein, J.L. (2008). NPC2 facilitates bidirectional transfer of cholesterol between NPC1 and lipid bilayers, a step in cholesterol egress from lysosomes. Proceedings of the National Academy of Sciences of the United States of America *105*, 15287-15292.

Ioannou, Y.A. (2000). The structure and function of the Niemann-Pick C1 protein. Molecular genetics and metabolism *71*, 175-181.

Ittner, L.M., Fath, T., Ke, Y.D., Bi, M., van Eersel, J., Li, K.M., Gunning, P., and Gotz, J. (2008). Parkinsonism and impaired axonal transport in a mouse model of frontotemporal dementia. Proceedings of the National Academy of Sciences of the United States of America *105*, 15997-16002.

Jankovic, J. (2008). Parkinson's disease: clinical features and diagnosis. J Neurol Neurosurg Psychiatry *79*, 368-376.

Janvier, K., Kato, Y., Boehm, M., Rose, J.R., Martina, J.A., Kim, B.Y., Venkatesan, S., and Bonifacino, J.S. (2003). Recognition of dileucine-based sorting signals from HIV-1 Nef and LIMP-II by the AP-1 gamma-sigma1 and AP-3 delta-sigma3 hemicomplexes. The Journal of cell biology *163*, 1281-1290.

Jeyakumar, M., Thomas, R., Elliot-Smith, E., Smith, D.A., van der Spoel, A.C., d'Azzo, A., Perry, V.H., Butters, T.D., Dwek, R.A., and Platt, F.M. (2003). Central nervous system inflammation is a hallmark of pathogenesis in mouse models of GM1 and GM2 gangliosidosis. Brain *126*, 974-987.

Kabeya, Y., Mizushima, N., Ueno, T., Yamamoto, A., Kirisako, T., Noda, T., Kominami, E., Ohsumi, Y., and Yoshimori, T. (2000). LC3, a mammalian homologue of yeast Apg8p, is localized in autophagosome membranes after processing. The EMBO journal *19*, 5720-5728.

Karpinar, D.P., Balija, M.B., Kugler, S., Opazo, F., Rezaei-Ghaleh, N., Wender, N., Kim, H.Y., Taschenberger, G., Falkenburger, B.H., Heise, H.*, et al.* (2009). Pre-fibrillar alpha-synuclein variants with impaired beta-structure increase neurotoxicity in Parkinson's disease models. The EMBO journal *28*, 3256-3268.

Kasper, D., Planells-Cases, R., Fuhrmann, J.C., Scheel, O., Zeitz, O., Ruether, K., Schmitt, A., Poet, M., Steinfeld, R., Schweizer, M.*, et al.* (2005). Loss of the chloride channel ClC-7 leads to lysosomal storage disease and neurodegeneration. The EMBO journal *24*, 1079-1091.

Kerr, J.F., Wyllie, A.H., and Currie, A.R. (1972). Apoptosis: a basic biological phenomenon with wide-ranging implications in tissue kinetics. Br J Cancer *26*, 239-257.
Khanna, R., Benjamin, E.R., Pellegrino, L., Schilling, A., Rigat, B.A., Soska, R., Nafar, H., Ranes, B.E., Feng, J., Lun, Y.*, et al.* (2010). The pharmacological chaperone isofagomine increases the activity of the Gaucher disease L444P mutant form of beta-glucosidase. FEBS J *277*, 1618-1638.
Kim, C., Ho, D.H., Suk, J.E., You, S., Michael, S., Kang, J., Joong Lee, S., Masliah, E., Hwang, D., Lee, H.J.*, et al.* (2013). Neuron-released oligomeric alpha-synuclein is an endogenous agonist of TLR2 for paracrine activation of microglia. Nat Commun *4*, 1562.
Kiselyov, K., Chen, J., Rbaibi, Y., Oberdick, D., Tjon-Kon-Sang, S., Shcheynikov, N., Muallem, S., and Soyombo, A. (2005). TRP-ML1 is a lysosomal monovalent cation channel that undergoes proteolytic cleavage. The Journal of biological chemistry *280*, 43218-43223.
Kitada, T., Asakawa, S., Hattori, N., Matsumine, H., Yamamura, Y., Minoshima, S., Yokochi, M., Mizuno, Y., and Shimizu, N. (1998). Mutations in the parkin gene cause autosomal recessive juvenile parkinsonism. Nature *392*, 605-608.
Knipper, M., Claussen, C., Ruttiger, L., Zimmermann, U., Lullmann-Rauch, R., Eskelinen, E.L., Schroder, J., Schwake, M., and Saftig, P. (2006). Deafness in LIMP2-deficient mice due to early loss of the potassium channel KCNQ1/KCNE1 in marginal cells of the stria vascularis. The Journal of physiology *576*, 73-86.
Kollmann, K., Damme, M., Markmann, S., Morelle, W., Schweizer, M., Hermans-Borgmeyer, I., Rochert, A.K., Pohl, S., Lubke, T., Michalski, J.C.*, et al.* (2012). Lysosomal dysfunction causes neurodegeneration in mucolipidosis II 'knock-in' mice. Brain *135*, 2661-2675.
Komatsu, M., Waguri, S., Koike, M., Sou, Y.S., Ueno, T., Hara, T., Mizushima, N., Iwata, J., Ezaki, J., Murata, S.*, et al.* (2007). Homeostatic levels of p62 control cytoplasmic inclusion body formation in autophagy-deficient mice. Cell *131*, 1149-1163.
Komatsu, M., Waguri, S., Ueno, T., Iwata, J., Murata, S., Tanida, I., Ezaki, J., Mizushima, N., Ohsumi, Y., Uchiyama, Y.*, et al.* (2005). Impairment of starvation-induced and constitutive autophagy in Atg7-deficient mice. The Journal of cell biology *169*, 425-434.
Kopito, R.R. (2000). Aggresomes, inclusion bodies and protein aggregation. Trends in cell biology *10*, 524-530.
Korschen, H.G., Yildiz, Y., Raju, D.N., Schonauer, S., Bonigk, W., Jansen, V., Kremmer, E., Kaupp, U.B., and Wachten, D. (2013). The Non-lysosomal beta-Glucosidase GBA2 Is a Non-integral Membrane-associated Protein at the Endoplasmic Reticulum (ER) and Golgi. The Journal of biological chemistry *288*, 3381-3393.
Kramer, M.L., and Schulz-Schaeffer, W.J. (2007). Presynaptic alpha-synuclein aggregates, not Lewy bodies, cause neurodegeneration in dementia with Lewy bodies. J Neurosci *27*, 1405-1410.
Kreutzberg, G.W. (1996). Microglia: a sensor for pathological events in the CNS. Trends Neurosci *19*, 312-318.
Kruger, R., Kuhn, W., Muller, T., Woitalla, D., Graeber, M., Kosel, S., Przuntek, H., Epplen, J.T., Schols, L., and Riess, O. (1998). Ala30Pro mutation in the gene encoding alpha-synuclein in Parkinson's disease. Nat Genet *18*, 106-108.
Kuronita, T., Eskelinen, E.L., Fujita, H., Saftig, P., Himeno, M., and Tanaka, Y. (2002). A role for the lysosomal membrane protein LGP85 in the biogenesis and maintenance of endosomal and lysosomal morphology. Journal of cell science *115*, 4117-4131.
Kuronita, T., Hatano, T., Furuyama, A., Hirota, Y., Masuyama, N., Saftig, P., Himeno, M., Fujita, H., and Tanaka, Y. (2005). The NH(2)-terminal transmembrane and lumenal domains

of LGP85 are needed for the formation of enlarged endosomes/lysosomes. Traffic (Copenhagen, Denmark) *6*, 895-906.
Kurzawa-Akanbi, M., Hanson, P.S., Blain, P.G., Lett, D.J., McKeith, I.G., Chinnery, P.F., and Morris, C.M. (2012). Glucocerebrosidase mutations alter the endoplasmic reticulum and lysosomes in Lewy body disease. J Neurochem *123*, 298-309.
Lachmann, R.H. (2006). Miglustat: substrate reduction therapy for glycosphingolipid lysosomal storage disorders. Drugs Today (Barc) *42*, 29-38.
Laemmli, U.K. (1970). Cleavage of structural proteins during the assembly of the head of bacteriophage T4. Nature *227*, 680-685.
Lamark, T., and Johansen, T. (2010). Autophagy: links with the proteasome. Curr Opin Cell Biol *22*, 192-198.
Langston, J.W., Ballard, P., Tetrud, J.W., and Irwin, I. (1983). Chronic Parkinsonism in humans due to a product of meperidine-analog synthesis. Science (New York, NY *219*, 979-980.
Lashuel, H.A., and Lansbury, P.T., Jr. (2006). Are amyloid diseases caused by protein aggregates that mimic bacterial pore-forming toxins? Q Rev Biophys *39*, 167-201.
Lashuel, H.A., Petre, B.M., Wall, J., Simon, M., Nowak, R.J., Walz, T., and Lansbury, P.T., Jr. (2002). Alpha-synuclein, especially the Parkinson's disease-associated mutants, forms pore-like annular and tubular protofibrils. J Mol Biol *322*, 1089-1102.
Lazzarino, D.A., and Gabel, C.A. (1988). Biosynthesis of the mannose 6-phosphate recognition marker in transport-impaired mouse lymphoma cells. Demonstration of a two-step phosphorylation. The Journal of biological chemistry *263*, 10118-10126.
Lee, M.K., Stirling, W., Xu, Y., Xu, X., Qui, D., Mandir, A.S., Dawson, T.M., Copeland, N.G., Jenkins, N.A., and Price, D.L. (2002). Human alpha-synuclein-harboring familial Parkinson's disease-linked Ala-53 --> Thr mutation causes neurodegenerative disease with alpha-synuclein aggregation in transgenic mice. Proceedings of the National Academy of Sciences of the United States of America *99*, 8968-8973.
Lefrancois, S., Zeng, J., Hassan, A.J., Canuel, M., and Morales, C.R. (2003). The lysosomal trafficking of sphingolipid activator proteins (SAPs) is mediated by sortilin. The EMBO journal *22*, 6430-6437.
Leonova, T., Qi, X., Bencosme, A., Ponce, E., Sun, Y., and Grabowski, G.A. (1996). Proteolytic processing patterns of prosaposin in insect and mammalian cells. The Journal of biological chemistry *271*, 17312-17320.
Leroy, E., Boyer, R., Auburger, G., Leube, B., Ulm, G., Mezey, E., Harta, G., Brownstein, M.J., Jonnalagada, S., Chernova, T.*, et al.* (1998). The ubiquitin pathway in Parkinson's disease. Nature *395*, 451-452.
Lesage, S., Anheim, M., Condroyer, C., Pollak, P., Durif, F., Dupuits, C., Viallet, F., Lohmann, E., Corvol, J.C., Honore, A.*, et al.* (2011). Large-scale screening of the Gaucher's disease-related glucocerebrosidase gene in Europeans with Parkinson's disease. Human molecular genetics *20*, 202-210.
Lin, Y.W., Yu, S.L., Shao, H.Y., Lin, H.Y., Liu, C.C., Hsiao, K.N., Chitra, E., Tsou, Y.L., Chang, H.W., Sia, C.*, et al.* (2013). Human SCARB2 Transgenic Mice as an Infectious Animal Model for Enterovirus 71. PloS one *8*, e57591.
Liu, Y., Fallon, L., Lashuel, H.A., Liu, Z., and Lansbury, P.T., Jr. (2002). The UCH-L1 gene encodes two opposing enzymatic activities that affect alpha-synuclein degradation and Parkinson's disease susceptibility. Cell *111*, 209-218.
Liu, Y., Suzuki, K., Reed, J.D., Grinberg, A., Westphal, H., Hoffmann, A., Doring, T., Sandhoff, K., and Proia, R.L. (1998). Mice with type 2 and 3 Gaucher disease point mutations generated

by a single insertion mutagenesis procedure. Proceedings of the National Academy of Sciences of the United States of America *95*, 2503-2508.
Livak, K.J., and Schmittgen, T.D. (2001). Analysis of relative gene expression data using real-time quantitative PCR and the 2(-Delta Delta C(T)) Method. Methods *25*, 402-408.
Manning-Bog, A.B., Schule, B., and Langston, J.W. (2009). Alpha-synuclein-glucocerebrosidase interactions in pharmacological Gaucher models: a biological link between Gaucher disease and parkinsonism. Neurotoxicology *30*, 1127-1132.
Marsh, M., Schmid, S., Kern, H., Harms, E., Male, P., Mellman, I., and Helenius, A. (1987). Rapid analytical and preparative isolation of functional endosomes by free flow electrophoresis. The Journal of cell biology *104*, 875-886.
Martin, L.J., Pan, Y., Price, A.C., Sterling, W., Copeland, N.G., Jenkins, N.A., Price, D.L., and Lee, M.K. (2006). Parkinson's disease alpha-synuclein transgenic mice develop neuronal mitochondrial degeneration and cell death. J Neurosci *26*, 41-50.
Martinez-Pineiro, L., Galicia de Pedro, I., Cisneros, J., Cuervo, E., Frias Iniesta, J., and Martinez-Pineiro, J.A. (1996). [New features of pharmacologic treatment of erectile dysfunction]. Arch Esp Urol *49*, 270-276.
Masliah, E., Rockenstein, E., Veinbergs, I., Mallory, M., Hashimoto, M., Takeda, A., Sagara, Y., Sisk, A., and Mucke, L. (2000). Dopaminergic loss and inclusion body formation in alpha-synuclein mice: implications for neurodegenerative disorders. Science (New York, NY *287*, 1265-1269.
Matsui, H., Nishinaka, K., Oda, M., Niikawa, H., Komatsu, K., Kubori, T., and Udaka, F. (2006). Disruptions of the fornix fiber in Parkinsonian patients with excessive daytime sleepiness. Parkinsonism & related disorders *12*, 319-322.
Mazzulli, J.R., Mishizen, A.J., Giasson, B.I., Lynch, D.R., Thomas, S.A., Nakashima, A., Nagatsu, T., Ota, A., and Ischiropoulos, H. (2006). Cytosolic catechols inhibit alpha-synuclein aggregation and facilitate the formation of intracellular soluble oligomeric intermediates. J Neurosci *26*, 10068-10078.
Mazzulli, J.R., Xu, Y.H., Sun, Y., Knight, A.L., McLean, P.J., Caldwell, G.A., Sidransky, E., Grabowski, G.A., and Krainc, D. (2011). Gaucher disease glucocerebrosidase and alpha-synuclein form a bidirectional pathogenic loop in synucleinopathies. Cell *146*, 37-52.
Meikle, P.J., Hopwood, J.J., Clague, A.E., and Carey, W.F. (1999). Prevalence of lysosomal storage disorders. JAMA *281*, 249-254.
Michelakakis, H., Xiromerisiou, G., Dardiotis, E., Bozi, M., Vassilatis, D., Kountra, P.M., Patramani, G., Moraitou, M., Papadimitriou, D., Stamboulis, E.*, et al.* (2012). Evidence of an association between the scavenger receptor class B member 2 gene and Parkinson's disease. Mov Disord *27*, 400-405.
Mizushima, N., Levine, B., Cuervo, A.M., and Klionsky, D.J. (2008). Autophagy fights disease through cellular self-digestion. Nature *451*, 1069-1075.
Moran, L.B., Croisier, E., Duke, D.C., Kalaitzakis, M.E., Roncaroli, F., Deprez, M., Dexter, D.T., Pearce, R.K., and Graeber, M.B. (2007). Analysis of alpha-synuclein, dopamine and parkin pathways in neuropathologically confirmed parkinsonian nigra. Acta neuropathologica *113*, 253-263.
Morris, R.G.M. (1981). Spatial Localization Does Not Require the Presence of Local Cues. Learn Motiv *12*, 239-260.
Mullen, R.J., Buck, C.R., and Smith, A.M. (1992). NeuN, a neuronal specific nuclear protein in vertebrates. Development (Cambridge, England) *116*, 201-211.

Mullis, K., Faloona, F., Scharf, S., Saiki, R., Horn, G., and Erlich, H. (1986). Specific enzymatic amplification of DNA in vitro: the polymerase chain reaction. Cold Spring Harb Symp Quant Biol *51 Pt 1*, 263-273.
Murphy, D.D., Rueter, S.M., Trojanowski, J.Q., and Lee, V.M. (2000). Synucleins are developmentally expressed, and alpha-synuclein regulates the size of the presynaptic vesicular pool in primary hippocampal neurons. J Neurosci *20*, 3214-3220.
Narendra, D., Tanaka, A., Suen, D.F., and Youle, R.J. (2008). Parkin is recruited selectively to impaired mitochondria and promotes their autophagy. The Journal of cell biology *183*, 795-803.
Nilsson, O., and Svennerholm, L. (1982). Accumulation of glucosylceramide and glucosylsphingosine (psychosine) in cerebrum and cerebellum in infantile and juvenile Gaucher disease. J Neurochem *39*, 709-718.
Nishioka, K., Hayashi, S., Farrer, M.J., Singleton, A.B., Yoshino, H., Imai, H., Kitami, T., Sato, K., Kuroda, R., Tomiyama, H.*, et al.* (2006). Clinical heterogeneity of alpha-synuclein gene duplication in Parkinson's disease. Annals of neurology *59*, 298-309.
Nixon, R.A., Cataldo, A.M., and Mathews, P.M. (2000). The endosomal-lysosomal system of neurons in Alzheimer's disease pathogenesis: a review. Neurochemical research *25*, 1161-1172.
Nuytemans, K., Theuns, J., Cruts, M., and Van Broeckhoven, C. (2010). Genetic etiology of Parkinson disease associated with mutations in the SNCA, PARK2, PINK1, PARK7, and LRRK2 genes: a mutation update. Human mutation *31*, 763-780.
O'Callaghan, J.P., and Jensen, K.F. (1992). Enhanced expression of glial fibrillary acidic protein and the cupric silver degeneration reaction can be used as sensitive and early indicators of neurotoxicity. Neurotoxicology *13*, 113-122.
Okochi, M., Walter, J., Koyama, A., Nakajo, S., Baba, M., Iwatsubo, T., Meijer, L., Kahle, P.J., and Haass, C. (2000). Constitutive phosphorylation of the Parkinson's disease associated alpha-synuclein. The Journal of biological chemistry *275*, 390-397.
Olzmann, J.A., and Chin, L.S. (2008). Parkin-mediated K63-linked polyubiquitination: a signal for targeting misfolded proteins to the aggresome-autophagy pathway. Autophagy *4*, 85-87.
Orvisky, E., Park, J.K., LaMarca, M.E., Ginns, E.I., Martin, B.M., Tayebi, N., and Sidransky, E. (2002). Glucosylsphingosine accumulation in tissues from patients with Gaucher disease: correlation with phenotype and genotype. Molecular genetics and metabolism *76*, 262-270.
Orvisky, E., Sidransky, E., McKinney, C.E., Lamarca, M.E., Samimi, R., Krasnewich, D., Martin, B.M., and Ginns, E.I. (2000). Glucosylsphingosine accumulation in mice and patients with type 2 Gaucher disease begins early in gestation. Pediatric research *48*, 233-237.
Overly, C.C., and Hollenbeck, P.J. (1996). Dynamic organization of endocytic pathways in axons of cultured sympathetic neurons. J Neurosci *16*, 6056-6064.
Owada, M., and Neufeld, E.F. (1982). Is there a mechanism for introducing acid hydrolases into liver lysosomes that is independent of mannose 6-phosphate recognition? Evidence from I-cell disease. Biochemical and biophysical research communications *105*, 814-820.
Pankiv, S., Clausen, T.H., Lamark, T., Brech, A., Bruun, J.A., Outzen, H., Overvatn, A., Bjorkoy, G., and Johansen, T. (2007). p62/SQSTM1 binds directly to Atg8/LC3 to facilitate degradation of ubiquitinated protein aggregates by autophagy. The Journal of biological chemistry *282*, 24131-24145.
Parente, M.K., Rozen, R., Cearley, C.N., and Wolfe, J.H. (2012). Dysregulation of gene expression in a lysosomal storage disease varies between brain regions implicating unexpected mechanisms of neuropathology. PloS one *7*, e32419.

Park, J.S., Mehta, P., Cooper, A.A., Veivers, D., Heimbach, A., Stiller, B., Kubisch, C., Fung, V.S., Krainc, D., Mackay-Sim, A.*, et al.* (2011). Pathogenic effects of novel mutations in the P-type ATPase ATP13A2 (PARK9) causing Kufor-Rakeb syndrome, a form of early-onset parkinsonism. Human mutation *32*, 956-964.
Parton, R.G., Simons, K., and Dotti, C.G. (1992). Axonal and dendritic endocytic pathways in cultured neurons. The Journal of cell biology *119*, 123-137.
Pentchev, P.G., Brady, R.O., Hibbert, S.R., Gal, A.E., and Shapiro, D. (1973). Isolation and characterization of glucocerebrosidase from human placental tissue. The Journal of biological chemistry *248*, 5256-5261.
Perandones, C., Micheli, F.E., Pellene, L.A., Bayly, M.A., Berkovic, S.F., and Dibbens, L.M. (2012). A case of severe hearing loss in action myoclonus renal failure syndrome resulting from mutation in SCARB2. Mov Disord *27*, 1200-1201.
Periquet, M., Fulga, T., Myllykangas, L., Schlossmacher, M.G., and Feany, M.B. (2007). Aggregated alpha-synuclein mediates dopaminergic neurotoxicity in vivo. J Neurosci *27*, 3338-3346.
Petersen, C.M., Nielsen, M.S., Nykjaer, A., Jacobsen, L., Tommerup, N., Rasmussen, H.H., Roigaard, H., Gliemann, J., Madsen, P., and Moestrup, S.K. (1997). Molecular identification of a novel candidate sorting receptor purified from human brain by receptor-associated protein affinity chromatography. The Journal of biological chemistry *272*, 3599-3605.
Pham, T.T., Giesert, F., Rothig, A., Floss, T., Kallnik, M., Weindl, K., Holter, S.M., Ahting, U., Prokisch, H., Becker, L.*, et al.* (2010). DJ-1-deficient mice show less TH-positive neurons in the ventral tegmental area and exhibit non-motoric behavioural impairments. Genes Brain Behav *9*, 305-317.
Platt, F.M., Neises, G.R., Dwek, R.A., and Butters, T.D. (1994). N-butyldeoxynojirimycin is a novel inhibitor of glycolipid biosynthesis. The Journal of biological chemistry *269*, 8362-8365.
Polymeropoulos, M.H., Lavedan, C., Leroy, E., Ide, S.E., Dehejia, A., Dutra, A., Pike, B., Root, H., Rubenstein, J., Boyer, R.*, et al.* (1997). Mutation in the alpha-synuclein gene identified in families with Parkinson's disease. Science (New York, NY *276*, 2045-2047.
Qi, L., Zhang, X.D., Wu, J.C., Lin, F., Wang, J., Difiglia, M., and Qin, Z.H. (2012). The role of chaperone-mediated autophagy in huntingtin degradation. PloS one *7*, e46834.
Qi, X., and Grabowski, G.A. (1998). Acid beta-glucosidase: intrinsic fluorescence and conformational changes induced by phospholipids and saposin C. Biochemistry *37*, 11544-11554.
Qiao, L., Hamamichi, S., Caldwell, K.A., Caldwell, G.A., Yacoubian, T.A., Wilson, S., Xie, Z.L., Speake, L.D., Parks, R., Crabtree, D.*, et al.* (2008). Lysosomal enzyme cathepsin D protects against alpha-synuclein aggregation and toxicity. Mol Brain *1*, 17.
Raben, N., Plotz, P., and Byrne, B.J. (2002). Acid alpha-glucosidase deficiency (glycogenosis type II, Pompe disease). Curr Mol Med *2*, 145-166.
Ramirez, A., Heimbach, A., Grundemann, J., Stiller, B., Hampshire, D., Cid, L.P., Goebel, I., Mubaidin, A.F., Wriekat, A.L., Roeper, J.*, et al.* (2006). Hereditary parkinsonism with dementia is caused by mutations in ATP13A2, encoding a lysosomal type 5 P-type ATPase. Nat Genet *38*, 1184-1191.
Reczek, D., Schwake, M., Schroder, J., Hughes, H., Blanz, J., Jin, X., Brondyk, W., Van Patten, S., Edmunds, T., and Saftig, P. (2007). LIMP-2 is a receptor for lysosomal mannose-6-phosphate-independent targeting of beta-glucocerebrosidase. Cell *131*, 770-783.
Reed, D.R., Lawler, M.P., and Tordoff, M.G. (2008). Reduced body weight is a common effect of gene knockout in mice. BMC Genet *9*, 4.

Reynolds, A.D., Glanzer, J.G., Kadiu, I., Ricardo-Dukelow, M., Chaudhuri, A., Ciborowski, P., Cerny, R., Gelman, B., Thomas, M.P., Mosley, R.L*., et al.* (2008). Nitrated alpha-synuclein-activated microglial profiling for Parkinson's disease. J Neurochem *104*, 1504-1525.
Rieker, C., Dev, K.K., Lehnhoff, K., Barbieri, S., Ksiazek, I., Kauffmann, S., Danner, S., Schell, H., Boden, C., Ruegg, M.A*., et al.* (2011). Neuropathology in mice expressing mouse alpha-synuclein. PloS one *6*, e24834.
Rijnboutt, S., Aerts, H.M., Geuze, H.J., Tager, J.M., and Strous, G.J. (1991). Mannose 6-phosphate-independent membrane association of cathepsin D, glucocerebrosidase, and sphingolipid-activating protein in HepG2 cells. The Journal of biological chemistry *266*, 4862-4868.
Ritz, B., and Yu, F. (2000). Parkinson's disease mortality and pesticide exposure in California 1984-1994. Int J Epidemiol *29*, 323-329.
Ron, I., and Horowitz, M. (2005). ER retention and degradation as the molecular basis underlying Gaucher disease heterogeneity. Human molecular genetics *14*, 2387-2398.
Ron, I., Rapaport, D., and Horowitz, M. (2010). Interaction between parkin and mutant glucocerebrosidase variants: a possible link between Parkinson disease and Gaucher disease. Human molecular genetics *19*, 3771-3781.
Rott, R., Szargel, R., Haskin, J., Bandopadhyay, R., Lees, A.J., Shani, V., and Engelender, S. (2011). alpha-Synuclein fate is determined by USP9X-regulated monoubiquitination. Proceedings of the National Academy of Sciences of the United States of America *108*, 18666-18671.
Russo, R., Berliocchi, L., Adornetto, A., Varano, G.P., Cavaliere, F., Nucci, C., Rotiroti, D., Morrone, L.A., Bagetta, G., and Corasaniti, M.T. (2011). Calpain-mediated cleavage of Beclin-1 and autophagy deregulation following retinal ischemic injury in vivo. Cell Death Dis *2*, e144.
Saito, Y., Suzuki, K., Hulette, C.M., and Murayama, S. (2004). Aberrant phosphorylation of alpha-synuclein in human Niemann-Pick type C1 disease. J Neuropathol Exp Neurol *63*, 323-328.
Sampathu, D.M., Giasson, B.I., Pawlyk, A.C., Trojanowski, J.Q., and Lee, V.M. (2003). Ubiquitination of alpha-synuclein is not required for formation of pathological inclusions in alpha-synucleinopathies. Am J Pathol *163*, 91-100.
Sardi, S.P., Clarke, J., Kinnecom, C., Tamsett, T.J., Li, L., Stanek, L.M., Passini, M.A., Grabowski, G.A., Schlossmacher, M.G., Sidman, R.L*., et al.* (2011). CNS expression of glucocerebrosidase corrects alpha-synuclein pathology and memory in a mouse model of Gaucher-related synucleinopathy. Proceedings of the National Academy of Sciences of the United States of America *108*, 12101-12106.
Sardi, S.P., Clarke, J., Viel, C., Chan, M., Tamsett, T.J., Treleaven, C.M., Bu, J., Sweet, L., Passini, M.A., Dodge, J.C*., et al.* (2013). Augmenting CNS glucocerebrosidase activity as a therapeutic strategy for parkinsonism and other Gaucher-related synucleinopathies. Proceedings of the National Academy of Sciences of the United States of America.
Sardiello, M., Palmieri, M., di Ronza, A., Medina, D.L., Valenza, M., Gennarino, V.A., Di Malta, C., Donaudy, F., Embrione, V., Polishchuk, R.S*., et al.* (2009). A gene network regulating lysosomal biogenesis and function. Science (New York, NY *325*, 473-477.
Sawkar, A.R., Adamski-Werner, S.L., Cheng, W.C., Wong, C.H., Beutler, E., Zimmer, K.P., and Kelly, J.W. (2005). Gaucher disease-associated glucocerebrosidases show mutation-dependent chemical chaperoning profiles. Chem Biol *12*, 1235-1244.
Sawkar, A.R., D'Haeze, W., and Kelly, J.W. (2006). Therapeutic strategies to ameliorate lysosomal storage disorders--a focus on Gaucher disease. Cell Mol Life Sci *63*, 1179-1192.

Schmid, J., Oelbe, M., Saftig, P., Schwake, M., and Schweda, F. (2012). Parallel regulation of renin and lysosomal integral membrane protein 2 in renin-producing cells: further evidence for a lysosomal nature of renin secretory vesicles. Pflugers Arch.

Schröder, J. (2008). Funktionelle Analyse der lysosomalen integralen
Membranproteine LIMP-1 und LIMP-2. In Biochemistry Institute (Kiel, Christian-Albrechts Universität).

Schroen, B., Leenders, J.J., van Erk, A., Bertrand, A.T., van Loon, M., van Leeuwen, R.E., Kubben, N., Duisters, R.F., Schellings, M.W., Janssen, B.J.*, et al.* (2007). Lysosomal integral membrane protein 2 is a novel component of the cardiac intercalated disc and vital for load-induced cardiac myocyte hypertrophy. The Journal of experimental medicine *204*, 1227-1235.

Schueler, U.H., Kolter, T., Kaneski, C.R., Blusztajn, J.K., Herkenham, M., Sandhoff, K., and Brady, R.O. (2003). Toxicity of glucosylsphingosine (glucopsychosine) to cultured neuronal cells: a model system for assessing neuronal damage in Gaucher disease type 2 and 3. Neurobiol Dis *14*, 595-601.

Seaman, M.N., McCaffery, J.M., and Emr, S.D. (1998). A membrane coat complex essential for endosome-to-Golgi retrograde transport in yeast. The Journal of cell biology *142*, 665-681.

Seibler, P., Graziotto, J., Jeong, H., Simunovic, F., Klein, C., and Krainc, D. (2011). Mitochondrial Parkin recruitment is impaired in neurons derived from mutant PINK1 induced pluripotent stem cells. J Neurosci *31*, 5970-5976.

Settembre, C., Di Malta, C., Polito, V.A., Garcia Arencibia, M., Vetrini, F., Erdin, S., Erdin, S.U., Huynh, T., Medina, D., Colella, P.*, et al.* (2011). TFEB links autophagy to lysosomal biogenesis. Science (New York, NY *332*, 1429-1433.

Settembre, C., Zoncu, R., Medina, D.L., Vetrini, F., Erdin, S., Huynh, T., Ferron, M., Karsenty, G., Vellard, M.C., Facchinetti, V.*, et al.* (2012). A lysosome-to-nucleus signalling mechanism senses and regulates the lysosome via mTOR and TFEB. The EMBO journal *31*, 1095-1108.

Sevlever, D., Jiang, P., and Yen, S.H. (2008). Cathepsin D is the main lysosomal enzyme involved in the degradation of alpha-synuclein and generation of its carboxy-terminally truncated species. Biochemistry *47*, 9678-9687.

Shachar, T., Lo Bianco, C., Recchia, A., Wiessner, C., Raas-Rothschild, A., and Futerman, A.H. (2011). Lysosomal storage disorders and Parkinson's disease: Gaucher disease and beyond. Mov Disord *26*, 1593-1604.

Shimura, H., Hattori, N., Kubo, S., Mizuno, Y., Asakawa, S., Minoshima, S., Shimizu, N., Iwai, K., Chiba, T., Tanaka, K.*, et al.* (2000). Familial Parkinson disease gene product, parkin, is a ubiquitin-protein ligase. Nat Genet *25*, 302-305.

Sidransky, E. (2005). Gaucher disease and parkinsonism. Molecular genetics and metabolism *84*, 302-304.

Sidransky, E., and Lopez, G. (2012). The link between the GBA gene and parkinsonism. Lancet Neurol *11*, 986-998.

Sidransky, E., Nalls, M.A., Aasly, J.O., Aharon-Peretz, J., Annesi, G., Barbosa, E.R., Bar-Shira, A., Berg, D., Bras, J., Brice, A.*, et al.* (2009). Multicenter analysis of glucocerebrosidase mutations in Parkinson's disease. The New England journal of medicine *361*, 1651-1661.

Sidransky, E., Sherer, D.M., and Ginns, E.I. (1992). Gaucher disease in the neonate: a distinct Gaucher phenotype is analogous to a mouse model created by targeted disruption of the glucocerebrosidase gene. Pediatric research *32*, 494-498.

Sidransky, E., Tayebi, N., Stubblefield, B.K., Eliason, W., Klineburgess, A., Pizzolato, G.P., Cox, J.N., Porta, J., Bottani, A., and DeLozier-Blanchet, C.D. (1996). The clinical, molecular, and

pathological characterisation of a family with two cases of lethal perinatal type 2 Gaucher disease. J Med Genet *33*, 132-136.
Sillence, D.J., and Platt, F.M. (2004). Glycosphingolipids in endocytic membrane transport. Semin Cell Dev Biol *15*, 409-416.
Singleton, A.B., Farrer, M., Johnson, J., Singleton, A., Hague, S., Kachergus, J., Hulihan, M., Peuralinna, T., Dutra, A., Nussbaum, R.*, et al.* (2003). alpha-Synuclein locus triplication causes Parkinson's disease. Science (New York, NY *302*, 841.
Sofroniew, M.V. (2009). Molecular dissection of reactive astrogliosis and glial scar formation. Trends Neurosci *32*, 638-647.
Specht, C.G., and Schoepfer, R. (2001). Deletion of the alpha-synuclein locus in a subpopulation of C57BL/6J inbred mice. BMC Neurosci *2*, 11.
Spillantini, M.G., Divane, A., and Goedert, M. (1995). Assignment of human alpha-synuclein (SNCA) and beta-synuclein (SNCB) genes to chromosomes 4q21 and 5q35. Genomics *27*, 379-381.
Sridhar, S., Botbol, Y., Macian, F., and Cuervo, A.M. (2012). Autophagy and disease: always two sides to a problem. J Pathol *226*, 255-273.
Sun, Y., Liou, B., Ran, H., Skelton, M.R., Williams, M.T., Vorhees, C.V., Kitatani, K., Hannun, Y.A., Witte, D.P., Xu, Y.H.*, et al.* (2010a). Neuronopathic Gaucher disease in the mouse: viable combined selective saposin C deficiency and mutant glucocerebrosidase (V394L) mice with glucosylsphingosine and glucosylceramide accumulation and progressive neurological deficits. Human molecular genetics *19*, 1088-1097.
Sun, Y., Qi, X., and Grabowski, G.A. (2003). Saposin C is required for normal resistance of acid beta-glucosidase to proteolytic degradation. The Journal of biological chemistry *278*, 31918-31923.
Sun, Y., Qi, X., Witte, D.P., Ponce, E., Kondoh, K., Quinn, B., and Grabowski, G.A. (2002). Prosaposin: threshold rescue and analysis of the "neuritogenic" region in transgenic mice. Molecular genetics and metabolism *76*, 271-286.
Sun, Y., Ran, H., Zamzow, M., Kitatani, K., Skelton, M.R., Williams, M.T., Vorhees, C.V., Witte, D.P., Hannun, Y.A., and Grabowski, G.A. (2010b). Specific saposin C deficiency: CNS impairment and acid beta-glucosidase effects in the mouse. Human molecular genetics *19*, 634-647.
Suzuki, K. (1998). Twenty five years of the "psychosine hypothesis": a personal perspective of its history and present status. Neurochemical research *23*, 251-259.
Suzuki, K., Iseki, E., Togo, T., Yamaguchi, A., Katsuse, O., Katsuyama, K., Kanzaki, S., Shiozaki, K., Kawanishi, C., Yamashita, S.*, et al.* (2007). Neuronal and glial accumulation of alpha- and beta-synucleins in human lipidoses. Acta neuropathologica *114*, 481-489.
Svennerholm, L., Vanier, M.T., and Mansson, J.E. (1980). Krabbe disease: a galactosylsphingosine (psychosine) lipidosis. Journal of lipid research *21*, 53-64.
Tabuchi, N., Akasaki, K., Sasaki, T., Kanda, N., and Tsuji, H. (1997). Identification and characterization of a major lysosomal membrane glycoprotein, LGP85/LIMP II in mouse liver. J Biochem *122*, 756-763.
Takahashi, K., Tanabe, K., Ohnuki, M., Narita, M., Ichisaka, T., Tomoda, K., and Yamanaka, S. (2007). Induction of pluripotent stem cells from adult human fibroblasts by defined factors. Cell *131*, 861-872.
Tan, E.K., Chai, A., Teo, Y.Y., Zhao, Y., Tan, C., Shen, H., Chandran, V.R., Teoh, M.L., Yih, Y., Pavanni, R.*, et al.* (2004). Alpha-synuclein haplotypes implicated in risk of Parkinson's disease. Neurology *62*, 128-131.

Tanaka, Y., Guhde, G., Suter, A., Eskelinen, E.L., Hartmann, D., Lullmann-Rauch, R., Janssen, P.M., Blanz, J., von Figura, K., and Saftig, P. (2000). Accumulation of autophagic vacuoles and cardiomyopathy in LAMP-2-deficient mice. Nature *406*, 902-906.
Taveggia, C., Feltri, M.L., and Wrabetz, L. (2010). Signals to promote myelin formation and repair. Nat Rev Neurol *6*, 276-287.
Thayanidhi, N., Helm, J.R., Nycz, D.C., Bentley, M., Liang, Y., and Hay, J.C. (2010). Alpha-synuclein delays endoplasmic reticulum (ER)-to-Golgi transport in mammalian cells by antagonizing ER/Golgi SNAREs. Molecular biology of the cell *21*, 1850-1863.
Thrower, J.S., Hoffman, L., Rechsteiner, M., and Pickart, C.M. (2000). Recognition of the polyubiquitin proteolytic signal. The EMBO journal *19*, 94-102.
Tybulewicz, V.L., Tremblay, M.L., LaMarca, M.E., Willemsen, R., Stubblefield, B.K., Winfield, S., Zablocka, B., Sidransky, E., Martin, B.M., Huang, S.P.*, et al.* (1992). Animal model of Gaucher's disease from targeted disruption of the mouse glucocerebrosidase gene. Nature *357*, 407-410.
Ueda, K., Fukushima, H., Masliah, E., Xia, Y., Iwai, A., Yoshimoto, M., Otero, D.A., Kondo, J., Ihara, Y., and Saitoh, T. (1993). Molecular cloning of cDNA encoding an unrecognized component of amyloid in Alzheimer disease. Proceedings of the National Academy of Sciences of the United States of America *90*, 11282-11286.
Usenovic, M., Tresse, E., Mazzulli, J.R., Taylor, J.P., and Krainc, D. (2012). Deficiency of ATP13A2 leads to lysosomal dysfunction, alpha-synuclein accumulation, and neurotoxicity. J Neurosci *32*, 4240-4246.
Vaccaro, A.M., Motta, M., Tatti, M., Scarpa, S., Masuelli, L., Bhat, M., Vanier, M.T., Tylki-Szymanska, A., and Salvioli, R. (2010). Saposin C mutations in Gaucher disease patients resulting in lysosomal lipid accumulation, saposin C deficiency, but normal prosaposin processing and sorting. Human molecular genetics *19*, 2987-2997.
van der Putten, H., Wiederhold, K.H., Probst, A., Barbieri, S., Mistl, C., Danner, S., Kauffmann, S., Hofele, K., Spooren, W.P., Ruegg, M.A.*, et al.* (2000). Neuropathology in mice expressing human alpha-synuclein. J Neurosci *20*, 6021-6029.
Vega, M.A., Rodriguez, F., Segui, B., Cales, C., Alcalde, J., and Sandoval, I.V. (1991). Targeting of lysosomal integral membrane protein LIMP II. The tyrosine-lacking carboxyl cytoplasmic tail of LIMP II is sufficient for direct targeting to lysosomes. The Journal of biological chemistry *266*, 16269-16272.
Vembar, S.S., and Brodsky, J.L. (2008). One step at a time: endoplasmic reticulum-associated degradation. Nature reviews *9*, 944-957.
Verhoef, L.G., Lindsten, K., Masucci, M.G., and Dantuma, N.P. (2002). Aggregate formation inhibits proteasomal degradation of polyglutamine proteins. Human molecular genetics *11*, 2689-2700.
Vielhaber, G., Hurwitz, R., and Sandhoff, K. (1996). Biosynthesis, processing, and targeting of sphingolipid activator protein (SAP)precursor in cultured human fibroblasts. Mannose 6-phosphate receptor-independent endocytosis of SAP precursor. The Journal of biological chemistry *271*, 32438-32446.
Vilarino-Guell, C., Wider, C., Ross, O.A., Dachsel, J.C., Kachergus, J.M., Lincoln, S.J., Soto-Ortolaza, A.I., Cobb, S.A., Wilhoite, G.J., Bacon, J.A.*, et al.* (2011). VPS35 mutations in Parkinson disease. American journal of human genetics *89*, 162-167.
Vitner, E.B., Dekel, H., Zigdon, H., Shachar, T., Farfel-Becker, T., Eilam, R., Karlsson, S., and Futerman, A.H. (2010). Altered expression and distribution of cathepsins in neuronopathic forms of Gaucher disease and in other sphingolipidoses. Human molecular genetics *19*, 3583-3590.

Vogiatzi, T., Xilouri, M., Vekrellis, K., and Stefanis, L. (2008). Wild type alpha-synuclein is degraded by chaperone-mediated autophagy and macroautophagy in neuronal cells. The Journal of biological chemistry *283*, 23542-23556.
Vogler, C., Levy, B., Grubb, J.H., Galvin, N., Tan, Y., Kakkis, E., Pavloff, N., and Sly, W.S. (2005). Overcoming the blood-brain barrier with high-dose enzyme replacement therapy in murine mucopolysaccharidosis VII. Proceedings of the National Academy of Sciences of the United States of America *102*, 14777-14782.
Volles, M.J., and Lansbury, P.T., Jr. (2002). Vesicle permeabilization by protofibrillar alpha-synuclein is sensitive to Parkinson's disease-linked mutations and occurs by a pore-like mechanism. Biochemistry *41*, 4595-4602.
Wahe, A., Kasmapour, B., Schmaderer, C., Liebl, D., Sandhoff, K., Nykjaer, A., Griffiths, G., and Gutierrez, M.G. (2010). Golgi-to-phagosome transport of acid sphingomyelinase and prosaposin is mediated by sortilin. Journal of cell science *123*, 2502-2511.
Waheed, A., Pohlmann, R., Hasilik, A., von Figura, K., van Elsen, A., and Leroy, J.G. (1982). Deficiency of UDP-N-acetylglucosamine:lysosomal enzyme N-acetylglucosamine-1-phosphotransferase in organs of I-cell patients. Biochemical and biophysical research communications *105*, 1052-1058.
Watanabe, Y., Tatebe, H., Taguchi, K., Endo, Y., Tokuda, T., Mizuno, T., Nakagawa, M., and Tanaka, M. (2012). p62/SQSTM1-Dependent Autophagy of Lewy Body-Like alpha-Synuclein Inclusions. PloS one *7*, e52868.
Webb, J.L., Ravikumar, B., Atkins, J., Skepper, J.N., and Rubinsztein, D.C. (2003). Alpha-Synuclein is degraded by both autophagy and the proteasome. The Journal of biological chemistry *278*, 25009-25013.
Weinreb, N.J., Charrow, J., Andersson, H.C., Kaplan, P., Kolodny, E.H., Mistry, P., Pastores, G., Rosenbloom, B.E., Scott, C.R., Wappner, R.S.*, et al.* (2002). Effectiveness of enzyme replacement therapy in 1028 patients with type 1 Gaucher disease after 2 to 5 years of treatment: a report from the Gaucher Registry. The American journal of medicine *113*, 112-119.
Westbroek, W., Gustafson, A.M., and Sidransky, E. (2011). Exploring the link between glucocerebrosidase mutations and parkinsonism. Trends Mol Med *17*, 485-493.
Willemsen, R., Tybulewicz, V., Sidransky, E., Eliason, W.K., Martin, B.M., LaMarca, M.E., Reuser, A.J., Tremblay, M., Westphal, H., Mulligan, R.C.*, et al.* (1995). A biochemical and ultrastructural evaluation of the type 2 Gaucher mouse. Mol Chem Neuropathol *24*, 179-192.
Wilms, H., Zecca, L., Rosenstiel, P., Sievers, J., Deuschl, G., and Lucius, R. (2007). Inflammation in Parkinson's diseases and other neurodegenerative diseases: cause and therapeutic implications. Curr Pharm Des *13*, 1925-1928.
Winklhofer, K.F., and Haass, C. (2010). Mitochondrial dysfunction in Parkinson's disease. Biochimica et biophysica acta *1802*, 29-44.
Winner, B., Jappelli, R., Maji, S.K., Desplats, P.A., Boyer, L., Aigner, S., Hetzer, C., Loher, T., Vilar, M., Campioni, S.*, et al.* (2011). In vivo demonstration that alpha-synuclein oligomers are toxic. Proceedings of the National Academy of Sciences of the United States of America *108*, 4194-4199.
Winslow, A.R., Chen, C.W., Corrochano, S., Acevedo-Arozena, A., Gordon, D.E., Peden, A.A., Lichtenberg, M., Menzies, F.M., Ravikumar, B., Imarisio, S.*, et al.* (2010). alpha-Synuclein impairs macroautophagy: implications for Parkinson's disease. The Journal of cell biology *190*, 1023-1037.

Witte, M.D., Kallemeijn, W.W., Aten, J., Li, K.Y., Strijland, A., Donker-Koopman, W.E., van den Nieuwendijk, A.M., Bleijlevens, B., Kramer, G., Florea, B.I*., et al.* (2010). Ultrasensitive in situ visualization of active glucocerebrosidase molecules. Nature chemical biology *6*, 907-913.

Wong, K., Sidransky, E., Verma, A., Mixon, T., Sandberg, G.D., Wakefield, L.K., Morrison, A., Lwin, A., Colegial, C., Allman, J.M*., et al.* (2004). Neuropathology provides clues to the pathophysiology of Gaucher disease. Molecular genetics and metabolism *82*, 192-207.

Xia, Q., Liao, L., Cheng, D., Duong, D.M., Gearing, M., Lah, J.J., Levey, A.I., and Peng, J. (2008). Proteomic identification of novel proteins associated with Lewy bodies. Front Biosci *13*, 3850-3856.

Xilouri, M., Vogiatzi, T., Vekrellis, K., Park, D., and Stefanis, L. (2009). Abberant alpha-synuclein confers toxicity to neurons in part through inhibition of chaperone-mediated autophagy. PloS one *4*, e5515.

Xu, Y.H., Barnes, S., Sun, Y., and Grabowski, G.A. (2010). Multi-system disorders of glycosphingolipid and ganglioside metabolism. Journal of lipid research *51*, 1643-1675.

Xu, Y.H., Quinn, B., Witte, D., and Grabowski, G.A. (2003). Viable mouse models of acid beta-glucosidase deficiency: the defect in Gaucher disease. Am J Pathol *163*, 2093-2101.

Xu, Y.H., Reboulet, R., Quinn, B., Huelsken, J., Witte, D., and Grabowski, G.A. (2008). Dependence of reversibility and progression of mouse neuronopathic Gaucher disease on acid beta-glucosidase residual activity levels. Molecular genetics and metabolism *94*, 190-203.

Xu, Y.H., Sun, Y., Ran, H., Quinn, B., Witte, D., and Grabowski, G.A. (2011). Accumulation and distribution of alpha-synuclein and ubiquitin in the CNS of Gaucher disease mouse models. Molecular genetics and metabolism *102*, 436-447.

Yamaguchi, Y., Sasagasako, N., Goto, I., and Kobayashi, T. (1994). The synthetic pathway for glucosylsphingosine in cultured fibroblasts. J Biochem *116*, 704-710.

Yamamoto, A., and Simonsen, A. (2011). The elimination of accumulated and aggregated proteins: a role for aggrephagy in neurodegeneration. Neurobiol Dis *43*, 17-28.

Yamayoshi, S., Yamashita, Y., Li, J., Hanagata, N., Minowa, T., Takemura, T., and Koike, S. (2009). Scavenger receptor B2 is a cellular receptor for enterovirus 71. Nature medicine *15*, 798-801.

Yang, Q., She, H., Gearing, M., Colla, E., Lee, M., Shacka, J.J., and Mao, Z. (2009). Regulation of neuronal survival factor MEF2D by chaperone-mediated autophagy. Science (New York, NY *323*, 124-127.

Yap, T.L., Gruschus, J.M., Velayati, A., Westbroek, W., Goldin, E., Moaven, N., Sidransky, E., and Lee, J.C. (2011). Alpha-synuclein interacts with Glucocerebrosidase providing a molecular link between Parkinson and Gaucher diseases. The Journal of biological chemistry *286*, 28080-28088.

Yap, T.L., Velayati, A., Sidransky, E., and Lee, J.C. (2013). Membrane-bound alpha-synuclein interacts with glucocerebrosidase and inhibits enzyme activity. Molecular genetics and metabolism *108*, 56-64.

Yildiz, Y., Matern, H., Thompson, B., Allegood, J.C., Warren, R.L., Ramirez, D.M., Hammer, R.E., Hamra, F.K., Matern, S., and Russell, D.W. (2006). Mutation of beta-glucosidase 2 causes glycolipid storage disease and impaired male fertility. The Journal of clinical investigation *116*, 2985-2994.

Young, J.E., Martinez, R.A., and La Spada, A.R. (2009). Nutrient deprivation induces neuronal autophagy and implicates reduced insulin signaling in neuroprotective autophagy activation. The Journal of biological chemistry *284*, 2363-2373.

Yu, R.K., Nakatani, Y., and Yanagisawa, M. (2009). The role of glycosphingolipid metabolism in the developing brain. Journal of lipid research *50 Suppl*, S440-445.

Zachos, C., Blanz, J., Saftig, P., and Schwake, M. (2012). A Critical Histidine Residue Within LIMP-2 Mediates pH Sensitive Binding to Its Ligand beta-Glucocerebrosidase. Traffic (Copenhagen, Denmark) *13*, 1113-1123.

Zarranz, J.J., Alegre, J., Gomez-Esteban, J.C., Lezcano, E., Ros, R., Ampuero, I., Vidal, L., Hoenicka, J., Rodriguez, O., Atares, B.*, et al.* (2004). The new mutation, E46K, of alpha-synuclein causes Parkinson and Lewy body dementia. Annals of neurology *55*, 164-173.

Zhang, W., Wang, T., Pei, Z., Miller, D.S., Wu, X., Block, M.L., Wilson, B., Zhou, Y., Hong, J.S., and Zhang, J. (2005). Aggregated alpha-synuclein activates microglia: a process leading to disease progression in Parkinson's disease. FASEB J *19*, 533-542.

Zhu, X.R., Maskri, L., Herold, C., Bader, V., Stichel, C.C., Gunturkun, O., and Lubbert, H. (2007). Non-motor behavioural impairments in parkin-deficient mice. Eur J Neurosci *26*, 1902-1911.

Zimprich, A., Benet-Pages, A., Struhal, W., Graf, E., Eck, S.H., Offman, M.N., Haubenberger, D., Spielberger, S., Schulte, E.C., Lichtner, P.*, et al.* (2011). A mutation in VPS35, encoding a subunit of the retromer complex, causes late-onset Parkinson disease. American journal of human genetics *89*, 168-175.

9 Appendix

9.1 Equipment, chemicals, kits and buffers

9.1.1 Machines

Table 9.1 *Machines*.

Machine	Model	Company
96 well plate reader	Synergy HAT	BioTek, Bad-Friedrichshall, DE
Agarose gel imaging	Gel Jet Imager UV system	Intas, Göttingen, DE
Agarose running chamber	Sub-Cell®GT	BioRad, Munich, DE
Autoclave	Tecnomara	Integra Biosciences, Fernwald, DE
Bacteria incubator	Multitron II	Infra-Hat, Sulzemoos, DE
Bench-top roller	RM5	Karl Hecht KG, Sondheim, DE
Cell culture incubator	HeraCell240	Heraeus, Hanau, DE
Chemiluminescence detection system	LAS 3000 and LAS4000	GE Healthcare, Munich, DE
Confocal laser scanning microscope	FV1000	Olympus. Hamburg, DE
Electroporation device	Pulse controller gene pulser	BioRad, Munich, DE
Fluorescence microscope	Axiovert 200M	Zeiss, Jena, DE
Electroporation device	Gene Pulser	BioRad, Munich, DE
Heating block	Thermostat 5320	Eppendorf, Hamburg, DE
Light microscope	CKX41 & SZ61	Olympus. Hamburg, DE
Magnetic stirrer	IKAMAG RCT, REO	IKA, Staufen, DE
Micropipette	10 µl	Eppendorf, Hamburg, DE
	200 µl	Gilson, Limburg-Offheim, DE
	1000µl	Gilson, Limburg-Offheim, DE
Microtome	Leica SM 2000R	Leica, Wetzlar, DE
PCR-Cycler	GenAmp 2400 PCR	Perkin Elmer, Rodgau-Jügesheim, DE
	Gene AMP PCR 9700	Applied Biosystems, Darmstadt, DE
pH-Meter	Digital-pH-Meter 646	Krick, Langenselbold, DE
Pipette Boy	Accu-jet®Pro	Integra Bioscience, Fernwald, DE
Powerpack	Powerpack 200/300	BioRad, Munich, DE
Pure water device	Milli-Q Plus	Millipore, Schwalbach, DE
Real-Time PCR Cycler	Light-Cycler 480 II	Roche, Mannheim, DE
SDS-Page Chamber	Mini-Protein 3-Electrophoresis system	BioRad, Munich, DE
Sensitive scales	L420P	Sartorius AG, Göttingen, DE
Sterile hood	VFR1806	CLAUS DAMM A/S, Alleroed, DE
Tabletop centrifuge	EM 900	Eppendorf, Hamburg, DE
Tabletop cooling centrifuge	Fresco21	Thermo Fisher, Schwerte, DE
Tank bloting device	Criterion™	BioRad, Munich, DE
Thermomixer	Thermomixer 5436	Eppendorf, Hamburg, DE
Tissue homogeniser	Precellys	PeqLab, Erlangen, DE
Ultracentrifuge	J2-HS	Beckman, Fullerton, US
UV-Table	Reprostar	Lamag, Berlin, DE
Vortexer	Vortex Genie	Bender & Hobein, Bruchsaal, DE
Waterbath	1083	GFL, Burgwedel, DE
Weighing scales	Kern 770	Kern & Son, Dürrwangen, DE

9.1.2 Materials

Table 9.2 *Laboratory material.*

Description	Company
12-Well-Plates	Sarstedt, Nümbrecht, DE
6-Well-Plates	Sarstedt, Nümbrecht, DE
96-Well-Plates	Sarstedt, Nümbrecht, DE
Conical flasks	Roth, Karlsruhe, DE
Coverslips	Assistent, Sondheim, DE
Cryo tubes	Sarstedt, Nümbrecht, DE
Electroporation cuvettes	Peqlab, Erlangen, DE
Filter Tips Biosphere	Sarstedt, Nümbrecht, DE
Glass beakers	Roth, Karlsruhe, DE
Gloves	Roth, Karlsruhe, DE
Graduated cylinders	Roth, Karlsruhe, DE
Needles	Becton Dickinson, Heidelberg, DE
Nitrocellulose membrane	Roth, Karlsruhe, DE
Objectives (histology)	Marienfeld Laboratory Glassware, Lauda-Königshofen, DE
Objectives (tissue culture)	Menzel Glass GmbH & Co. KG, Braunschweig, DE
Parafilm	American National Can™,Chicago, IL, US
Pasteur pipettes	Assistant, Sondheim, DE
PCR tube strips (8x)	Sarstedt, Nümbrecht, DE
PCR tubes	Sarstedt, Nümbrecht, DE
Pipette tips	Sarstedt, Nümbrecht, DE
Policeman´s rubber	Sarstedt, Nümbrecht, DE
Reaction tubes	Eppendorf, Hamburg, DE
Sterile filter (0,2 µm pore size)	Sarstedt, Nümbrecht, DE
Sterile plastic tubes	Sarstedt, Nümbrecht, DE
Surgical preparation tools	FST, Heidelberg, DE
Surgical scalpel	Aesculap, Tuttlingen, DE
Syringes	Becton Dickinson, Heidelberg, DE
Tissue culture dishes	Sarstedt, Nümbrecht, DE
Transfer pipettes, 3,5 ml	Sarstedt, Nümbrecht, DE
Ultracentrifuge 1.5 ml tubes	Beckman, Fullerton, US
Whatman paper	Roth, Karlsruhe, DE

9.1.3 Chemicals

Table 9.3 ***Reagents.***

Description	Company
1 X Trypsin/EDTA	PAA-Laboratories, Linz, AT
2-Mercaptoethanol (p.a.)	Roth, Karlsruhe, DE
30% Acrylamide / 0,8% bisacrylamide, rotiphorese 30	Roth, Karlsruhe, DE
4, 4,-difluoro-1, 3, 5, 7, 8-pentamethyl-4-bora-3a, 4a-diaza-s-indacene (Bodipy®493/503)	Invitrogen, Darmstadt, DE
Acetic acid	Sigma Aldrich, Steinheim, DE
Agarose	Lonza, Cologne, DE
Ammonium Persulfate (APS)	Roth, Karlsruhe, DE
Ampicillin	Melford Laboratories, Chelsworth, UK
B27-Supplement	Invitrogen, Darmstadt, DE
Bovine serum Albumin(BSA)	Sigma Aldrich, Steinheim, DE
Bromphenol blue	Canalco, Bethesda, US
Calcium Chloride dehydrated	Merck, Darmstadt, DE
Citric acid	Merck, Darmstadt, DE
Complete Protease Inhibitor Cocktail	Roche, Mannheim, DE
Cytosine arabinoside (AraC)	Fluka, Buchs, CH
DAB (3,3 Diaminobenzidine tetrahydrochloride)	Sigma Aldrich, Steinheim, DE
DABCO (1,4-Diazobicyclo[2.2.2]octane)	Sigma Aldrich, Steinheim, DE
DAPI (4‘,6-Diamidine-2-phenylindol)	Sigma Aldrich, Steinheim, DE
Desoxyribonucleosidetrisphosphates (NTPs) (2 mM/ 10 mM)	Fermentas, St. Leon-Rot, DE
Di-Calcium-hydrogen-phosphate	Roth, Karlsruhe, DE
Di-Sodium hydrogen phosphate	Roth, Karlsruhe, DE
DMEM, High Glucose	PAA, Laboratories, Linz, AT
DMEM/F12 media	Invitrogen, Darmstadt, DE
DMSO (Dimethylsulfoxide)	Serva, Heidelberg, DE
DNA-Ladder (100 bp, 1 kb)	Roche, Mannheim, DE
DNA-Polymerase (Taq, Pfu)	Fermentas, St. Leon-Rot, DE
DTT (Dithiothreitol)	Sigma Aldrich, Steinheim, DE
Eosin	Merck, Darmstadt, DE
Ethanol 99,8% p.a.	Roth, Karlsruhe, DE
Ethidiumbromide	Roth, Karlsruhe, DE
Ethylendiamintetra acetic acidEDTA)	Roth, Karlsruhe, DE

Eukitt	Sigma Aldrich, Steinheim, DE
EZ-Link Sulfo-NHS-LC-Biotin	Thermo Fisher Scientific, Rockford, US
Fetal Bovine serum	Invitrogen, Darmstadt, DE
Fetal calf serum (FCS)	PAA, Laboratories, Linz, AT
Glucose	Sigma Aldrich, Steinheim, DE
GlutaMAX™	Invitrogen, Darmstadt, DE
Glycerol	Sigma Aldrich, Steinheim, DE
Glycine	Roth, Karlsruhe, DE
Goat serum	PAA-Laboratories, Linz, AT
Haematoxylin by Harris	Roth, Karlsruhe, DE
Hibernate E®	Invitrogen, Darmstadt, DE
Hydrogen peroxide (30 % H_2O_2)	Merck, Darmstadt, DE
Isopropanol (p.a.)	Roth, Karlsruhe, DE
Kanamycin	Sigma Aldrich, Steinheim DE
Magnesium chloride	Merck, Darmstadt, DE
Methanol (p.a.)	Roth, Karlsruhe, DE
Milk powder	Roth, Karlsruhe, DE
Mowiol	Calbiochem, La Jolla CA, US
N,N,N',N'-Tetramethylethylendiamine (TEMED) (p.a.)	Roth, Karlsruhe, DE
N-butyl-deoxynojirimycin (Miglustat)	Tocris biosciences, Bristol, UK
Neurobasal media	Invitrogen, Darmstadt, DE
Page Ruler Prestained Protein Ladder Plus	Fermentas, St-Leon-Rot, DE
Paraformaldehyde	Fluka, Buchs, Switzerland
Penicillin/Steptomycin	PAA-Laboratories, Linz, AT
Poly-D-Lysine	Sigma Aldrich, Steinheim, DE
Potassium Chloride	Roth, Karlsruhe, DE
Potassium dihydrogen-phosphate	Roth, Karlsruhe; DE
Potassium-hydrogen carbonate	Roth, Karlsruhe, DE
Restriction enzymes	Fermentas, St-Leon-Rot, DE
RotiHistol	Roth, Karlsruhe; DE
Schiff's reagent	Roth, Karlsruhe, DE
Sodium chloride	Roth, Karlsruhe, DE
sodium dodecyl sulfate (SDS)	Roth, Karlsruhe, DE
Sodium hydrogen carbonate	Roth, Karlsruhe, DE
Sodium hydroxide	Riedel-de-Haen, Seelze, DE

Sodiumcitrate	Merck, Darmstadt, DE
Tetracyclin	Merck, Darmstadt, DE
Tris(hydroxymethyl)-aminomethane (TRIS)	Roth, Karlsruhe, DE
Triton X-100	Sigma Aldrich, Steinheim, DE
Trypan blue 0.4 %	Invitrogen, Darmstadt, DE
Turbofect® transfection reagent	Fermentas, St-Leon-Rot, DE
Tween-20	Sigma Aldrich, Steinheim, DE
Xylol	Roth, Karlsruhe, DE

9.1.4 Enzymes/Kits

Table 9.4 ***Enzymes.***

Description	Company
Dream Taq	Fermentas, St-Leon-Rot, DE
DNase	Roche, Mannheim, DE
Restriction enzymes	Fermentas, St-Leon-Rot, DE
Trypsin/EDTA	Invitrogen, Darmstadt, DE

Table 9.5 ***Kits.***

Description	Company
ApopTag®Peroxidase *In situ* Apoptosis Detection Kit	Millipore (Schwalbach, DE)
BCA-Protein Assay Kit	Thermo Fisher Scientific, Rockford, US
DNA-Extraction kit	Analytik Jena, Jena, DE
ECL Advanced/Plus Western Blot Detection Kit	GE Healthcare, Munich, DE
Elite DAB staining kit	Enzo Life Sciences, Lörrach, DE
High Pure PCR-Purification Kit	Roche, Mannheim, DE
NucleoSpin® RNA easy Kit	Macherey-Nagel, Düren, DE
PureYield Plasmid Midiprep System	Promega, Mannheim, DE
Plasmid Miniprep Kit	Fermentas, St-Leon-Rot, DE
RevertAid™ First Strand cDNA Synthesis Kit	Fermentas, St-Leon-Rot, DE
SYBR®Green Master mix	Takara, Shiga, JP
Vector Laboratories ABC kit	Enzo Life Sciences, Lörrach, DE
One-step quick mutagenesis kit	Stratagene/Agilent Technologies, Böblingen, DE)

9.1.5 Buffers, solutions and routine culture media

Table 9.6 ***Buffers for protein biochemistry.***

Name of buffer	*Reagents*
Enzyme activity assay citrate buffer	0.2 M Sodium citrate 0. 04 % NaN_3 0.2 % BSA pH 4.6
Enzyme activity assay stop solution	0.4 M Glycine pH to 10.4 with NaOH
Lysis Buffer cell pellets	50 mM Tris-NaOH 150 mM NaCl 2 mM EDTA Complete™ 1 % Triton-x 100 2 mM $MgCl_2$ pH 7.4
Phosphate buffer (o.1 M PB)	77.4 ml 1M Na_2HPO_4 22.6 ml 1M Na_2HPO_4 Fill to 1L with ddH_20, pH 7.4
Phosphate buffered saline solution (PBS)	137 mM NaCl 2.7 mM KCl 4.3 mM Na_2HPO_4 1.4 mM KH_2PO_4 Fill to 1L with ddH20, pH 7.4
SDS soluble buffer (Mazzulli et al., 2006)	2 % SDS, 50 mM Tris-HCl-pH7.4
SDS-PAGE-buffer 10x	1.92 M Glycine 250 mM Tris-HCl 35 mM SDS
SDS-PAGE-loading buffer (Laemmli) (5x)	2.5 ml Tris/HCl pH6.8 1 g SDS 5.8 ml 86 % Glycerol 0.05 % Bromophenol blue Fill to 10 ml with ddH20 + 5 x end concentration DTT
Stacking gel buffer	0.5 M Tris 0.4 % (w/v) SDS pH 6.8
Seperation gel buffer	1,5 M Tris 0.4 % (w/v) SDS pH 8.8

Stripping buffer	200 ml 10 % SDS stock solution 62.5 ml Tris/HCl pH 6.8 8.3 ml β-mercaptoethanol Fill to 1L with ddH20
Tank-Blot-Transfer-Buffer (10X)	250 mM Tris 2 M Glycine pH 8.3
Tank-Blot-Buffer (1X)	1 x Tank-Blot-Buffer 10x 20 % Methanol Fill to 1L with ddH2O
TBS-T	20 mM Tris HCl 150 mM NaCl pH 7.5 0.1 % Tween20
Triton soluble buffer (Mazzulli et al., 2006)	1 % triton x-100 20 mM HEPES 150 mM NaCl 10 % glycerol 1 mM $MgCl_2$ 50 mM NaF 2 mM $NaVO_3$ Complete™ pH 7.4
Western Blot blocking buffer	5 g Milk powder dissolved in TBS/T

Table 9.7 Routine media.

Name of buffer	***Reagents***
DMEM High Glucose (+additives)	DMEM 10 % FCS 50 µg/ml Penicillin & Streptomycin
LB-agar plates	10 g Trypton/Peptone from Casein 5 g Yeast extract 10 g NaCl in 950 ml ddH_2O, pH 7.0 15 g Agar 1000 ml ddH_2O Autoclave, pour into 10ml sterile 10cm plates
LB-medium	10 g Trypton/Peptone from Casein 5 g Yeast extract 10 g NaCl in 950 ml ddH_2O, pH 7.0

Table 9.8 ***Solutions used in immunofluorescence of cells grown on coverslips (IF) and histological sections (IH).***

Name of buffer	Reagents
Fixation solution	PBS, 4 % PFA
Washing /permeabilisation buffer (IF)	PBS, 0.2 % saponin
Masking buffer (IF)	PBS, 0.2 % saponin /0.12 % Glycine
Blocking buffer (IF)	10 % FCS, 0.2 % saponin
H_20_2 solution (IH)	PB, 0.3 % H_20_2
Washing solution (IH)	PB, 0.25 % Triton-x-100
Blocking/antibody solution (IH)	PB, 0.25 % Triton-x-100, 4 % normal goat serum
DAPI-Solution	PBS, 1 mg/ml DAPI
Mounting IF/IH (immunofluorescence only)	1 ml Mowiol solution (17 % Mowiol/33 % glycerol/ PBS) 100 µl DABCO (end conc. 50 mg/ml) 1 µl DAPI-solution (end conc. 1 µg/ml)
Citric acid immunohistology unmasking solution	10 mM Citric acid (pH 6 - NaOH)

10 List if figures and tables

10.1 Figures

10.2 Tables

11 Abbreviations

Ab/Am	Antibiotics/Antimycotics
AC	Anterior commissure
AMRF	Action myoclonus renal failure
AP	Alkalische Phosphatase
APS	Ammoniumperoxodisulfate
ATP	Adenosintriphosphate
BCA	Bicinchonic acid
bp	Base pair
BSA	Bovine albumin serum
CA	Cornu ammonis
Cblm	Cerebellum
CC	Corpus callosum
CD68	Cluster of differentiation 68
cDNA	Complementary DNA
CMA	Chaperone mediated autophagy
CO_2	Carbon dioxide
Cx	Cortex
ddH_2O	Double distilled water
DG	Dentate gyrus
DMEM	Dulbecco's minimal essential medium
DMSO	Dimethylsulfoxide
DNA	Deoxyribonucleic acid
Dnase	Deoxyribonuclease
dNTP	Deoxyribonucleotidetriphosphate
DTT	Dithiothreitol
E. coli	Escherichia *coli*, bacteria
ECL	Enhanced chemoluminescence
EDTA	Ethylene, diamine tetra-acetic acid
eGFP	Enhanced green fluorescent protein
ER	Endoplamatic reticulum
ERAD	ER associated degradation
FBS	Foetal bovine serum
FCS	Foetal calf serum
Fig	Figure
Fx	Fornix
G	Granular cell layer
g	Gramme
GAPDH	Glyceraldehyde 3-phosphate dehydrogenase
GD	Gaucher disease
GFAP	Glial fibrillary acidic protein

GluCer	Glucosylceramide/Glucosylceramid
GSLs	Glycosphingolipids
h	human
H&E	Haematoxylin and Eosin
H_2O	Water
HeLa	Henrietta Lacks (cervical cancer cells)
HLC	Hind-limb clasping
HRP	Horse raddish peroxidase
iPSCs	Inducible pluripotent stem cells
kb	Kilo bases
kDA	Kilo Dalton
LAMP-1	Lysosomal associated protein type 1
LAMP-2	Lysosomal associated protein type 2
LAMP-2a	LAMP-2 isoform a
LC3I/II	Light-chain-3-I/II
LIMP-2	Lysosomal integral membrane protein type 2
LIMP-$2^{-/-}$	LIMP-2 knockout
LPS	Lipopolysaccharide
M	Molecular cell layer ro medulla
M-6-PR	Mannose-6-phosphate receptor
MB	Midbrain
MEF	Mouse embryonic fibroblast
mg	Milligramme
mL	Milliliter
mM	Millimolar
mRNA	Messenger ribonucleic acid
OB	Olfactory bulb
P	Purkinje cell layer
P	Pons
PAS	Periodic acid-Schiff
PBS	Phosphate buffered saline
PCR	Polymerase chain reaction
PD	Parkinson´s disease
pH	Potential hydrogen
PME	progressive myoclonic epilepsy
qRT-PCR	Quantitative real time polymerase chain reaction
RNA	Ribonucleic acid
SCARB2	LIMP-2 gene
SDS-PAGE	Natriumdodecylsulfate-Polyacrylamide-Gel electrophorseis
SHSY-5Y	Human neurobalstoma cells (sub-clone 5Y)
siRNA	Small interfering RNA

SN	Substantia nigra
SNCA	α-synuclein gene
SQSTM1/p62	Sequestosome 1/p62
TAE	Tris-Acetate-EDTA
TFEB	Transcription factor E box
Tris	Tris-(hydroxymethyl)-aminomethan
TUNEL	Terminal deoxynucleotidy transferase (deoxyuridine triphosphate) dUTP Nick End Labelling
UCHL-1	Ubiquitin carboxy-terminal hydrolase like-1
V	Volt
Wm	White matter
WT	wild-type
ZNS	Zentralnervensystem
α-syn	α-Synuclein
β-GC	Beta-Glucocerebrosidase
µg	Mikrogramm
µL	Mikroliter
µM	Mikromolar
%	Percent
-/-	Knockout
+/+	Wild-type
°C	Degree Celsius

12 Curriculum vitae

Name: Michelle Danaher

Date of birth: 11.09.1983

Nationality: Irish

Birthplace: Limerick, Ireland

Marital status: Single

Doctoral training:

From 09/2008: In Prof. Dr. Paul Saftig`s working group at the Biochemistry Institute, Christian Albrechts-Universität, Kiel, Germany.

Qualifications:

- 2005 to 2006: Master of Science in Biotechnology and Molecular Biology at the University of Hull, UK.
  Thesis work in the laboratory of Prof. Dr. Jörg Hardege.
  Theme: "Bioaccumulation of alkylphenols in *Nereis diversicolor* "
- 2001 to 2005: Bachelor of Science in biochemistry at the University College Cork, Ireland.
- 1996 to 2001: St. Mary´s secondary school, Charleville, Co. Cork, Ireland.
  Leaving certificate.

Publications:

Ram JL, Fei X, **Danaher SM**, Lu S, Briethaupt T, Hardege JD (2008) Finding females: pheromone-guided reproductive tracking behavior by male *Nereis succinea* in the marine environment. **J Exp Biol** 211, 757-765.

13 Acknowledgements

I am sincerely and heartily grateful to my advisors, Dr. Judith Blanz, PD Dr. Michael Schwake and Prof. Dr. Paul Saftig, for their support and guidance during my doctoral studies and the writing of my dissertation. I must also acknowledge Prof. Dr. Markus Glatzel, Hermann Altmeppen and Michaela Schweizer for their collaboration and helpful discussions. I recognise that this research would not have been possible without excellent technical assistance provided by Maike Langer and I am particularly grateful for the expert scientific skills provided by Meryem Senkara these past years. I owe sincere and earnest thankfulness to Mirka Allerding for her precise pickiness while editing this work but most of all for her friendship and support. I would also like thank Johannes Prox and Friederike Zunke for their time and effort in perfecting this thesis. I am obliged to all other colleagues, both past and present, who supported over the years and have endeavoured to promote a stimulating and welcoming academic and social environment. My family have given me their support throughout, as always, for which my mere expression of thanks does not suffice. Above all, I would like to thank Tobias Rothaug for his unequivocal support, patience and resolution to keep me sane.

14 Declaration

Herewith I declare that:

i. apart from the supervisor`s guidance, the content and design of this dissertation is my own work.

ii. this thesis has not been submitted partially or wholly as part of a doctoral degree to another examining body.

iii. parts of this work have been submitted for scientific publication.

iv. this thesis has been prepared according to the Rules of Good Scientific Practice of the German Research Foundation.

Kiel, March 2013

Michelle Danaher